ONWI

Ac. #3004
LBL-11566
UC-70
CONF 800267
ONWI-240

PROCEEDINGS

WORKSHOP ON NUMERICAL MODELING OF THERMOHYDROLOGICAL FLOW IN FRACTURED ROCK MASSES

February 19-20, 1980
Berkeley, California

September 1980

This work was supported by the Assistant Secretary for Nuclear Energy, Office of Waste Isolation of the U.S. Department of Energy under Contract No. W-7405-ENG-48. The contract is administered by the Office of Nuclear Waste Isolation at Battelle Memorial Institute, Columbus, Ohio

Organized by:

Earth Sciences Division
Lawrence Berkeley Laboratory
University of California

LEGAL NOTICE

LBL-11566
CONF 800267
ONWI-240

PROCEEDINGS OF THE WORKSHOP ON NUMERICAL MODELING OF THERMOHYDROLOGICAL FLOW IN FRACTURED ROCK MASSES

February 19-20, 1980

Berkeley, California

Earth Sciences Division
Lawrence Berkeley Laboratory
University of California
Berkeley, California 94720

This work was supported by the Assistant Secretary for Nuclear Energy, Office of Waste Isolation of the U. S. Department of Energy under Contract No. W-7405-ENG-48. The contract is administered by the Office of Nuclear Waste Isolation at Battelle Memorial Institute, Columbus, Ohio.

TABLE OF CONTENTS

PREFACE v

INTRODUCTIONS

P. A. Witherspoon
Fracture Flow 1

M. M. Lemcoe
Welcome 2

OVERVIEWS

J. S. Y. Wang
Introduction to Numerical Modeling of Thermohydrologic Flow in Fractured Rock Masses 3

F. J. Bourke
UK Modelling of Thermal Effects on Leakage from Hard Rock Depositories 14

FRACTURE MODELINGS

T. N. Narasimhan
Multidimensional Numerical Simulation of Fluid Flow in Fractured Porous Media 16

J. C. Bernard
Flow in Fractured Porous Media. 33

R. K. Thorpe
An Example of Rock Fracture Characterization for Modeling Purposes 37

J. Noorishad, M. S. Ayatollahi, and P. A. Witherspoon
A Finite Element Method for Coupled Stress and Fluid Flow Analysis in Fractured Rock Masses 43

REPOSITORY STUDIES

A. F. Runchal
A Porous Media Fluid Flow, Heat and Mass Transport Model with Rock Stress Coupling. 50

A. B. Pahwa and P. T. Baxley
Detection of Fractures from Well Testing. 60

A. S. Burgess and J. L. Ratigan
Modeling of Groundwater Flow in Fractured Rocks for Radioactive Waste Repository Studies 65

S. K. Gupta, C. R. Cole, C. T. Kincaid, and F. E. Kaszeta
Description and Applications of the FE3DGW and CFEST Three-Dimensional Finite-Element Models 77

GEOTHERMAL MODELS

K. H. Coats
Geothermal Model 86

C. R. Faust and J. W. Mercer
The Role of Numerical Models in Applications to Thermo-hydrological Flow in Fractured Rock Masses 47

J. W. Pritchett
Geothermal Reservoir Simulation Capabilities at Systems, Science and Software. . . . . '

K. Pruess
SHAFT79 . . . . . ''

G. S. Bodvarsson and M. J. Lippmann
Numerical Model CCC . . . . . '.

RECENT DEVELOPMENTS

R. Hofmann
Development of an Explicit Finite-Difference Fluid Flow Model. . . . . :::

R. R. Eaton and D. E. Larson
The Importance of Including Fractures in Thermohydrological Modeling of Flow Through Porous Media . . . . . ::

PANEL DISCUSSION

J. C. Duguid, Chairman; J. S. Y. Wang, Editor; and K. H. Coats, J. E. Gale, R. E. Goodman, G. Hocking, and C. R. Wilson, Panelists . . .

PROGRAM . . . . . '.

LIST OF PARTICIPANTS . . . . . 2.

PREFACE

This workshop on modeling thermohydrologic flow in fractured rock masses is a result of the attention currently being given to the isolation of nuclear wastes in geological formations. The workshop provided a forum for the 60 participants from the fields of waste isolation, groundwater hydrology, geothermal energy, and petroleum engineering to discuss the discrete and continuum approaches, the generic repository studies, and the experiences of modeling thermohydrologic flow in different fields.

The workshop was organized by the Earth Sciences Division, Lawrence Berkeley Laboratory, under the guidance of Professor Paul A. Witherspoon, and sponsored by the Office of Nuclear Waste Isolation, U. S. Department of Energy. Drs. Joseph S. Y. Wang and Chin Fu Tsang were the workshop co-chairmen and Werner J. Schwarz was the workshop coordinator. The assistance and advice of Drs. James O. Duguid, Michael M. Lemcoe, and Michael Wigley of ONWI are much appreciated.

Included in these Proceedings are presentations from the workshop and summaries of the panel discussions. Papers from outside the Lawrence Berkeley Laboratory were prepared by the authors and are being reproduced without editing. Lawrence Berkeley Laboratory papers were reviewed by the Earth Sciences Division's Publication Committee.

Joseph S. Y. Wang

FRACTURE FLOW

Paul A. Witherspoon
Earth Sciences Division
Lawrence Berkeley Laboratory
University of California
Berkeley, California 94720

Welcome to the workshop of modeling thermo-hydrological flows in fractured systems. This problem is of critical importance in the underground isolation of radioactive waste where one is concerned with flows through nearly impermeable rock formations.

An idealization of a fracture in the "open" and "closed" positions is illustrated in Figure 1. For an open fracture, the surfaces are not in contact. In the simple case of a fracture closing under normal stress, the asperities will close off part of the flow path. The flow field is complex with the presence of contact areas and rough surfaces.

The asperities may withstand large normal stress and the fracture is difficult to close under compression. The flow through the fracture depends highly nonlinearly on the stress. Figure 2 illustrates the behavior of radial flow through a tension fracture in a granite core over the stress range from 0 to 20 MPa. There are also the effects of hysteresis during cyclic loading, as clearly evident on Figure 2. The treatment of the highly nonlinear behavior of discrete fractures under variations in stress is another interesting problem.

With all the complexities of a fracture closing under stress, one might question the validity of the cubic dependence of the flow on the fracture

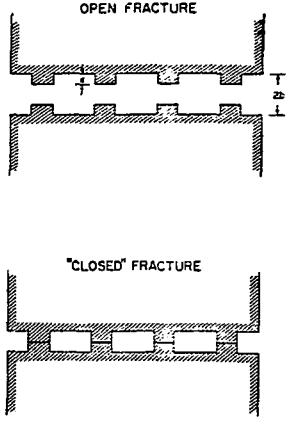

Fig. 1. Idealized fracture showing the mating of asperities as the fracture surfaces are closed under stress (after Witherspoon et al., 1980). XBL 797-7589

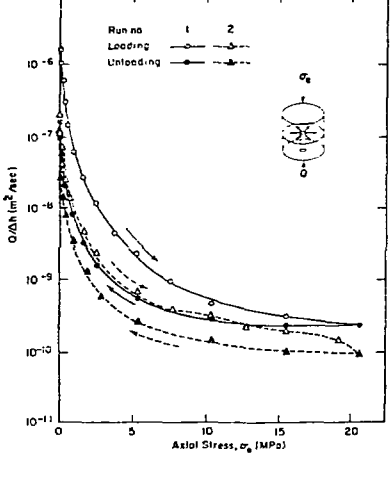

Fig. 2. Effect of cyclic loading on permeability of tension fracture in granite with radial flow (after Iwai, 1976). XBL 797-7578A

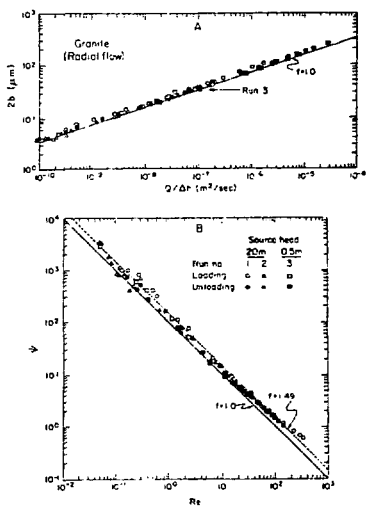

Fig. 3. Comparison of experimental results for radial flow through tension fracture in aperture with cubic law. In Run 3, fracture surfaces were no longer in contact during unloading when aperture exceeded value indicated by arrow (after Witherspoon et al., 1980). XBL 797-7564A

aperture. The cubic law is based on highly idealized concepts with laminar flow in an "open" fracture with parallel planar surfaces. Under the experimental conditions of normal stress and at ambient temperature, Figure 3 shows that the cubic law seems to still hold whether the fracture is open or closed.

For a network of discrete fractures under deformable conditions, the fractures will have both normal and shear motions. The coupling effects of thermal pulse and stress changes from an underground repository on the flow through the fractures are complex problems. This workshop presents an excellent opportunity to discuss the treatment of these coupling processes in discrete fractures and the validity of using porous medium approximations for the flows through the rocks.

References

Iwai, K., 1976. Fundamental Studies of Fluid Flow Through a Single Fracture. Ph.D. thesis, University of California, Berkeley, California.

Witherspoon, P. A., Wang, J. S. Y., Iwai, K., and Gale, J. E., 1980. Validity of Cubic Law for Fluid Flow in a Deformable Rock Fracture. Water Resources Research, V. 16, No. 6., p. 1016-1024.

WELCOME

M. M. Lemcoe
Office of Nuclear Waste Isolation
Battelle Memorial Institute
Columbus, Ohio 43201

On behalf of ONWI, it is indeed a pleasure to welcome you to this modeler's meeting on thermal-hydrology. I know we will all go away with a better overall understanding of these models and that out of this workshop a document will be forthcoming that significantly adds to our store of knowledge on thermal-hydrological codes. I do hope that, as the discussion proceeds, particular attention will be paid to addressing the key questions: "Where do we go from here?" and "What additional work has to be done in order to address the most important technical issues?"

We are presently in a constant budget mode; therefore, we will not be able to fund everything in our shopping lists. So, it becomes especially important that we prioritize the needs and identify them as specifically and concisely as we possibly can. One final question to be addressed is: "How can we best utilize these thermal-hydrological models to develop the thermal-mechanical-hydrological models for repository design and investigation of possible nuclide pathways to the biosphere?"

Thank you.

INTRODUCTION TO NUMERICAL MODELING OF THERMOHYDROLOGIC FLOW IN FRACTURED ROCK MASSES

J. S. Y. Wang
Earth Sciences Division
Lawrence Berkeley Laboratory
University of California
Berkeley, California 94720

INTRODUCTION

More attention is being given to the possibility of nuclear waste isolation in hard rock formations.[1,2] The waste will generate heat which raises the temperature of the surrounding fractured rock masses and induces buoyancy flow and pressure change in the fluid. These effects introduce the potential hazard of radionuclides being carried to the biosphere, and affect the structure of a repository by stress changes in the rock formation. The thermohydrological and thermomechanical responses are determined by the fractures as well as the intact rock blocks. The capability of modeling fractured rock masses is essential to site characterization and repository evaluation.

The fractures can be modeled either as a discrete system, taking into account the detailed fracture distributions, or as a continuum representing the spatial average of the fractures. If the flow through the rock blocks is not negligible, the fractured rock mass can be approximated as two overlapping continua with two porosities, one representing the fractures and another the porous rock blocks. The choice among the discrete, double-porosity, and porous medium models depends on the one hand on the characteristics of the fracture network, the size of the region, and the physical processes of interest; and on the other hand it depends on the availability of data and the limitation of the computational capability. For near-field simulation, it may be necessary to model the detailed fluid movement in order to understand the radionuclide transport, thermal convection, and rock displacement in the fracture network. For far-field phenomena, it may be sufficient to model the average behavior of fluid flow in the rock mass.

The capability of modeling subsurface fluid flow has been developed in hydrology, petroleum engineering, and other geological fields. More recently, the interest in geothermal energy has also contributed to the advancement of this capability, especially in modeling nonisothermal flows. Although the focus of each field is different, many models which have been developed are relevant and can in some cases, be adapted to the study of the various thermohydrologic processes associated with nuclear waste repositories. Table 1 summarizes the main characteristics of several major thermohydrological models[4-16]. These models were selected for a recent detailed review[3] to bring out their strengths, methods of approach, and other characteristics. The selection is somewhat arbitrary and emphasizes those in the published literature that could be applied to fractured systems.

A numerical model is characterized by the governing equations, the numerical methods, the computer codes, the validations, and the applications. These elements of the thermohydrological models will be discussed in the following five sections. Along with the general review, some of the considerations in modeling fractures will also be discussed. Some remarks on the research needs in modeling fractured rock mass will conclude the paper.

GOVERNING EQUATIONS

The formulation of the governing equations are the starting point of any numerical model. The mathematical description of the state of a moving fluid through pores and fractures is given by functions of the Darcy velocity $\bar{q}$ and any two thermodynamic quantities pertaining to the fluid, for instance the pressure P and the temperature T. The fluid velocity within individual pores and fractures, $\bar{v}$, is related to the macroscopically averaged Darcy velocity, $\bar{q}$, by the porosity ϕ:

$$\bar{v} = \frac{\bar{q}}{\phi}$$

in the porous medium approximation. The choice of pressure and temperature as variables is arbitrary. All thermodynamic quantities are determined by the values of any two of them, together with the equation of state. Density, ρ, internal energy, U, enthalpy, H, and others can be used to determine the state of the moving fluid. The governing equations for the moving fluid are based on the conservation laws of mass, momentum, and energy.

Fluid Flow Equation

The conservation of fluid mass is the balance of the rate of change, the flux, and the prescribed source/sink of fluid mass

$$\frac{\partial(\phi\rho)}{\partial t} + \nabla \cdot (\rho\bar{q}) = \zeta_F$$

This equation of continuity is applicable either within a fracture with $\phi = 1$ or for a porous medium with $\phi < 1$. We will first discuss the porosity and density in the transient term.

Porosity is a formation-related property and depends on the mechanical properties of the rock medium. In any one of the models, one of the following approximations for the porosity is used:

Table 1. Some of the Major Thermohydrological Models.

Model	Current Development	Main Characteristics
ROCMAS	J Noorishad, UCB	stress-flow-(heat), fracture-porous, 2D, FE, hydrology, geotechnical
TRUST TERZAGHI	T. Narasimhan, LBL	saturated-unsaturated flow-consolidation, 3D, IFD, hydrology, soil mechanics
CCC	M. Lippmann, LBL	flow-heat-consolidation, 3D, IFD, geothermal, aquifer storage, waste isolation
Duguid	J. Duguid, ONWI	flow, double-porosity, 2D, FE, hydrology
O'Neill	K. O'Neill, CRRE Z. Shapiro, Princeton	flow-heat, double-porosity, 3D, FE, geothermal
GWTHERM	A. Runchal, ACR	flow-heat-(transport), 2D, IFD, waste isolation
FINI	A. Burgess, Acres	flow-heat, 2D, FE, waste isolation
CFEST FE3DGW	S. Gupta, BPNL	flow-heat-solute, 3D, FE, hydrology, waste isolation
SWIFT	S. Pahwa, Intera	flow-heat-solute-(transport), 3D, FD, waste isolation
Coats	K. Coats, Intercomp	flow-heat, two-phase, 3D, FD, geothermal, petroleum
Faust-Mercer	C. Faust, J. Mercer, Geotrans	flow-heat, two-phase, 3D, FD, geothermal
MUSHRM	J. Pritchett, S. Garg, S^3	flow-heat-solute, two-phase, 3D, FD, geothermal, geopressure
SHAFT79	K. Pruess, LBL	flow-heat, two-phase, 3D, IFD, geothermal, waste isolation

(a) ρ is constant.

(b) ρ change is linear in pressure change, $\Delta\rho = \beta_p \Delta P$, where the compressibility of pores β_p is assumed to be constant (pressure-independent).

(c) ρ change is nonlinear in ΔP. Compressibility is a function of effective stress, $\sigma' = \sigma - P$, but the total stress σ is given.

(d) ρ change is coupled to the stress-strain changes. The pressure change affects the stress field of the rock blocks which in turn changes the strain or porosity.

Most of the models assume (b). For a double-porosity model, there are two porosities and two fluid flow equations coupled by fracture-porous flow. The two porosities may be coupled by the compressibility of fluid β_p in addition to the compressibility of rock (or pore). In the double-porosity model, the pressure at a point is the sum of the pressures representing the fractures and the pressure representing the porous medium blocks, $P = P^f + P^m$.

The density of fluid ρ will also change in response to pressure and temperature changes. The approximations for the density change are:

(a) ρ is constant. The fluid is incompressible.

(b) ρ is slightly compressible, $\Delta\rho = \beta_p \rho \Delta P$, with constant compressibility β_p. This equation of state is frequently used for isothermal, saturated flow.

(c) ρ is slightly compressible with pressure increase and expandible (with expansivity β_T) with temperature increase, $\Delta\rho = \beta_p \rho \Delta P - \beta_T \rho \Delta T$. This is for nonisothermal, saturated flow. For a fluid with dissolved substance, ρ can also change with concentration C.

(d) ρ is very compressible. This is the case for the steam-water, two-phase flow. The change of fluid density with pressure and temperature is determined by the equation of state (steam table). For a two-phase state with saturation S for the liquid water and 1-S for the vapor, $\rho = S\rho^l + (1 - S)\rho^v$. In the two-phase region with temperature determined by the pressure, $T = T_s(P)$, the saturation can be treated as a variable.

The approximations for the porosity change $\Delta\phi$ and the density change $\Delta\rho$ in different models determine the treatment of the transient term $\partial(\phi\rho)/\partial t$ in the fluid flow equation. For some saturated flow models, this transient term is expressed in terms of constant total compressibility of the formation or the coefficient of specific storage S_s:

$$\frac{\partial(\phi\rho)}{\partial t} = \frac{S_s}{g} \cdot \frac{\partial P}{\partial t}$$

Fluid Velocity

The fluid velocities within the fractures are of particular interest in determining the radionuclids transport. The flux velocity $\bar{q}$ in the fluid flow equation is determined by the permeability, the viscosity, and the driving forces for fluid moving through a formation

$$\bar{q} = -\frac{\bar{k}}{\mu}\cdot(\nabla P - \rho \bar{g})$$

This is Darcy's law for the equation of motion. Darcy's law is an approximation of the general Navier-Stokes equation for momentum conservation.

Permeability $\bar{k}$ is a formation-dependent property. The approximations for $\bar{k}$ are:

(a) k is constant for isotropic, homogeneous formations
(b) $\bar{k}(\bar{r})$ is anisotropic and heterogeneous
(c) $\bar{k}$ is reduced by the relative permeabilities for the liquid and vapor flow in two-phase regions. The relative permeabilities, k_r^l and k_r^v, depend on the saturation.
(d) $\bar{k}$ is a function of porosity or void ratio e and depends on the loading history (hysteresis)
(e) $\bar{k}$ is a function of pressure, temperature and/or stress. The effective stress-displacement calculations and/or thermo-mechanical calculations are used to determine the dependence of permeability on these parameters.

Most of the models have some capability for handling anisotropic and heterogeneous (position-dependent) permeability functions. The fractures can be modeled with the equivalent fracture permeabilities assigned to the locations of the discrete fractures. However, the complex responses of the fractures to pressure, temperature, and stress changes may require detailed treatment of the fracture permeabilities.

With a parallel-plate model for a planar fracture of aperture b, the equivalent fracture permeability for steady laminar flow averaged between the plates is

$$k^f = \frac{b^2}{12} .$$

The corresponding flux of fracture flow is proportional to b^3. As a result of the nonlinear dependence, the fracture flow is sensitive to the displacement of the fracture surfaces due to stress changes in the rock blocks.

The smooth parallel-plate is an idealization of a real fracture. A fracture has rough surfaces with contacts between the surfaces. The aperture changes vary nonlinearly with applied normal and shear stresses. Under a given stress field, the aperture may depend on the block size (scale effect). The fracture may also contain in-fill material. These characteristics of a real fracture may reduce the fracture permeability and retard the flow.

For large-scale modeling of a highly fractured rock mass, it is unrealistic to model all its fractures. Simple geometric models can be used to approximate the fracture sets with an equivalent permeability tensor. If sufficient data are available on the apertures, spacings, orientations, areal extent, and other fracture parameters, a statistical treatment will be necessary. Although each individual fracture is highly permeable, the total permeability may be small if there are high degrees of discontinuity and disconnectivity in the fracture network. Not all the fractures and void spaces are paths for fluid flow. The correlation between permeability and porosity does not always exist.

In addition to the permeability, the Darcy velocity, $\bar{q}$, also depends on the dynamic viscosity μ and the driving forces. The following are approximations for μ in the different models.

(a) μ is constant. The constant viscosity μ_o can be combined with the permeability as hydraulic conductivity

$$K = \frac{k\rho_o g}{\mu_o}$$

(b) $\mu(T)$ is for nonisothermal saturated flow.
(c) $\mu(P, T)$ is for two-phase flow. The viscosity of steam is sensitive to the pressure change.

Pressure gradient and gravitational force are the driving forces of Darcy velocity. The following are approximations for the driving forces.

(a) Constant gravitational force. The hydrostatic pressure can be subtracted from the pressure

$$P' = P - \rho_o g z$$

The incremental pressure P', or the hydraulic head $h = P'/\rho_o g$, are frequently used as the variable in isothermal flow models.

(b) Boussinesq approximation for the gravitational force imbalance between hot and cold water (buoyancy force)

$$(\rho - \rho_o)\bar{g} = -\rho_o \beta_T (T - T_o)\bar{g} .$$

The density variation with temperature is considered only in the buoyancy force and is neglected in other terms of the governing equations.

(c) $\nabla P - \bar{q}$ for nonisothermal, saturated flow
(d) $\nabla P - \rho\bar{g}$, $i = l, v$, for the liquid and vapor of two-phase flow
(e) $\nabla P^i - \rho^i\bar{g}$, $i = l, v$, for two-phase flow with capillary pressure, $P_c(S) = P^v - P^l$, taken into account.
(f) Inertial force included. This force is important for regions where the flow

velocity is high, e.g., within large fractures near a wellbore. At high velocity, transition from laminar flow to turbulent flow occurs. The pressure loss in a turbulent region decreases the effective pressure driving force.

Heat Transfer Equation

Heat transfer through the formation depends on the conduction and dispersion through the rock, convection by the fluid, and the strength of the heat source.

$$\frac{\partial(\rho U)}{\partial t} + \nabla \cdot (\rho \bar{q} H) - \nabla \cdot \bar{\bar{K}}_H \cdot \nabla T = Q_H$$

The conservation of energy is expressed in terms of the rate of change of internal energy U, the convective flux of enthalpy H, and the diffusive flux driven by the temperature gradient. The thermodynamic functions U and H can be expressed in terms of temperature and/or pressure.

For the internal energy accumulation, the different approximations used in the models are:

(a) $\frac{\partial(\rho U)}{\partial t} = C \frac{\partial T}{\partial t}$

with a constant heat capacity C of the formation

(b) $\frac{\partial(\rho U)}{\partial t} = [\phi \rho c + (1 - \phi)\rho^r c^r] \frac{\partial T}{\partial t}$,

with dependence of the total heat capacity on the water heat capacity c within the pores and on the rock heat capacity c^r.

(c) in terms of internal energies of liquid U^ℓ and vapor U^v for two-phase flow,

$$\frac{\partial(\rho U)}{\partial t} = \frac{\partial}{\partial t} [\phi S \rho^\ell U^\ell + \phi(1 - S)\rho^v U^v + (1 - \phi)\rho^r c^r T]$$

(d) in terms of enthalpies,

$$H^i = U^i + \frac{P}{\rho^i}, \quad i = \ell, v.$$

The convective flux of enthalpy $\nabla \cdot (\rho \bar{q} H)$ can be expressed

(a) in terms of temperature, $\rho c \bar{q} \cdot \nabla T$;
(b) in terms of H for saturated flow;
(c) in terms of H^ℓ, H^v, for the two-phase flow

$$\nabla \cdot (\rho^\ell \bar{q}^\ell H^\ell + \rho^v \bar{q}^v H^v).$$

(d) in terms of internal energies

$$U^i = H^i - \frac{P}{\rho^i}, \quad i = \ell, v$$

Two approximations are used to describe the diffusive flux $-\bar{\bar{K}}_H \cdot \nabla T$. The tensor $\bar{\bar{K}}_H$ can depend on either

(a) conduction through the rock ($\bar{\bar{K}}_T$), or
(b) both conduction and dispersion in water-saturated rock ($\bar{\bar{K}}_T + \bar{\bar{K}}_D$). The thermal dispersion depends on the fluctuations of microscopic velocities. The dispersive contribution can be regarded as an enhancement to heat conduction in the presence of fluid. The dispersivity $\bar{\bar{K}}_D$ depends (usually assumed linearly) on the components of the microscopic velocity $v = q/\phi$. The longitudinal dispersivity along the flow may differ from the transverse dispersivity normal to the flow.

For a double porosity model, there are two temperature equations coupled by the fracture-porous heat transfer. The temperature at a point is related to the temperatures representing the fractures and to the temperature representing the porous medium blocks by:

$$T = \frac{\phi^f T^f + \phi^m T^m}{\phi^f + \phi^m}$$

Coupling of Fluid Flow and Heat Transfer

The fluid flow equation and the heat transfer equation are coupled through the fluid velocity $\bar{q}$ in the flux terms and through the temperature and pressure dependences of the fluid properties (ρ, μ) and formation properties (k, ϕ). In most models using the Darcy approximation, the flow velocity equation is substituted into the fluid flow equation and the heat transfer equation. The elimination of $\bar{q}$ simplifies the set of governing equations for thermohydrologic flow to two equations for the pressure and temperature fields. After these fields are determined, the fluid velocity $\bar{q}$ or the microscopic velocity $\bar{v}$ is calculated from the pressure gradient and the gravitational force.

For a low-permeability formation with a small fluid flow, the convection and dispersion contributions to the heat transfer are small compared with the conduction contribution. In this case, the temperature field is independent of the fluid flow, and the temperature equation with heat conduction only can be decoupled from the pressure equation. However, the fluid flow field depends on the temperature field. The heat generated by the wastes affects the fluid flow directly through changes of fluid properties and indirectly through changes in rock stresses which may alter the permeability and porosity of a formation. The complete determination of the fluid flow field requires thermal-hydrological-mechanical calculations. For fractured rock masses with very deformable fractures, the couplings may be strong. With the fluid flow field determined, the radionuclide transport can be modeled.

NUMERICAL METHODS

In this section we will discuss the general features of numerical methods for solving the governing equations. The space discretization, the time difference, and the solution scheme of different models will be summarized.

The governing equations for thermohydrological flows have diffusive terms, e.g., $\nabla\cdot(\bar{\bar{k}}/\mu)\cdot\nabla P$ and $\nabla\cdot\bar{\bar{K}}\nabla T$; convective terms, e.g., $\rho c\bar{q}\cdot\nabla T$; and storage capacity terms, e.g., $S_S(\partial P/\partial t)$ and $C(\partial T/\partial t)$. The numerical approximation for evaluating these terms, together with the treatments of initial conditions, boundary conditions, and source/sink, will be reviewed below.

Spatial Difference

Within the region to be modeled, the unknown variables are solved at discrete nodal points. The distribution of nodes can be regular with uniform or nonuniform spacings, or irregular in one-, two-, or three-dimensional space. The spatial gradients of the variables in the governing equations are expressed in terms of the neighboring nodal values. The finite-difference method and the finite-element method are frequently used to approximate the differential gradient operators.

In the finite-difference method, a gradient of a variable is directly expressed in terms of the difference of the neighboring nodal values. For example, the $\partial P/\partial x$ in $\nabla\cdot(\bar{\bar{k}}/\mu)\cdot\nabla P$ is approximated by $(P_{i+1} - P_i)/(x_{i+1} - x_i)$ between the nodes indexed by i+1, i along the x-axis. The coefficients $\bar{\bar{k}}/\mu$ are evaluated at the interfaces i + 1/2 between i+1 and i. The interface i+1/2 can be midway between i+1, i or at other locations specified by the user or the program. The region surrounding a node bounded by the interfaces is referred to as a node block or cell. The coefficients at the interface can be evaluated as the arithmetic mean, e.g.

$$\left(\frac{\rho}{\mu}\right)_{i+1/2} = \frac{\left(\frac{\rho}{\mu}\right)_{i+1} + \left(\frac{\rho}{\mu}\right)_{i}}{2}$$

or as the harmonic mean, e.g.,

$$\left(\frac{1}{k}\right)_{i+1/2} = \frac{\left(\frac{\Delta x}{k}\right)_{i+1} + \left(\frac{\Delta x}{k}\right)_{i}}{\Delta x_{i+1} + \Delta x_i}$$

where $\Delta x_i = |x_{i+1/2} - x_i|$. These finite-difference approximations can be generalized for an irregular grid. For example, the factor 1/2 in the arithmetic mean can be replaced by other fractional weighting factors, the Δx_i in the harmonic mean can be replaced by the normal distance from the node to the interface between the neighboring nodes if the neighboring nodes are not along the coordinates in an irregular grid system.

For the convective term $c\bar{q}\cdot\nabla T$ (or $\nabla\cdot\bar{q}H$) in the temperature equation, the central difference in space, or central weighting,

$$\frac{T_{i+1/2} - T_{i-1/2}}{x_{i+1/2} - x_{i-1/2}}$$

with $T_{i+1/2} = 0.5(T_{i+1} + T_i)$ can be used for $\partial T/\partial x$. However, there is a tendency for the solutions with central weighting to oscillate artificially at high flow velocity. The convective flux associated with the flow velocity $\bar{q}$ carries heat downstream, a nodal point between an upstream and a downstream node will have temperature closer to the upstream value. The central weighting scheme does not take into account this convective effect. In the upstream weighting scheme, the interface temperature is set equal to the upstream value, i.e., $T_{i+1/2} = T_{i+1}$ if fluid flows from i+1 to i. In other words, a backward difference, $T_{i+1} - T_i$, is used for the convective term at node i. One can also use partial upstream weighting $T_{i+1/2} = aT_{i+1} + (1 - a)T_i$ with $0.5 < a < 1$. The central weighting scheme ($a = 0.5$) yields a lower space-discretization error but has the problem of numerical oscillation. The upstream weighting ($a = 1$) eliminates the oscillation but introduces a space-discretization error which is virtually equivalent to physical diffusion. To minimize the numerical oscillation and the numerical diffusion, the grid size for the space discretization will be limited.

The finite-element method differs from the finite-difference method in evaluating the spatial gradient terms. An element is the region bounded by curves connecting the nodes. For example, a two-dimensional linear triangular element is a triangle with three nodal vertices, a quadrilateral element has four corner nodes, and a three-dimensional orthorhombic element has eight corner nodes. Within a model, different elements can be used. For example, the fractures can be treated with special long, thin elements. A variable within an element is interpolated in terms of the values of the variable at the corner nodes. Simple polynomials (linear, quadratic, or cubic) are frequently used as linearly independent basis functions for the interpolation. The simple basis function is a cubic polynomial (Hermite polynomial) for interpolating in terms of its value and its partial derivatives at each corner node.

In the Galerkin finite-element scheme, the trial solution with basis function interpolation is substituted into the differential equations. The space-differential operators operate on the basis functions. The residue of the trial solutions is integrated over the element weighted by the basis functions. The integration is usually carried out using two- or three-point Gaussian integration for each dimension. If the solution is expanded in terms of a complete (infinite) set of linearly independent functions in the elements, the trial solution is exact and the residue would vanish. In the Galerkin weighted residual method, the residue is forced to be zero by requiring the orthogonality of the residual to the finite number of basis functions which are also used in the expansion of the trial solution.

An equivalent expression of the governing partial differential equations is in terms of variation of functionals. A functional is an integral over space with the integrand bilinear in the variable function. Upon variational operation on a functional, the corresponding differential equation emerges. The variational approach for fluid flow is based on the same minimum energy principle or Lagrangian formulation as that used to study the equilibrium states in mechanics or stress analysis. In the fluid-stress coupled model (ROCMAS), the variational approach is used. In the variational approach to the finite-element method, the trial solutions, as expansions in basis functions, are substituted into the functional integrals. The differential operators in the functional operate on the basis functions in a manner similar to that in the weighted residual procedure of the Galerkin formulation.

With the use of the Gaussian algorithm for element integration in the finite element method, the coefficients, like $\bar{k}/\mu$ in the pressure equation and ρc_p in the temperature convection, can be evaluated at the Gaussian points within an element. This is different from the finite difference method with the coefficient calculated at the interfaces between blocks. For the convective terms, the problems of numerical oscillation and numerical diffusion also exist in the finite-element method. The upstream weighting is handled by using upstream basis functions.

The conductive term $\nabla \cdot \bar{K}_T \cdot \nabla T$ in the heat transfer equation, like the $\nabla \cdot (\bar{k}/\mu) \cdot \nabla P$ in the fluid flow equation, is a diffusive term. If the dispersivity $\bar{K}_D$ is added to the thermal conductivity $\bar{K}_T$ the temperature equation is coupled to the fluid flow not only in the convective flux but also through the sensitive dependence of $\bar{K}_D$ on fluid velocity. As the velocity changes direction and magnitude, the effective diffusive conductivity-dispersivity $\bar{K}_D + \bar{K}_T$ changes. This may slightly complicate the treatment of the diffusive term but may stabilize the numerical oscillation or decrease the relative importance of the numerical diffusion.

Table 1 summarizes the dimension and the space discretization method. The integrated finite difference (IFD) method and the finite difference (FD) method both evaluate gradients in the same way. The IFD emphasizes the straightforward formulation of the numerical equations from the integral form of the governing equations, or equivalently, from the conservation laws over finite-volume blocks. Furthermore, in IFD method, the block shape is not limited to the regular two-dimensional rectangular or three-dimensional orthorhombic shape used in most finite difference models.

Time Difference

From the conservation laws or the governing equations, the fluxes, evaluated at the interfaces in the finite difference method or at the Gaussian points in the finite element method, are balanced by the rates of change of mass and energy. In the integrated finite difference and finite difference methods, the value of the variable at a given node represents the average of the values within the block enclosed by the surrounding interfaces. The balance between the rate of accumulation within the block and the net flux across the interfaces is clearly shown. In the finite element method, each element is shared by the corner and boundary nodes and each node is surrounded by several elements. The block enclosing a node is the sum of the fractions of each neighboring element. Although the rate of change or the transient term can be handled easily in the weighted residual formulation, the numerical problem of convergence may occur. In the diagonal or lumped capacity approach, the time derivative in the governing equation is determined independently of the orthogonalization process.

The analysis of the transient equation results in a system of equations of the matrix form

$$[A]\left[\frac{df}{dt}\right] + [B]\{f\} + \{R\} = 0$$

where the column $\{f\}$ contains the nodal values of pressure, temperature, or other thermodynamic variables. The coefficient matrix $[A]$ contains the coefficients of fluid storage or heat capacity term associated with the time derivative $\{df/dt\}$, $[B]$ contains the spatial approximations (finite difference or finite element) of the fluxes, and $\{R\}$ contains the known information such as source/sink or boundary conditions. The time derivatives in the governing equations are generally handled by first-order temporal finite difference from time t to $t+\Delta t$

$$\frac{df}{dt} \approx \frac{\{f\}_{t+\Delta t} - \{f\}_t}{\Delta t}.$$

To solve the unknown $\{f\}_{t+\Delta t}$ from the known solution $\{f\}_t$, the other terms in the governing equations can be interpolated between $t+\Delta t$ and t. The matrix equation can be written in the form

$$\frac{[A]}{\Delta t}(\{f\}_{t+\Delta t} - \{f\}_t) + [B](\lambda\{f\}_{t+\Delta t} +$$

$$(1-\lambda)\{f\}_t) + \lambda\{R\}_{t+\Delta t} + (1-\lambda)\{R\}_t = 0$$

For the forward differencing explicit scheme with interpolation factor $\lambda = 0$, the $\{f\}_{t+\Delta t}$ can be easily determined by multiplying the matrix equation with $\Delta t[A]^{-1}$. The explicit scheme generally requires a minimum of computational effort. However, it is only conditionally stable. Usually the implicit schemes with the interpolation factor $0.5 \leq \lambda \leq 1$ are stable. The central differencing Crank-Nicholson scheme ($\lambda = 0.5$) is accurate in Δt to the second order. The backward differencing implicit scheme ($\lambda = 1.0$) is usually unconditionally stable and is correct in time to the first order.

Time stepping, together with the consideration of spatial truncation, determine the numerical stability, convergence, error, and efficiency of a model. In many models, the choice of the internal-

ation factor λ for time difference, and the choice of the upstream weighting factor α for convective spatial difference, are determined by the user. In some cases, various stability criteria are programmed into the algorithms for automatic control of time stepping.

In the above discussion about the implicit schemes we have not taken into consideration the dependence of the coefficient matrices [A] and [B] on time. In general, the fluid storage or the heat capacity coefficients in [A] and the hydraulic conductivity $\rho\bar{k}/\mu$, the thermal conductivity-dispersivity $\bar{K}_T + \bar{K}_D$, or the convective flux $\rho\bar{q}$ for [B], depend on the time-dependent variables. These time-dependences of the coefficients cannot be neglected, especially for the two-phase flows with sensitive dependence of fluid properties ρ, μ on P, T, and the relative permeabilities k_r of liquid and vapor on the saturation. For the discrete fracture modeling, this nonlinear dependence of the coefficient matrix on P, T is also a problem with the sensitive dependence of the fracture permeability on the aperture of the fracture which is determined by stress-flow coupling and thermomechanical coupling.

In a fully implicit scheme, the coefficient matrices [A] and [B] are also evaluated at $t+\Delta t$. In such a case, the matrix equation is no longer linear in $\{f\}_{t+\Delta t}$, and iterative procedures are needed to handle these nonlinearities. The Newton-Raphson procedure, or predictor-corrector method, is frequently used. The Newton-Raphson procedure involves approximating the nonlinear equations with a first-order Taylor series expansion about an assumed solution. The derivatives of the nonlinear coefficients are calculated at the values of variables at old iteration and the changes in the variables are solved by the linearized equation. The iteration proceeds until it converges to a specified criterion. In the structure analysis for nonlinearly deformable fractures, the variable stiffness method and the load transfer method are modifications of the Newton-Raphson scheme.

Solution Scheme

After temporal finite difference, spatial discretization, and linearization of the coefficients in the governing equations, the partial differential equations are transformed into a system of simultaneous linear algebraic equations or a matrix equation of the form

$$[A]\{f\} = \{F\}.$$

The size of the matrix depends on the number of nodes and the number of variables. For example, in a region with m nodes for two variables P and T, the matrix is 2m x 2m in size. The solution for the 2m unknown nodal values of P and T at time $t+\Delta t$ in $\{f\}$ can be obtained through the use of direct elimination methods or the use of iterative methods.

Many of the direct methods are variations of the Gaussian elimination procedure. In this procedure, one unknown is eliminated from one equation at a time. The procedure works in a systematic way so that a general matrix equation is reduced to a triangular system. The lower-triangular system has the first equation with the first unknown, the second equation has two unknowns, etc. The triangular system can be solved step by step with the first unknown determined by the first equation, the second unknown determined by the second equation after the first solution is substituted into the second equation. The forward substitution proceeds until all the unknowns are solved. Similarly, the upper-triangular system can be solved by backward substitution.

The L-U decomposition is one method of Gaussian elimination. With matrix [A] decomposed into a lower- and an upper-triangular matrix [A] = [L][U], then $[A]\{f\} = \{F\}$ is equivalent to two triangular systems

$$[L]\{g\} = \{F\} \qquad \text{and} \qquad [U]\{f\} = \{g\}.$$

If the matrices [L] and [U] are known, the matrix equation can be solved by forward and backward substitution. With a given n x n matrix [A], the matrices [L] and [U] are not unique. There are n^2 elements in [A] and $0.5n(n+1)$ unknown elements in [L] and the same number in [U]. Therefore, there are $n(n+1) - n^2 = n$ elements which can be set to any value. In the Doolittle method, the diagonal elements of [L] are set to unity. With the n diagonal elements fixed, other elements in [L] and [U] can be determined algebraically. Alternatively in the Crout method, the diagonal elements of [U] are set to unity instead. The Crout and Doolittle methods are two popular direct elimination solution schemes.

In the matrix equation, one can interchange one row with another row, or one column with another column. This procedure is called pivoting. In general, it is necessary to perform pivoting to ensure numerical stability and minimize round-off errors if there are zero or nearly zero elements in the matrix during elimination.

The ordering of the nodal labeling, the storage of the matrices, the elimination sequence, and the approach to avoid large round-off errors, all affect the computational efficiency and the core storage requirement of a solution scheme. Although the direct elimination methods can be used for any nonsingular matrices, special matrices may be solved by a special method. For example, the tridiagonal banded matrices, frequently encountered in the application of finite-difference methods, can be easily solved by the well-known tridiagonal algorithm (Thomas' algorithm). In the alternating direction implicit (ADI) finite-difference method for a regular grid system in two- or three-dimensional space, the partial differentials along dimensional space, the partial differentials along different directions are updated sequentially for a fractional time step. Each quasi-one-dimensional finite difference results in a tridiagonal system which can be solved with the tridiagonal algorithm.

If the matrix is sparse and large, iterative methods instead of direct methods may offer certain advantages. An iterative method starts from a first approximation which is successively improved

until a sufficiently accurate solution is obtained. Some examples of iterative methods are briefly described here to demonstrate the steps involved.

If one diagonally splits a matrix [A] into lower and upper triangular systems, [A] = [D] + [L] + [U]. The matrix equation [A] $\{f\}$ = $\{F\}$ can be rewritten as

$$([D] + [L])\{f\} = -[U]\{f\} + \{F\}.$$

If the right-hand side is known at the kth step and the left-hand side is known at the (k+1)th step, we have

$$\{f\}^{k+1} = ([D] + [L])^{-1}(-[U]\{f\}^{k} + \{F\}).$$

This is the matrix form of Gauss-Seidel's method. The inverse of ([D] + [L]) can be handled by forward substitution. If the residual from kth to (k+1)th step is denoted by $\{r\}^k = \{f\}^{k+1} - \{f\}^k$, the generalized iterative method $\{f\}^{k+1} = \{f\}^k + w\{r\}^k$ is the successive overrelaxation (SOR) method. In matrix form, the new solution is

$$\{f\}^{k+1} = ([D] + w[L])^{-1}(((1 - w)[D] - w[U])\{f\}^{k} + w\{F\}).$$

The relaxation factor w should be chosen so that the rate of convergence is optimized. Eigen-value analyses are frequently used for determining the best relaxation factor. For real, symmetric, and positive-definite matrices, $0 < w < 2$. Similar to SOR, other relaxation or acceleration schemes can be constructed.

Each iterative method and direct solution method has its strength and weakness. The choice of a given method is determined by the nature of the matrices. Combinations of different methods can also improve the efficiency. In the block iterative methods, the coefficient matrix is partitioned into blocks and all elements of a block are operated on during one iterative step. If the block is tridiagonal, it can be solved by a direct solution scheme.

With the rapid development of computing capability and the storage capacity of computers, more and more models are switching from iterative methods to direct solution methods. Direct methods usually require larger core storage space but minimize convergent tests.

COMPUTER CODES

After formulation of the governing equations and the selection of the numerical methods, the implementation of the computer code is a major effort in the development of a model. A general purpose code should be easy to use by both the developers and others. In this section, some of the practical aspects of using a code will be discussed. Although detailed knowledge of the governing equations and the numerical methods are helpful, a new user interested in using a code may be more interested in its capabilities and the input-output of the code. For each computer code, the following subjects are important considerations.

Documentation and Availability

The user's manual, the code listing, the computer systems used, and the background of code development are of general interest.

Spatial Grid

Versatility in grid mesh design and discretization of the spatial domain is important for a model to be applicable for fracture simulation.

Material Properties

A user is interested to know the required input of material properties for the model and the capabilities to treat heterogeneity, anisotropy, pressure-, temperature-, and stress-dependence. The major material properties are permeability, porosity, rock medium compressibility, heat capacity, thermal conductivity, dispersivity, etc.

Fluid Properties

The input data and calculations for fluid properties need to be described. The dependence of density and viscosity on temperature and pressure can be calculated either from a given formula or interpolated from tabulated values.

Sources and Sinks

Some of the model applications require the availability of fluid and heat source and sink terms for simulation. The localized, time-dependent heat sources from the radioactive decay of the waste in a repository are the driving force for buoyancy flow.

Initial Conditions

The input data at initial and program restart times are important for the treatment of the transient problem.

Boundary Conditions

The flexibility of treating various boundary conditions by the program is important.

Time Stepping and Solution Control

The time steps can be specified by the user or controlled by the program according to specified criteria. It is also of interest to discuss the procedures used in the program for checking accuracy or convergence of solutions. Since the fluid velocity is proportional to the pressure gradient, a reliable determination of the fluid velocity, to be used in radionuclide transport calculations, requires high accuracy in the pressure solutions.

Output

The printer and graphic output are important for the analysis and presentation of the results of modeling.

VALIDATIONS

Testing of a code is important in checking the mathematical validity, the numerical stability, and the versatility of the model. The numerical results can be validated, on the one hand against analytic solutions and numerical codes to test the accuracy of the code, and on the other hand against laboratory data and field experiments to determine the usefulness of the model. In this section, some frequently used analytic solutions are briefly described and in addition, other validation procedures are discussed.

Analytic Solutions

For simple (linear, cylindrical, or radial) systems with constant or simple coefficients and well-defined initial and boundary conditions, the pressure or the temperature equation may be solved in terms of elementary analytic functions or special functions. In some cases, the solution exists in the form of a simple integral which can be easily evaluated numerically. Some examples of transient analytic or semianalytic solutions are listed below.

1. Radial Flow to a Well

If a well is producing at a constant rate, the pressure near the well drops and the drawdown propagates radially outward. The classic solution to this problem, with fully penetrating line source well in an infinite homogeneous aquifer, is the Theis solution or the exponential integral solution.

The Theis solution can be generalized to cases with variable flow rates, a finite well radius, wellbore storage and skin effects, finite aquifers, leaky aquifers, partial penetration of a well, multi-aquifers, etc.

In double-porosity models, semianalytic solutions exist, showing the delayed pressure responses due to the porous medium after the early response due to fracture flow.

For two-phase flow, the radial propagation of a flashing front due to mass production can be described by modified exponential solutions.

2. Linear Convective-Diffusive Solution

A popular solution for testing the temperature equation with a convective term is the linear hot water injection problem. The propagation of the temperature front is used to test the problems of numerical oscillation and numerical diffusion for various upstream weighting schemes.

The horizontal hot water injection problem with heat loss due to vertical conduction to overburden and underburden has a solution due to Avdonin.

3. Instantaneous and Continuous Sources

In addition to the line-source solution (Theis solution) in the cylindrical coordinate system, the solutions for other source shapes can be easily derived using the Green function technique. Examples of others are the point source, the planar source, the disk source, the finite line source, the finite cylindrical source, etc.

4. Single Fracture Solutions

For single horizontal or vertical fractures intercepting a well in porous medium formulations, solutions using superposition of point sources have been developed in petroleum literature.

History Matching

Besides being verified against analytic solutions, a model should be severely tested in an attempt to match the history of field data over a long period of time. Even in a field with many wells the subsurface conditions are so complicated that the input parameters characterizing the reservoir are usually very difficult to estimate. Nevertheless, reasonable success in matching long-term data and in predicting the future are important factors to be considered in reviewing a model. The success of history matching and prediction depends not only on the soundness of the code but also on the knowledge of the geological and physical processes to be modeled; and the experience of the modelers who perform the study.

APPLICATIONS

A well-developed model can often be used for the study of processes in several fields. The versatility and range of applicability of a model can be illustrated by the variety of problems solved by the code. Improvements and developments of a code are frequently associated with new applications. In the following, major areas of application of the models are discussed. The focus will be mainly on fracture-related phenomena and thermally-induced phenomena.

Fracture Well Testing

The first direct study of a geological formation is the drilling of a well to the depth of interest. After core studies and geophysical logging have been done, a variety of well tests can be performed to study the hydraulic properties of the formation. The tests can be transient or steady, with single well or with multiple wells, with a packed interval for detailed studies or with the well left open for integrated studies, and with various driving mechanisms to induce pressure changes (production, injection, shut-in, pulse, etc.). In petroleum engineering, where the interest is in improving production by hydraulic fracturing, the focus of fracture well testing is to determine the extent and orientation of single, large fractures in fluid producing formations, and to estimate enhanced productivity. In geothermal engineering many reservoirs are known to be fractured. Man-made fractures are also of interest for hot dry rock geothermal studies. However, in waste isolation studies, it may be more difficult to perform and analyze conventional well tests. For example, the formation may be too tight to conduct a constant flow rate test within a reason-

able period of time. The propagation of pressure perturbations through the complicated fracture network may be highly anisotropic and difficult to detect.

Convection and Generic Studies

The buoyancy force due to density change of hot fluid will induce convective fluid movement around a repository. The development of convection cells in porous media has been of great interest for geological and geothermal studies. Due to the slow decay of the nuclear waste, the buoyancy flow induced by the waste heat will persist over thousands of years.

CONCLUSION

In repository studies, numerical modeling is essential in every phases. The characterization of formations, the evaluation of thermal effects, the analysis of field data, and the assessment of enviromental impact all require such models. With more field studies and larger computer capacities, the modeling capability will be continuously enhanced. There is much work to be done in the improvements, the validations and the applications of numerical models in order to investigate and understand the in-situ thermohydrological processes in fractured rock masses.

In general, porous medium models are quite well developed. Most of the modeling methodologies are originally designed for porous systems. Their applicability to fractured systems is not well established. Most of the models are verified against a few analytical solutions. More verifications of the numerical code should be made, especially against fracture flow solutions. Model should be validated against data from laboratory experiments or field test sites before applying the model results.

One of the problems in the use of porous medium models and double porosity models for fractured systems is the uncertainty in the range of applicability of the continuum approaches. When the extent and spacings of the fractures are comparable with the dimensions of the region of interest, it is difficult to define the equivalent permeability and pososity which are representative of the flow averaged over the grid blocks. There is very little modeling experience for complex fracture systems and very limited field testing over large rock masses. Both modeling and testing are required to gain insight into the representations of the fractured system to make it amenable to modeling.

For fracture flow, there is only an empirical understanding when one tries to go beyond the parallel-plate model. Studies of fluid movements through natural or induced fractures are needed.

Fractures are easily deformable and the stress-displacement dependencies are highly nonlinear. Since fluid flow is sensitive to the fracture aperture, the coupling between the flow with the mechanical or thermally induced deformation may be strong under certain field conditions. In general fluid flow, heat transfer, rock deformations, and chemical transport are coupled. The limits of validity of uncoupled or partially coupled modeling need to be determined.

Even with extensive field testing, most of the properties can not be determined exactly because of the heterogeneity of the formations and the intrinsic uncertainty of the experiments. Therefore, models should be constructed to handle statistical distributions of parameters. The basic understanding of the relationship between the distributions of discrete data and the uncertainties of continuum parameters is yet to be developed.

REFERENCES

1. Proceedings of GAIN Symposium, Berkeley, California, July 16-20, 1978. LBL-7096, Lawrence Berkeley Laboratory.

2. Proceedings of Workshop on Thermomechanical Modeling for a Hardrock Waste Repository, Berekely, California, June 25-27, 1979. UCAR-10043, Lawrence Livermore Laboratory, ONWI-98, Office of Nuclear Waste Isolation.

3. Wang, J.S.Y., Sterbentz, R.A., and Tsang, C.F., The state-of-the-art of numerical modeling of thermohydrological flow in fractured rock masses. LBL-10524, Lawrence Berkeley Laboratory, Berkeley, California, June, 1980.

4. Ayatollahi, M.S., Noorishad, J. and Witherspoon, P.A., A finite element method for stress and flow analysis in fractured rocks. LBL-11430, Lawrence Berkeley Laboratory, Berkeley, California, 1980.

5. Narasimhan, T.N., Witherspoon, P.A., and Edwards, A.L., Numerical model for saturated-unsaturated flow in deformable porous media. 2. The algorithm. Water Resources Research, 14(2), 255-261, April 1978.

6. Lippmann, M.J., Tsang, C.F., and Witherspoon, P.A., Analysis of the response of geothermal reservoirs under injection and production procedures. SPE-6537, 47th Annual California Regional Meeting of the Society of Petroleum Engineers of AIME, Bakersfield, California, April 13-15, 1977.

7. Duguid, J.O., and Lee, P.C.Y., Flow in fractured porous media. Water Resources Research, 13(3), 558-566, June 1977.

8. O'Neill, K., The transient three-dimensional transport of liquid and heat in fractured porous media. Ph.D. thesis, Dept. of Civil Engineering, Princeton University, Princeton, New Jersey, January 1978.

9. Runchal, A., Treger, J., and Segal, G., Program EP21 (GWTHERM): Two-dimensional fluid flow, heat, and mass transport in porous media. TN-LA-34, Advanced Tech-

nology Group, Dames & Moore, Los Angeles, California, September 1979.

10. Ratigan, J.L., Burgess, A.S., Skiba, E.L., and Charlwood, R., Groundwater movements around a repository, repository domain groundwater flow analyses, part 1 permeability perturbations, part 2 inflow to repository, part 3 thermally induced flow. KBS-54:05, Hagconsult AB, Karnbranslesakerhet, Stockholm, Sweden, September, 1977.

11. Gupta, s.K., Cole, C.R., and Bound, F.W., Finite element three-dimensional ground-water (FE3DGW) flow model - formulation, program listings and user's manual. PNL-2652, Battelle Pacific Northwest Laboratory, Richland, Washington, December 1979.

12. Dillon, R.T., Lantz, R.B., and Pahwa, S.B., Risk methodolgy for geologic disposal of radioactive waste: the Sandia waste isolation flow and transport (SWIPT) model. SAND78-1267, NUREG/CR-0424, Sandia Laboratories, Albuquerque, New Mexico, October 1978.

13. Coats, K.H., Geothermal reservoir modeling. SPE-6892, 52nd Annual Fall Technical Conference and Exhibition of the Society of Petroleum Engineers of AIME, Denver, Colorado, October 1977.

14. Faust, C.R., and Mercer, J.W., Geothermal reservoir simulation: 2. Numerical solution techniques for liquid- and vapor-dominated hydrothermal systems. Water Resources Research, 15(1), 31-46, February 1979.

15. Brownell, D.H., Jr., Garg, S.K., and Pritchett, J.W., Computer simulation of geothermal reservoirs. SPE-5381, 45th Annual California Regional Meeting of the Society of Petroleum Engineers of AIME, Ventura, California, April 1975.

16. Pruess, K., and Schroeder, R.C., SHAFT79 user's manual. LBL-10861, Lawrence Berkeley Laboratory, Berkeley, California, January 1980.

UK MODELLING OF THERMAL EFFECTS ON LEAKAGE FROM HARD ROCK DEPOSITORIES

P. J. Bourke
Environmental Safety Group
Harwell Laboratory
Oxfordshire OX11 ORA, UK

Introduction

Mathematical hypotheses have been developed for predicting temperature fields and some of their effects on the return of radionuclides to the surface following the burial of heat emitting waste in hard rock.

The main thermal effects on individual waste packages will be increased rates of leaching of radioactivity and corrosion of containers. These effects will depend on local temperatures. They can be quantified without elaborate modelling once these temperatures are specified and the relevant experimental data, now being obtained, are available.[1-3]

In addition to these local effects, raised temperatures through and around depositories will reduce the density of water in fractures in the rock and cause it to rise towards the surface. Further, the heating of the rock through the depository will cause expansion and induce tensile stress and possible increased fracturing of the surrounding, cooler rock. Both these phenomena will tend to increase waterborne movement of radionuclides which is the most likely means of leakage from depositories to the surface.[4] Assessments of their importance are being attempted and progress with these is summarized here.

Prediction of Temperature Fields

Heat transfer from hard rock depositories will be mainly by conduction through the rock and convection has been shown to be negligible.[5] The maximum temperatures which will be produced and the times for these maxima to decay will depend on transient conduction for up to a millenium through about 100 m of rock surrounding the depository.[6] There is considerable uncertainty in extrapolating existing, mainly laboratory, measurements of conductivity of small samples of rock for short times to these conditions. Hence, a field heating experiment[7] has been made to measure conduction over 25 m for two years. The results show almost constant conductivity and it is thought that, by using them, reliable predictions of depository temperature fields can now be made.

A typical prediction is given in Figure 1 which shows the temperature field at 10, 100 and 1000 years after burial of about 7,000 'Harvest' blocks in a cubic array. The effects on maximum temperatures and their decay times of relevant depository variables, size, shape, depth, number of blocks, etc., have been analysed to allow the depository design to be optimised.[8,9]

Thermally Induced Water Flow

The pressure gradients causing flow due to thermal buoyancy can be assessed directly, without further assumption, from predicted temperature fields. For a 1000 m deep, compact depository for the probably HLW arisings until 2000 AD of 10,000 'Harvest' blocks from existing UK power stations, the thermally induced average pressure gradient to the surface will be greater than likely values of the natural pressure gradient for more than 10,000 years after burial.[5] This effect can be reduced by increasing the horizontal dimensions and/or depth of the depository[10] but it is still concluded that thermal flow will remain a major cause of leakage for long times.

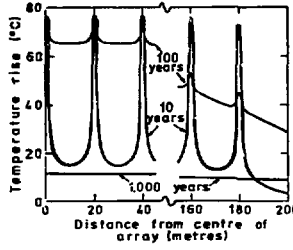

It was therefore decided to analyse this flow in more detail. This has been done[11] by assuming probable ranges of the relevant rock properties; permesbility and porosity, and calculating the time taken for water to rise from the depository to the surface. A typical example is given in Figure 2 which shows the paths to the surface and journey times for water starting from various positions in a 1000 m deep, 10,000 block depository.

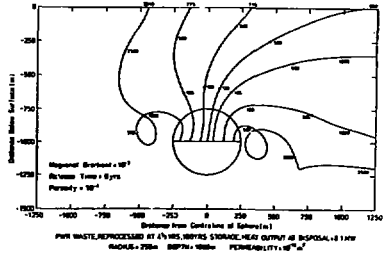

The times to reach the surface are not considered reliable because of uncertainty in the assumed rock permeability and porosity but most of times calculated for the assumed rock property ranges have been between 1000 and 10,000 years which is considererd undesirably short. Radionuclides are, however, expected to travel with much slower speeds because of diffusion and sorption from the water flow into the rock. It is concluded that reliable field data for the rock properties and for retardation of the readionuclide movement are urgently needed. Experimental studies[12] of the former are being started and of the latter being planned.

Thermal Stressing and Fracturing

Thermally induced stress through and around depositories have been calculated[13-15] assuming the rock to have constant mechanical properties obtained from laboratory measurements and ignoring the effects of existing fractures. After allowing for probable values of the natural stress field, regions of net tension and high shear stress which might cause new fractures were found.

This analysis is, however, not yet considered to be reliable because of uncertainty about the above assumptions. Further, even if it is accurate, it is incomplete because it is still not possible to relate quantitatively calculated stresses to changes in permeability and porosity due to changes in existing fractures or initiation of new ones. Accordingly, further theoretical work is being done to plan an underground study of the effects of heating on a well defined fracture. Measurements of strain and modulus will be made to investigate the validity of the mechanical assumptions and hydraulic data will be obtained to relate stress to resistance to flow. It is hoped that further analysis will then allow an assessment of the importance of thermal stress round a depository to be made.

References

1. J. A. C. Marples, C. Sombret and C. Marlow; Thermal effects of HLW products, First CEC Radioactive Waste Management Conference, Luxembourg, May 1980.
2. H. Beale, H.J. Englemann, A. Boulangier, M.P.P. Mayence and G. Hamstra, Conceptual designs of depositories, First CEC Radioactive Waste Management Conference, Luxembourg, May 1980.
3. H.C. Heremans, E. Barbreau, P. J. Bourke and H. Gies; Thermal aspects of waste burial, First CEC Radioactive Waste Management Conference, Luxembourg, May 1980.
4. P. J. Bourke and D. P. Hodgkinson; Far field effects in burial of radioactive waste, NEA-OECD Heating Experiments Seminar, Ludvica, September 1978.
5. P. J. Bourke and D. P. Hodgkinson; Thermally induced water flow, NEA/IAEA Low Permeability Workshop, Paris, March 1979.
6. P. J. Bourke; Heat transfer aspect of burial of radioactive waste, AERE-R-8790, 1976.
7. P. J. Bourke, D. P. Hodgkinson and A. S. Batchelor; Field heating experiments, NEA-OECD Heating Experiments Seminar, Ludvica, September 1978.
8. P. J. Bourke and D. P. Hodgkinson; Temperatures versus size, shape and depth of depositories, AERE M-2900, 1977.
9. H. Beale, P. J. Bourke and D. P. Hodgkinson; Thermal aspects of radioactive waste disposal, IAEA/OECD International Symposium, Helsinki, July 1979.
10. P. J. Bourke and P. C. Robinson; Effects of depository width and depth on thermal water flow, AERE-R-9951, in preparation.
11. D. P. Hodgkinson; Hydrothermal convection around a radioactive waste dpository, AERE-R-9149, 1979.
12. P. J. Bourke, J. E. Gale, D. P. Hodgkinson, and P. A. Witherspoon; Tests of permeability of hard rock, NEA/IAEA Low Permeability Workshop, Paris, March 1979.
13. A. S. Batchelor, P. J. Bourke, P. Hacket and D. P. Hodgkinson; Initial assessment of thermal expansion of granitic depository, AERE-R-9017, 1979.
14. D. P. Hodgkinson; Thermal stress field, AERE-R-8999, 1978.
15. D. P. Hodgkinson and P. J. Bourke; Thermal stress around a radioactive waste depository, J. Nucl. Sci., in press.

MULTIDIMENSIONAL NUMERICAL SIMULATION OF FLUID FLOW IN FRACTURED POROUS MEDIA

T. N. Narasimhan
Earth Sciences Division
Lawrence Berkeley Laboratory
University of California
Berkeley, California 94720

ABSTRACT

Fluid flow in fractured porous media can be simulated with considerable ease and generality using an integral finite-difference scheme (IFDM). The three commonly used conceptualizations of fractured systems, namely, discrete fracture systems, equivalent porous media systems, and double- or composite-porosity systems are all contained within the IFDM formulation. The theoretical basis of the IFDM is briefly described and the method is compared and contrasted with the finite difference and the finite element methods. Six illustrative examples are provided to demonstrate the applicability of the method to fractures with fixed or variable geometry, to advective-diffusive chemical transport in a fractured system and to a double-porosity system.

INTRODUCTION

At present there is considerable interest in the possibility of disposing nuclear wastes in extremely low permeable geological environments such as those obtained in igneous and metamorphic rocks or in ancient argillaceous materials. Though lacking in primary permeability, these rocks are known to contain fractures down to several kilometers below land surface. Moreover, the stress-relief accompanying the underground openings and the associated shafts will also lead to the creation of artificial fractures that may extend to at least a distance of a few shaft or repository diameters. The fractures, which may have apertures as small as 1 to 10 microns, may, over a period of thousands or years, provide pathways for migrating groundwaters from the repository to the biosphere. Long-term acceptability of deep waste-disposal sites is therefore very much dependent on our ability to simulate the evolution of the groundwater regimes in such fractured rock systems.

Approaches to Modeling Fractured Systems

Fractured rocks-systems of interest in radioactive waste disposal consist of extremely low permeability rocks (10^{-9} to 10^{-4} darcies) intersected by one or more fracture sets. The fractures, whose permeability is directly related to their apertures, provide the main conduits for water movement with some diffusive leakage into the rock matrix. Modeling the flow of water in such systems involves the simulation of a highly heterogeneous system with complex geometry. Even with the current availability of powerful computers, a detailed handling of such systems requires capabilities of handling enormous quantities of data, not economically feasible at the present time, except when the flow region is relatively small (e.g., the region immediately adjoining the repository).

In general, three approaches have been proposed in the literature to handle fractured-porous systems. These are:

a. Equivalent Porous Medium Approach: In this approach, the fractured system is grossly treated as an equivalent non-isotropic statistical continuum. The tacit assumption is that physical quantities such as potential, porosity, pressure and so on, are averaged over sufficiently large blocks of rock containing a large number of fractures. Obviously, the sizes of such a representative block will increase with increased fracture spacing. Computations based on this model will, in general, be relevant only to field observations made with measuring devices with large characteristic lengths (e.g. wells with large open intervals). From a practical standpoint, there is general agreement among many workers that the equivalent porosity model is a reasonable method to analyze the fluid flow regime far away from the repository. One of the serious drawbacks of this approach is that there is as yet no well-defined method for computing the gross, porous media parameters, even if the fracture details are completely prescribed. This is because the gross parameters are very much dependent on scale and there is reason to believe that the gross system may in general truly be anisotropic, rather than orthotropic as is commonly assumed in the literature.

b. Double-Porosity Approach: The double-porosity approach was originally proposed by Barenblatt et al., 1960, to analyze flow in fractured-porous media. In this approach, the flow region is mathematically idealized as a complex of two interacting media, one representing the fissured-regime and the other representing the porous regime. The fissured regime is characterized by very high permeability and very low storage while the porous block regime is characterized by low permeability and high storage. Such a system may be described by two conservation equations, one for each aforesaid regime. These two equations are to be coupled by a fluid transfer-term expressed as a nonlinear source term, dependent on the potential difference between the regimes at the location of interest. This double porosity model enabled the development of several useful analytical solutions for well-test analysis in the petroleum literature (e.g., Warren and Root, 1963; Odeh, 1965) for naturally fractured reservoirs. The double-porosity approach, or better still, the interacting double-continuum approach is truly a mathematical approximation whose exact relation to physics is ill-defined. For example, the analytic solution of the double porosity system yields two values for potential at every point in the system, one for the fracture-regime and one for the porous-regime. How do these quantities

relate to the actual physical measurement at the location? Moreover, the source-term which couples the two regimes is proportional to the difference in the two potentials through a coefficient whose physical significance is not well-defined. Yet, when one is not interested in a detailed description of what happens within the reservoir, the above deficiencies can be overlooked and the double porosity system can be used as a practical tool for modeling and prediction. Such indeed is the case when one chooses to use this model for analyzing well-test data from naturally fractured reservoirs.

The utility of the double porosity model in regard to waste-isolation studies depends on the manner in which the model output is to be utilized. For example, for modeling chemical transport problems, the double-porosity model output will not be reliable since a fairly well-defined fluid flux field is a necessary input for solving the transport equation. Furthermore, it is not clear to this writer that the double-porosity concept is needed at all when one chooses to solve the over-all problem by numerical methods. As we shall see later, numerical models, developed directly from the basic integral equation, help not only in dispensing with hard-to-define internal boundary conditions, but also provide a great deal of flexibility in modeling any part of the flow region with any desired degree of fineness. Thus, in a numerical model of a fractured medium, the double porosity model can be treated realistically as a limiting case in which the porous blocks are discretized very coarsely.

c. The Discrete Fracture Approach: In this very general approach, the fractures and the porous matrix are separately discretized into volume elements and the conservation equations are solved for each such volume element. A principal drawback of this approach is the amount of detail that is required as input and the accompanying effort involved in obtaining numerical solutions. Nevertheless, it appears that such a detailed effort is necessary to analyze the flow regime in the vicinity of the underground opening. Also, very little is known at present about the factors that govern the transformation of parameters from one scale to another (e.g. permeability of individual fractures). In order to gain insight into the question of scale transformation, the discrete fracture model is a tool of fundamental necessity.

Purpose and Scope

The purpose of this paper is to present a general, multidimensional numerical model for simulating fluid flow in fractured porous media. The model is inherently sufficiently general to include the three approaches described above as particular cases. Conceptual-theoretical discussions are provided to develop the problem in an integrated fashion. Some numerical results are presented to substantiate the theoretical arguments. In scope, the paper is restricted to isothermal fluid flow.

THEORY

Conceptual Framework

The basic law of mass conservation is applicable to any elemental volume ℓ of the flow region, whether that elemental volume comprises a portion of a fracture, a portion of the rock matrix, or even a combination of both. According to the law of mass conservation, the algebraic sum of the fluxes crossing the surface enclosing volume element and the arbitrary withdrawal of fluids from ℓ (the sources) equals the rate of change of fluid mass in ℓ, thus,

$$\rho_\ell G_\ell + \int_{\Gamma_\ell} \rho K \vec{\nabla}\phi \cdot \vec{n} d\Gamma = \frac{\partial M_{w,\ell}}{\partial t} \tag{1}$$

where ρ_ℓ is average fluid density within ℓ; G_ℓ is the volumetric rate of fluid generation from ℓ; ρ is fluid density at $d\Gamma$; K is the hydraulic conductivity at $d\Gamma$; $\phi = z + \psi$ is the fluid potential where z is elevation and ψ is pressure head; $\vec{n}$ is unit outernormal to $d\Gamma$; $M_{w,\ell}$ is the mass of water contained in ℓ and Γ_ℓ is the closed surface bounding the volume element ℓ. Should the system be fully saturated with water, and should the fluid potential vary smoothly over the volume element, then $M_{w,\ell}$ can be related to the average pressure head ψ_ℓ at an interior nodal point in the system by the relation,

$$M_{w,\ell} = M^*_{w,\ell} + (dM_{w,\ell}/d\psi_\ell)\bar{\psi}_\ell \tag{2}$$

and

$$dM_{w,\ell}/d\psi_\ell = V_\ell \rho_\ell S_{s,\ell} \tag{3}$$

where $M^*_{w,\ell}$ is the mass content of ℓ at $\bar{\psi}_\ell = 0$, V_ℓ is the volume of ℓ and $S_{s,\ell}$ is the specific storage of the material in ℓ given by

$$S_{s,\ell} = \rho_\ell g(n\beta + m_{v,\ell}) \tag{4}$$

where g is acceleration due to gravity, n is porosity, β is compressibility of water and $m_{v,\ell}$ is the coefficient of volume change (rate of change of bulk volume with external pressure) of the material in element ℓ. Additionally, if we neglect time-dependent changes in elevation of the nodal points due to very small deformations, then, $\Delta\bar{\psi}_\ell = \Delta\bar{\phi}_\ell$. Moreover, Γ_ℓ may either be completely interior to the flow region ($\Gamma_{\ell,i}$) or portions of it may coincide with the external bounding surface of the system ($\Gamma_{\ell,b}$). Hence we may rewrite (1) as

$$\rho_\ell G_\ell + \int_{\Gamma_{\ell,i}} \rho K \vec{\nabla}\phi \Gamma \cdot nd + \int_{\Gamma_{\ell,b}} \rho K \vec{\nabla}\phi \cdot nd\Gamma = M_{c,\ell} \frac{\partial \phi_\ell}{\partial t} \tag{5}$$

where $M_{c,\ell} = dM_w/d\psi$ is the fluid mass capacity of the volume element ℓ, defined as the change in mass of water in ℓ due to a unit change in head under conditions of drainage. In heat-flow problems, the analagous quantity is the heat capacity of an arbitrary mass of material.

The integral representation in (5) may be applied to any volume element, finite or infinitesimal. If one applies (5) to an infinitesimal element, and divides both sides through by V_ℓ, the result is the well known differential expression,

$$\rho_\ell q_\ell + \text{div } K\vec{\nabla}\varphi = m_{c,\ell}\frac{\partial \varphi_\ell}{\partial t} \qquad (6)$$

where q_ℓ is G_ℓ/V_ℓ and $m_{c,\ell} = M_{c,\ell}/V_\ell$.

However, since our purpose is to develop a numerical model and since the numerical approach consists in applying the conservation equation to finite subdomains of the flow region, we may directly proceed from (5) and write down the discretized equations. We will not follow the redundant step of integrating (6) to obtain (5). Note also that in (5) the second integral on the right hand side incorporates the known boundary conditions either in the form of known φ (prescribed potential condition) or in the form of known $K\vec{\nabla}\varphi\cdot\vec{n}$ (prescribed flux condition). That is, (5) imbeds the boundary condition into the conservation statement.

For purposes of numerical computations, if one chooses the volume element to be sufficiently small so that (2) is satisfied at all times with reference to φ_ℓ measured at the representative nodal point, then one may directly apply (5) to ℓ. Also, if Γ_ℓ and t are divided into a finite number of segments, then, the integrals may be replaced by finite sums and the differentials by finite differences to obtain,

$$\rho_\ell G_\ell + \sum_m \rho_{\ell m} K_{\ell m}(\vec{\nabla}\varphi\cdot\vec{n})_{\ell m}\Delta\Gamma_{\ell m} + \sum_b \rho_{\ell b} K_{\ell b}(\vec{\nabla}\varphi\cdot\vec{n})_{\ell b}\Delta\Gamma_{\ell b} = M_{c,\ell}\frac{\Delta\varphi_\ell}{\Delta t} \qquad (7)$$

in which m denotes all interior surface segments and b denotes all exterior surface segments. Note that (7) applies to any arbitrary volume element and hence it is an invariant statement. As shown in Fig. 1, (7) may be applied to a portion of a fracture or a portion of a porous medium. When (7) is applied to a fracture (Fig. 1B), then, for the segment of Γ_ℓ representing the fracture-rock interface ($\Delta\Gamma_{\ell,r}$ in Fig. 1B), one has to use $K_{\ell,r}$ in applying (7) where $K_{\ell,r}$ is the hydraulic conductivity of the rock-fracture interface. It is of interest to note here that in the double porosity model, the flux across this surface is treated as a source term included in G_ℓ. This source term is the internal boundary condition linking the fissure-regime and the porous regime. Thus, in the double-porosity model, the term $(\rho_\ell K_{\ell m}\vec{\nabla}\varphi\cdot\vec{n}d\Gamma)$ for the fracture rock interface is replaced by an equivalent term $\rho_\ell\alpha^* K_m(\varphi_m - \varphi_\ell)$ where φ_m is the average potential in the block, φ_ℓ is the potential in the fracture, $K_{\ell m} = K_m$ in the matrix hydraulic conductivity and α^* is a function of the surface area of the fracture interface and a characteristic length

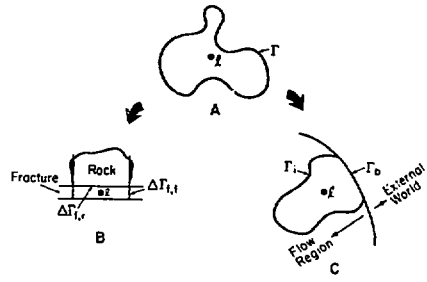

Fig. 1. Examples of volume elements, nodal points, and bounding surfaces. (XBL 807-7236)

of the block. As we shall see later, the model described in this paper is flexible enough to handle either of the two methods of handling the fracture rock interface.

It is not difficult to see in this regard that in a rock system with irregular fracture distributions α^* should vary widely from one location to another in the flow region. Yet, the double-porosity model assumes this factor (or a factor α related to α^* by $\alpha = \alpha^*/V$) be constant everywhere in the flow region. Obviously, the double porosity approach is extremely simplistic for naturally fractured systems. Conversely, estimates of α obtained indirectly from interpretation of well tests can only be model coefficients with very limited use. Application of the α to a detailed modeling of the reservoir can lead to unrealistic estimates of fluid potentials and fluxes over the flow region.

The Chosen Approach

In the present work we shall choose the approach of directly applying (7) to well defined subdomains of the flow region. Additionally, we shall choose to evaluate the quantity $(\vec{\nabla}\varphi\cdot\vec{n})$ at each interface between volume elements by the finite difference approximation

$$\vec{\nabla}\varphi\cdot\vec{n}\Big|_{\ell,m} \sim \frac{\varphi_m - \varphi_\ell}{D_{\ell,m}} \qquad (8)$$

where $D_{\ell,m}$ is the distance between the nodal points ℓ and m. Equation (8) presupposes that the line joining ℓ and m coincides with the normal to the interface $\Delta\Gamma_{\ell m}$. Figure 2 is a sketch of a volume element ℓ of arbitrary shape in the rock matrix which communicates with other rock or fracture elements. In Fig. 2, $D_{\ell,m} = d_{\ell,i} + d_{m,i}$, where $d_{\ell,i}$ and $d_{m,i}$ denote, respectively, the perpendicular distances from nodes ℓ and m to the interface $\Delta\Gamma_{\ell,m}$.

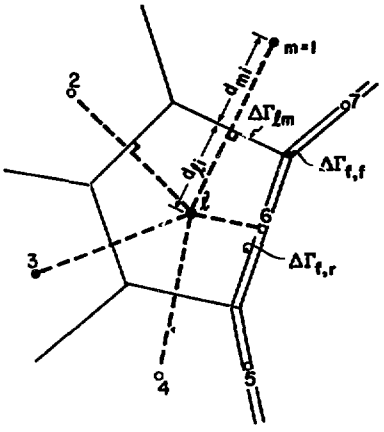

Fig. 2. Philosophy of mesh discretization for the Integral Finite Difference Method. (XBL 807-7234)

This approach has been termed the Integral Finite Difference Method (IFDM; Narasimhan and Witherspoon, 1976) since this method directly evaluates the surface integrals and the associated volume averages and since it uses the finite difference approach for evaluating gradients of potential. This approach, which has been known since the early 50's (MacNeal, 1953; Dusinberre, 1961) was translated into a very powerful computer program called TRUMP by Edwards (1972). Many of the ideas inherent in the following discussions have originated from Edwards.

The discretized IFD equations now become,

$$\rho_\ell G_\ell + \sum_{\substack{m \\ \ell \neq m}} U_{\ell m}(\phi_m - \phi_\ell) + \sum_b U_{\ell b}(\phi_b - \phi_\ell) = \rho_\ell V_\ell S_{s,\ell} \frac{\Delta\phi_\ell}{\Delta t} \quad (\ell = 1,2,3,\ldots,L) \qquad (9)$$

where $U_{\ell,m}$ is the conductance of the interior surface $\Delta\Gamma_{\ell,m}$, given by

$$U_{\ell,m} = \frac{\rho K_{\ell,m} \Delta\Gamma_{\ell,m}}{D_{\ell,m}} \qquad (10)$$

$U_{\ell,b}$ is the conductance of the external surface segment, $\Delta\Gamma_{\ell,b}$ given by

$$U_{\ell,b} = \frac{K_\ell \Delta\Gamma_{\ell,b}}{D_{\ell,b}} \qquad (11)$$

L is the total number of nodes in the flow region for which $\Delta\phi_\ell$ is to be computed. m denotes a volume element having an interface with volume element ℓ. Rearranging terms in (9), we get

$$\rho_\ell G_\ell - \phi_\ell \left[\sum_m U_{\ell,m} + \sum_b U_{\ell,b}\right] + \sum_m U_{\ell,m}\phi_m + \sum_b U_{\ell,b}\phi_b = \rho_\ell V_\ell S_{s,\ell} \frac{\Delta\phi_\ell}{\Delta t} \qquad (12)$$

Equations (9) and (12) are central to the IFDM. Apart from the source terms and the material properties, a key task in the IFDM is to provide the geometric quantities $D_{\ell m}$, $\Delta\Gamma_{\ell,m}$ and V_ℓ that are needed to evaluate $U_{\ell,m}$, $U_{\ell,b}$ and $M_{\ell,\ell'}$. In the IFDM these quantities are provided directly as input, for each interface and volume element in the flow region. Equation (9) is in a form very convenient for writing the iterative procedure used in the computer program TRUMP, and its derivatives while (12) is convenient to express the equation in a global matrix form for direct solution purposes. We shall return to (12) later when comparing IFDM with other methods.

Marching in the Time Domain

In (9) ϕ_m and ϕ_ℓ are both functions of Δt and we have to use appropriate mean values, $\bar{\phi}_m$ and $\bar{\phi}_\ell$ such that

$$U_{\ell m}(\bar{\phi}_m - \bar{\phi}_\ell) = \int_{t_o}^{t_o+\Delta t} U_{\ell,m}(\phi_m - \phi_\ell)dt \qquad (13)$$

and

$$U_{\ell b}(\bar{\phi}_b - \bar{\phi}_\ell) = \int_{t_o}^{t_o+\Delta t} U_{\ell,b}(\phi_b - \phi_\ell)dt \qquad (14)$$

To achieve this (Narasimhan et al., 1978, Edwards, 1972), express these mean values by

$$\bar{\phi}_\ell = \phi_\ell^\circ + \lambda\Delta\phi_\ell \qquad (15)$$

$$\bar{\phi}_m = \phi_m^\circ + \lambda\Delta\phi_m \qquad (16)$$

where ϕ_ℓ° and ϕ_m° are the initial values corresponding to time t_o and $0 \leq \lambda \leq 1$ is a weighting factor. For $\lambda = 0$, leads to a set of explicit expressions for the $\Delta\phi$'s. However, the explicit expression for any element ℓ will violate maximum principle when Δt exceeds the critical time constant for the element. This critical value, called a stable time-

step, is the ratio of capacity of ℓ to the sum of its surface conductance,

$$\Delta t_{stab,\ell} = \frac{M_{c,\ell}}{\sum_m U_{\ell,m} + \sum_b U_{\ell,b}} \qquad (17)$$

for a stable solution, therefore, when $\Delta t > \Delta t_{stab,\ell}$ we substitute (15) and (16) into (9) to arrive at an implicit set of equations (simultaneous equations). For convenience, we rearrange terms to express $\Delta\phi_\ell$ in terms of an explicit part and an implicit part. Thus,

$$\Delta\phi_{\ell,explicit} + \frac{\lambda\Delta t}{M_{c,\ell}} \left\{ - \sum_b U_{\ell,b}\Delta\phi_\ell + \sum_m U_{\ell m}(\Delta\phi_m - \Delta\phi_\ell) \right\} = \Delta\phi_\ell \qquad (18)$$

where

$$\Delta\phi_{\ell,explicit} = \frac{\Delta t}{M_{c,\ell}} \left\{ \rho_\ell G_\ell + \sum_m U_{\ell,m}(\phi^o_m - \phi^o_\ell) + \sum_b U_{\ell,b}(\phi^o_b - \phi^o_\ell) \right\} \qquad (19)$$

We now reason that we could first compute the $\Delta\phi_{\ell,explicit}$ values for every ℓ in the flow region and then evaluate the second quantity on the left-hand side of (18) only for those ℓ for which $\Delta t > \Delta t_{stab,\ell}$. This has been called the mixed explicit-implicit approach. In applying (18) thus, if, for a given ℓ and m

$$\Delta t > \Delta t_{stab,\ell} \quad \text{but} \quad \Delta t < \Delta t_{stab,m}$$

then, we replace

$$U_{\ell,m}(\Delta\phi_m - \Delta\phi_\ell) \text{ by } U_{\ell,m}(\Delta\phi_{m,explicit} - \Delta\phi_\ell).$$

The mixed explicit-implicit approach thus does the implicit calculations only in those parts of the flow region where stability is violated. In other words, if isolated areas of instability are separated in a flow region by areas of stability, then the unstable regions are essentially decoupled from one another within each time step. Under these circumstances, the mixed explicit-implicit strategy helps us to partition the large global matrix and obtain solution by solving several small submatrices. For details of this strategy see Edwards (1972), Narasimhan et al (1978), and Neuman and Narasimhan (1977).

Computer Programs

The basic IFD model was originally developed by Edwards (1972) for heat transport with conduction, convection, and radiation and incorporated into a program called TRUMP. Subsequently, this model was adapted at the Lawrence Berkeley Laboratory to solve porous media fluid flow problems. These programs include: TRUST, for solving saturated-unsaturated flow in deformable media (Narasimhan et al., 1978); TERZAGI, for saturated flow in deformable media; CCC, for heat and water transport in deformable media (Lippmann et al., 1977); and SHAFT 79, for two-phase transient flow of heat and mass (Pruess et al., 1979). The discussions that follow in regard to simulating fractures are applicable to all the aforesaid programs subject to suitable modifications. However, the actual applications that follow have been carried out with TERZAGI, except for one case analyzed with TRUMP.

Simulation of Fractured Rock Systems

We have already stated that there are three different ways in which fractured rock systems can be simulated. These include: systems with discrete fractures; double-porosity systems; and equivalent porous media systems. The last of these does not require any further attention since literature is voluminous on modeling porous systems. We will now consider the first two cases.

Systems with discrete fractures: In modeling a porous medium with discrete fractures with the IFDM, we recognize that (9) or (12) are very general in nature and can be applied to an elemental volume, either in a fracture or in the rock matrix, as in Fig. 2. Computationally, a major difference between a matrix element and a fracture element is that the former is usually characterized by higher capacities ($M_{c,\ell}$) and lower hydraulic conductivities and hence large time constants. The latter, on the other hand, are usually characterized by very low capacities and very high hydraulic conductivities and hence very small time constants.

Note from (9) or (12) that in setting up the final matrix of simultaneous equations, the quantities needing greatest attention in computation are the conductances $U_{\ell,m}$ and $U_{\ell,b}$, since $\rho_\ell G_\ell$ and $M_{c,\ell}$ are directly provided as input. For computing the conductances proper, equations (10) and (11) one needs the hydraulic conductivity at the interface $K_{\ell,m}$, the distance between nodal points $D_{\ell,m}$ and the surface area $\Delta\Gamma_{\ell,m}$. In particular, handling the conductance between a fracture and a matrix element is worth discussing. Because of the much higher hydraulic conductivity of the fractures, the potential gradients along the fracture will be relatively small compared to that within the block and hence, a single fracture element may be connected to one or more rock elements along a given fracture surface. Moreover, since gradient potential across the fracture opening can be neglected, the fracture rock conductance, $U_{f,r}$, is determined by

$$U_{f,r} = \frac{\omega K_r \Delta\Gamma_{f,r}}{d_{r,i}}$$

where K_r is the hydraulic conductivity of the rock matrix, $\Delta\Gamma_{f,r}$ is the interface area and $d_{r,i}$ is the distance from the nodal point of the rock element to the interface $\Delta\Gamma_{f,r}$.

It is now appropriate to discuss the fracture parameters. Insofar as adjoining fracture elements are concerned, we need to use the hydraulic conductivity of the fracture, K_f in computing conductance. It is now well established that K_f is related to 2b, the fracture aperture. Experimental evidence (Witherspoon et al., 1979) suggests that laminar fluid flow in a fracture can be very closely approximated by the relation,

$$Q_f = \frac{(2b)^2 \rho g}{12\mu} \cdot (2b\Delta\ell_f) \cdot \frac{\partial\phi}{\partial x} \tag{21}$$

where Q_f is the flux in the x direction, 2b is the fracture aperture, μ is the coefficient of viscosity and $\Delta\ell_f$ is the length of the fracture trace on the plane across which Q_f is measured. For the sake of a definition, if we let $\Delta\ell_f = 1$ and $\partial\phi/\partial x = 1$, then, $w_f = (2b)^3\rho g/12\mu$. Hence the expression "cubic law" is used to characterize fluid flow in fractures. Realistically, therefore, we could define the fracture hydraulic conductivity to be

$$K_f = \frac{(2b)^2 \rho g}{12\mu} \tag{22}$$

Finally, we discuss the meaning of the storage parameter for a fracture element. For a fracture element ℓ, if we neglect the compressibility of the rock grains, the quantity of water released from storage per unit change in pressure head is given by

$$M_{c,\ell} = \frac{d(V_{v,f}\rho)}{d\psi} = V_{v,f}\frac{d\rho}{d\psi} + \rho\frac{dV_{v,f}}{d\psi} \tag{23}$$

where $V_{v,f}$ is the volume of voids in the fracture element ℓ. However, for convenience, we may normalize $V_{s,f}$ with reference either to bulk volume $V_{b,f}$ or solid volume $V_{v,f}$ of the fracture element. If we are to normalize (23) with reference to $V_{b,f}$ and recognize that $p = \rho g\psi$, where p is pressure, we obtain,

$$M_{c,\ell} = V_{b,f}\,\rho g[n_f\beta + m_{v,f}] \tag{24}$$

where $n_f = V_{v,f}/V_{b,f}$ is "porosity" of the fracture element and $M_{v,f} = -dn_f/dp$ is the coefficient of volume change (Lambe and Whitman, 1969) of the fracture element.

Or, as has been done is TERZAGI in which the volume element is always defined as having the same volume of incompressible solids, it is more convenient to normalize (23) with reference to $V_{s,f}$. Thus,

$$M_{c,\ell} = V_{s,f}\rho g[e_f\beta + a_{v,f}] \tag{25}$$

where e_f is the void ratio of the fracture and $a_{v,f} = -de_f/dp$ is the coefficient of compressibility for the fracture. Note that whether one uses V_b with n and m_v, or one uses V_s with e and a_v, the final quantity $M_{c,\ell}$ is the same as long as one is consistent.

We note here that in the case of a volume element in a fracture, the element itself is made only of the voids. However, for convenience we may associate any arbitrary solid volume $V_{s,f}$ with the fracture and define a fictitious bulk volume $V_{b,f} = V_{s,f} + V_{v,f}$ for the fracture element. Since $V_{s,f}$ is arbitrarily chosen, we can, in fact choose it in such a fashion that e_f becomes exactly equal to 2b, tha fracture aperture. This can be achieved by letting $V_{s,f}$ numerically equal to A_f, where A_f is the surface area of the fracture wall. In this case,

$$e_f = \frac{A_f(2b)}{A_f} = 2b \tag{26}$$

If we use this procedure for $a_{v,f}$ in (25) we may use experimental data directly on fracture closure as a function of stress, i.e., $a_{v,f} = -d(2b)/dp$.

It is apparent from the foregoing that once we have defined the appropriate conductances for fracture-fracture, fracture-rock and rock-rock interfaces and have defined the physically appropriate storage parameters for volume elements in the fracture or in the rock, the solution of the discrete fracture problem merely reduces to solving (9) or (12) through direct or iterative techniques.

Systems idealized by double porosity: It is perhaps best to discuss the relation of the double porosity model to a simple idealized system of horizontal fractures as shown in Fig. 3. Consider a system of I horizontal fractures with spacing S. The thickness, H, of this system is given by $H = (I + 1)S$. It is clear that in this system water moves horizontally in the fractures and water drains vertically from the intervening blocks to the fractures bounding the matrix. We will now replace this system by two interacting continua, each of thickness H, one representing the flow phenomenon in the fractured milieu and the other, that in the matrix milieu. Obviously, the fracture continuum is characterized only by horizontal flows while the matrix continuum only by vertical flows.

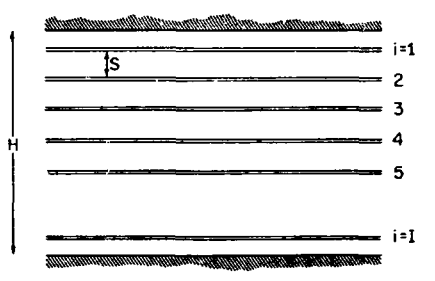

Fig. 3. System of horizontal fractures in a permeable medium. (XBL 809-2844)

If we assume that flow in the fracture obeys the cubic law, then the total horizontal flux in the horizontal direction in the layer equals I times the flux in each fracture. We may therefore define the average hydraulic conductivity, K_f^*, of the fracture continuum by,

$$K_f^* = \frac{I(2b)^3 \rho g}{12 \mu H} \tag{27}$$

Similarly if $S_{s,f}$ is the storativity for one fracture, then, $S_{s,f}$, the average storativity, for the fracture continuum is,

$$S_{s,f}^* = \frac{I(S_{s,f}(2b))}{H} \tag{28}$$

Since the fracture aperture is far smaller than the fracture spacing, $K_r^* \sim K$ and $S_{s,r}$, where K_r^* and $S_{s,r}^*$ are the average hydraulic conductivities and storativities of the rock continuum.

Consider an area A_f at the interface between a fracture and an adjoining matrix block. The flux from the block to the fracture is given by

$$w_{f,r} = \frac{K_r^* A_f}{0.5S} (\phi_r^* - \phi_f^*) \tag{29}$$

and the total flux from blocks to fractures is given by $Iw_{f,r} = (IK_r^* A_f/0.5S)$. In (29), ϕ_r^* and ϕ_f^* are average potentials in the element of each continuum.

If we consider two volume elements at a given location, one in the fracture continuum and one in the porous continuum, each element having an area of cross section A_f and height H, then $V_f^* = V_m^* = A_f H$. For each of these volume elements we may now write a conservation equation.

Fracture continuum element

$$\int_\Gamma (\rho K_f^* \nabla \phi_f^* \cdot \hat{n} d\Gamma) + \frac{\rho I K_r^* A_f}{0.5S} \cdot (\phi_r^* - \phi_f^*) = \rho V_f^* S_{s,f}^* \frac{\partial \phi_f^*}{\partial t} \tag{30}$$

Rock continuum element

$$\frac{-\rho I K_r^*}{0.5S} A_f (\phi_r^* - \phi_f^*) = \rho V_r^* S_{s,r}^* \frac{\partial \phi_r^*}{\partial t} \tag{31}$$

Noting that $V_r^* = V_f^* = A_f H$ and dividing through by V_f^* in (30) and V_r^* in (31) and letting the elements tend to zero in the limit, we now obtain the differential equation,

$$-\text{div}\, \rho K_f^* \hat{\nabla} \phi_f^* + \alpha K_m^* (\phi_m^* - \phi_f^*) = \rho S_{s,f}^* \frac{\partial \phi_f^*}{\partial t} \tag{32}$$

$$-\alpha K_r^* (\phi_r^* - \phi_f^*) = \rho S_{s,r}^* \frac{\partial \phi_r^*}{\partial t} \tag{33}$$

where

$$\alpha = \frac{2I}{0.5SH} = \frac{4}{S^2}.$$

Since $H = IS$, obviously α is a factor controlled by the spacing and the specific surface of the rock blocks. Note also that in the fracture continuum water flows within the continuum as well as across an imaginary interface to the matrix continuum. Hence, (32) has a source term as well as a divergence term on the left hand side. However, it is assumed that, due to the strong permeability contrast between the fracture and the blocks, flow of water within the blocks is restricted to lines normal to fracture-block interfaces. Hence, in (33) the divergence term is absent.

In view of (30) and (31) we may now proceed to apply (9) to a double-porosity system. First, we discretize the flow region into $i = 1, 2, 3, \ldots L$ subdomains to represent the elements of the fracture continuum with K_f^* and $S_{s,f}^*$ defined as in (27) and (28). For each of these subdomains we shall provide all required input data such as $G_{i,j}$, interior connection data, exterior connection data and bulk volumes so that one equation such as (9) can be developed for each of the L elements. Simultaneously we assume that at the location of each $i = 1,2,3,\ldots L$ fracture continuum element there exists a matrix continuum element $j = 1, 2, 3, \ldots L$ such that $V_i = V_j$ for $i = j$. In order to couple the two continua we will now connect, for each $i = j$, the fracture continuum element i with the matrix continuum element j in such a fashion that the conductance $U_{i,j}$ is given by,

$$U_{i,j} = \frac{I\rho K_r^* \Delta f_{i,j}}{d_{j,i}} = \frac{I\rho K_r^* A_f}{0.5S} = \rho V_r \alpha K_r^* \tag{34}$$

We thus end up with conservation equations for 2L volume elements in all, with one equation for each fracture-continuum and matrix-continuum element. Note that the time-constant for the respective elements shall be given by

$$\Delta t_{\text{stab},i} = \frac{V_f^* S_{s,f}^*}{\sum_m U_{i,m} + \sum_j U_{i,j}} \tag{35}$$

where i, m are fracture continuum elements, j is a matrix continuum element, and $j = i$ and

$$\Delta t_{\text{stab},j} = \frac{V_m^* S_{s,m}^*}{U_{i,j}} \tag{36}$$

where j is a fracture continuum elements, i is a matrix continuum element, and $j = i$.

Since the IFDM is so structured that the geometric quantities ($\Delta f_{i,m}$ and $D_{i,m}$) needed for computing the conductances are directly provided as input data, the handling of $V_r \alpha$ needed as input

for computing $U_{\ell,j}$ in (34) poses no special problem. Also, since the 2L simultaneous equations are formulated, they can be solved by the mixed explicit-implicit method. Indeed, since the double-porosity model gives rise to a stiff matrix (due to the *marked differences in the time-constants between* the fracture-continuum elements and the matrix-continuum elements), the mixed explicit-implicit method is particularly desirable for solution.

Comparison of IFDM with Other Approaches

Having described the utility of the IFD approach to handle a variety of fracture-simulation problems, it is of interest to see how this approach compares with other numerical techniques, notably, the conventional finite difference method (FDM) and the finite element method (FEM).

IFDM and FDM: The basic difference between these two approaches is that the latter is applied specifically to volume elements with faces perpendicular to the coordinate axes while the former is applied in general to arbitrarily shape elements. The reason for this is that the FDM seeks to directly approximate the partial differential equation, which includes second derivatives of potential in space. Note that the partial differential equation expresses the conservation law per unit volume of the volume element. This volume-normalization, coupled with the regular shape of the volume element helps obtain the second-derivatives in space. The IFDM, however, chooses not to use the volume normalization procedure and expresses the conservation law for arbitrary an volume element. Yet, if one applies the IFDM to a mesh involving regularly shaped volume elements, then the IFDM and FDM equations shall be identical except for division by the bulk volume. Thus, the FDM may be treated as a limiting case of the IFDM.

IFDM and the FEM: The conceptual similarity between these two techniques lie in the fact that both are integral methods in which intensive properties such as potential are expressed as averages over finite volume elements. However, these two methods differ a) in the manner of carrying out integration operations and b) in the approach employed for evaluating gradients of potentials. In order to compare the integration procedures adopted in the IFDM and the FEM, it is instructive to recall equations (9) and (12) that are central to the IFDM. For convenience, we may write (12) in matrix notation as

$$\sum_{m=1}^{L} A_{\ell m}\,\phi_m - \rho_\ell V_\ell S_{s,\ell}\,\frac{\Delta\phi_\ell}{\Delta t} = B_\ell \qquad (37)$$

where

$$A_{\ell,\ell} = \frac{1}{M_{c,\ell}}\left\{\sum_m U_{\ell,m} + \sum_m U_{\ell,b}\right\}$$

$$A_{\ell,m} = \frac{U_{\ell,m}}{M_{c,\ell}}$$

and

$$B_\ell = -\rho_\ell G_\ell + \sum_b U_{\ell,b}\phi_b$$

In (37) the $A_{\ell,m}$'s denote the conductances between elements ℓ and m. If an element ℓ communicates with an element m across some common interface then $A_{\ell,m} > 0$. Or else $A_{\ell,m} = 0$. Also, ρ_ℓ, V_ℓ, $S_{s,\ell}$ and B_ℓ are known, while ϕ_m is a function of initial conditions and the $\Delta\phi_m$ is the variable to be solved for. In setting up (37) a major task is to evaluate the coefficients $A_{\ell,m}$ and V_ℓ in order to set up the equations. Note that $A_{\ell,m}$ includes in itself certain geometric quantities in addition to the material properties. In the handling of the geometric quantities inherent in $A_{\ell,m}$ IFDM and FEM choose different approaches. Thus, the IFDM explicitly defines each volume element by defining its bounding surface segments and directly provides the required geometric inputs $\Delta\Gamma_{\ell,m}$ and $D_{\ell,m}$ required for computing $A_{\ell,m}$. On the other hand, the FEM, as it is commonly employed, chooses an indirect approach to achieve the same purpose. In the FEM, the geometric inputs consist of the coordinates of the nodal points as well as a description of the connectivity between specific nodal points. From this information the geometric quantities inherent in $A_{\ell,m}$ are generated through a process of weighted volume integration. A consequence of this approach is that one avoids the need to explicitly describe the surface segments $\Delta\Gamma_{\ell,m}$ between communicative volume elements. The volume elements are implicitly described, as it were. While this appears to be desirable in that one bypasses the need quantitatively for describing surface segments, the volume integration leads to a different type of computational requirement. That is, the volume integration requires the differential volume element of integration dV to have a simple geometrical shape such as a triangle, a rectangle, a toroid, a tetrahedron or a parallelipiped. As a result, the integration in the volume integral has to be expressed with reference to a specific coordinate system. In comparison, the IFDM evaluates each conductance term locally in a single one-dimensional form and hence is independent of any coordinate system. Thus, an important difference between the FEM and the IFDM is that in the former conductances are computed through a process of volume integration, while the latter the conductances are computed directly as a product of the required input data. While it would appear that the latter may require greater input effort, it must be stated that an ability to directly prescribe conductances in a simple fashion is extremely helpful in handling certain special cases. For example, such an ability is of help in connecting a well or a single fracture element to several matrix elements. Although one could handle this with the finite element method (e. g., Narasimhan et al., 1978) there is an extra effort involved in

implementing this with the FEM. Moreover, one could argue that by following the IFD approach one essentially removes the geometric aspects from the mainstream of calculations and in, certain cases, the geometric quantities could be computed with any desired degree of precision before one sets out to solve the conservation equations.

Apart from the integration aspect, the major difference between the IFDM and the FEM consists in the manner in which spatial gradients of potential are evaluated. In fact, it is in regard to this that one should really exercise judgement in choosing between the IFDM and the FEM for handling any given class of problems. As discussed by Narasimhan and Witherspoon (1976), the IFDM employs a simple finite difference approximation for measuring gradients. This demands that for measuring gradient along any given direction, one simply computes the slope in that direction. It follows that the finite difference approximation is capable of giving only one gradient measurement at a time.

Instead, in the FEM, an equation is set up for the variation potential within a region bounded by 3 or more nodal points and gradients are evaluated at any point and in any given direction by partially differentiating the surface fitting the potential variation. Herein lies the unique power of the FEM, which is especially useful when application of Darcy's law at an arbitrarily oriented surface in an anisotropic medium requires gradient of potential in more than one direction. Even here one could argue that one could interpolate the required additional gradients from associated finite difference gradients. However, an added advantage of the finite element approach is that by choosing a sufficiently large number of nodal points to fit the equation of the variation in potential, one could effectively introduce higher order terms in the expression for gradient, presumably increasing the accuracy of the evaluated gradients. Whether these higher order terms (which, incidentally lead to increased computational effort) lead ultimately to highly accurate solutions in all cases has not yet been firmly established, particularly for transient problems.

In summary, therefore, the differences between the IFDM and the FEM are limited to certain methods of implementing geometric operations. Awareness of these differences show that each of these methods offer unique flexibility and power to handle certain classes of problems. Both of them, used properly, can give results of comparable accuracy. For systems with isotropic materials or with very general three-dimensional configurations, the IFDM provides a model capable of handling complex geometries and variations in symmetry within the flow region. For systems with arbitrarily varying anisotropy or systems in which the mesh deforms in time, the FEM provides flexibility of computations. Indeed, it is possible, in principle, to combine these two methods of handling geometry into a well-organized, single computer program so that within the same flow region each method could be employed as needed for maximum efficiency.

A BRIEF DESCRIPTION OF PROGRAM TERZAGI

Before proceeding to substantiate the preceding theoretical discussions with illustrative examples, it is pertinent here to briefly describe the input organization of program TERZAGI. The input data of this one-, two-, or three-dimensional IFD program is organized into blocks, each block handling one category of information: control parameters (Block 1); material properties (Block 2); fluid properties (Block 3); volume element geometries (Block 4); internal surface connections (Block 5); external surface connections (Block 6); boundary potentials (Block 7); variable sources (Block 8); and initial conditions, constant sources and preconsolidation pressures (Block 9). While a detailed description of the program is out of place here, the following aspects should prove to be of interest to the reader:

- The solution is started with a small time-step and the time-step is increased gradually by not more than a factor of 2 at a time, depending on the progress of solution. Should the convergence be slow or the nonlinear parameters change too rapidly, the time-step is automatically cut down. If desired, the time-step can be manually controlled.

- The implicit solution process is achieved by a point-iterative scheme with an acceleration factor. The implicit weighing factor λ is varied during the solution from 0.57 to 1 depending on the maximum rate of change of potential, in order to minimize time integration errors. Options are available to override this by using forward-, central- or backward differencing modes.

- The required material properties include void ratio, effective stress, coefficient of compressibility, preconsolidation stress, absolute permeability, specific storage, etc. Some of this data could be mutually exclusive. The required fluid properties include fluid viscosity, density and compressibility.

- The required volume element properties include bulk volume, type of material contained, and average elevation.

- The required data for interior surface connections include the nodal point designations on either side of the interface, the distance between the nodal points, and the magnitude of the surface area.

- Material properties as well as boundary potentials and sources can all be functions of time or potential.

- The model uses the simple effective stress principle that change in effective stress is equal and opposite in sign to change in pore pressure.

Application to some Fractured Systems

We will now present some illustrative examples on the application of the IFDM to simulate fluid flow in fractured media. The list of these examples is as follows:

Porous Medium with Discrete Fractures: (1) Flow to a well intercepting a single horizontal fracture; (2) Flow to a well intercepting a single vertical fracture; (3) Pulse test in a well intercepting an inclined fracture; (4) Simulation of a hydraulic fracturing experiment; (5) Advective-diffusive transport in a fractured system with spherical particles.

Double Porosity Medium: (6) Flow to a well intercepting a system of horizontal fractures separated by porous blocks.

1. Flow to a well intercepting a single horizontal fracture. Consider a well of finite radius, r_w, fully piercing an aquifer with a horizontal fracture of radius r_f and width w (=2b). The well pumps at a constant rate Q, starting with hydrostatic initial conditions. The problem is to predict the evolution of fluid potential around the well. Gringarten and Ramey (1974) solved this problem analytically and obtained a solution assuming that the fracture is infinitely conducting and that the rate of flux is constant throughout the fracture. Furthermore, the presence of the well was ignored and the fracture was considered to be a discoidal source.

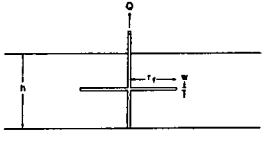

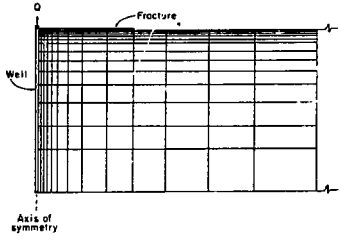

Fig. 4. Single horizontal fracture in permeable rock: problem description. (XBL 804-7003)

Bodvarsson and Narasimhan (manuscript under preparation) have studied a class of well-flow problems involving a horizontal fracture. The geometry of the system studied by them is given in Fig. 4. As a first step in their study they solved the problem of Gringarten and Ramey using the IFDM program TERZAGI. A comparison of their results with the analytic solution are presented (Fig. 5) in terms of the dimensionless time $T_{D_f} = K_z t/S_{s,r} r^2$ and dimensionless fracture pressure $P_D = (2\pi Krh\Delta\phi)/Q$, where K_r is the hydraulic conductivity of the aquifer, h is the aquifer thickness, $S_{s,r}$ is specific storage of the aquifer, and $\Delta\phi$ is the drawdown is potential in the fracture. As may be seen the agreement is excellent.

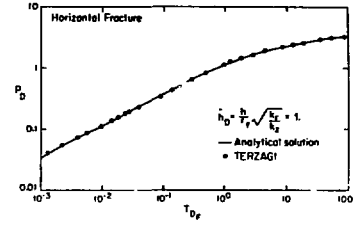

Fig. 5. Horizontal fracture problem: comparison of analytical and numerical results. (XBL 809-2843)

In a series of subsequent runs, the study was extended to finite-conductivity fractures in the pr ence of a realistic wellbore, within which fluid level changes with fluid production. The results of the studies (for which no analytical solution is available) is given in Fig. 6 in the form of a set of type curves.

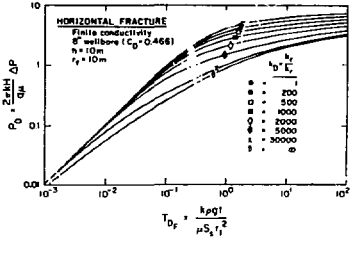

Fig. 6. Horizontal fracture problem: type curves for finite fracture conductivity (after Bodvarsson and Narasimhan, 1981). (XBL 804-6297)

2. Flow to a well intercepting a single vertical fracture. Narasimhan and Palen (1979) studied the problem of fluid flow to a well intercepting a single vertical fracture using the program TERZAGI. Both the well and the fracture fully pierce the aquifer. The geometry of the problem is given in Fig. 7. Analytical solutions have been presented in the literature for infinite conductivity (Gringarten et al., 1974) as well as for finite conductivity vertical fractures (Cinco-Ley et al., 1978). To validate their numerical model, Narasimhan and Palen used a mesh as given in Fig. 8. As shown in Fig. 9, they obtained excellent agreement with the analytical results of Cinco-Ley et al. (1978). The small departures for early time results for C_r = 1 and C_r = 0.2 are primarily due to well-bore storage effects, not considered in the analytical solution. The small departures for $T_{Df} > 8 \times 10^2$ observed with C_r = 0.2 or C_r = 1.0 are due to the closed external boundaries simulated in the numerical model.

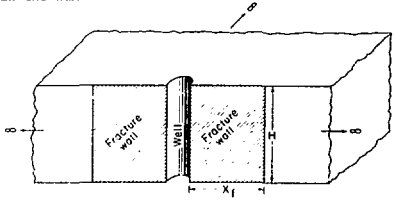

Fig. 7. Single vertical fracture in permeable rock: problem description.

(XBL 809-2845)

The numerical model is especially suited for simulating deformable fractures for which fracture permeability varies with fracture aperture. This problem is somewhat difficult to handle analytically due to the nonlinearity involved. The results of four cases of flow within a deformable fracture are presented in Fig. 10.

In Fig. 10, Curve 1 relates to a deformable fracture with an initial aperture w = 1 mm and x_f = 10m. The fracture deformability, quantified by $a_{v,f} = -de_f/dp = -d(2b)/dp$ is assumed to be 3.28×10^{-10} pascal^{-1} and fracture permeability is allowed to vary with aperture according to the cubic law. We will use this curve to be the standard against which we shall compare the remaining three cases.

Curve 2 represents the case in which all factors are the same as in Curve 1, but K_f is assumed to be constant, corresponding to the initial aperture of 1 mm and independent of fracture aperture. As one would expect, Curve 2 shows lesser values of P_D then Curve 1. Curve 3 incorporates the effect of a 0.1 m-radius well into the problem relating to Curve 1. The unit slope for $T_{Df} < 0.2$ represents

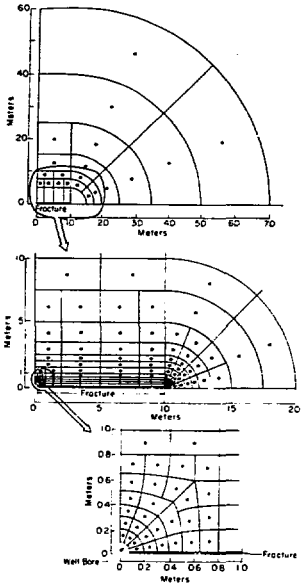

Fig. 8. Vertical fracture problem: mesh design. (Narasimhan and Palen, 1979).

(XBL 792-5744)

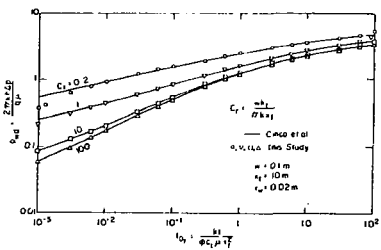

Fig. 9. Vertical fracture problem: comparison of numerical and analytical results (Narasimhan and Palen, 1979).

(XBL 792-5741)

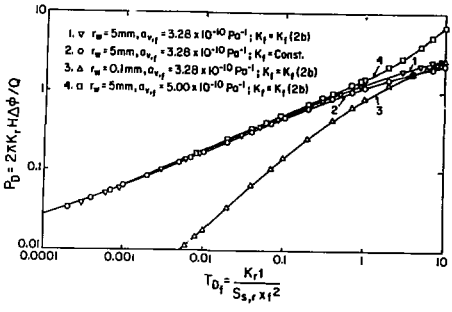

Fig. 10. Vertical fracture problem: effect of fracture deformation. (XBL 809-2841)

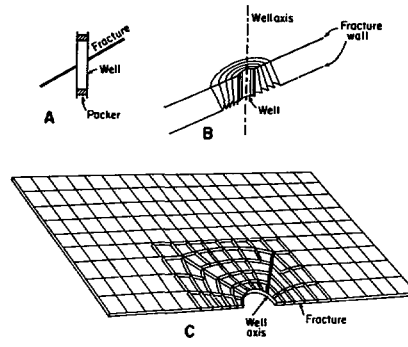

Fig. 11. Single inclined fracture in a permeable medium: problem description (Juprasert, personal communication). (XBL 810-2846)

withdrawal of fluid from storage. As is to be expected, for $T_{Df} > 10$, Curve 3 tends to merge gradually with Curve 1.

Curve 4 relates to a problem which was designed to study the effect of fracture compressibility on the pressure transient. In this case the fracture compressibility, $a_{v,f}$, was increased by 48 per cent from 3.28×10^{-10} Pa^{-1}. As seen from the figure, this solution begins to depart makedly from Curve 1 for $T_{Df} > 1.0$. The results show that the pressure transient is extremely sensitive to fracture compressibility of deformable fractures.

3. Pulse-test in a well intercepting an inclined fracture. For studying transient fluid flow in tight fractures, the method of pulse-testing is of interest (Wang et al., 1978). Unlike the conventional well test, the pulse test consists in packing of an interval of the formation, charging the well with a pulse of water at a pressure higher than the formation pressure and letting the pressure decay in the well as a function of time. Analytic solution to this problem with respect to a horizontal fracture in a tight rock has been discussed by Wang et al. Sirisak Juprasert (1979; personal communication) numerically studied the pulse-test problem for an inclined fracture using program TERZAGI. A major effort in this regard was to develop an IFDM mesh with associated geometric quantities. As shown in Fig. 11, the fracture plane is divided into a number of volume elements with the elements assuming radial shapes close to the well. In the immediate vicinity of the well elliptically shaped volume elements were designed to account for the fact that the well pierces the fracture plane in an oblique fashion. Using the mesh shown in Fig. 11, a number of runs were made with various fracture inclinations. Results from three of these runs are presented in Fig. 12. The results indicate that with higher fracture inclination, the pressure pulse dissipates faster in the wellbore. Conversely if one were to match data from an inclined fracture system against the horizontal fracture solution, one would overestimate the hydraulic conductivity of the fracture.

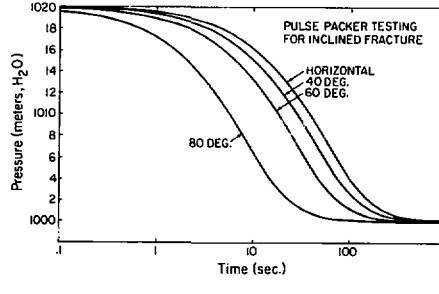

Fig. 12. Inclined fracture problem: solutions for various inclinations (Juprasert, personal communication). (XBL 809-2842)

4. Simulation of a hydraulic fracturing experiment. Since the late 1950's hydraulic fracturing of in situ rocks has been extensively used to stimulate oil and gas reservoirs through the creation of *massive* hydraulic fractures extending up to several hundred meters from the stimulated well. On a smaller scale, hydraulic fracturing experiments are also used to determine in situ rock stresses (e.g. Haimson and Fairhurst, 1970).

Palen (1980) adapted the TERZAGI model to analyze the pressure transient data from a hydraulic fracturing experiment in granite and to estimate the in situ stresses as well as the fracture parameters. The experiment was conducted at Monticello in South Carolina by the U.S. Geological Survey (Zoback, pers. com, 1979). The hydraulic fracturing was performed at a depth of approximately 300 m below surface over an interval 3 m. An oil-water mixture with a viscosity of 2.35×10^{-3} kg/m.sec (2.35 cp) was used as the injecting fluid. The well was of 0.1524 m (6 inches) diameter and communicated with surface injection equipment through a .0508 m (2.0 inches) diameter tubing. The actual experiment consisted of several injection cycles separating shut-in and bleed-off periods. For illustrative purposes, the observed injection rates and injection pressures are given in Fig. 13.

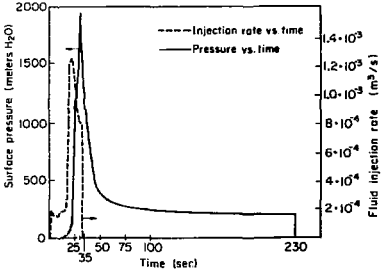

Fig. 13. Simulation of hydraulic fracturing: field data on injection rate and pressure (after Palen, 1980). (XBL 807-3481)

Numerical simulation of the hydraulic fracturing process requires the modeling of the energy build-up in the well itself, prior to the initiation of the fractures as well as the propagation of the fracture with time. The former aspect requires the treatment of the well as a volume element of the flow region and the latter requires an ability to handle time-dependent geometry, based on fracture extension. While the wellbore aspect is quite easily handled in the standard IFD formulation, appropriate criteria had to be incorporated into the algorithms to extend the fracture. Palen (1980) used two criteria to extend the fractures; (a) that the fluid pressure near the tip of the fracture be in excess of the least principal stress in the horizontal plane and (b) there be enough potential energy in the system to create new fracture surface to overcome the strength of the rock at the fracture tip. Assuming the fracture to grow in the shape of a "penny", and by adjusting initial fracture aperture, fracture compressibility, minimum in situ stress, and fracture toughness, the fit given in Fig. 14 was obtained. Independent estimates by Zoback (pers. com., 1979) suggests that the minimum principal stress estimated in the simulation closely matched Zoback's estimate.

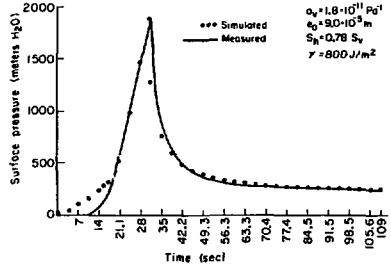

Fig. 14. Simulation of hydraulic fracturing: comparison of numerical results and field observations (after Palen, 1980). (XBL 807-3479)

5. Advective-diffusive transport in a fractured system with spherical particles. We shall now consider a general problem in which flow in the fracture as well as that in the rock matrix is considered in detail. Rather than the diffusion equation which has been of concern so far, we shall now consider an advective-diffusion problem.

Consider a set of parallel, uniform fractures separated by a distance S (Fig. 15). Water enters this semi-infinite region through the fracture at $z = 0$, at a constant velocity, v_f, and with a solute concentration $C(z = 0, t) = C_0 e^{-\lambda_d t}$ where λ_d is a decay constant. The solute is transported by advection and longitudinal dispersion, D_L, within the fracture and by diffusion perpendicular to the fracture interface into the rock matrix. Rasmuson and Neretnieks (1980) studied this problem analytically by assuming the rock blocks to be replaced by spherical particles of the same surface to volume ratio. The problem then can be expressed by two partial diferential equations, one for advective-dispersion in the fracture, the other for radial diffusion into the spheres. These two are coupled by the transfer of solute between the fracture and the sphere and are subject to the boundary condition, $C(z = 0, t) = C_0 e^{-\lambda_d t}$ and the initial condition $C = 0$ everywhere in the flow region.

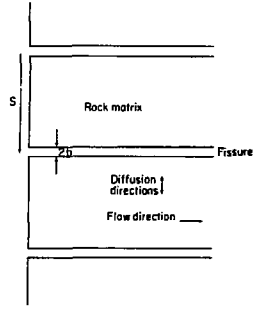

Fig. 15. Chemical transport in a fissured medium: problem description (after Rasmuson et al. 1980). (XBL-8010-2956)

Rasmuson et al., (1980) simulated the same problem with the IFD program TRUMP in order to validate the program. The problem considered was subject to the following parameters, considered to be realistic for geologic disposal of high level radioactive wastes: S = 1 m; D_L = 1.35 x 10^{-4} m^2/s; K, volume equilibrium constant = 10^4 m^3/m^3; D_p, diffusivity of rock matrix = 10^{-12} m^2/sec; v_f, velocity of fluid in the fracture = 3 x 10^{-7} m/sec, 2b = 10^{-5} m, and r_0, the radius of the spherical particle = 1.5 m. The decay constant used was λ_d = 2.311 x 10^{-9} $year^{-1}$, corresponding to a half-life of 3 x 10^8 years.

The problem was solved with 25 elements along the fracture with length varying from 15 m (10 elements), 30 m (10 elements) and 100 m (5 elements), and each spherical particle divided 15 concentric elements with Δ_r = 0.1 m. In Fig. 16, the numerical solution obtained with TRUMP for a point in the fracture at Z = 225 m is shown compared with the analytic solution. As can be seen, except for a slightly earlier breakthrough predicted by the numerical solution, the two solutions agree to within 10^{-3} per cent for most of the period simulated.

6. A double-porosity problem. The final illustrative problem is concerned with a fractured system idealized as an equivalent system of two interacting continua. To provide a physical feel for the illustration, we shall consider a system of 10 horizontal fractures, each with a uniform aperture of 10^{-4} m and separated by matrix slabs 1 m in thickness. The aggregate thickness of the rock and fracture is 10 m. If cubic law is assumed, each fracture has an absolute permeability of k_f = 8.333 x 10^{-10} m^2. But if we assume that the combined effect of the fractures can be replaced by a fracture continuum 10 m thick, then, the equivalent permeability of the fissured continuum amounts

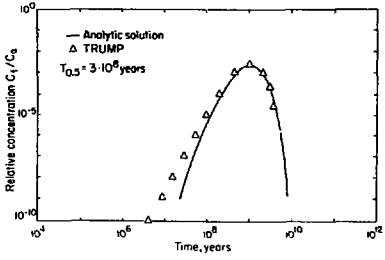

Fig. 16. Chemical transport in a fissured rock: comparison of numerical and analytical results (after Rasmuson et al. 1980). (XBL 809-2840)

to k_f^* = 8.333 x 10^{-14} m^2. Similarly, if the fracture compressibility is assumed negligible, the specific storage of the fracture continuum is approximately $S_{s,f}^*$ = 1 x 10^{-9} m^{-1} of water. It is reasonable to assume that the permeability of the matrix may be smaller than k_f^* by one to three orders of magnitude or more, while a value of 10^{-5} m^{-1} is reasonable for the specific storage of the rock, $S_{s,r}$.

Let us now consider the mechanics of fluid transfer between the fissured and the matrix continua. Obviously, in the actual problem, water will drain vertically from the matrix slab upward and downward into adjoining fractures, with the centerline of the slab forming a line of symmetry. If we consider a thin prism of a matrix slab with cross sectional area A, then the amount of water draining from a slab to one adjoining fracture is given by

$$Q_{f,r} = \frac{k_r \rho_r}{\mu} \cdot A \cdot \frac{\psi_r - \psi_f}{D_{f,r}} \qquad (38)$$

$$= \frac{k_r \rho g}{\mu} \alpha^* (\psi_r - \psi_f) \qquad (39)$$

where $\alpha^* = A/D_{f,r}$ and $D_{f,r}$ = 0.5 m. Now since each slab is doubly-draining, the actual volume of water transfer from a given prism of the matrix continuum of thickness H to the prism of fracture continuum at the same location is 20 times $Q_{f,r}$ and is equal to $(k_r \rho g/\mu)(20\alpha^*)(\psi_r - \psi_f)$.

It is of interest here to compare α^* with the geometric parameter often used to quantify the coupling term in the differential expression of the double-porosity model. For this, consider a prism of each medium at the same location, with cross sectional area A and height H, where H is the thickness of the media. Then, if we normalize α^* with

reference to bulk volume, we get a volume-normalized parameter related to α. That is, α has a dimension of reciprocal area and in the present case, α is related $1/(S)(H)$.

In order to solve this interacting-continua problem using TERZAGI, a problem that has been studied by Barenblatt et al (1960), Warren and Root (1963), Odeh (1965), and many others, was chosen. The problem involves a well piercing the fractured-continuum that is areally infinite. The well is produced at a constant rate Q. As has been done by Warren and Root (1963), this problem can be analyzed in terms of four dimensionless groups,

$$T^*_{D_f} = \frac{k^*_f \rho g t}{S^*_{s,f} \mu r_w^2} \tag{40}$$

$$P^*_{D_f} = \frac{2\pi k^*_f \rho g \Delta\psi}{Q\mu} \tag{41}$$

$$\lambda = \alpha r_w^2 \frac{k_r}{k^*_f} \tag{42}$$

and

$$\omega = \frac{S^*_{s,f}}{S^*_{s,f} + S_{s,r}} \tag{43}$$

The problem was studied using TERZAGI. A number of runs were made to study the effect of varying λ, ω and the magnitude of wellbore storage capacity. In addition, one run was made with spatially varying k^*_f to consider "skin" effect near wellbore as well as increased fracture intensity beyond about 110 m from the well axis. The results are summarized in three double-logarithmic plots, Figs. 17, 18, and 19.

In Fig. 17 the double porosity results are compared with the Theis solution for three values of λ. Increasing λ implies increasing matrix permeability. In the numerical model a 0.1 m radius well was assumed. In order to approximate the line source solution, the well was assumed to be packed-off and hence deriving storativity purely from water compressibility. In one case the well was assumed to have a fluctuating free surface. In the former case, the capacity of the wellbore was assumed to be 10^{-6} m^3 of water per meter of head change while in the latter it was $(0.1)^2\pi$. As can be seen from Fig. 17, the different cases clearly show effects of delayed drainage from the blocks in the range $10^1 < t_{D_f} < 10^6$, when the wellbore storage is small. It is, however, interesting to note that a realistic wellbore radius of 0.1 m with free fluid surface in the well gives a solution which totally masks all the effects that one could hope to see due to variable λ or, equivalently, variable matrix permeability.

Study of the double-porosity system by many workers has showed that the late-time behavior of the system is dominated by the combined storativities of the matrix and the fractured media while the intermediate-time behavior is influenced by ω, *the ratio of the fissure storativity to matrix* storativity. In Fig. 18, two cases are compared, $\omega = 10^{-4}$ and $\omega = 10^{-2}$. As should be expected, the late-time solutions for these two cases are distinct from each other.

The final case shown in Fig. 19 was actually chosen to illustrate the generality of the numerical approach over the analytical approach. In a general integral, numerical model, the system is described as a complex of several isolated continua, each interacting with the other. Insofar as the numerical approach is concerned, the double-porosity

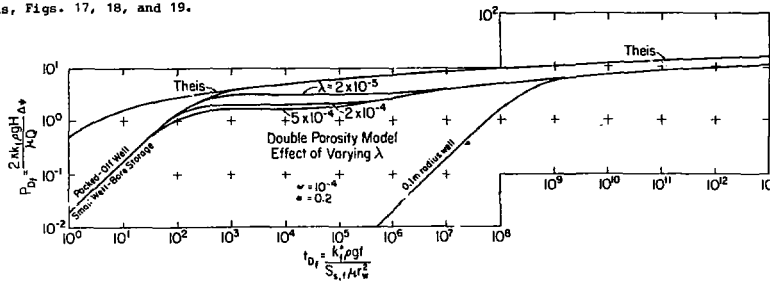

Fig. 17. Simulation of a double-porosity medium: effect of varying λ. (XBL 810-2849)

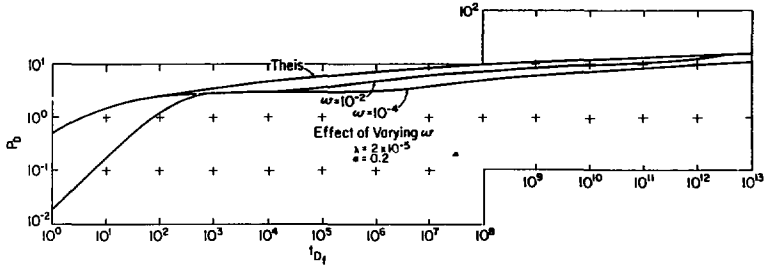

Fig. 18. Simulation of flow in a double-porosity medium: effect of varying ω. (XBL 810-2848)

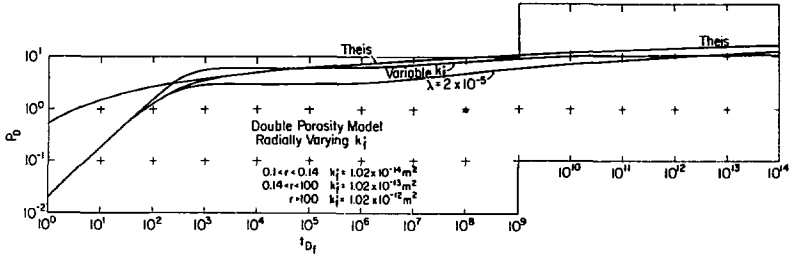

Fig. 19. Simulation of a double-porosity medium: effect of spatially varying permeability. (XBL 810-2847)

problem is a simplified special case which can be handled with ease. The case considered in Fig. 19 considers the fissure-continuum to have radially varying k_f^a, to simulate the existence of a low-permeability skin close to the well and to account for increased permeability due to fracturing beyond about 100 m from the well.

As can be seen from Fig. 19, the presence of the low-permeability skin causes much higher drawdowns than the $\lambda = 2 \times 10^{-5}$ case, after $t_{D_f} \sim 10^2$. For $r > 100$ m, the two cases have identical parameters except for the skin. Detailed study of the printouts showed that the pressure transient extended beyond about 100 m for $t_{D_f} > 10^{10}$. As a result, the variable k_f^a flattens markedly after that time and eventually crosses the $\lambda = 2 \times 10^{-5}$ curve at $t_{D_f} \sim 10^{12}$.

CONCLUSIONS

The Integral Finite Difference Method (IFDM) combines the power of an integral formulation with the simplicity of finite-difference gradients to constitute a powerful tool for simulating fluid flow in a variety of fractured rock systems. The conventional finite-difference method is a subset of the IFDM and is included in it as a limiting case. The principal difference between the IFDM and the Finite-Element Method (FEM) lies in the ability of the latter to facilitate generalized gradient evaluations. A unique feature of the IFDM is that the information required to generate conductances between communicating volume elements are handled as input in a simple fashion. This feature provides unique advantages in handling heterogeneous systems such as fractured porous media with sharply-varying material properties.

Insofar as simulating fluid flow in fractured systems is concerned, we do possess fairly sophisticated abilities. The chief problem that now confronts us is that of obtaining the relevant data from the field to provide input to the computational model. The information required to be handled for characterizing all the discrete fractures of even a small system is too voluminous and difficult to obtain. To minimize this problem one may desire to replace the discrete system with an equivalent macroscopically average system. While such equivalent systems are conceptually interesting, they have two disadvantages when one desires to utilize them in situations where a high degree of certainty is desired (e.g., radioactive waste isolation). The first is that very little is known as yet about the quantitative relationships that exist between the small- and large-scale parameters. Secondly, by their very nature, the macroscopic parameters possess inherent uncertainty or imprecision about them. This may suggest that these parameters cannot be expected to answer questions beyond a certain level of accuracy. In regard to waste isolation, the required degree of precision may be finer than the uncertainties associated with the macroscopic parameters.

ACKNOWLEDGEMENTS

In obtaining the various results presented in this paper, I have had many interesting discussions with the following colleagues to whom my sincere thanks are due: G. Bodvarsson, S. Juprasert, W. A. Palen, A. Rasmuson, and J. S. Y. Wang. This work was supported by the Division of Geothermal Energy, U. S. Department of Energy under contract W-7405-ENG-48.

REFERENCES

Barenblatt, G. E., I. P. Zheltov, and I. N. Kochina, "Basic concepts in the theory of homogeneous liquids in fissured rocks." J. Appl. Math Mech. 24 5., 1286-1303, 1960.

Gringarten, A. C., P. Samaniego, and N. Dominguez, "Transient behavior for a well with a finite conductivity vertical fracture. Paper SPE 6014, 51 Annual Meeting, Soc. Pet. Eng. AIME, 1976.

Carslaw, H. S., Heat transfer calculations by finite differences. Int'l Text Book Co., Scranton, Pennsylvania, 1961.

Edwards, A. L., "TRUMP: A computer program for transient and steady state temperature distributions in multidimensional systems." Rept. UCRL 14754, Revision III, National Technical Information Service, Springfield, VA., 1972.

Gringarten, A. C. and H. J. Ramey, Jr., "Unsteady-state pressure distributions created with a single horizontal fracture, partial penetration or restricted entry." Soc. Pet. Eng. J., Aug. 1977, 413-426.

Haimson, B. and Fairhurst, C., "In situ stress determination at great depth by means of hydraulic fracturing." in Rock Mechanics: Theory and Practice, Proc. Eleventh Intl. Symp. on Rock Mech., W. H. Somerton, ed., 1970.

Lippmann, M. J., C. F. Tsang, and P. A. Witherspoon, "Analysis of the response of geothermal reservoirs under injection and production procedures, Paper No. SPE 6537, Soc. Pet. Eng. AIME, 47th Calif. Annual Meeting, Bakersfield, Calif., 1977.

Macneal, R. H., "An asymmetrical finite difference network." Quart. Appl. Math., 11, 295-310, 1953.

Narasimhan, T. N. and W. A. Palen, "A purely numerical approach for analyzing flow to a well intercepting a vertical fracture." Preprint No. 7983, Soc. Pet. Eng. AIME, California Regional Meeting, Ventura, April, 1979.

Narasimhan, T. N. and P. A. Witherspoon, "An integrated finite-difference method for analyzing fluid flow in porous media." Water Resources Res., 12(1), 57-643, 1976.

Narasimhan, T. N., P. A. Witherspoon, and A. L. Edwards. "Numerical model for saturated-unsaturated flor in deformable porous media, Part 2: the algorithm." Water Resources Res., 14(2), 255-261, 1978.

Neuman, S. P. and T. N. Narasimhan, "Mixed explicit-implicit iterative finite element method for diffusion-type problems, Part I. Theory." Int. J. Num. Meth. in Eng. 11, 309-323, 1977.

Odeh, A. S., "Unsteady behavior of naturally fractured reservoirs." Soc. Pet.Eng. J., Sept. 1965, 245-

Palen, W. A., "The roles of fluid pressure and fluid flow in the hydraulic fracturing process." Ph.D. dissertation, Dept. of Mechanical Eng., Univ. of California, Berkeley, June 1980.

Pruess, K., and R. C. Schroeder, SHAFT79, User's Manual, Rept. LBL-10861, Lawrence Berkeley Laboratory, Berkeley, California, March 1980.

Rasmuson, A., T. N. Narasimhan, and I. Neretnieks, "Chemical transport in a fissured rock: validation of a numerical model." Manuscript in preparation.

Rasmuson A. and I. Neretnieks, "Exact solution of a model for diffusion in particles and longitudinal dispersion in packed beds." Am Inst. Chem. Eng. J., in press, 1980.

Wang, J. S. Y., T. N. Narasimhan, C. F. Tsang, and P. A. Witherspoon, "Transient flow in tight fractures." Proc. Invitational Well Testing Symposium, Report No. LBL-7027, Lawrence Berkeley Laboratory, Berkeley, California, pp. 103-116, 1977.

Warren, J. E. and P. J. Root, "The behavior of naturally fractured reservoirs." Soc. Pet. Eng. J., Sept. 1963, 245-255.

Witherspoon, P. A., J. S. Y. Wang, K. Iwai, and J. E. Gale, "Validity of cubic law for fluid flow in a deformable rock fracture." Water Resources Res., 1980 (in press).

FLOW IN FRACTURED POROUS MEDIA

James O. Duguid
Office of Nuclear Waste Isolation
Battelle Memorial Institute
Columbus, Ohio 43201

SUMMARY

The equations governing fluid flow through fractured porous media consist of two equations of motion and two continuity equations. These equations are coupled by an interaction term that represents the mass flux of fluid from the primary pores into the fractures. Numerical (finite element) solution of the governing equations was used to investigate the relative magnitude of some of the terms of the equations. The acceleration term in the equation of motion for the fractures was found to be small and for the cases investigated can be neglected. Elimination of this acceleration term allows the governing equations to be greatly simplified, a simplification that allows for the numerical solution of the governing equations on a larger region.

INTRODUCTION

The formulation of a theory for flow in fractured porous media is hampered by the range in size of the openings found in the medium. The primary pores, which were formed during deposition or crystallization, are small; however, they make up roughly 10% of the volume of the medium. The fractures (or joints), which are formed after deposition or crystallization, are large, widely spaced conduits constituting less than 1% of the volume of the medium. The magnitude of the permeability, which is dependent on the size of openings, is larger for the fractures than for the primary pores. This produces a larger fluid flow in fractures. Thus, in fractured porous media, the fractures (a relatively small volume of the medium) carry the bulk of the fluid flow through the medium.

Based on the frequency of fractures relative to the extent of the formation, an investigator can formulate the governing equations in two ways: (1) using the continuum approach when a representative elemental volume can be defined that is small as compared to the extent of the region under investigation and (2) using the discrete fracture approach, where the fracture is composed of parallel plates, when the fracture spacing is large as compared to the region under investigation. The primary pores can be treated as a continuum for either approach.

The equations discussed in this paper were formulated using the continuum approach. The details of their formulation can be found in Duguid and Lee[3]; Duguid and Abel[2]; and Duguid and Lee[4].

DISCUSSION OF RESULTS

Equations

The governing set of equations, formulated in detail in Duguid and Lee[4] are:

$$\bar{V}_{1s} = -\frac{K_1}{\mu}\nabla\sigma_1$$

$$(1-\phi_2)\phi_1\beta\frac{\partial\sigma_1}{\partial t} + (1-\phi_2)\phi_2\beta\frac{\partial\sigma_2}{\partial t} + \frac{\Gamma}{\rho} + \nabla\cdot\bar{V}_{1s} = 0$$

$$\bar{V}_{2s} = -\frac{\bar{\bar{K}}_2}{\mu}\cdot\left[\nabla\frac{\partial\bar{V}_{2s}}{\partial t} + \nabla\sigma_2\right] \qquad (1)$$

$$(1-\phi_1)\phi_1\beta\frac{\partial\sigma_1}{\partial t} + (1-\phi_1)\phi_2\beta\frac{\partial\sigma_2}{\partial t} - \frac{\Gamma}{\rho} + \nabla\cdot\bar{V}_{2s} = 0$$

where:

- K_1 is the intrinsic permeability of the primary block (scalar),
- $\bar{\bar{K}}_2$ is the intrinsic permeability tensor for the fractures,
- t is time,
- $\bar{V}_{1s}$ is the flux of fluid relative to solid in the primary pores,
- $\bar{V}_{2s}$ is the flux of fluid relative to solid in the fractures,
- β is the coefficient of compressibility of water,
- Γ is the fluid interaction term,
- μ is the coefficient of fluid viscosity,
- ρ is the fluid density,
- σ_1 and σ_2 are the incremental pressures in the primary pores and fractures, respectively, and
- ϕ_1 and ϕ_2 are the primary and fracture porosities, respectively.

The fluid interaction term describes the transient mass flux of the fluid out of the primary blocks and into the fractures (Duguid and Lee[3]). This interaction is expressed as:

$$\Gamma = \frac{4K_1\phi_2\rho}{\pi c^2\mu}(\sigma_1 - \sigma_2)\left[1 + \sum_{n=1}^{\infty} e^{-D}\right] \qquad (2)$$

$$= \alpha(\sigma_1 - \sigma_2)$$

where:

$$D = \frac{K_1 n^2 \pi^2 t}{2\phi_1\beta\mu\ell^2}$$

- c is the half-width of an average fracture,
- ℓ is the characteristic half-dimension of a primary block, and
- t is the elapsed time.

Equations (1) are six equations in six variables for a two-dimensional space. The variables are pressure in the primary pores, pressure in the fractures, and two components of flux in both the primary pores and the fractures. This system may be reduced to four equations by elimination of the

term $\bar{v}_{1s}$ between the first two equations of the system. The reduced system may be used for problems where the Dirichlet boundary conditions are given in terms of pressure. If the boundary conditions are given in terms of discharge, the division of discharge between the primary pores and the fractures must be known, or all six equations must be used. If all six are retained, a boundary condition or flux may be used.

The numerical solution of equations (1) was achieved using the Galerkin finite element method. The theoretical formulation of the Galerkin finite element method for this system of equations is presented by Duguid and Abel[2].

Constant Discharge Problem

For the constant discharge problem a fractured porous aquifer is intersected by a stream and is initially at equilibrium with the stream. At time t = 0 the stream level is assumed to decrease in such a way that the total discharge from the aquifer is constant. The first response is assumed to occur in the fractures. The aquifer is confined above by an impermeable formation and is semiconfined below. The leakage along the lower boundary is assumed to occur in both the primary pores and the fractures (Fig. 1). This problem of lowering of stream level is not likely to occur in nature, but the problem is of interest to investigate the division of discharge between the primary pores and the fractures.

$$w_1 = \frac{-K_1'\sigma_1}{d'\mu}\left(1 + \sum_{n=0}^{\infty} e^{-(K_1'n^2\pi^2 g/2d'^2\mu\phi_1'\beta)}\right)$$

$$w_2 = \frac{-K_{zz}'\sigma_2}{d'\mu}\left(1 + \sum_{n=0}^{\infty} e^{-(K_{zz}'n^2\pi^2 t/2d'^2\mu\phi_2'\beta)}\right)$$

where d is the thickness of the aquifer and the coefficients with prime superscripts refer to properties of the lower semifonfining unit. The leakage boundary conditions were obtained from the solution of the one-dimensional storage equation in the lower unit (Bredehoeft and Pinder[1]). The material properties used in the numerical solution of this problem are:

$c = 1.6 \times 10^{-3}$ ft	$\alpha = 5.95 \times 10^{-14}$
$d = 40.0$ ft	$\beta = 2.50 \times 10^{-8}$ ft^2/lb
$d' = 100.00$ ft	$\mu = 2.74 \times 10^{-5}$ lb-sec/ft^2
$K_1 = 1.5 \times 10^{-14}$ ft^2	$\rho = 1.94$ lb-sec^2/ft^4
$K_1' = 2.74 \times 10^{-16}$ ft^2	$\phi_1 = 0.29$
$K_{xx} = 4.5 \times 10^{-12}$ ft^2	$\phi_1' = 0.25$
$K_{zz} = 4.0 \times 10^{-12}$ ft^2	$\phi_2 = 0.005$
$K_{zz}' = 2.74 \times 10^{-14}$ ft^2	$\phi_2' = 0.0025$
$\ell = 1.0$ ft	

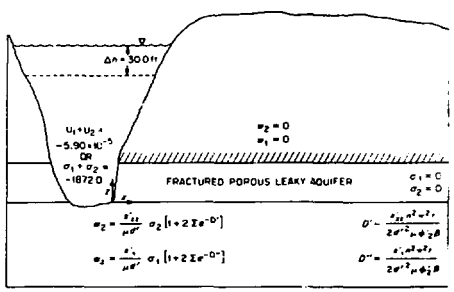

Fig. 1. Physical Interpretation of Boundary Conditions

The boundary conditions for the problem are:

$x = 0 \quad t = 0 \quad u_2 = -5.90 \times 10^{-5}$ ft/sec

$x = 0 \quad t > 0 \quad u_1 + u_2 = -5.90 \times 10^{-5}$ ft/sec

$x \to$ large $t > 0 \quad \sigma_1 = \sigma_2 = 0$

$z = d \quad t > 0 \quad w_1 = w_2 = 0$

$z = 0 \quad t > 0$

The solution of this problem indicated that the incremental pressure in the primary pores is approximately the same as the pressure in the fractures. The pressure in the fractures was observed to be slightly lower than the pressure in the primary pores, and the first response occurs in the fractures. This result is attributed to the large size of the fractures as compared to the primary pores.

The solution for horizontal flux in the primary pores and the fractures at the outflow surface is shown in Fig. 2. From this figure it is observed that the components of horizontal flux are approximately constant for all time. The variation

of flux in the primary pores is attributed to the initial assumption of zero flux. Another result that may be obtained from Fig. 2 is the ratio of flux in the primary pores to flux in the fractures is proportional to the respective ratios of horizontal permeability.

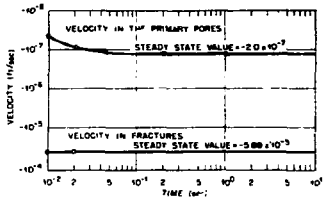

Fig. 2. Velocity at the Outflow Surface for Constant Discharge

Figure 2 also indicates that, for the material properties used, the acceleration term in the equation for flow in the fractures can be neglected in constant discharge problems.

Step Drawdown Problem

The step drawdown problem is identical to the constant discharge problem except that a step decrease in pressure is assumed at the outflow surface. At time t = 0, the stream level is assumed to decrease instantaneously by 30 ft. (Fig. 1.).

The boundary conditions at the outflow surface are expressed as:

$x=0 \quad t=0 \qquad \sigma_2=-1872.0 \text{ lb/ft}^2$

$x=0 \quad t>0 \qquad \sigma_1+\sigma_2=-1872.0 \text{ lb/ft}^2$

The solution for incremental pressure at a point 30 ft. in from the outflow surface is shown in Fig. 3. The incremental pressure in the fractures is lower than the pressure in the primary pores (i.e., a greater negative value). Figure 3 shows that the incremental pressure and the pressure gradient in both the primary pores and the fractures are nearly equal.

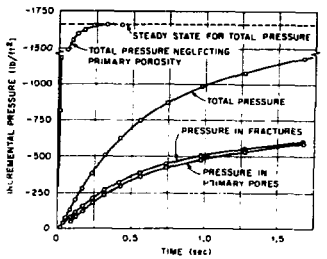

Fig. 3. Incremental Pressure 30 ft from Outflow Surface for Step Drawdown

The solution of this problem was used to investigate the magnitude of the acceleration term that appears in the equation of motion of fluid in the fractures. For step drawdown this term should have its greatest effect as a result of the rapid change of flux over a relatively short time interval. The solution of this problem was obtained both with and without the accereration term, and the solutions were compared at all nodal points within the domain. Only a negligible difference in the total pressure and in the pressure in the fractures was observed at any node.

Because the primary permeability is low, an investigator might be tempted to neglect the flow in the primary pores. This has the effect of terminating the supply of fluid to the fracture and results in a rapid aquifer response (the uppermost curve in Fig. 3).

CONCLUSIONS

From the solution of the constant discharge problem it was observed that the division of discharge between the fractures and the primary pores is proportional to the ratio of their respective horizontal components of permeability. This ratio is apparent theoretically if the acceleration term in the equation of motion for fluid flow in the fractures is neglected and the respective pressure gradients are approximately equal.

From the solution of the step drawdown problem, it was found that the acceleration term for fluid flowing in the fractures is small and can be neglected. The pressure and the pressure gradient in the fractures were also found to nearly equal to the pressure and pressure gradient in the primary pores, respectively.

Based on these conclusions the system of six equations can be reduced to a set of two equations that describe the pressure in the primary pores and the pressure in the fractures. The division of discharge between the fractures and the primary pores can be formulated from knowing that the ratio of primary discharge to fracture discharge is proportional to the ratios of the respective horizontal components of permeability. The reduced set of equations lend themselves to use on quasi three-dimensional regional flow problems (two-dimensional flow in a leaky aquifer).

The rapid response in the fractures when the influence of the primary pores is neglected shows that the primary pores cannot be neglected. This is especially true for interpretation of rapid drawdown tests. More flow simulations are needed over a range of permeabilities and porosities to determine whether very small values of primary permeability can be neglected.

REFERENCES

1. Bredehoeft, J., and Pinder, G., "Digital Analysis of Areal Flow in Multiaquifer Groundwater Systems: A Quasi Three-Dimensional Model", Water Resources Research, 6(3), 883-888, June 1970.

2. Duguid, J.O. and Abel, J.F., "Finite Element Galerkin Method for Analysis of Flow in Fractured Porous Media", in Finite Element Methods in Flow Problems, ed. by J.T. Oden, O.C. Zienkiewicz, R.H. Gallagher, and C. Taylor,

University of Alabama, UAH Press, Huntsville, 599-615, 1974.

3. Duguid, J.O. and Lee, P.C.Y., "Flow in Fractured Porous Media", Research Report 73-WR-1, Dept. Civil and Geological Engineering, Princeton University, 101p., May 1973.

4. Duguid, J.O. and Lee, P.C.Y., "Flow in Fractured Porous Media", Water Resources Research, 13(3), 558-566, June 1977.

AN EXAMPLE OF ROCK FRACTURE CHARACTERIZATION FOR MODELING PURPOSES

Richard K. Thorpe
Earth Sciences Division
Lawrence Berkeley Laboratory
University of California
Berkeley, California 94720

INTRODUCTION

The spatial definition of geologic discontinuities in a rock mass is an important part of the modeling process. This paper illustrates the type of observational information available to the analyst and how it can be developed. The example for the discussion is the characterization of natural fracturing around the "Time-Scale" Heater Experiment at the Stripa Mine in south-central Sweden.[1] This experiment is one of several field tests in the Swedish-American Co-operative Waste Storage Research Program[2] that focus on the thermomechanical aspects of potential nuclear waste storage in crystalline rock. It is intended that the information presented here will be incorporated into numerical models of the local rock mass in the future.

SITE DESCRIPTION

A general description of the geology and fracture system at Stripa is given by Olkiewicz, et al.,[3] and only a brief summary is supplied here. Situated in south-central Sweden, the Stripa iron ore body lies in a synclinal formation of leptite, which is a gray to brownish metavolcanic rock of Precambrian age. The syncline plunges 20° to the northeast, and the underground site is in fine-grained granite in contact with the northwestern limb. The granite post-dates the leptite, and may be associated with several post-orogenic Precambrian plutons in the region. Fracturing in the test area, located at a depth of about 335 m, is pervasive, yet the absence of gneissic structures suggests that tectonism since the intrusion has been relatively mild.

METHODOLOGY AND RESULTS

Two approaches are used here to characterize the local fracture system. First, major discontinuities are identified in the test area so that they can be modeled as discrete elements of weakness. While these features probably have a major role in the rock mass behavior, they comprise only a small percentage of the fracturing. Most of the other fractures are discontinuous in their own planes, hence the second aspect of the characterization involves defining all fracturing in terms of orientation, spacing, and length of joints. While it is impracticable to define or model such ubiquitous joints as they actually exist, a stochastic representation should be possible. Compatibility of the two sets of results will be demonstrated.

Characterization of Major Discontinuities

The success to which major discontinuities can be delineated within a rock mass depends on their continuity and the quality of subsurface information from which they are to be identified. Surficial mapping is an aid in assessing the continuity of fractures, and at Stripa, the walls and floors of the heater experiment drifts have been mapped in detail to show all fractures longer than about 0.3 m. The outcrops of features were mapped at a scale of 1:20, using a 1-by-1 m reference grid painted on the rock surface. Information such as rock type variations, fracture fillings, or clear signs of faulting was noted during the mapping. The detailed fracture map developed in this manner for the time-scale drift floor is shown in Fig. 1.

Heaters for the experiment are placed 10 m below the drift floor, therefore only the most prominent and continuous features in the map are likely to extend through the heated region and affect the rock mass behavior. Accordingly, only the prominent faults striking transverse to the drift were extrapolated downward and correlated with features in the borehole fracture logs. The correlation of the features was based on observational evidence; i.e., similarity of orientations, coatings, and surface characteristics and proximity to the extrapolated position. Other significant discontinuities may exist near the heaters and not intersect the drift, however, none could be identified with confidence using the observational technique. Results of the discrete characterization are illustrated by Fig. 2, which shows the inferred profile of four shear surfaces that pass through the heater array. These features offset or truncate other discontinuities, and the r filling minerals of chlorite, calcite, epidote, and clay are several times thicker than the fillings of other fractures. Fault number 3, which is the most prominent and well-defined of the set, apparently offsets a 20 cm-wide pegmatite dike as shown in the figure. The three-dimensional configurations of these faults can be represented by a series of contiguous triangular surfaces, the vertices of which are the actual borehole intercepts of the faults.

Characterization of Jointing

In order to describe the abundant jointing between the major features, it is preferable to adopt a statistical approach that incorporates both borehole and surficial data. The important parameters are the dominant joint orientations, i.e., joint sets, and the distributions of joint spacings and trace lengths. Fracture logs of the oriented core from the instrumentation boreholes in the time-scale experiment supplied orientation and spacing data. Figure 1 yielded trace length information.

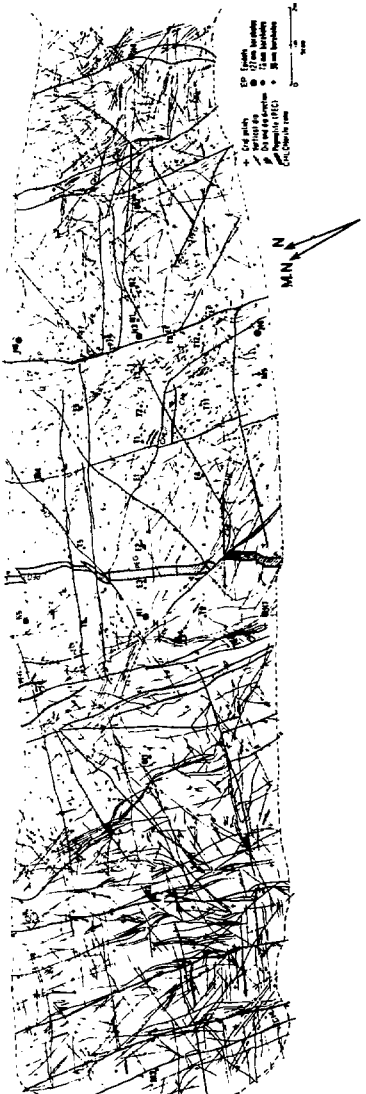

Fig. 1. Detailed fracture map of the floor of the time-scale experiment drift.

The jointing can be separated into four distinct sets according to the pole clusters in Fig. 3. Assigning these set designations to fractures in Fig. 1 allows a compilation of trace lengths to be made. A typical histogram of the data for one joint set is shown in Fig. 4. When these values are plotted in lognormal probability form, the cumulative frequency distributions in Fig. 5 are obtained. The least-squares linear fit through each distribution is of the form

$$\log x = \overline{\log x} + K \cdot \sigma_{\log x} \qquad (1)$$

where x is the trace length in meters, $\overline{\log x}$ is the logarithmic mean and $\sigma_{\log x}$ is the standard deviation. K is related to the normal probability function by

$$P(X>x) = (1/\sqrt{2\pi}) \cdot \int_{-\infty}^{K} \exp(-k^2/2)dk \qquad (2)$$

where P(X>x) is the probability of exceeding the value x.

Joint spacing distributions can be described in a similar manner by assigning appropriate set designations to fractures logged in the boreholes. Vertical spacings are then computed as the distance between consecutive fractures of the same set. Fig. 6 is a lognormal probability plot of the data with the respective distribution equations shown.

Several errors are inherent in the above approach. First, inclined fractures are underrepresented by vertical boreholes.[4] This bias could be reduced by incorporating the floor map in the spacing analysis. For the data presented here, the spacing normal to joints is found by multiplying the vertical spacing by the cosine of the mean dip angle of the set. Similarly, horizontal features are missing from the floor map, hence their length distributions are not given. Also, there are biases in the trace length data caused by (a) the minimum length of fractures that were mapped (0.3 m) and (b) the dimensions of the drift. These biases prevent the distributions from being used to predict extreme values outside the range of data upon which they are based.

DISCUSSION

The virgin state of stress has been measured in the underground test site,[5] and this information helps to validate the above findings. Fig. 7 is a stereographic plot of the principal stresses and the mean pole directions to the four fracture sets in the time-scale experiment. The pole of joint set 1, $\hat{n}_1$, corresponds to that of the four faults traced through the rock mass. Resolving the principal stresses into shear and normal components on the mean fault plane, as shown in Fig. 8 yields a theoretical shearing azimuth of 242°. The azimuth of slickensiding on the faults was measured as 240° by field observation and inspection of the fracture intercepts in the core.[1] Reconstruction of the inferred configuration of the fractures by orthographic projection and physical modeling shows the intercept

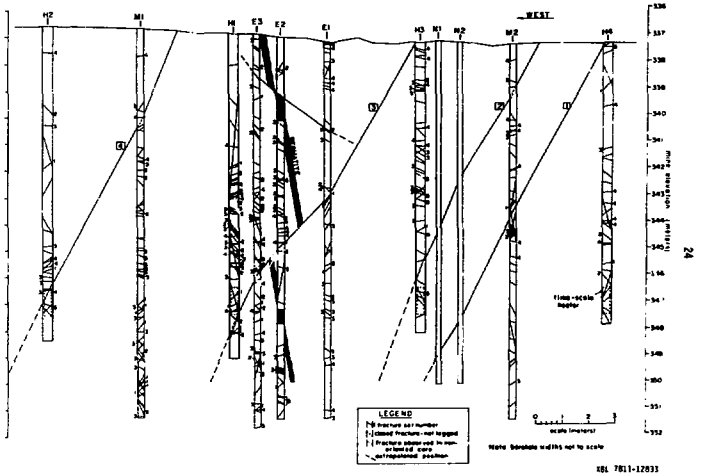

Fig. 2. Subsurface profile of fractures along centerline of time-scale drift.

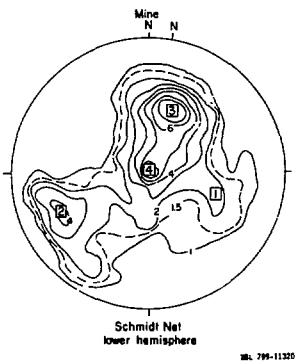

Fig. 3. Stereonet plot of fractures poles for time-scale experiment.

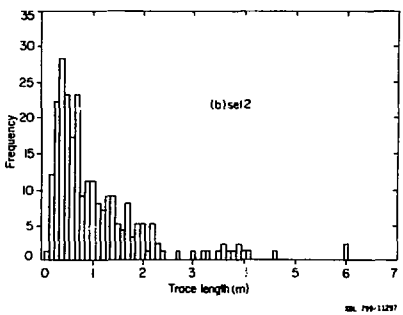

Fig. 4. Histogram of joint lengths.

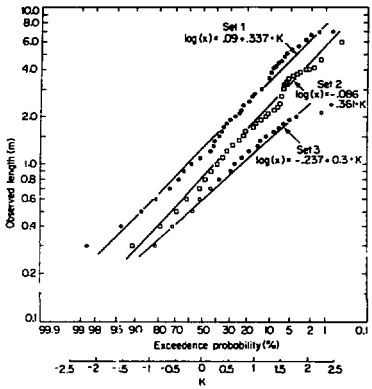

Fig. 5. Lognormal joint length distribution.

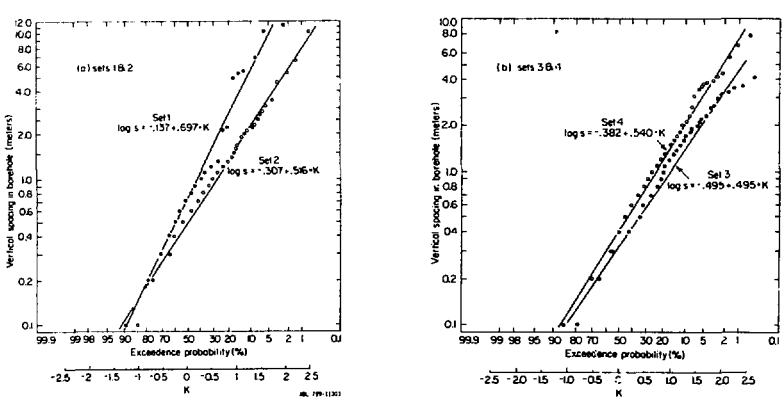

Fig. 6. Lognormal plots of joint spacings for (a) sets 1 & 2 and (b) sets 3 & 4.

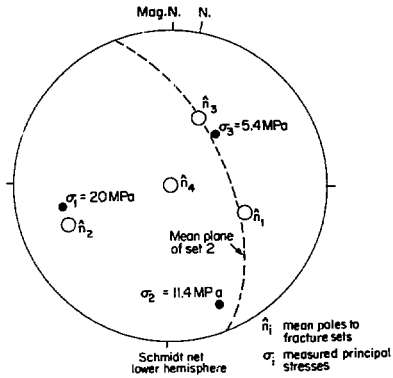

Fig. 7. Stereographic plot of principal stresses and joint set poles in the time-scale experiment.

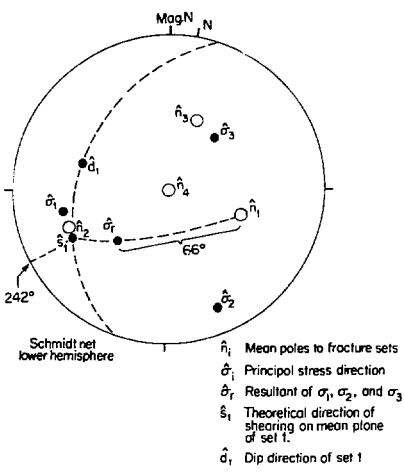

Fig. 8. Stereographic determination of stress components on mean plane of joint set 1.

points to be nearly colinear in this direction.[1] In light of this corroboration, the inferred configurations of the faults are quite reasonable.

The origins of the jointing are still uncertain, but it appears likely that set 3 is the youngest of the four sets and may be associated with continuing post-glacial uplift. Three observations in support of this claim are offered: (1) The set lies perpendicular to the existing minimum principal stress (Fig. 7). (2) Joints of this set are predominantly filled with calcite rather than the more common chlorite found in other joints, which suggests a relatively recent transport and deposition. (3) The joints tend to cross or offset nearly all other joints when observed in the core samples.[1]

Statistically, joints of set 3 are shorter and more closely spaced than are the others (Figs. 5 and 6). A shear-to-normal stress ratio of 4.70 has been calculated for the mean plane of the set, which is over twice that for the other joint sets.[1] Thus, if thermal loading or some other perturbation were to propagate or coalesce these fractures, stability problems might arise. The likelihood of this has not yet been addressed in the Stripa analysis, but it appears that some attention is warranted.

The origins of joint sets 1, 2 and 4 are also uncertain in the absence of structural information on the Stripa granite. Fractures in set 2 tend to be rough or irregular, suggesting an extension mechanism. Clearly, these could not result from the state of stress reported here, but more likely from a condition where the major principal stress was perpendicular to its present orientation. Such conditions could occur by (a) glacial loading, in which the major principal stress would be closer to vertical, (b) stress changes during cooling of the pluton, or (c) viscous drag during the intrusion process. The othogonality of the joint sets indicates that there is probably a reasonable explanation for their occurrence, yet it is tenuous to speculate on this with limited knowledge of the regional geology.

Regardless of their genesis, certain observations can be made regarding the engineering significance of joint sets 1, 2, and 4. First, with set 2 lying perpendicular to the major principal stress it would be unlikely for these joints to deform appreciably or otherwise affect the stability of the rock mass under moderate stress perturbations. Secondly, radial stress relief around the opening has reduced the compression across the horizontal joints, which should increase the nonlinearity of their deformation behavior. The third point concerns the modeling of joint set 1. The set is effectively represented by the four faults in Fig. 2, since most instability along planes at this orientation would be accommodated by these major weaknesses. The faults are anisotropic, however, due to their lack of planarity transverse to the direction of slickensiding.[1] This anisotropy will be properly represented if numerical models utilize the irregular surface configurations that have been inferred,[1] or alternatively, if strength parameters that vary with direction are assigned.

CONCLUSIONS

The results discussed here pertain to near-field behavior of a rock mass, and as such they represent a practical limit to the degree to which discrete subsurface discontinuities can be defined by surface mapping and cross-correlation of observational borehole data. Discontinuities on the scale of the rock mass being studied can dominate its response, and should therefore be described deterministically. Alternatively, if the size or continuity of a feature is much less than the scale of the rock mass in question, a statistical approach is appropriate.

It has been demonstrated that in addition to facilitating a discrete characterization of major features, detailed mapping of fractures and thorough logging of core samples can yield valuable statistical information. Efficient collection of data requires prior knowledge of the engineering significance of parameters to be measured, and sensitivity modeling would be of benefit in this regard.

REFERENCES

1. Thorpe, R.,1979. Characterization of discontinuities in the Stripa granite - time-scale experiment, Lawrence Berkeley Laboratory report LBL-7083, SAC-20, Berkeley, Cal.

2. Witherspoon, P.A. and O. Degerman, 1978. *Swedish-American cooperative program on radioactive waste storage in mined caverns - program summary*, Lawrence Berkeley Laboratory report LBL-7049, SAC-01, Berkeley, Cal.

3. Olkiewicz, A., J. Gale, R. Thorpe, and B. Paulsson, 1979. The geology and fracture system at Stripa, Lawrence Berkeley Laboratory report LBL-7083, SAC-20, Berkeley, Cal.

4. Terzaghi, R., 1965. Sources of error in joint surveys, Geotechnique, 15.

5. Carlsson, H., 1978. Stress measurements in the Stripa granite, Lawrence Berkeley Laboratory report LBL-7078, SAC-04, Berkeley, Cal.

A FINITE ELEMENT METHOD FOR COUPLED STRESS AND FLUID FLOW ANALYSIS OF FRACTURED ROCK MASSES

J. Noorishad, M. S. Ayatollahi, P. A. Witherspoon
Earth Sciences Division
Lawrence Berkeley Laboratory
University of California
Berkeley, California 94720

SUMMARY

Following a delineation of the constitutive and governing equations of fluid flow through deformable fractured rock masses, a Gurtine-type variational formulation for general initial and boundary fluid flow and load deformation conditions as well as fluid body forces is presented. Subsequent finite-element discretization offers a numerical technique capable of analyzing quasi-static stress and fluid flow behavior of deformable fractured rock masses. The method is verified and applied with the help of a few examples.

INTRODUCTION

Biot's work [2,3,4,5] on general theory of consolidation has provided the constitutive stress-strain relationship on which analysis of stress and fluid flow in deformable porous elastic media is based. Numerical solution to Biot's formulation by different investigators [6,7,8,13] has led to the solution of quasi-static and dynamic problems of seepage, consolidation, and liquifaction.

Analysis of stress and fluid flow in deformable fractured media was approached in a different manner. Noorishad [12], using explicit coupling, solved two sets of finite element formulations: (1) static equilibrium force-displacement equation, and (2) steady-state fluid flow equation, to obtain a compatible stress and pressure field within the fractured medium. This work was later extended by Hilber et al [9] to dynamic range, where fault stick-slip phenomena due to injection of incompressible fluid into nonporous fractured rock was studied. Ayatollahi [1], by extending Biot's formulation for nonlinear material, was able to develop a finite-element method for the analysis of stress and fluid flow in deformable fractured rock masses.

In this paper, a complete and general approach to quasi-static stress and fluid flow analysis of rock masses is offered. Finite-element modeling of rock masses under general initial and boundary fluid flow and load deformation conditions, and fluid body forces is made possible.

FIELD EQUATIONS

Field equations for the behavior of the media under consideration are set up in two steps. First, the porous elastic portions of the medium are considered, then in the following segment, fractures are dealt with. Following a general approach [7], the displacement field for fully saturated porous elastic media is defined by two field variable quantities: the components of the displacement vector of the solid u_i, and the components of the fluid displacement vector U_i. The components of the fluid displacement U_i are defined in such a way that the volume of the fluid displaced through a unit area perpendicular to axis x_i is nU_i, where n is porosity. Relative displacement of fluid with respect to solid is defined as $w_i = n(U_i - u_i)$.

The solid and fluid strain quantities, explained in terms of displacement, will be

$$e_{ij} = \frac{1}{2}(u_{i,j} + u_{j,i})$$
$$\zeta = w_{i,i} \tag{1}$$

where e_{ij} are components of the solid strain tensor and ζ is the volumetric strain of the fluid.

Letting the components of the bulk stress tensor and fluid pressure be denoted by τ_{ij} and π, respectively, the stress-strain relationship for isotropic cases are:

$$\tau_{ij} = 2\mu e_{ij} + \lambda_c \delta_{ij}\delta_{kl}e_{kl} + \alpha M\delta_{ij}\zeta$$
$$\pi = \alpha M\delta_{ij}e_{ij} + M\zeta \tag{2}$$

where $\lambda_c = \lambda + \alpha^2 M$, or alternatively,

$$\tau_{ij} = 2\mu e_{ij} + \lambda\delta_{ij}\delta_{kl}e_{kl} + \alpha\delta_{ij}\pi$$
$$\zeta = -\alpha\delta_{ij}e_{ij} + \frac{1}{M}\pi \tag{3}$$

where μ and λ are Lamé constants for solid skeleton and α and M are material properties defined by porous matrix compressibility, solid bulk compressibility, fluid compressibility, and porosity.

In the event of a highly incompressible matrix material, $\alpha \approx 1$ and M approaches the fluid incompressibility. Assumption of fluid incompressibility leads to $M \approx \infty$ and reduces Eq. 3 to the following:

$$\tau_{ij} = 2\mu e_{ij} + \lambda\delta_{ij}\delta_{kl}e_{kl} + \delta_{ij}\pi$$
$$\zeta = -\delta_{ij}e_{ij} \tag{4}$$

Darcy's law, governing the flow of fluid with respect to solid and neglecting the effect of body forces on fluid, is given by

$$\frac{\partial w_i}{\partial t} = \frac{k}{\eta} \pi_{,i} \tag{5}$$

where k is the specific permeability coefficient of the solid and η is the fluid viscosity. It is also assumed that the solid is isotropic relative to the flow.

Taking divergence of Eq. 5 leads to an expression for the volumetric change of the fluid

$$\frac{\partial \zeta}{\partial t} = \left(\frac{k}{\eta} \pi_{,i}\right)_{,i} \tag{6}$$

Considering the fact that τ_{ij} as written in Eq. 3 embodies the fluid pressure, the equation of equilibrium for the bulk of the fluid-filled elastic media takes the following familiar form

$$\tau_{ij,j} + \rho_s f_i = 0 \tag{7}$$

where ρ_s is the bulk mass density and f_i is the component of the body force vector.

Eqs. 1, 3, 6, and 7 completely define and govern the behavior of the saturated porous elastic portions of the media.

A medium composed of fractures, with its mechanical and flow behavior thoroughly defined on a parallel basis to porous elastic media, though very different, can be approached from the standpoint of the coupled stress-flow analysis in a similar manner. This requires that the Biot constants α and M be similarly defined for fractures. In general, one can expect that both α and M for a fracture should depend upon parameters such as roughness of fracture surfaces, filling material, and the state of stress. However, assumption of α equal to unity and M equal to fluid incompressibility for clean fractures seems to be reasonable. In case of fractures with filling materials, fluid incompressibility divided by filling material porosity provides a meaningful estimate of M. The value of α in this case could be less than unity and the correct estimate can possibly be obtained from tests similar to those explained by Biot and Willis [5] for solid materials.

Having defined α and M, constitutive and governing equations for fractures, parallel to those for solids, are formulated in local coordinates by the following:

$$\begin{aligned}
F_i &= \delta_{ij} c^f_{ij} u'_i + \alpha^f \delta_{i1} \pi \qquad i,j = 1,2 \\
\zeta^f &= -\alpha \frac{u'_\zeta}{2b} + \frac{1}{M^f} \pi \\
\frac{\partial \zeta^f}{\partial t} &= \frac{k^f}{\eta} (\pi_{,i})_{,i} \\
F_i\Big|_{US} &+ F_i\Big|_{LS} = 0
\end{aligned} \tag{8}$$

The first and second equations are nonlinear constitutive relationships in terms of the local fracture force components F_i and average net fracture deformation components u'_i. C^f_{ij} represents the 2 x 2 diagonal fracture stiffness matrix (8), and 2b is the fracture aperture. The third relation explains the flow governing equation along the fracture. Finally the last equation, representing the static equilibrium law, equates the sum of the normal and the tangential forces on the upper and lower surfaces of the fracture to zero value.

INITIAL AND BOUNDARY CONDITIONS

Initial conditions and fluid body load have been avoided for the sake of simplicity of variational formulations and will be considered later The boundary and initial conditions for the saturated fractured solid mass are

$$\begin{aligned}
&u_i(\underline{x}, t) = \hat{u}_i(\underline{x}, t) && \text{on } A_1 \times [0, \infty) \\
&t_{ij}(\underline{x}, t) \cdot n_j(\underline{x}) = \hat{G}_i(\underline{x}, t) && \text{on } A_2 \times [0, \infty) \\
&\pi(\underline{x}, t) = \hat{\pi}(\underline{x}, t) && \text{on } B_1 \times [0, \infty) \\
&\frac{k^s}{\eta} (\pi_{,i}) \cdot n_i(\underline{x}) = \hat{Q}^s(\underline{x}, t) && \text{on } B_2 \times [0, \infty) \\
&\frac{k^f}{\eta} (\pi_{,i}) = \hat{Q}^f && \text{flow in or out of the fracture} \\
&u_i(\underline{x}, o) = 0 && \text{on } V^s, V^f \\
&\tau_{ij}(\underline{x}, o) = \hat{\tau}_{oij} && \text{on } V^s, V^f \\
&\pi(\underline{x}, o) = 0 && \text{on } V^s, V^f
\end{aligned} \tag{9}$$

where $n_i(\underline{x})$ is normal unit vector of the surface and f and s refer to fracture and solid parts.

Equations 1, 3, 6, 7, and 8, along with boundary conditions and initial conditions, completely define the mixed boundary value problem.

VARIATIONAL PRINCIPLE

Application of the Gurtin type variational formulation to the problem of flow through saturated elastic media, initially given by Sandhu [6] and later extended by Ghabousi [7] to account for the compressibility of the solid particles and the fluid, is generalized for the problem of the flow of compressible fluids through deformable, saturated, porous, fractured rock masses.

Let $R = \{u, \pi\}$ be an admissable state in J, defined in V x $[0, \infty)$ and the functions u and π possess the appropriate continuity and differentiality conditions. J is the set of all admissable states and V is the region of space occupied by the fluid-porous fractured rock mixture. A functional $\mathcal{U}_t(R)$ over J for each time $t \in [0, \infty)$ is defined

$$\mathcal{U}_t(R) =$$

$$\int_{V^{s,f}} \left(e_{ij} * C^{s,f}_{ijk\ell} e_{k\ell} - 2\rho_s f_i * u_i \right.$$

$$+ 2e_{ij} * \hat{\tau}_{oij} - 2\pi * \alpha^{s,f} \delta_{ij} e_{ij}$$

$$\left. - 1 * \pi_{,i} * \frac{k^{s,f}}{\eta} \pi_{,i} - \pi * \frac{1}{M^{s,f}} \pi \right) dv^{s,f}$$

$$- 2 \int_{A^2} G_i * u_i ds^s - 2 \int_{B^2} 1 * \hat{Q} * \pi ds^s$$

$$- 2 * \hat{Q}^f * \pi \quad (10)$$

It can be shown that

$$\mathcal{U}_{\bar{R}}(R) = \frac{d}{d\lambda} \mathcal{U}(R + \lambda \bar{R}) \Big|_{\lambda=0} = 0 \quad \text{for every } \bar{R} \in J$$

if and only if R is a solution state of the mixed boundary-value problem.

FINITE-ELEMENT DISCRETIZATION

The field variables u and π within the elements of the solid rock are discretized through the following expressions:

$$u^{ns} = \underline{\varphi}_u^{ns\,T} \underline{u}$$

$$\pi^{ns} = \underline{\varphi}_\pi^{ns\,T} \underline{\pi} \quad (11)$$

where $\underline{u}$ and $\underline{\pi}$ are the set of values of the field variables at finite number nodes and $\underline{\varphi}_u$ and $\underline{\varphi}_\pi$ are interpolation functions. Since fractured regions are treated as another medium with different properties, their discretization follows from the work of Goodman et al. [10] in regard to displacement field, and the work of Wilson and Witherspoon [13] in regard to pressure field.

$$u'^{nf} = \underline{\varphi}_{u'}^{nf\,T} \underline{u}$$

$$\pi^{nf} = \underline{\varphi}_\pi^{nf} \underline{\pi} \quad (12)$$

where u' is the net local average relative movement of the faces of the fracture element in a direction vertical to the fracture plane and along the fracture. u', being a measure of fracture deformation, is equivalent to the strain in the continuum. $\underline{\varphi}_\pi^{nf}$ differs from $\underline{\varphi}_\pi^{ns}$ in that it defines π along the fracture as a function of two end-point pressures of the fracture element.

Substitution of eqs. 11 and 12 in the variational formulation, eq. 10, gives the discrete form of $\Omega_t(R)$. (Derivation of the proper terms for fracture is done in local coordinates and transferred by matrix $\underline{T}^{nf}$.)

$$\mathcal{U}_t(R) = \underline{u}^T * \underline{K}^{s,f} \underline{u} + \underline{u}^T * \underline{C}^{s,f} \underline{\pi} - 1 * \underline{\pi}^T * \underline{H}^{s,f} \underline{\pi}$$

$$- \underline{\pi}^T * \underline{E}^{s,f} \underline{\pi} - 2\underline{u}^T * \underline{F}^s + 2 * \underline{\pi}^T * \underline{Q}^{s,f} \quad (13)$$

where

$$\underline{K}^{s,f} = \underline{K}^s + \underline{K}^f$$

$$\underline{K}^s = \sum_{ns=1}^{m} \int_{V^{ns}} \underline{\varphi}_e^{ns} C^{ns} \underline{\varphi}_e^{ns} dv^{ns}$$

$$\underline{K}^f = \sum_{nf=m+1}^{N} \underline{T}^{nf\,T} \left[\int_{S^{nf}} \underline{\varphi}_{u'}^{nf} \underline{C}^{nf} \underline{\varphi}_{u'}^{nf} ds^{nf} \right] \underline{T}^{nf} \quad (14)$$

$$\underline{C}^{s,f} = \underline{C}^s + \underline{C}^f$$

$$\underline{C}^s = \sum_{ns=1}^{m} \int_{V^{ns}} \underline{\varphi}_\pi^{ns} \alpha^{ns} \underline{1}^{ns} \underline{\varphi}_e^{ns\,T} dv^{ns}$$

$$\underline{C}^f = \sum_{nf=m+1}^{N} \left[\int_{V^{nf}} \underline{\varphi}_\pi^{nf} \underline{1}^{nf} \underline{\varphi}_{u'}^{nf} dv^{nf} \right] \underline{T}^{nf}$$

$$\underline{H}^{s,f} = \underline{H}^s + \underline{H}^f$$

$$\underline{H}^s = \sum_{ns=1}^{m} \int_{V^{nf}} \underline{\varphi}_\sigma^{ns} \frac{k^{ns}}{\eta} \underline{\varphi}_\theta^{ns\,T} dv^{ns}$$

$$\underline{H}^f = \sum_{nf=m+1}^{N} \int_{V^{ns}} \underline{\varphi}_\theta^{nf} \frac{k^{nf}}{\eta} \underline{\varphi}_\theta^{nf\,T} dv^{nf}$$

$$\underline{E}^{s,f} = \underline{E}^s + \underline{E}^f$$

$$\underline{E}^s = \sum_{ns=1}^{m} \int_{V^{ns}} \underline{\varphi}_\pi^{ns} \frac{1}{M^{ns}} \underline{\varphi}_\pi^{ns\,T} dv^{ns}$$

$$\underline{E}^f = \sum_{nf=m+1}^{N} \int_{V^{nf}} \underline{\varphi}_\pi^{nf} \frac{1}{M^{nf}} \underline{\varphi}_\pi^{nf\,T} dv^{nf}$$

$$\underline{r}^{s} = \sum_{ns=1}^{m} \int_{A_2^{ns}} \underline{\Phi}_u^{ns} \underline{\Phi}_u^{ns^T} \underline{\hat{G}}\, ds^{ns}$$

$$+ \sum_{ns=1}^{m} \int_{V^{ns}} \underline{\Phi}_u^{ns} \rho^{ns} \underline{f} dV^{ns}$$

$$+ \sum_{ns=1}^{m} \int_{V^{ns}} \underline{\Phi}_e^{ns} \underline{\tau}_o^{ns} dV^{ns}$$

$$+ \sum_{nf=n+1}^{N} \underline{T}^{nf^T} \left[\int_{V^{nf}} \underline{\xi}_u^{nf^T} \underline{\tilde{\tau}}^{nf} ds^{nf} \right]$$

$$\underline{Q}^{s,t} = \sum_{ns=1}^{m} \int_{A_2^{ns}} \underline{\Phi}_\pi^{ns} \underline{\Phi}_\pi^{ns^T} \underline{\hat{Q}}\, ds^{ns} + \sum_{nf=m+1}^{N} \underline{\hat{Q}}^{nf}$$

$$\underline{1}^{ns} = \begin{Bmatrix} 1 \\ 1 \\ 1 \\ 0 \end{Bmatrix} \text{ and } \underline{1}^{nf} = \begin{Bmatrix} 1 \\ 0 \end{Bmatrix}$$

$$\underline{T}^{nf} = \begin{bmatrix} \underline{D} & & & 0 \\ & \underline{D} & & \\ 0 & & \underline{D} & \\ & & & \underline{D} \end{bmatrix}$$

where

$$\underline{D} = \begin{bmatrix} \cos\alpha & \sin\alpha \\ -\sin\alpha & \cos\alpha \end{bmatrix} \quad \text{and} \quad \alpha = \text{Arctan} \frac{y_\ell - y_k}{x_\ell - x_k}$$

$(x, y)_{k,\ell}$ marks the end coordinates of the fracture element side. $\underline{C}^{ns}$ and $\underline{C}^{nf}$ are elasticity and force-deformation matrices for solid and fracture elements, respectively, and Φ_e and Φ_θ are obtained from Φ_u and Ψ_π by appropriate differentiation. The above equations will have to be modified, if the effect of gravitational force on flow is to be taken into account. Boundary conditions and governing equations for flow will take the following forms.

$$\frac{\partial w_i}{\partial t} = \frac{k^{s,f}}{\eta} (\pi_{,i} + \rho_f g \hat{1}_z) \quad +$$

$$\frac{\partial \zeta}{\partial t} = \left(\frac{k^{s,f}}{\eta} (\pi_{,i} + \rho_f g \hat{1}_z) \right)_{,i} \qquad (16)$$

$$\frac{k^{s}}{\eta} (\pi_{,i} + \rho_v g \hat{1}_z) = \hat{Q}^{s}(\underline{x}, t)$$

$$\frac{k^{f}}{\eta} (\pi_{,i} + \rho_f g \hat{1}_z) = \hat{Q}^{f}$$

† Symbol $\underline{1}$ is a unit vector along the z global axis of the coordinate system, i.e., $\begin{Bmatrix} 0 \\ 0 \\ 1 \end{Bmatrix}$.

Then, the functional of Eq. 10 has to include:

$$- \int_{V^{s,f}} 2 * \rho_f g \hat{1}_z \pi_{,i} dV$$

which will bring the following contributions to the $\underline{Q}$ vector Eq. 15 of the discrete form of the variational equation

$$- \sum_{ns=1}^{m} \int_{V^{ns}} \underline{\Phi}_\theta^{ns} \frac{k^{ns}}{\eta} \rho_f g \hat{1}_z dV^{ns}$$

$$- \sum_{n=m+1}^{N} \int_{V^{nf}} \underline{\Phi}_\theta^{nf} \frac{k^{nf}}{\eta} \rho_f g \hat{1}_z dV^{nf}$$

Also, additional modifications will be necessary if initial pressures are to be taken in account. If the initial pressure distribution vector is denoted by π_o, the following terms have to be added to the $\underline{Q}^{\dagger}$ vector of Eq. 15:

$$- \sum_{n=1}^{m} \left[\int_{V^{ns}} \underline{\Phi}_\pi^{ns} \frac{1}{M^{ns}} \underline{\Phi}_\pi^{ns^T} \right] \pi_o$$

$$- \sum_{n=m+1}^{N} \left[\int_{V^{nf}} \underline{\Phi}_\pi^{nf} \frac{1}{M^{nf}} \underline{\Phi}_\pi^{nf^T} dV^{nf} \right] \pi_o \qquad (18)$$

and following contributions to the $\underline{F}$ vector of Eq. 15 accordingly

$$+ \sum_{n=1}^{m} \left[\int_{V^{ns}} \underline{\Phi}_\pi^{ns} \alpha \underline{1}^{ns^T} \underline{\Phi}_e^{ns} dV \right] \pi_o$$

$$+ \sum_{nf=m+1}^{N} \left\{ \left[\int_{V^{nf}} \underline{\Phi}_\pi^{nf} \alpha \underline{1}^{nf^T} \underline{\Phi}_{u'}^{T} \right]^{T} \underline{1}^{nf} \right\} \pi_o \qquad (19)$$

Taking the variation $\Omega_t(R)$ of Eq. 15 with respect to π and $\underline{u}$ results in the following matrix equations:

$$\underline{K}^{s,f} \underline{u} + \underline{C}^{s,f} \underline{\pi} = \underline{F}^{s}$$

$$\underline{C}^{s,f^T} \underline{u} - (\underline{E}^{s,f} + \underline{1} * H^{s,f}) \underline{\pi} = -\underline{1} * \underline{Q}^{s,f} \qquad (20)$$

Discretization in Time Domain: Time integration of Eq. 16 is performed by using a predictor-corrector scheme, Eq. 13. The solution is first predicted at $t+\theta\Delta t$. In doing so, $1 * \underline{\pi}_{t+\theta\Delta t}$ is written as

† This contribution to flow load is not time-integrated.

$$1 * \underline{\pi}_{t+\theta\Delta t} = \underline{A}(t + \theta\Delta t) = \underline{A}(t) + \frac{1}{2}\theta\Delta t(\underline{\pi}_t + \underline{\pi}_{t+\theta\Delta t})$$

which results in the following form for Eq. 16.

$$\begin{bmatrix} \underline{K}^{s,f} & \underline{C}^{s,f} \\ \underline{C}^{s,f^T} & -\frac{\theta\Delta t}{2}\underline{H}^{s,f} - \underline{E}^{s,f} \end{bmatrix} \begin{Bmatrix} \underline{u}_{t+\theta\Delta t} \\ \underline{\pi}_{t+\theta\Delta t} \end{Bmatrix} =$$

$$= \begin{Bmatrix} \underline{F}^{s}_{t+\theta\Delta t} \\ -\frac{\theta\Delta t}{2}\left(\underline{Q}_t^{s,f} + \underline{Q}_{t+\theta\Delta t}^{s,f}\right) + \left(\underline{A}(t) + \frac{\theta\Delta t}{2}\underline{\pi}_t\right)\underline{H}^{s,f} \end{Bmatrix}$$

where $\underline{A}(t)$ is obtained from the previous time step by writing

$$1 * \underline{\pi}_{t+\theta t} = \underline{A}(t + \Delta t) = \underline{A}(t) + \frac{\Delta t}{2}(\underline{\pi}_t + \underline{\pi}_{t+\theta\Delta t})$$

The solution is then corrected to give the value of the unknowns $\underline{u}$ and $\underline{\pi}$ at time $t+\Delta t$

$$\underline{X}_{t+\Delta t} = \underline{X}_t + \frac{1}{\upsilon}(\underline{X}_{t+\theta\Delta t} + \underline{X}_t)$$

where $\underline{X}$ is either $\underline{u}$ or $\underline{\pi}$. The coefficient θ in the above equations is a measure of an artificial viscosity to fluctuating transient response which is used at the expense of slightly slowing down the convergence.

Computations of the stresses and flows within each element are easily obtained when the unknown displacements and pressures are determined at each time step. The problem of the peculiar behavior of the fracture element is dealt with with the stiffness perturbation technique [10] during each time step.

Caution must be exercised in the choice of time steps in the various problems. For a uniform mesh, a measure of the relative size of the elements of the matrices $\underline{K}$, $\underline{H}$ is given by $\upsilon = k\Delta t/(\lambda+2\pi)$.[7] In the event $\upsilon \times 10^n$ is smaller than unity, numerical difficulties can be expected, n being the number of available digits in the computer.

VERIFICATION AND APPLICATION

Due to the fact that there is no other method of coupled stress and fluid flow analysis in fractured media, full comparison of the effectiveness of this method is not possible. However, assignment of zero value to Biot's coupling coefficient, mobilizes partial capability of the method that could be utilized to solve the class of fluid flow problems in unfractured or fractured saturated porous media. In doing so, Biot's constant, M, must also be changed to $1/S_s$, the reciprocal of aquifer specific storage coefficient, to make the flow formulation compatible. The method, in this capacity, resembles some of the available fluid flow finite element techniques used for modeling of groundwater hydrology problems. Using this capability, a number of problems, for which exact or

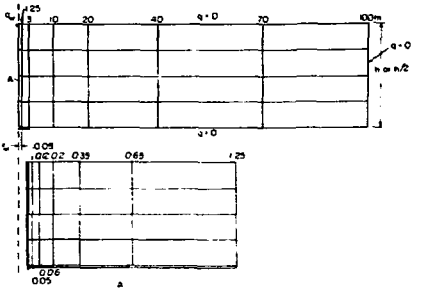

Fig. 1. Axisymmetric finite-element mesh. (XBL 802-4690)

groundwater hydrology problems. Using this capability, a number of problems, for which exact or other analytical solutions exist, were solved. One of the more interesting ones is the problem of an axisymmetric confined reservoir with a horizontal fracture at the center intersecting the production well. Figure 1 shows the finite element mesh used to model the reservoir. This mesh was originally used to model the axisymmetric confined, *porous elastic aquifer flow* into a well for duplication of Theis behavior. However, due to time restrictions, the same mesh, with little change for placement of a row of fracture elements at the bottom, was used to represent the upper half of the flow domain for the problem at hand. Due to the unfit nature of the mesh to simulate flow in the fractured region of the mesh, the results of this stage are only used to cast some light on the reservoir behavior and should therefore be considered preliminary.

Results of the reservoir behavior are plotted in Figure 2. As expected, only late-time behavior agreement with the available solution [11] is

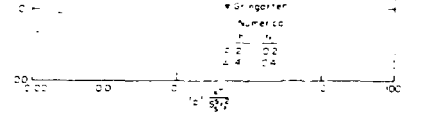

Fig. 2. Dimensionless pressure in well versus dimensionless time for uncoupled analysis. (XBL 802-4693)

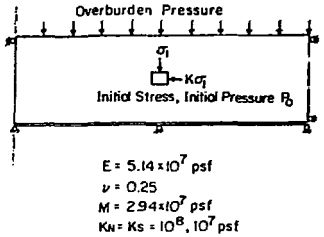

Fig. 3 Loading conditions and deformation constants of the model. (XBL 802-4685)

achieved. Subsequent analysis with a refined mesh provided a complete match. Having verified partial capability of the method, we began to use its main potential to investigate the realistic behavior of the reservoir through coupled stress and flow analysis. In doing so, initial and boundary conditions of the system, in regard to both fluid flow and structural analysis, has to be provided. Figure 3 shows such data for the problem. For this problem, initial aperture of the fracture, a measure of its conductivity, was assumed to be 0.1 mm.

Results of the analysis for different fracture lengths and stiffness are presented in Figs. 4 and 5. Uncoupled results for the same problems are also plotted in order to provide a basis for the comparison of the coupled behavior. As shown in these figures, early-time results of the coupled behavior for different fracture stiffness are practically the same. However, soft fractures close markedly and induce larger pressure drops. Uncoupled results are also the same as coupled results for the case of hard fractures. Had the same value of S_s been used for t_D, instead of 1/H in the coupled case, the results, presently parallel, would have coincided.

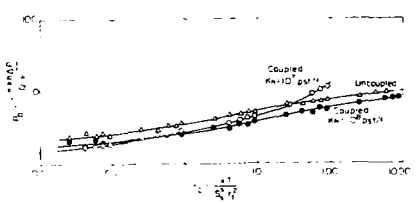

Fig. 4. P_D versus t_D for coupled and uncoupled analysis of the model for a finite conductivity 10 feet radius fracture (XBL 802-4689)

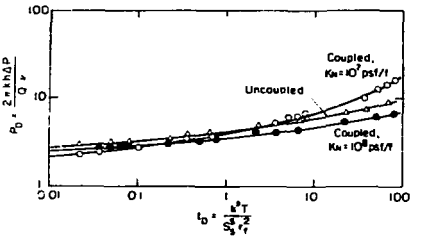

Fig. 5 P_D versus t_D for coupled and uncoupled analysis of the model for a finite conductivity 30 feet radius fracture. (XBL 802-4691)

To get a better feel for the reservoir's realistic behavior, pressure drops along the fracture have been plotted for the two different fracture lengths in coupled and uncoupled analysis on ordinary coordinates. In coupling analysis, pressure drops near the well are almost twice those of uncoupled results. Implications of such findings are that fluid flow analysis alone may lead to underestimation of pressure drops and overestimation of the production capacity of fractured reservoirs. This, in the face of the generally irreversible nature of the fracture deformation behavior, could result in permanent closure of the fractures.

CONCLUSION

The method of analysis presented here provides a new technique for more realistic investigation of fluid flow behavior in fractured porous media. To achieve this, mechanical as well as fluid flow parameters of both porous media and fractures are used in an extension of Biot's three-dimensional theory of consolidation. A finite-element analysis

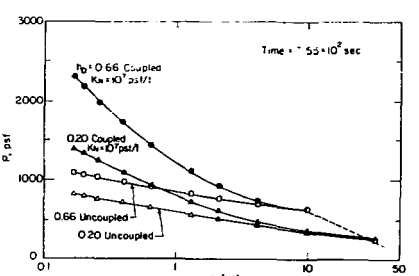

Fig. 6. Pressure response along sift finite conductivity fractures of different lengths (XBL 802-4686)

method, capable of modeling coupled stress and fluid flow phenomena in fractured rock masses has been developed. Plane or axisymmetric problems under general initial and boundary conditions could be solved. To show the method's general capability, the problem of a deep confined aquifer with a horizontal fracture at the center was solved. Coupled analysis showed drastic reduction in well pressure due to closing of fractures in response to fluid withdrawal. The degree of closing is mainly controlled by the fracture stiffness.

REFERENCES

1. Ayatollahi, M. S., "Stress and Flow in Fractured Porous Media," Ph.D.dissertation, University of California, Berkeley, 1978.

2. Biot, M. A., "General Theory of Three Dimensional Consolidation," Journal of Applied Physics, Vol. 12, February, 1941, pp. 155-164.

3. Biot, M. A., "Theory of Elasticity and Consolidation for a Porous Anisotropic Media," Journal of Applied Physics, Vol. 26, 1955, pp. 182-185.

4. Biot, M. A., "Theory of Deformation of a Porous Viscoelastic Anisotropic Solid," J. Applied Physics, V. 27, 1956.

5. Biot, M. A. and Willis, D. C., "The Elastic Coefficients of the Theory of Consolidation," Paper No. 57-APM-44, presented at the Applied Mechanics Division Summer Conference, Berkeley, California, June 13-15, 1957.

6. Sandhu, R. S. and Wilson, E. L., "Finite-Element Analysis of Seepage in Elastic Media," J. of Engineering Mechanics, Division ASCE, Vol. 95, No. EM3, 1969, p. 641-652.

7. Ghaboussi, J. and Wilson, E. L., "Flow of Compressible Fluids in Porous Media," SESM Report No. 72-12, University of California, 1971.

8. Ghaboussi, J., "Dynamic Stress Analysis of Porous Elastic Solids Saturated with Compressible Fluids," Ph.D. Thesis, University of California, Berkeley, California, 1971.

9. Hilber, H. and Taylor, R. L., "A Finite Element Model of Fluid Flow in Systems of Deformable Fractured Rock," Report No. UC-SESM 76-5, Department of Civil Engineering, University of California, Berkeley, 1976.

10. Goodman, R. E., Taylor, R. L., and Brekke, T. L., "A Model for the Mechanics of Jointed Rocks," J. of Soil Mechanics and Found. Division, ASCE, Vol. 94, N.S.M. 3, May 1968.

11. Gringarten, A. C. and Ramey, H. J., "Unsteady State Pressure Distribution Created by a Well with a Single Horizontal Fracture, Partial Penetration or Restricted Entry," SPE Journal, p. 413, August 1974.

12. Noorishad, J., "Finite-Element Analysis of Rock Mass Behavior under Coupled Action of Body Forces, Flow Forces, and External Loads," Ph.D. dissertation, University of California, Berkeley, 1971.

13. Wilson, C. and Witherspoon, P. A., "An Investigation of Laminar Flow in Fractured Porous Rock," Ph.D. thesis, University of California, Berkeley, California, 1970.

14. Taylor, R. L., "Analysis of Flow of Compressible or Incompressible Fluids in Porous Elastic Solids," Consulting report to the Naval Civil Engineering Laboratory, Port Hueneme, California, 1974.

A POROUS MEDIA FLUID FLOW, HEAT, AND MASS TRANSPORT MODEL WITH ROCK STRESS COUPLING

Akshai K. Runchal
Analytic & Computational Research, Inc.*
12029 Clover Avenue
Los Angeles, California 90066

SUMMARY

This lecture describes the physical and mathematical basis of a general purpose porous media flow model. The mathematical basis of the model is obtained from the coupled set of the classical governing equations for the mass, momentum and energy balance.

These equations are embodied in a computational model which is then coupled externally to a linearly elastic rock-stress model. This coupling is rather exploratory and based upon empirical correlations. The coupled model is able to take account of time-dependent, inhomogeneous and anisotropic features of the hydrogeologic, thermal and transport phenomena. A number of applications of the model have been made. Illustrations from the application of the model to nuclear waste repositories are included.

FORWARD

The material presented here is an edited version of the lecture presented by the author at the workshop on "Numerical Modeling of Thermo-hydrological Flow in Fractured Rock Masses," at Lawrence Berkeley Laboratory, Berkeley, February 19-20, 1980. The material presented refers to the computational model GWTHERM. Since the workshop, a more versatile, advanced and faster model, PORFLOW, has been developed. The mathematical basis of PORFLOW is more general than, and the program structure is radically different from, that of the GWTHERM. This has allowed for considerable economy in computer time and a high degree of flexibility in the number of transport equatons to be solved, the specificaion of boundary conditions, and the physical options of PORFLOW.

The focus of my presentation is a porous media flow model, GWTHERM (Slide 1). Though the primary incentive for the development of this model was its application to numerical modeling of nuclear waste repositories in geologic media, it is really a general purpose model for fluid flow, heat and mass transport in porous, or equivalent porous, media.

1

PHYSICAL AND MATHEMATICAL BASIS
OF
GWTHERM

Presented by Akshai K. Runchal

at

Workshop on
Numerical Modeling of Thermo-Hydrological
Flow in Fractured Rock Masses
Lawrence Berkeley Laboratory
Berkeley, February 19-20, 1980

What GWTHERM stand for and what it is, is shown in a nutshell in this slide (Slide 2). The name itself is not very important. It stands for Ground Water flow with THERMal gradients, so I guess a model without a name is like a fish without a bicycle, so you need some name to tag onto a model.

GWTHERM - GENERAL FEATURES 2

GWTHERM stands for Ground Water flow with THERMal gradients.

GWTHERM is a general mathematical model for coupled analysis of fluid flow, heat and multi-component mass transport in porous or equivalent porous media.

GWTHERM takes account of the changes in hydrological properties of rock masses due to the thermally or mechanically-induced rock stresses by dynamic coupling with a rock stress model called DAMSWEL.

*At the time of the workshop, the author was employed by Dames & Moore as Manager, Advanced Technology Group, Los Angeles.

This slide (Slide 3) shows an outline of the presentation. The conceptual basis of the model will be presented followed by some transport equations and auxiliary relations as well as some results of model applications (Slide 3). I am sure you are all very familiar with the equations, so I will try to skim through them so that they cause you the least amount of wasted time. But, since I am presenting a model, I do think I should write them down so that everyone knows what the framework of the model is.

We have experimented in a preliminary way with coupling the fluid and thermal energy flow with a rock stress model, DAMSWEL. It is a very preliminary way, and we are not quite sure that this is the way to go. I will present the basis of this coupling and then I will talk about some salient features, capabilities and limitations of the model.

My conceptualization of the medium is shown on this slide (Slide 4). I guess we start with some kind of geologic, hydrologic, mechanical, and thermal data. I am sure some of those slides that we saw from the previous talks were a very sobering influence on all of us as to what this data consists of or what it might look like in real life. Nonetheless, we try to interpret it in some simpler parametric terms and we come up with some fluid properties and parameters as well as some rock mass properties.

Then, of course, the question is how do we conceptualize a fractured medium. There are, I guess, a number of approaches, but basically you can treat them as either equivalent porous medium or the discrete fracture medium approach. The model, GWTHERM, that we are talking about, is the one that you see appearing in the lower right-hand corner and falls into the equivalent porous medium category.

Here is one way of looking at where we are in terms of the conceptual models of transport processes (Slide 5). The clear areas that you see there represent the least complicated set of models which deal with really just the convective transport. From hydrological and transport properties, we obtain the ground water flow and transport equations and come up with some convective and radionuclide transport model. This is a kind of a standard model; not very complicated. The next level of complexity which almost all models for a nuclear waste repository have to have is that of the thermal transport. The vertically hatched structure shows that from another set of data, some thermal properties are derived and heat transport is coupled with the flow by means of convective transport and water properties. The situation becomes a little more complicated because now we have a coupling effect between the fluid flow and the heat transport. For most rocks, the convective heat transport is much smaller than the heat transport by diffusion

---

PURPOSE OF THE PRESENTATION 3

- To present the conceptual basis of the model.
- To present the transport equations and auxiliary relations which comprise the mathematical model.
- To outline the dynamic coupling between GWTHERM and the rock stress model DAMSWEL.
- To discuss the salient features, capabilities and limitations of GWTHERM.

4

CONCEPTUALIZATION OF THE MEDIUM

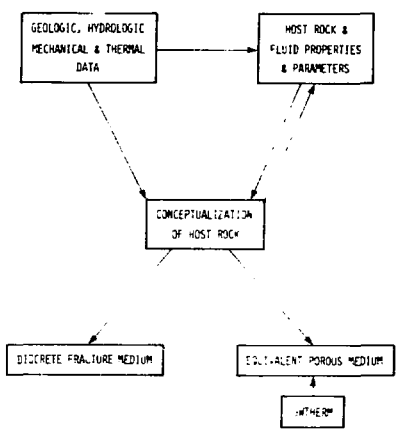

in the rock; so, this is usually not a first-order coupling. The heat transport, on the other hand, modifies the water properties; the main ones being the density and the viscosity of the fluid and they have a very strong influence on the ground water flow--it is a very strong coupling. Another complexity arises from the rock stress coupling, shown as the inclined hatched structure in the slide. This coupling has not attracted much attention so far. I think John showed some slides of such a coupling. The presently more developed models are where only the rock stress and the elastic properties are included in a flow model. So I guess, what is missing from the model that John showed is the heat transport components of the overall picture. At least in the vicinity of the repositories, I guess, we would need models which have all the components though presumably a little further away we would not have to worry too much about the rock stresses. Even further out, such as at the extremity of the regional scale, we may perhaps just be able to get away with the flow and transport modul s and need not consider either rock stresses or heat transport.

CONCEPTUAL MODEL OF THE TRANSPORT PROCESSES 5

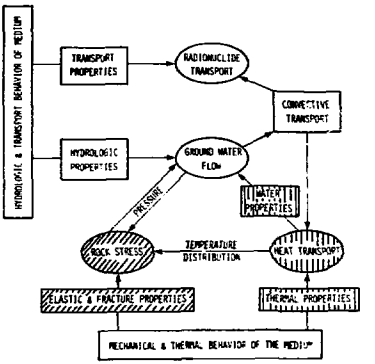

The essential feature of the model that we are talking about here (Slide 6) is a mechanism for coupled solution of fluid flow, pressure, temperature distribution, and mass concentration. It deals with saturated flow in porous media only. The rock stress coupling is through the hydrologic properties. It can be used to model either axially symmetric or two-dimensional cartesian geometry in either a real or cross sectional model. Temperature-dependent viscosity and density are included and it ... account of the inhomogeneities anisotropies, and time-dependence of properties. A simple arrhenious one-step chemical reaction, radioactive decay, and mig.ation retardation are also included.

SALIENT FEATURES OF GWTHERM 6

- Coupled solution of fluid flow, fluid pressure, temperature distribution and mass concentration
- Saturated, porous or equivalent porous media,
- Rock stress coupling through hydrologic properties,
- Transient or steady state system,
- 2-D cartesian or 3-D axisymmetric geometry,
- Temperature-dependent density and viscosity,
- Inhomogeneous, anisotropic and time-dependent properties,
- Radioactive decay, arrhenious one-step chemical reaction and migration retardation.

There are some limitations (Slide 7). There are a few listed on this slide, not because there are only a few limitations of the model, but because we are talking only within a framework and I did not want to put all the other millions of limitations that there are to this model. Within this framework, the features one could possibly need would be compressibility, pressure-dependent properties, general three-dimensionality, and more complex chemical reactions or radioactive decay chains. All of these do not extend the conceptual limits so much as the limits of computer memory or time or resources.

LIMITATIONS OF GWTHERM 7

- Absence of compressibility,
- Saturation or pressure independent properties,
- Absence of general three-dimensionality,
- Simple one-step chemical reaction or decay.

I am now just going to go through some of the governing equations (Slide 8). The only difference that you see in the equations that are presented here from those that, I am sure you are used to, is that of some notation. There is the continuity equation expressing the principles of mass conservation with the accumulation, the convection, and the mass injection/withdrawal terms. The notation is shown in the slide and the radius, r, is included to take account of any axi-symmetric feature; cartesian equations are obtained when it is equated to unity.

I guess the only thing I might add is that there may at times be a justification for using an average system of equations, especially if you have an areal aquifer flow situaton where h would need to be included, which then gets related to the thickness of the aquifer or the pressure, depending on whether we are talking of a confined or an unconfined aquifer. For a cross sectional flow, or one without any averaging, h is simply put to unity.

Nothing new about the momentum equations shown in this slide (Slide 9). Some assumptions are inherent in these equations. As you can see, no acceleration terms are included in these equations and the buoyancy effects are included via a Boussinesq's approximation.

The thermal transport equation is, again, fairly standard (Slide 10). The concept of the equivalent specific heat and thermal conductivity for the rock/fluid is employed in deriving these equations.

Another equation in the same mode is the species transport equation (Slide 11) except that a retardation factor and a first-order chemical reaction or radioactive decay term is included. D, of course, is the dispersivity tensor and contains both the hydrodynamic dispersivity and the mass diffusivity.

GOVERNING EQUATIONS: CONTINUITY EQUATION 8

$$\frac{\partial}{\partial t}(n\rho h) + \frac{1}{r}\frac{\partial}{\partial x_i}(rhG_i) = \dot{m}\, h$$

$$G_i = n\rho u_i$$

with:

- t = time [s]
- n = porosity
- ρ = fluid density [kg m^{-3}]
- h = width or depth for averaged equations [m], unity otherwise
- G_i = mass flux in i-th direction [kg m^{-2}s^{-1}]
- u_i = velocity in i-th direction [m s^{-1}]
- $\dot{m}$ = rate of mass injected (+) or withdrawn (-) per unit volume [kg m^{-3}s^{-1}]
- r = radius [m]
- x_i = mutually-orthogonal coordinates [m]

GOVERNING EQUATIONS: MOMENTUM 9

$$u_i = -\frac{k_{ij}}{n\mu}\left(\frac{\partial p}{\partial x_j} + \rho g \frac{\partial z}{\partial x_j}\right)$$

with:

- u_i = velocity component in i-th direction [m s^{-1}]
- k_{ij} = intrinsic permeability [m^2]
- μ = dynamic viscosity [kg m^{-1} s^{-1}]
- p = thermodynamic pressure [kg m^{-1} s^{-2}]
- g = gravitational constant [m s^{-2}]
- z = vertical coordinate [m] oriented in a direction opposite to that of the gravitational attraction

---

GOVERNING EQUATIONS: THERMAL TRANSPORT 10

$$\frac{\partial}{\partial t}(n\rho h\, C_e T) + \frac{1}{r}\frac{\partial}{\partial x_i}(rhG_i C_f T) = \frac{1}{r}\frac{\partial}{\partial x_i}\left(rkh\frac{\partial T}{\partial x}\right) + Sh$$

$$C_e = C_f + \frac{1-n}{n}\frac{\rho_s}{\rho}C_s$$

with:

- C_e = equivalent specific heat [J kg^{-1} °C^{-1}]
- C_f = fluid specific heat [J kg^{-1} °C^{-1}]
- C_s = solid specific heat [J kg^{-1} °C^{-1}]
- ρ_s = solid density [kg m^{-3}]
- T = temperature [°C]
- k = equivalent thermal conductivity [W m^{-1} °C^{-1}]
- S = rate of heat gain (+) or loss (-) per unit volume [W m^{-3}]

GOVERNING EQUATIONS: SPECIES TRANSPORT 11

$$\frac{\partial}{\partial t}(n\rho h R_d C) + \frac{1}{r}\frac{\partial}{\partial x_i}(rhG_i C) = \frac{1}{r}\frac{\partial}{\partial x_i}\left(rn\rho hD\frac{\partial C}{\partial x_i}\right) +$$

$$+ S_c h - R_c n\rho h R_d C$$

with:

- R_d = retardation coefficient
- C = species concentration [kg/kg]
- D = dispersion coefficient tensor [kg m^{-1}s^{-1}]
- S_c = rate of gain (+) or loss (-) of the species per unit volume [kg m^{-3}s^{-1}]
- R_c = chemical reaction or time-decay constant (s^{-1})

We go to a standard derivation of pressure equation (Slide 12). I don't see Paul Witherspoon in the audience here. He'll have trouble measuring this reference pressure in the field; it uses a reference density rather than the actual fluid density. It does not lead to any loss of generality in the model and proves convenient from a mathematical point of view.

Now all the equations that we are talking of so far, are incorporated in the model GWTHERM. These equations can all be represented by a general transport equation as shown on this slide (Slide 13). The present version does not include a time-dependent average aquifer depth, h, and the formulation of the source term and density variations is rather restricted. It is intended that a more versatile version will be created in the future.

This slide (Slide 14) presents some salient features of the numerical technique employed. It employs an integrated finite difference (IFD) scheme and as a result, it is intrinsically flux conservative in the sense that you do get out what you put in; a property which you can have trouble with in some of the numerical schemes. It employs a second-order ADI scheme. For spatial integration a second-order central difference scheme is employed as a standard option. In case there is a likelihood of numerical instability, the model has an automatic built-in convective shift to use donor-cell scheme. The shift is employed when the local Peclet number is greater than two; otherwise straightforward central differencing is used. It uses staggered-grid approach which gives a better resolution and the equations are solved by an efficient tri-diagonal matrix inversion algorithm.

Some of the other features of the numerical technique are shown on this slide (Slide 15). It is seen that the model provides for a high flexibility in terms of the specification of both the physical input and the control input.

PRESSURE EQUATION DERIVATION 12

Let $\Phi = \frac{p}{\rho_0 g} + (z - z_0)$

where

Φ = a reference pressure (m)

Combination of the continuity equation and the momentum equations with the Boussinesq's assumption for density variation leads to:

$$h\, S_s \frac{\partial \Phi}{\partial t} + n \frac{\partial h}{\partial t} = \frac{1}{r} \frac{\partial}{\partial x_i} \left[rh\, K_{ij} \left(\frac{\partial \Phi}{\partial x_j} + R \frac{\partial z}{\partial x_j} \right) \right] + m_v h$$

where m_v is the volumetric flow withdrawal or input.

The darcy velocity may now be written as:

$$U_i = n u_i = -K_{ij} \left(\frac{\partial \Phi}{\partial x_j} + R \frac{\partial z}{\partial x_j} \right)$$

A GENERAL TRANSPORT EQUATION 13

The governing equations of GWTHERM can be expressed in the form of a general transport equation

$$\alpha \frac{\partial}{\partial t}(n\rho hF) + \frac{1}{r} \frac{\partial}{\partial x_i} (\beta rhG_i F - rh \Gamma_{ij} \frac{\partial F}{\partial x_j}) = h(S_p - S_m F)$$

where:

- F is the transported property
- α is an equivalent fluid-solid matrix property coefficient
- β is a fluid property
- Γ_{ij} is an equivalent dispersion coefficient tensor
- S_p and S_m are source and sink terms.

NUMERICAL TECHNIQUE: SALIENT FEATURES I 14

- An intrinsically conservative algorithm, based upon Integrated Finite Differences (IFD).
- A second-order accurate time integration scheme with a fractional step (A.D.I.) method.
- A second-order accurate space integration scheme with central difference scheme.
- Automatic convective shift to donor cells for cell Peclet number greater than 2 to assure enhanced stability.
- Improved accuracy with a staggered grid approach.
- Economical solution algorithm based upon a Tri-Diagonal Matrix Algorithm (TDMA).

NUMERICAL TECHNIQUE: SALIENT FEATURE II 15

- Arbitrarily nonuniform spatial resolution.
- Arbitrarily varying time steps.
- Inhomogeneous and anisotropic fluid and host medium properties.
- Time-dependent changes in properties, sources or boundary conditions.
- Highly flexible and conversational free-format input system which allows input changes during the course of simulation.

An illustrative example for grid selection is shown in this slide (Slide 16). The region of interest is covered by a nonuniform lattice of rectangular "elements" or "cells" and the set of governing equations is integrated over each of the cells.

GRID SELECTION: ILLUSTRATIVE EXAMPLE 16

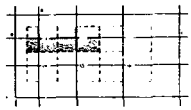

- Region of interest is covered completely by contiguous rectangular elements called "cells".
- The centers of the cells are connected by the primary grid where the dependent variables are defined.
- The "faces" of the cells are contiguous and across these convective and diffusive fluxes are transmitted from cell-to-cell.

This slide (Slide 17) shows an example of the spatial integration procedure, employing the concept of integrated finite differences for one of the differential terms in the general transport equations. The other terms in the equations are approximated in the same way.

SPATIAL INTEGRATION: ILLUSTRATION EXAMPLE 17

A typical integration step over a cell is carried out, thus:

$$I=\int_{\delta t}\int_{\delta x}\int_{\delta y}\frac{\partial}{\partial x}\left(AF-B_x\frac{\partial F}{\partial x}\right)dt\,dx\,dy$$

$$= \delta t\,\delta Y\left[A_eF_e-A_wF_w-B_x\left.\frac{\partial F}{\partial x}\right|_e+B_x\left.\frac{\partial F}{\partial x}\right|_w\right]$$

$$F_e = f_e F_E+(1-f_e)F_P$$

$$\left.\frac{\partial F}{\partial x}\right|_e = (F_E-F_P)/(x_E-x_P)$$

and so on....

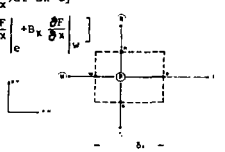

The essence of the solution algorithm is shown in this slide (Slide 18). The governing partial differential equations are reduced to a set of simultaneous, tridiagonal, algebraic equations by integrated finite difference. These equations are then solved by a tridiagonal matrix inversion algorithm.

SOLUTION ALGORITHM: I 18

- The first half step finite-difference equation may be written as:

  $a(F_P^*-F_P^n) = L_xF^* + L_yF^n + S$

- Here "*" values are unknown and "n" values are known at "old" time level, L_x and L_y are difference operators and S represents source/sink terms.
- Each grid point, in turn, gives rise to an equation which can be rearranged as:

  $A_PF_P^* + A_EF_E^* + A_WF_W^* = C$

- Ultimately there will be m equations for (m-2) grid points, and two boundary conditions
- These equations are solved by a particularly efficient TDMA

This slide (Slide 19) shows the governing equation for the rock-stress interaction model, DAMSWEL. The model is an adapted version of a widely used model developed at the University of Swansea, Wales, UK. It is based on an implicit finite-element methodology.

ROCK STRESS INTERACTION MODEL: DAMSWEL 19

- The DAMSWEL rock stress model is based upon:

$$\frac{\partial}{\partial x_i}\sigma_{ij} + \frac{E}{3(1-2\nu)H}\frac{\partial p}{\partial x_i} = \frac{\alpha E}{(1-\nu)}\frac{\partial T}{\partial x_i}$$

where:

σ_{ij}	= stress in the rock
E	= elastic modulus
ν	= Poisson's ratio
α	= linear thermal expansion coefficient
H	= external compressive stress to cause a unit change in pore fluid volume
p	= pore water pressure

- The solution algorithm is based upon an implicit finite-element methodology.

The coupling between the porous-media model, GWTHERM and the rock-stress model, DAMSWEL is based on an experimental correlation obtained by Iwai (1976) (Slide 20). The permeabilities are modified by a polynomial relation which employs the ratio of the effective normal stress to a reference value of the stress. The effective porosity is assumed to be directly related to the changes in fracture aperture. The schematic of the coupled model is outlined in this slide (Slide 21).

21

SCHEMATIC OF THE COUPLED GWTHERM-DAMSWEL MODEL

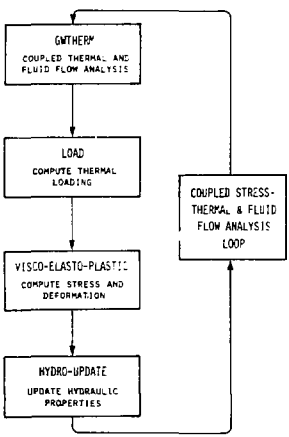

The auxiliary information required by the model is summarized in this slide. There are no surprises here (Slide 22).

Some illustrative examples relating to the application of the model to geologic repository problems will now be shown (Slide 23).

This slide (Slide 24) shows a generic stratigraphic section of a repository in granitic rock. The properties and the regional setting are shown in the slide. It should be noted that the horizontal and vertical scales are different.

GWTHERM - DAMSWEL COUPLING 20

- GWTHERM-DAMSWEL coupling is based upon the experimental data of Iwai (1976)

$$\frac{K}{K_r} = [1+A(\frac{\sigma_n}{\sigma_r})^t]^{-3}$$

where:

K and K_r are the permeabilities at effective normal stresses σ_n and σ_r, respectively.
σ_n is effective normal stress acting on the host rock.
σ_r is a reference stress for the rock.
A and t are empirical constants.

- The effective porosity is assumed to be directly related to fracture aperture.
- Other expressions can be employed at discretion.

AUXILIARY INFORMATION REQUIRED 22

- Initial conditions
- Boundary conditions
- Fluid properties
  - density, viscosity, specific heat, thermal and mass diffusivities
- Host medium properties
  - density, permeabilities, specific heat, thermal diffusivity, porosity, storativity, mechanical and chemical properties
- Sources, sink terms, generation and decay rates
- Geometry, properties and pertinent features of the system components

23

ILLUSTRATIVE EXAMPLES

RELATING TO GEOLOGIC REPOSITORIES

24

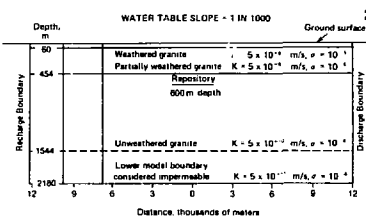

GENERIC GRANITE STRATIGRAPHIC SECTION IN ITS REGIONAL SETTING

The evolution of the flow field for this repository scenario is shown in these three slides (Slides 25 through 27). It is seen that because of the thermal convective instability, a strong vertical convection pattern emerges with time and later decays to near horizontal flow when the heat generated due to radioactive decay becomes negligible.

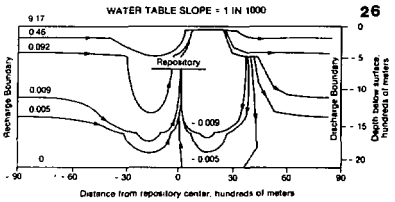

STREAM FUNCTION CONTOURS AT APPROXIMATELY 4,000 YEARS

The effect of variations in the supposed repository parameters is shown in these three slides (Slides 28 through 30). It is seen that a basic pattern of thermal instability persists though specific modifications occur for different conditions.

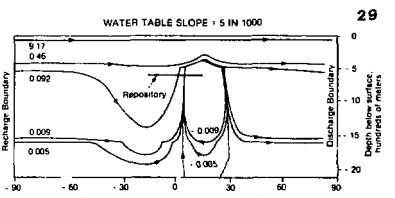

STREAM FUNCTION CONTOURS AT APPROXIMATELY 4,000 YEARS WITH WATER TABLE SLOPE OF 5 IN 1,000

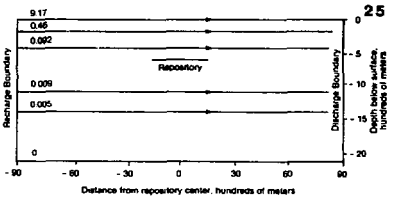

STREAM FUNCTION CONTOURS FOR NATURAL GROUNDWATER FLOW IN GENERIC GRANITE FORMATION

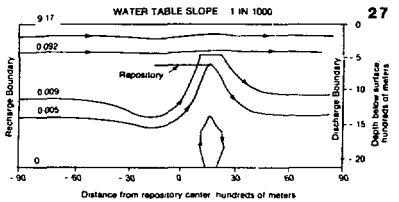

STREAM FUNCTION CONTOURS AT APPROXIMATELY 100,000 YEARS

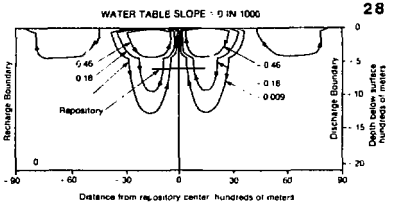

STREAM FUNCTION CONTOURS AT APPROXIMATELY 4,000 YEARS WITH ZERO WATER TABLE SLOPE

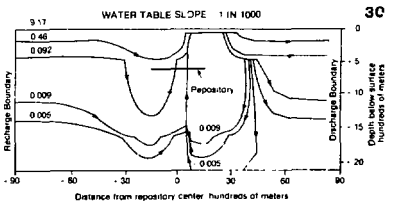

STREAM FUNCTION CONTOURS AT APPROXIMATELY 4,000 YEARS IN THE PRESENCE OF A VERTICAL FAULT

A conceptual repository in a Basaltic rock is shown in this slide (Slide 31) along with the properties employed for the study. Further details of this study are available in Hardy & Hocking (1978).

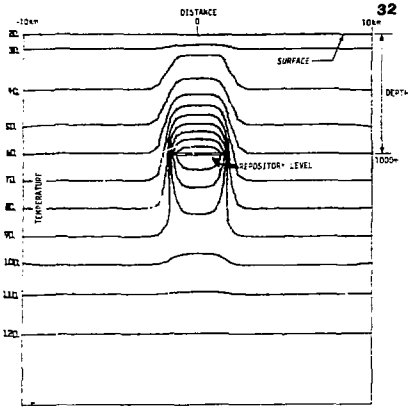

TEMPERATURE CONTOURS AROUND REPOSITORY AT 5000 YEARS

CONCEPTUAL NUCLEAR WASTE REPOSITORY
IN BASALT; THERMAL LOADING: 25W/m^2

The temperature contours, the particle flow velocity vectors, and the isopleths of Technitium-99 concentrations for this conceptual repository at 5,000 years after decommissioning, are shown in these slides (Slides 32 through 34). As in the case of the granitic repository, a strong vertical convection pattern is indicated.

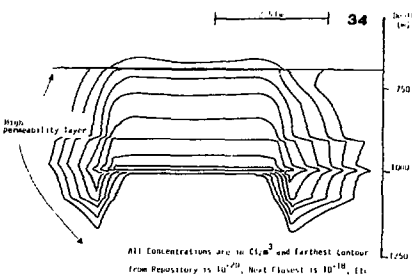

CONCENTRATION CONTOURS FOR TECHNETIUM 99 AT AN ELAPSED TIME OF 5,000 YEARS (b) CASE II

CONCEPTUAL NUCLEAR WASTE REPOSITORY
IN BASALT; THERMAL LOADING: 25W/m^2

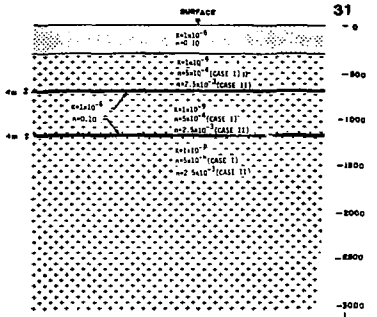

CONCEPTUAL NUCLEAR WASTE REPOSITORY
IN BASALT; THERMAL LOADING: 25W/m^2

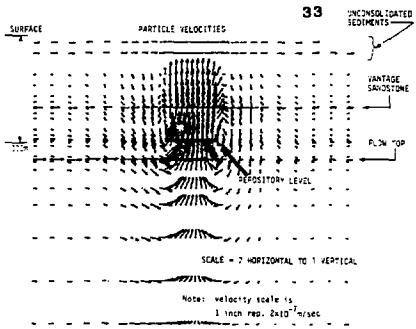

PARTICLE FLOW VELOCITIES FOR CASE I AT 5000 YEARS

CONCEPTUAL NUCLEAR WASTE REPOSITORY
IN BASALT; THERMAL LOADING: 25W/m^2

This slide (Slide 35) shows some preliminary results for particle path trajectories for particles released at the repository level with both the absence and the presence of rock-stress coupling. The numbers on the trajectories denote the years after release of the particle. It is seen that the rock-stress coupling causes some significant changes in the particle trajectories; however, the overall pattern in this case stays unchanged.

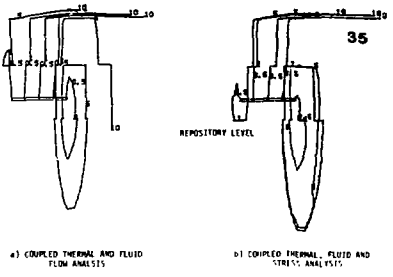

CONCEPTUAL NUCLEAR WASTE REPOSITORY IN BASALT; THERMAL LOADING: 25W/m^2

In conclusion (Slide 36), it can be stated that the model GWTHERM is a versatile, powerful, and flexible tool for a wide range of flow problems. Though the primary thrust of the model development has been toward applications in the nuclear waste repository analysis, a number of other applications to problems in the ground water pollution and aquifer storage have also been successfully attempted.

CONCLUSION **36**

- GWTHERM is a general, flexible and versatile tool for analysis of a range of ground water flow problems.
- In particular, GWTHERM has been extensively employed for analysis of the impact of nuclear waste repositories on ground water flow.
- Coupled analysis of flow, heat and mass transport is at times a very essential part of the analysis.
- Under certain conditions, rock stresses may significantly alter the nuclide migration pathways.
- The illustrative problems give an indication of some of the capabilities of GWTHERM.

I will now conclude my talk by thanking you for your patience.

REFERENCES

1. Hardy, M. P. & G. Hocking, 1978. Numerical modeling of rock stresses within a basaltic nuclear waste repository, Rockwell Hanford Operations, Prime Contract EY-77-C-06-1030, U.S. Dept. of Energy.

2. Iwai, K., 1976. Fundamental Studies of Fluid Flow Through a Single Fracture. Ph.D. Thesis, Dept. of Civil Engineering, Univ. of California, Berkeley.

3. Runchal, A. K., and T. Maini, 1980. The impact of a high level waste repository on the regional ground water flow, to appear in Intn'l Journal of Rock Mechanics.

DETECTION OF FRACTURES FROM WELL TESTING

Suresh B. Pahwa and Phillip T. Baxley
Intera-Environmental Consultants, Inc.
11999 Katy Freeway, Suite 610
Houston, Texas 77079

INTRODUCTION

Modeling of flow and transport through fractured porous media has been a topic of concern and interest in the groundwater modeling community. Detection and characterization of fractures is an important and difficult part of fracture modeling. Detection of fractures from single well slug and recovery tests is presented in this paper.

During a slug or a pulse test, a known quantity of water is instantaneously released into a wellbore and the decrease of water level with time is measured in the wellbore. In a recovery test, the wellbore is bailed out and the increase in water level is measured with time. In both the slug and recovery tests, the final or steady-state is the bottom-hole pressure equal to the formation pressure. In one case, the initial condition is a completely filled wellbore versus a completely empty one in the other case. A variation of these tests, known as drill stem test, is employed in petroleum reservoir engineering where the bottom-hole pressure is measured as a function of time by opening and shutting off the valve in cycles.

The slug and recovery tests can be interpreted using analytical solutions of the total mass conservation equation (pressure equation) in graphical forms. An example of the slug test interpretation approach is Cooper, Bredehoeft, and Papadopulos' (1967) method. They solved the flow equation for transient conditions around a well incorporating wellbore storage in their solution. Their solution is in terms of H/H_0 vs. Tt/r_c^2, where H is the water level, H_0 the inital water level, T the transmissivity, t the time, and r_c is the radius of the well casing. The analytical solution was computed numerically and a set of curves were obtained. The transmissivity is obtained by a simple curve matching procedure. This approach is entirely rigorous for homogeneous formations with ideal well completions and is quite adequate for most applications. Alternatively, a numerical model can be used to detect any unusual features - heterogeneities, fractures, or skin effects.

There are three ways of using the slug or recovery test data as input to the numerical model. These are:

(1) Input the flow rate (injection or withdrawal) and match the bottom-hole pressures.

(2) Input the bottom-hole pressures and match the flow rate based upon bottom-hole pressure limited injection of withdrawal.

(3) Input the initial water level and, based upon the bottom-hole pressure, let the model calculate the water level flow rate into the well, indicating a change in wellbore storge due to injection or withdrawal. In this case, the calculated vs. observed water levels are matched.

In this paper, use of the third method with one modification is presented. We attempted to match both water level and the rate of change of water level with time. This method assures internal consistency between the water level and the rate curves. Since the total fluid volume is constant (wellbore volume), overprediction of rate during initial times must imply underprediction during later times. Since the water level curve is integral of the rate curve, the degree of match in one curve is reflected in the other.

As will be shown in this paper, some test data can be well matched if only water level match is attempted but presents difficulty if both water level and its slope are matched. This is a positive indication of deviation from a homogeneous porous meduim formation. In the test results presented here, fractures are believed to be present and a dual porosity model is used to obtain satisfactory matches.

TESTS

The slug and recovery tests presented here were conducted by Sandia Laboratories, Albuquerque and the U.S. Geological Survey in site characterization work related to Waste Isolation Pilot Plant (WIPP). A geological cross-section near the WIPP site is shown in Figure 1 (Mercer and Orr, 1979). Above the salt layer, Salado, the Rustler is essentially the only water-bearing formation. The Rustler primarily consists of anhydrite and all the water in the Rustler is present in two relatively thin dolomite beds contained within the Rustler. From a site characterization standpoint, these two formations are of most importance. The tests presented in this paper were conducted in two dolomite formations known as Magenta and Culebra. The formations are approximately 750 feet below the ground surface. The Magenta and Culebra beds vary in thickness from 10 to 30 feet. The formations are believed to be fractured but the extent of these fractures is not known. There is no information available relative to size and distribution of these fractures.

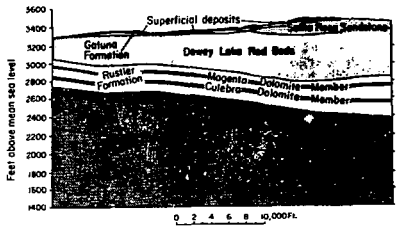

Figure 1. Geologic section near WIPP site.

Interpretations of four tests are presented here, three slug and one recovery. Two of the slug tests were done in the Culebra and one in the Magenta. The recovery test was in the Culebra formation. These had been interpreted earlier by the U.S. Geological Survey (Davis, 1979) using Cooper, Bredehoeft, and Papadopolous' method. Best match transmissivity (T) and storativity (S) values are calculated from well tests. As mentioned before, the present numerical analysis was done to detect unusual features in the system. In principle, both transmissivity (T) and storativity (S) values are calculated from well tests. However, as is commonly known, well test results are very insensitive to storativity. Storativity, or storage coefficient, can be defined as follows:

$$S = \phi b(C_W + C_R)$$

where ϕ is the porosity, b is the aquifer thickness and C_W and C_R are the water and rock compressibilities, respectively. In the numerical model used in this work, each of the parameters on the right-hand side of the above equation are explicitly included. It is worthwhile back-calculating expected range of storativity in the test formations. Compressibility of water is 1.4×10^{-6}/feet of water (3.2×10^{-6}/psi), compressibility of rocks is typically in the range 10^{-6} to 4×10^{-6}/feet (2×10^{-6} to 8×10^{-6}/psi), thickness is 5 to 30 feet, and porosity is of the order of 10% (0.1). Therefore, the storativity should be in the 10^{-6} to 10^{-5} range.

DUAL POROSITY MODELING

The dual porosity modeling done here is conceptually simple. One or more fractures are assumed to be either intercepted by the well or formed by drilling and extend away from the well. In either case, fluid injected into the well can directly enter some fractures without any matrix in between. It is also assumed that the matrix permeability is not negligible relative to the fracture permeability and, therefore, both systems must be simultaneously modeled. Not knowing the number, location or spacing of the fractures, both fracture and matrix media are superimposed within the same volume of total rock and fluid media. A conceptualization is presented in Figure 2. It is important to remember that the fluid transport characteristics of the total rock and fluid media are being modeled and, for simplification, the two fluid transport components of the medium are separated, but modeled simultaneously.

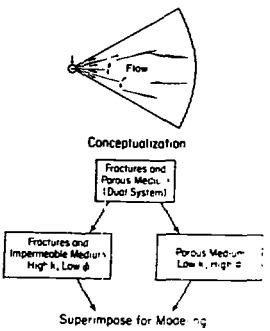

Figure 2. Conceptualization of a Fractured Porous Medium and Dual Porosity Modeling.

ANALYSIS

As mentioned before, interpretation of four tests are presented in this paper. Interpretation of the first test did not require any fracture flow modeling, whereas the other three did. The first test results are included here to show the distinctly different behavior of those wells which exhibited fractures.

Slug Test: The well H2C is completed in the Culebra formation. The perforation interval is 624 to 652 feet below ground surface. A two inch diameter tubing is placed inside the cased hole. Two packers were set at 608 and 735 feet to isolate the perforated interval. The tubing was placed in the packed interval for filling and conducting the slug test.

The observed water level and flow rate curves are shown in Figure 3. The USGS interpreted the data to calculate transmissivity and storativity values of 0.32 feet^2/day and 1.8×10^{-5}, respectively. A homogeneous value of 0.32 feet^2/day for the transmissivity and 0.1 for the porosity were used in the numerical model. This gave a good match of the data (see Figure 3). This could be interpreted to mean that the fractures were not intercepted by well H2C, or that the fractures present around the other wellbores (as will be shown later) are localized around those wells.

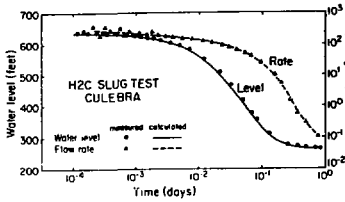

Figure 3. Comparison of calculated results and measured data for the H2C well slug test using T = 0.32 feet^2/day and ϕ = 0.1.

Slug Test: This hole, H2B, is also completed in the lower dolomite member of the Rustler formation - Culebra. The hole is 661 feet deep out of which the upper 611 feet are cased, leaving the lower 50 feet as the open hole interval for testing. A 4.75 inch tubing extends to the open hole interval. The tubing and the open hole are isolated from the casing annulus using a packer at roughly 601 feet depth. The water level and the flow rate curves as functions of time are shown in Figure 4. The water level curve is smooth and monotonic in behavior, however, the flow rate curve shows an inflection point and two distinctive behaviors.

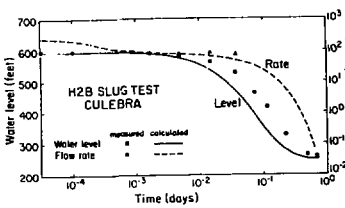

Figure 4. Comparison of calculated results and measured data for the H2B well slug test using T = 0.39 feet^2/day and $\phi = 1.8 \times 10^{-5}$.

The USGS interpretation of the test showed a transmissivity value of 0.39 feet^2/day and storativity of 1.8×10^{-9}. Using the aquifer thickness and compressibilities stated previously, these correspond to a hydraulic conductivity of 0.013 feet/day and porosity on the order of 10^{-5}.

Formation transmissivity is directly related to the slope of the water level curve. As can be seen in Figure 4, using the above mentioned values, slopes of the calculated and observed values match reasonably well, indicating a degree of confirmation for the transmissivity value of 0.39 feet^2/day. However, the time values (at the same water level) differ by roughly a factor of 2. Also, the rate curve match is unsatisfactory. The porosity was then varied and, as is generally the case with these tests, found to have relatively little effect on the calculated curves. When the transmissivity was increased by a factor of 3, it was possible to match the first part of both the curves, but not the second. This is shown in Figure 5. At this point, heterogeneity was introduced. Transmissivity near the well was increased to 0.5 feet^2/day. The results are drawn in Figure 6. In this case, a good match of the water level curve was obtained, but the initial portion of the rate curve and the inflection point could not be matched. This shows the possible presence of fractures in the system. Dual porosity modeling gave an excellent match of both the curves.

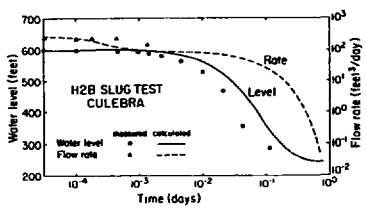

Figure 5. Comparison of calculated results and measured data for the H2B well slug test using ϕ = 0.1 and T = 1.17 feet^2/day.

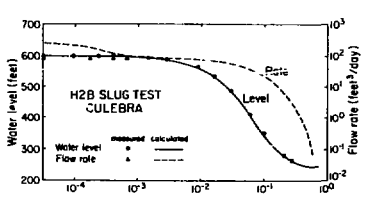

Figure 6. Comparison of calculated results and measured data for the H2B well slug test using ϕ = 0.1, T = 0.5 feet^2/day near the well and 0.39 feet^2/day away from it.

The dual porosity match is shown in Figure 7 with matrix transmissivity of 0.39 feet^2/day, porosity of 0.1, and fracture transmissivity of 1.17 feet^2/day, porosity of 0.001. When the slug test starts, fluid is taken by the fractures. The initial rate is 650 feet^3/day and it stays high for the initial period of 10^{-3} day. Once the fracture system is filled and pressurized, fluid goes into the rock matrix both directly from the well and through the fractures. Subsequently, the well behavior is totally dominated by the matrix system and a homogeneous matrix response is seen in both rate and water level curves.

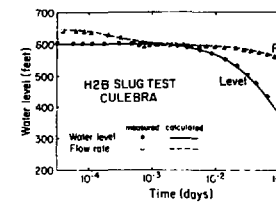

Figure 7. Comparison of calculated results and measured data for the H2B well slug test using a dual porosity system. Fracture system T = 1.17 feet^2/day, : = .001 matrix system T = 0.39 feet^2/day, : = 0.1.

It should be pointed out that essentially the same match could be obtained using different sets of values for the fracture system porosity and length from the wellbore. As long as the fracture volume was kept the same, length and porosity could be varied up to factors of 3 without any noticeable change in the match. It implies that it is difficult to estimate fracture spacing and length from these types of tests.

Recovery Test: Transmissivity and porosity values calculated from the slug test were used in the recovery test in Well H2B. Comparison of the calculated values with the observed data is shown in Figure 8. The match is excellent providing a confirmation of the previously calculated transmissivity and porosity values. As mentioned before, it was difficult to calculate the extent of the fractures. From these tests, it is reasonable to say that the region around the well H2B is fractured. However, it is difficult to say whether these fractures are local, possibly caused by drilling operations, or extend over a much larger area. The slug and recovery tests measure properties only in the close vicinity of the wellbore. Changing the aquifer properties away from the wellbore did not show any impact on the well test interpretations. The relative transmissivity values indicate that the magntude of flow in fractures is comparale to the magnitude of flow in the matrix and is not dominated by either of the two systems.

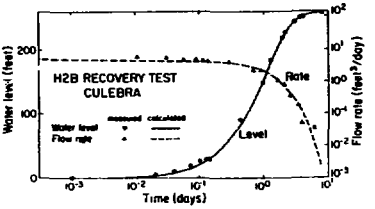

Figure 8. Comparison of calculated results and measured data for the H2B well recovery test using the same dual porosity match parameter obtained from the slug test.

Slug Test: The H2A well is completed in the Magenta, the upper dolomite formation. The open hole inteval is 511 to 563 feet below land surface. The packer is set at 505 feet. The tubing diameter is approximately 2 inches. The water level and the flow rate curves are shown in Figure 9. The behavior is qualitatively similar to the H2B slug test discussed in the previous subsection. The water level changes monotonically along a smooth curve, but the flow rate actually increases at roughly 10^{-2} days and shows discontinuities. These are probably data measurements but two distinctive behaviors are certain. Again in this case, a dual porosity parameterization was required to match the observed behavior qualitatively and quantitatively.

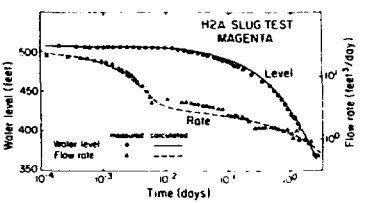

Figure 9. Comparison of calculated results and measured data for the H2A well slug test using a dual porosity system. Fracture system T = 0.05 feet^2/day, = 0.001, matrix system T = 0.005 feet^2/day, : = 0.1.

The USGS calculated a transmissivity value of 0.005 feet^2/day and a storativity of 1.8×10^{-4} which would indicate an extremely high porosity (of the order of 1.0). This again points out the difficulty of being able to calculate porosity or storativity from single well aquifer tests. The best match dual porosity parameters were 0.005 feet^2/day and 0.1 for matrix transmissivity and porosity. The corresponding values for the fracture system were 0.05 feet^2/day and 0.001.

CONCLUSIONS

General conclusions that can be drawn from the interpretation of these tests are as follows:

(1) Interpretation of single well slug and recovery tests can be done more accurately by matching both water level and flow rate instead of matching only water level as is done in conventional interpretation methods.

(2) The numerical method of slug and recovery test interpretation described in this paper can be used to determine existence of fractures.

(3) This method cannot be used to characterize fractures in terms of determining orientation, spacing, width, and length. If fractures are determined by this method, other tests are needed to characterize fractures.

(4) The Magenta dolomite and Culebra dolomite in the vicinity of the two wells definitely give indications fo being fractured.

REFERENCES

Cooper, J.J., Jr., Bredefhoeft, J.D., and Papadopulos, I.S., "Response of a finite-diameter well to an instantaneous charge of water", Water Res. Res., 3:1, 263 (1967).

Davis, Paul, U.S. Geological Survey, Water Resources Division, Albuquerque, New Mexico, Personal Communication (1979).

Mercer, J.W., and Orr, B.R., "Interim data report on the geohydrology of the proposed waste isolation plot plant site in southeast New Mexico". U.S. Geological Survey, Water Res. Res., Inv. 79-78 (1979).

MODELING OF GROUNDWATER FLOW IN FRACTURED ROCKS FOR RADIOACTIVE WASTE REPOSITORY STUDIES

A. S. Burgess and J. L. Ratigan
Acres American Inc. — RE/SPEC Inc.
Buffalo, New York — Rapid City, South Dakota

MODELING REQUIREMENTS

A model is a representation of a real or a planned system. Thus all models are approximate, uncertain and incomplete. However, they are easier to understand, construct and manipulate than the system they represent. The model to be used is determined by the questions being asked and the process being represented. Thus, modeling a system requires

- a statement of the objective
- conceptualization of the system
- development of the model
- application of the model.

Modeling Objectives

The prediction of the groundwater flow regime in a fractured rock may have a different objective depending on the nature of the problem. Thus, models used for geothermal, radioactive waste, dam foundations, oil recovery, water supply, or product storage will each have significant differences. In this paper, considerations will be primarily for the modeling of groundwater flow in fractured rock in connection with radioactive wast repositories. For this, the objective is to define the groundwater flow regime in and around the repository for subsequent use in nuclide transport calculations and estimates of dose to man.

Conceptualization of Fractured Rock for Modeling

Conceptualization of fractured rock for modeling must be based on observations, particularly of outcrops or excavations, which indicate

- fracture density (total length per unit area) may vary widely over short distances
- in general, there are fewer major fractures (i.e., long, single open fracture or multiple fractures in limited zones) than minor fractures (discontinuous, closed)
- many fractures are grouped in similar orientations
- the larger groundwater seepages are generally associated with the major fractures
- seepages frequently occur only at localized places along a fracture

Figures 1 through 2 show maps of fractures in crystalline rock terrain at two different scales. Without reference to the scale for each, it is difficult to determine whether the area represented is on a scale of feet or miles. A filtering of the data, thus, occurs in any representation. From satellite imagery or high level aerial photography, only major features (lineaments) are identifiable (Figure 1). Features with lengths of less than about 500 m are usually not considered significant at this scale. By comparison, detailed mapping of the dam foundation shown in Figure 2 identifies all features down to length of approximately 3 m. Even at this scale, however, multiple fractures are frequently plotted as fracture zones, rather than discrete fractures. The same principle can be taken even further and examination of rock cores indicates a series of microcracks which are ignored in outcrop mapping.

To characterize a rock mass for groundwater flow, data on the following are required

- fracture orientations
- fracture lengths
- fracture spacings
- fracture surfaces, infillings, apertures
- relationships between fracture.

Analyses of joint spacing by Snow[1], Priest and Hudson[2] indicate that joint spacings have a Poisson distribution. Data on apertures by Snow[3] shows that these tend to be log normally distributed. The length of joints appears to have a log normal or negative exponential distribution (Ringdal[4]).

The cross-correlation between these characteristics has not been established. However, positive correlation might be expected between aperture and length. Geological observations indicated that fewer major faults occur in an area than minor faults and joints. This indicates a negative correlation of fracture density with fracture length. Data from Canada and Sweden of fracture density versus length, plotted on log scales in Figure 3 shows a negative correlation (Burgess[5]). Because of the method of sampling, each data point represents the total density for fractures having lengths of average length L ± 0.5 log cycle in meters. Thus, an average length of 10 km includes all fractures in the range 3.16 to 31.6 km. This is based on the assumed sensitivity of the different sampling methods, i.e., outcrop survey will yield data primarily in the range 1 - 10 m; air photo interpretation will yield data primarily in the range 0.5 - 5 km. Much more data is required to determine if series of curves exists for each curve representing a different tectonic region fracture density and length relationship.

The choice between representing the rock mass by an equivalent porous medium or a series of discrete fractures will depend on the size of area being modeled, and the data availability.

Three models are proposed which are capable of explicitly recognizing the range of likely conditions. These are

- regional models in which discrete identifiable features can be modeled in a deterministic manner.
- site models representing the areas between the discrete major features in the above model. In

FIGURE 1: MAJOR LINEAMENTS IN AREA OF CANADIAN SHIELD (STEVENSON, J.S. 1962. THE TECTONICS OF THE CANADIAN SHIELD)

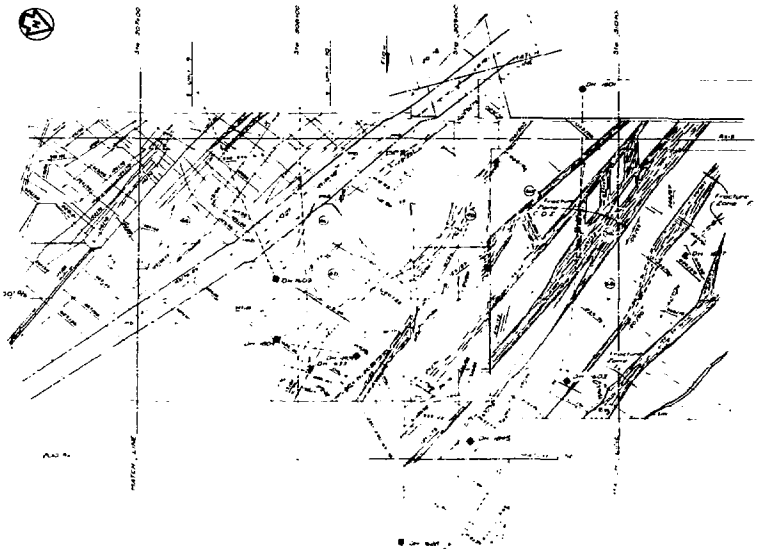

FIGURE 2: FRACTURE MAPPING FOR DAM FOUNDATION

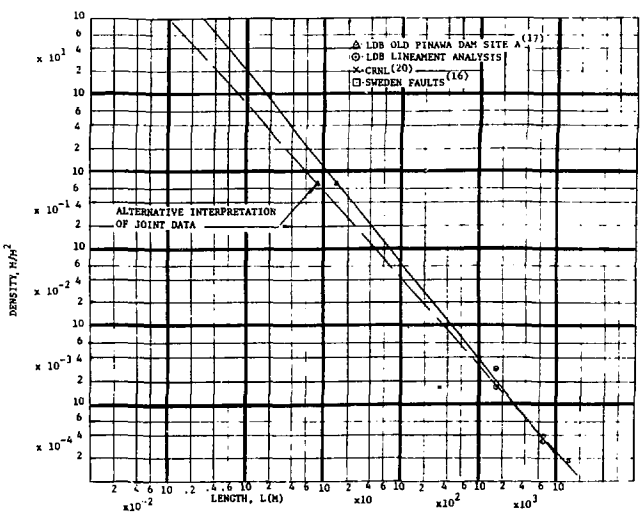

FIGURE 3: FRACTURE DENSITY RELATIONSHIP

these regions, the fracture distribution will be unkown and an equivalent porous medium model will be used. Coupling will be important between heat and groundwater flow, and possibly between stress and permeability.

- local models. These will model the area of the emplacement drill hole and room. Intact rock properties are reasonably definable. However, the distance and distribution of any significant fractures in and around the repository or the potential distribution and gradients in the room/canister region will not be known. For this region, a probabilistic approach is preferred. The influence of stress on permeability due to fracture aperture changes or fracture growth will require consideration.

The analysis logic for groundwater flow and contaminant transport is shown in Figures 4a and 4b.

The choice between discrete fracture and equivalent porous medium modeling are made on the basis of available data and discretization scale in the model. Thus, fractures which would be significant on the scale of discretization employed in a model should be defined as discrete features. If their location and characteristics cannot be defined deterministically, than a probabilistic approach must be adopted.

Parameters

For groundwater flow, the principal parameter of concern is the hydraulic conductivity of the individual fractures or rock mass. For transport considerations, i.e., velocity, the effective flow porosity is also required.

At present, measurements of the hydraulic conductivity of fractured rocks are limited, particularly at the depths for which the repositories are being considered. A summary of the available data is shown in Figure 5. Individual measurements made for intervals of about 2 m have been averaged over 50 m, since this is the approximate element size employed in the finite element modeling. In general, there is a decrease of hydraulic conductivity with depth to about 200 m, below which data variability obscures any trend. An envelope has been drawn to encompass the majority of the points. In addition, the depth-hydraulic conductivity relationship used in the KBS study by the authors is shown for reference. This relationship was developed based on limited information prior to the field data shown in the figure being available.

Porosity estimates made by assuming a simple parallel plate model appear to underestimate actual flow porosity by one to two orders of magnitude (Burgess[6]). This is attributed to the variations in aperture along a fracture and the tortuous flow path. Tracer testing is required to provide a reasonable data base for flow porosity.

FINI COMPUTER CODES

Groundwater modeling around conceptual repositories has been performed using the Acres FINI series of codes. FINI 500 is a finite element program for two-dimensional isothermal saturated flow in a porous medium for transient or steady-state conditions. FINI 520 is a nonisothermal version for thermally induced flow. The time-dependent temperature equation is combined with the quasi-steady pressure equation to account for the density buoyancy effect. Six noded isoparametric elements are used in both codes. Other element types available are 3-noded loading line element for source or sink and 6-noted gap/film elements. Full descriptions of the models are given in Burgess[6] and Ratigan et al[7].

MODELING FOR KBS

This section presents the results of studies of groundwater movements around a conceptual high-level radioactive waste repository in crystalline rock in Sweden. The work was carried out for KBS in 1977[6, 7, 8, 9, 10, 11, 12]. The results are summarized by Burgess[13].

Methodology

The objective of this study was to assess the groundwater movements around a repository using the best available data and analytical techniques. The finite element method was used to model thermal, mechanical and groundwater conditions.

To study groundwater flow around the repository, the coupling of thermal, mechanical and geohydrological parameters was recognized (Figure 6) together with time dependency of the thermal loading. At present, the coupling functions are inadequately defined. Some of the coupling was, therefore, performed separately from the main analyses, allowing the sensitivity of the interdependencies to be assessed.

The study commenced with analyses of the conductive heat transfer and of the initial groundwater conditions. The advective transfer of heat by seepage fluxes and investigated and shown to be insignificant. Following the development of a stress-permeability function, construction and postemplacement groundwater flow conditions were analyzed. Finally, long-term residual conditions were modeled. This represented the time span following the period of significant heat production. The analyses assumed equivalent porous media flow and used permeability and porosity values which were available from conventional packer tests.

Input Parameters

Repository Layout. The repository geometry, defined by other study groups, consists of rooms approximately 3,5 m in diameter at 25 m center to center at a dpeth of 500 m. The waste canisters would be emplaced in 1.0-m diameter vertical drill holes, spaced 4.0 m in the floor of the rooms. On completion, the entire repository would be suitably backfilled and sealed. The gross thermal loading for this arrangement is 5 W/m^2 on emplacement.

Thermal and Mechanical Properties. Rock mechanics and thermal parameters were determined from literature review and specific testing.

Permeabilities. Permeability values were based on a review of existing data for the Baltic Shield. Relevant averaged permeability depth profiles from available packer test results were used, and a log-log polynomial fitted to a median curve and extrapolated to 2,000 m

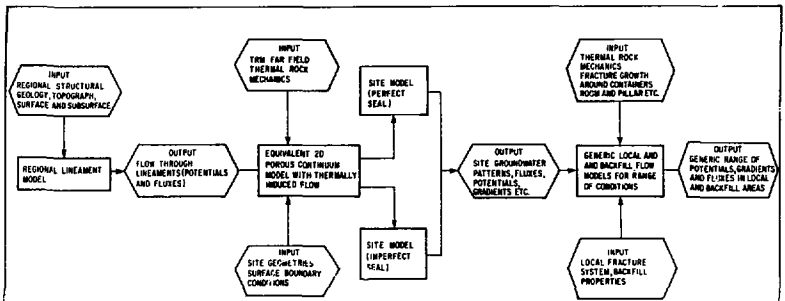

FIGURE 4a : GROUNDWATER MODELLING

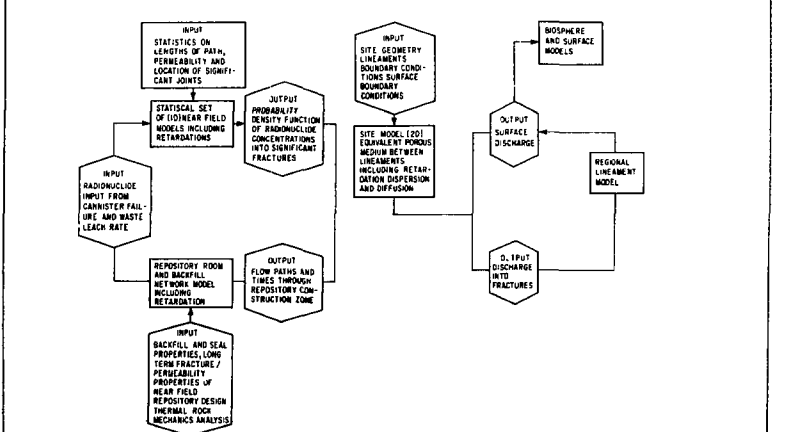

FIGURE 4b : CONTAMINANT SOURCE AND TRANSPORT MODELS FOR SAFETY ANALYSIS

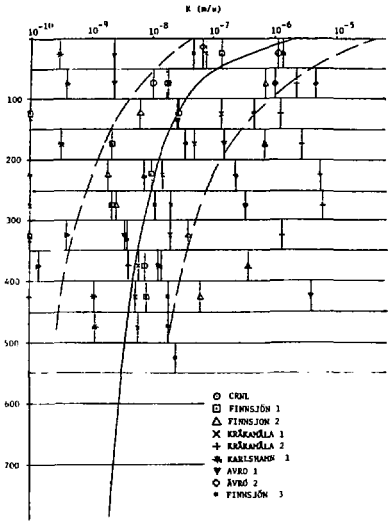

FIGURE 5: SUMMARY OF DEEP PERMEABILITY TEST DATA

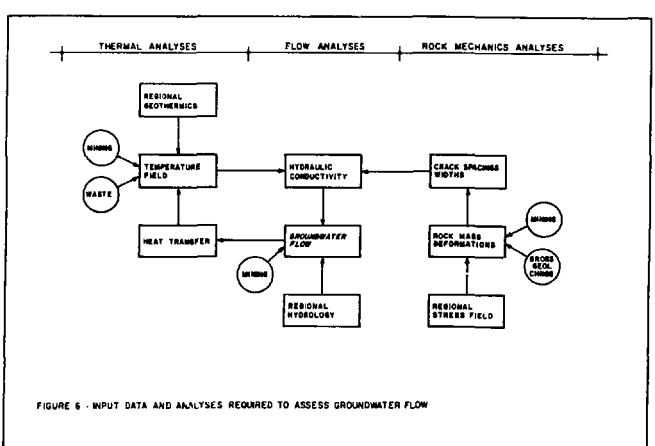

FIGURE 6 - INPUT DATA AND ANALYSES REQUIRED TO ASSESS GROUNDWATER FLOW

depth (Figure 3). Rock mass permeability tests undertaken subsequent to this study indicate that standard packer test results may overestimate permeability by one to two orders of magnitude. The implicaton of this is discussed later in this paper. The actual permeability of a particular limited section of a drill hole, however, may vary from the limit of measureable permeability of about 10^{-6} m/s or even higher.

To completely describe the permeability of a continuum, it is necessary to define the principal values of permeability and the direction of the principal axes in space. The analysis of most field tests assume the medium to be isotropic. However, as noted by Snow[14], isotropy is the exception rather than the rule in groundwater hydrology.

In situ stress measurements in the Baltic Shield show that the horizontal stress is greater than the vertical stress. Fracture aperture and hence permeability are inversely proportional to the normal stress on the aperture. Anisotropy of the permeability may, therefore, be expected. In general, permeability data are obtained from vertical drill holes and preferentially measure the horizontal permeability.

In this study, three permeability depth relationships were used:

Case 1 - Permeability homogeneous isotropic constant

$$K = 1.0 \times 10^{-8} \text{ m/s}$$

Case 2 - Permeability isotropic, decreasing with depth according to the empirical function

$$\log K = -5.57 + 0.362 (\log Z) - 0.978 (\log Z)^2 + 0.167 (\log Z)^3$$

where Z = depth in metres

Case 3 - Permeability anisotropic

$$K_Z = 1.0 \times 10^{-9} \text{ m/s}$$

$$\log K_R = -5.57 + 0.362 (\log Z) - 0.078 (\log Z)^2 + 0.167 (\log Z)^3$$

The objective of using these distributions was to investigate, for a given set of boundary conditions, the sensitivity to decreasing permeability with depth and the effect of anisotropy. While the authors believe that anisotropy is likely, it must be emphasized that this is based solely on circumstantial evidence (in situ stress, observations of near-surface excavations). Such existence in the prototype remains to be proven.

Porosities. The porosity of crystalline rocks is rarely measured in the field or laboratory. It is, however, a very important parameter in the determination of the pore velocity. Empirically or theoretically derived relationships between porosity and permeability may be used to determine the porosity where only the permeability has been measured.

The most widely used are Kozeny-Carmen (see Fisher[15] for application to fractured rocks) and the parallel plate model developed by Snow[1].

Norton and Knapp[16] report laboratory porosity measurements on crystalline rock samples showing flow porosities three to four order of magnitude smaller than total porosities. Porosity and permeability values of small granite samples were measured by Fisher[15] in connection with geothermal studies in the Los Alamos granite. Porosity values for Canadian crystalline rocks of 0.27 percent to 1.39 percent have been reported[17]. No details of the method of measurement or of the corresponding permeability values are given.

Webster[18] measured travel times for radioactive tracers in deep crystalline rocks in the Savannah basin. The effective porosity value computed was 8×10^{-4} for a permeability estimated at between 1.633×10^{-6} and 7.424×10^{-6} m/s.

At Studsvik, in situ tests were carried out by AB Atomenergi and SGU on a joint at a depth of 60 m to determine pore velocities and retardation characteristics[19]).

At Stripa Mine, average rock mass permeability and porosity values of 4×10^{-11} m/s and 1.3×10^{-4} m/s, respectively have been obtained by tracer methods[20]).

These field and laboratory results are plotted in Figure 7. It may be noted that empirical porosity values measured directly are higher than those calculated by the above porosity/permeability relationships for the same permeability value.

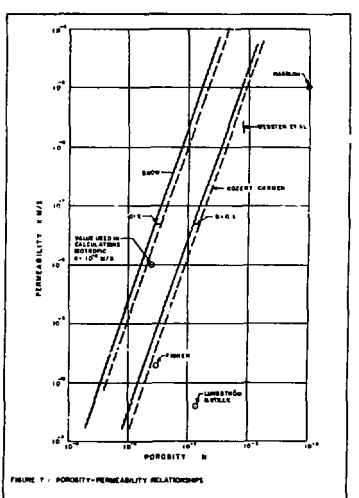

FIGURE 7 : POROSITY-PERMEABILITY RELATIONSHIPS

For a given permeability, the computed porosity may vary over about three orders of magnitude depending on the theoretical or empirical relationship selected. For this study, porosity values were based on Snow's parallel plate model for a constant joint spacing of 1.8 m. The joint spacing was based on the only fully detailed information available at the beginning of the study, and observations of personnel familar with excavations in Swedish Precambrian rock. The application of this model results in high estimates of pore velocities. However, since the porosity has been calculted from the permeability in a consistent manner throughout the analyses, the reported pore velocities may be readily modified as further field data become available on site-specific permeability-porosity relationships.

Boundary Conditions. Because of the relatively high rainfall in Sweden compared to infiltration, the groundwater surface is, in general, within 3 to 4 m of the ground surface. For this study, the water table was assumed coincident with the ground surface. For all models, the lower boundary has been taken as impervious, i.e., a flow line at a depth of between 1,000 and 2,000 m, depending on the model. Both constant potential and zero flux (flow line) vertical boundaries have been used in the analyses.

Models for Initial Conditions

Studies of the Finnsjön site are described in this paper. It is located 15 km from the Forsmark nuclear generating station site on the Baltic coast. The area exhibits subdued local relief of about 10 m; the major low-lying areas are occupied by lakes and the general elevation is about 35 m.

The terrain inland from the site is similar, with the average elevation rising about 1 m in 2 km. At a distance of about 100 km, between Sandviken and Avesta, the relief becomes more pronounced, typically 100 m and locally up to 300 m. This topography continues westward to the Norrland Mountains area.

The bedrock of the region comprises Precambrian Svecofennian gneisses and gneissic granites with some leptites and minor areas of younger granitic and basic intrusions.

The regional groundwater flow is considered to take place primarily in the major tectonic features and possibly also in the upper portion of the bedrock where subhorizontal joints are well developed. In the Forsmark area, the regional groundwater gradient is about 1 in 1,000. Idealized flow lines were drawn orthogonally to the groundwater contours. However, the real flow paths are primarily along the major tectonic features.

For local models, representative potential distributions and/or fluxes from the regional model were used to define the boundary conditions for smaller areas. In particular, the major tectonic features were used as model boundaries to enable the response of the intervening rock block to be studied for various material parameter values and boundary conditions.

To study possible groundwater flow patterns in a typical repository zone, a two-dimensional vertical finite element model of the study area was used. The goundwater surface and consequently the upper boundary potentials were assumed coincident with the ground surface. The relief of the ground surface itself, however, was not included in the model. Two major tectonic features bounded the area of study. The features ` approximately 1,750 m apart and are perpendicular to the regional groundwater gradient with surface potentials of 28.1 m and 24.5 m.

The bounding discontinuities were represented by 10-m wide zones with an isotropic permeability of 1.0×10^{-5} m/s. Two types of boundary conditions for these discontinuities have been considered: a vertical equipotential, and a vertical streamline. The field potential distribution is expected to lie between these two extremes.

The three permeability assumptions were analyzed with the two possible boundary conditions above resulting and following conclusions were drawn.

- For the same material properties, the change of boundary conditions has only a slight effect on the pore velocity magnitudes. The directions are modified, especially near the bounding discontinuities.
- The pore velocities at 500-m depth decrease successively for the cases of isotropic constant permeability, isotropic permeability decreasing with depth, and anisotropic permeability decreasing with depth, respectively. The anisotropic cases show that a quiescent zone could be expected at repository depths.

Models for Construction Emplacement Thermal Periods

The short-term conditions reflect the period from construction through emplacement of the waste, decommissioning of the repository, and the principal period of heat generation. During construction and the thermal cycle, changes in stress around the repository will result in changes in permeability. Analyses based on permeability of a fracture being a function of normal stress indicate that the major permeability changes would be due to construction, with changes due to the thermal cycle being much less significant.

Besides causing changes in stress and consequently permeability, the existence of the heat generating waste can cause thermally induced flow within the groundwater. This was studied using a fully coupled heat and mass transfer finite element method. Without a regional cross-flow, convection cells could theoretically occur (Figure 8). However, with a regional cross-flow, the cells degenerate into minor perturbations to the natural flow pattern (Figure 9). This indicates that a slight cross-flow through the repository site may be beneficial in that it eliminates convection cells and possible relatiely short pathways to the biosphere.

Models for Long-Term Conditions

For the analysis of the groundwater flow for the long-term residual effect conditions, the vertical section model was modified to include the repository plane. The repository was 1,250 m long and equidistant (250 m) from the bounding discontinuities.

The results of the groundwater studies of the initial conditions showed that the flow pattern was not sensitive to changes in boundary conditions, due to the high permeability assumed for the bounding discontinuities. For these analyses, therefore, the constant potential

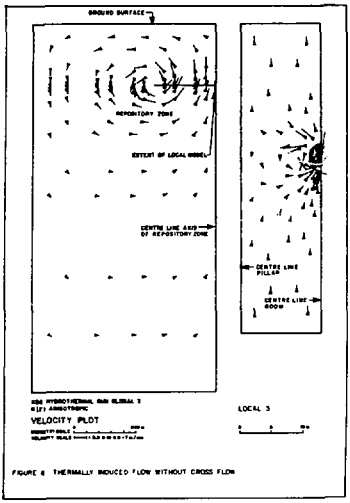

FIGURE 8 THERMALLY INDUCED FLOW WITHOUT CROSS FLOW

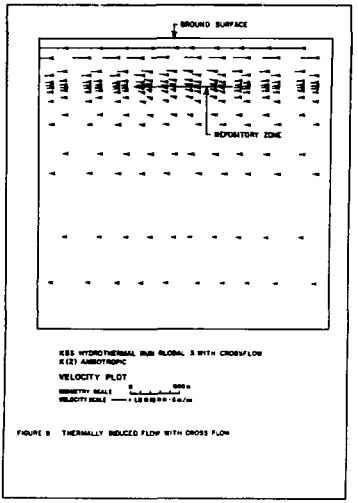

FIGURE 9 THERMALLY INDUCED FLOW WITH CROSS FLOW

vertical boundary condition only was modeled. The potential was taken as the elevation of the ground surface.

The potentials specified on the upper boundary of the model were equal to the ground surface elevation. The lower boundary of the model was considered impervious, i.e., a streamline.

Analyses were made for the three nominal permeability distributions used for the initial conditions study In addition, for comparative purposes, the effect on travel times of a permeability 5 x 10^{-11} m/s at 500-m depth was assessed for the anisotropic conditions (Case 3). This value was obtained from large-scale in situ permeability results at the Stripa Mine[20].

For the repository, two extreme permeability distributions have been considered.

(a) Impervious Backfill. For this condition, it is assumed that the room will be backfilled with impervious material of permeability characteristics similar to the surrounding rock mass. In addition, the rock is assumed to maintain its prerepository permeability characteristics. Under these assumptions, groundwater flow patterns will be identical to the undisturbed natural conditions, and thus represent a bound to the possible range of conditions.

(b) Pervious Backfill. For this condition, the rooms are assumed to be left void or loosely backfilled with pervious material. Over the long term, deterioration may result in an equivalent continuum at the repository plane having a thickness of 5 m, with a permeability of 1 x 10^{-3} m/s and porosity of 20 percent. This value represents a room permeability of 6 x 10^{-3} m/s for a long-term cross-sectional area of twice the initial cross-sectional area, or a room permeability of about 3 x 10^{-3} m/s for a long-term or cross-sectional area of 4 times the intial value. For these analyses, it has been assumed that the rooms are aligned parallel to the groundwater flow direction.

For an isotropic constant permeability distribution, Case 1 (Figure 10) the flow pattern is strongly influenced by the upper boundary condition (topography). The flow is generally downward through the repository and laterally toward the vertical boundaries. For the impervious backfill case, the equipotentials are strongly curved in the vicinity of the repository, becoming near vertical adjacent to the vertical boudaries. The pervious backfill, however, results in the equipotentials becoming near horizontal immediately above and below the repository. The nature of the backfill also affects the fluxes and pore velocities. For the pervious backfill condition, the fluxes and pore velocities are increased around the margins of the repository and reduced through the central portion.

For the case of isotropic permeability decreasing with depth, Case 2 (Figure 11), the flow patterns are similar to Case 1, being strongly influenced by the topography. The flow is downward throughout the repository area for both backfill conditions. The differences between the equipotential patterns for the two backfill cases are also similar to Case 1. For the impervious backfill condition, they are strongly curved in the repository area; for the pervious backfill condition, however, they are nearly horizontal immediately above and below the repository. Compared with the impervious backfill, the fluxes and pore velocities are

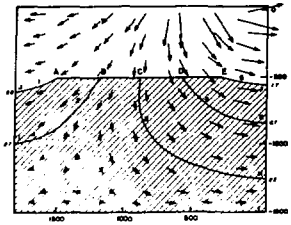

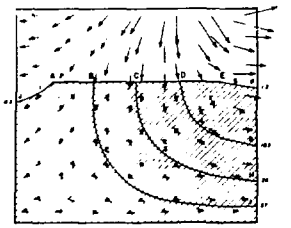

FIGURE 10 PATHWAYS AND TRAVEL TIMES CASE 1 ISOTROPIC HOMOGENEOUS PERMEABILITY DISTRIBUTION

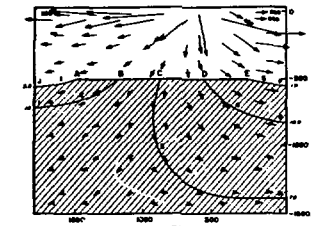

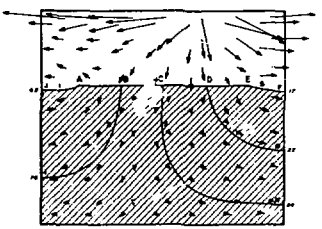

FIGURE 11 PATHWAYS AND TRAVEL TIMES CASE 2 ISOTROPIC NON-HOMOGENEOUS PERMEABILITY DISTRIBUTION

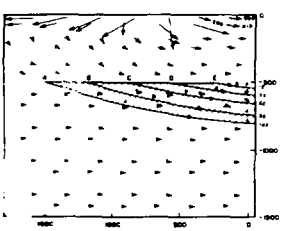

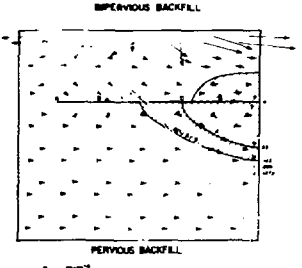

FIGURE 12 PATHWAYS AND TRAVEL TIMES CASE 3 ANISOTROPIC PERMEABILITY DISTRIBUTION

increased around the margins of the pository and reduced in the center.

The flow patterns for the anisotropic permeability distribution, Case 3 (Figure 12), is markedly different to those for isotropic conditions. With both pervious and impervious backfill, there is a strong, topography-induced lateral flow in the upper 200 m. For the impervious backfill conditions, the flow paths below 200-m depth are nearly horizontal across the site. These conditions are modified with pervious backfill within a region 200 m to 300 m above and below the repository. Flow is drawn into the repository on the upstream side, travels through the repository, and is discharged downstream. Over the upstream third, flow is into the roof and floor; over the center third, flow is into the roof and out from the floor; and over the downstream third, flow is out from the roof and the floor. The asymmetry is due to the regional cross-flow having a slight downward component across the site.

Discussion of Results

The permeability distributions used in the analyses were selected primarily to determine the sensitivity of flow patterns to the hydraulic properties. The travel times should, therefore, be considered on a comparative rather than an absolute basis.

For the impervious backfill case, the exit pathways from all locations in the repository are below the repository. For the pervious backfill case, the quickest pathways will be through, above or below the repository, depending on the starting point. The velocity of flow through the pervious repository zone is largely independent of the host rock permeability, being controlled by the porosity characteristics of the backfill. The travel times through the repository assume that the rooms are oriented parallel to the groundwater flow direction, i.e., parallel to the plane of the model.

An interesting and important paradox is seen in these results: travel times from an emplaced canister can be increased by using a porous pervious backfill. In addition, with impervious backfill, the flow paths do not pass through the repository plane after passing the canisters. Consequently, any benefits of retardation by geochemically engineering the backfill within the rooms would not be obtained. The geohydrologic properties of the backfill must, therefore, be specified with due considerations of the surrounding rock.

When the flow reaches the bounding major tectonic feature, the flow path will depend on the flow within and through the feature, within which the flow will undergo dilution mixing and dispersion. Some of the flow from the repository will, therefore, travel within the feature, and some will pass out into the adjacent rock. The partition of the flow and hence the concentration of any leached nuclides will depend on the relative hydraulic characteristics (permeability, gradient) of the bedrock block and the structural feature.

Considering the discharge plume from the repository to the bounding feature, the total quantity of flow is given by the surface integral of the flux over the boundary between the pathway limits.

The flux within the structural feature will be a function of the permeability and boundary conditions. The dilution of the repository plume will depend on the width of the structural feature, the flux and extent of mixing and dispersion. The transport times will be a function of the flux and porosity within the feature.

Modeling of groundwater flow around a conceptual repository, therefore, identified the need for methods and field data to assess

- the extent of anisotropy within the rock
- the rock mass permeability compared to the individual fracture permeability
- the rock mass flow porosity and its relationship (theoretical or empirical) to permeability
- the coupling between stress and permeability on an individual fracture basis and, perhaps more importantly, on a rock mass basis due to extension of fractures increasing overall fracture continuity.

CONCLUSIONS

Groundwater modeling represents only a part of the complete analysis which is required to define the effects of release of radionuclides and the dose commitment resulting to man. Other factors important in contaminant transport include dispersion, sorption of various species, reaction between the various species and the fractured media, release rate, dilution, and uptake into the food chain and the pathway to man. Besides the geologic barrier, engineering barriers must also be taken into account, including the waste form, cannister, overpack, and any other backfill material.

In the studies reported above, only freshwater was considered. Density effects due to thermal heating were included, but those due to groundwater geochemistry were neglected because of the lack of data. Recent drilling in the Canadian Precambrian Shield, however, has indicated that saline groundwaters do occur at depth. Future modeling should, therefore, include the effect of natural density differences. The siting potential of largely static saline groundwaters, for example, in crystalline rocks beneath sedimentary sequences, requires further research.

The principal needs at present are for more field data on permeability and flow porosity, and the opportunity to test models against realistic field conditions. Further analytical refinement at this time is of lesser importance.

ACKNOWLEDGEMENTS

The views expressed in this paper are those of the authors and do not necessarily represent those of agencies sponsoring the studies. The studies for KBS were undertaken by Hagconsult AB in association with Acres Consulting Services Limited and RE/SPEC Inc. The studies for AECL on pluton hydrogeology were undertaken by Acres Consulting Services Limited. The authors gratefuly acknowledge the useful discussions with their co-workers, Dr. R. G. Charlwood, Dr. P. F. Gnirk, Dr. U. E. Lindblom and Dr. H. Stille.

REFERENCES

[1]Snow, D. T. "Rock Fracture Spacings, Opening and Porosities". ASCE J. Soil Mech. and Found. Engrg Div. Vol 94. SM1 pp 78 - 91. 1968.

[2]Priest, S. D., and J. A. Hudson. "Discontinuity Spacings in Rock". Int. J. Rock Mech. Min. Sci. and Geomech. Abstr. Vol 13. pp 135 - 148

[3]Snow, D. T. "The Frequency and Apertures of Fractures in Rock". Int. J. Rock Mech. and Min. Sci. Vol 7. pp 23 - 40. 1970.

[4]Ringdal, F., Gjoystadl, H. and Husebye, E. S. "*Seismotectonic Risk Modeling for Nuclear Waste* Disposal in the Swedish Bedrock". KBS Tek.isk Rapport 51. Kärnbränslesäkerhet. Stockholm. 1977.

[5]Burgess, A. S. "Pluton Hydrogeology". Atomic Energy of Canada Limited. Technical Record TR73.

[6]Burgess, A. S. "Groundwater Movements Around a Repository. Regional Groundwater Flow Analyses. Part 1 Initial Conditions. Part 2 Long Term Residual Conditions". KBS Teknisk Rapport 54:03. Kärnbränslesäkerhet. Stockholm. 1977.

[7]Ratigan, J. L., Burgess, A.S., Skiba, E. L. and Charlwood, R. G. "Groundwater Movements Around a Repository. Repository Domain Groundwater Flow Analyses. Part 1 Permeability Perturbations. Part 2 Inflow to Repository. Part 3 Thermally Induced Flow". KBS Teknisk Rapport 54:05. Kärnbränslesäkerhet. Stockholm.

[8]Lindblom, U. E. "Groundwater Movements Around a Repository, Phase 1, State of the Art and Detailed Study Plan". KBS Teknisk Rapport 06. Kärnbränslesäkerhet. Stockholm. 1977.

[9]Stille, H., Burgess, A. S. and Lindblom, U. E. "Groundwater Movements Around a Repository. Geological and Geotechnical Conditions". KBS Teknisk Rapport 54:01. Kärnbränslesäkerhet. Stockholm. 1977.

[10]Ratigan, J. L. "Groundwater Movements Around a Repository. Thermal Analyses. Part 1 Conduction Heat Transfer. Part 2 Advective Heat Transfer". KPS Teknisk Rapport 54:02, Kärnbränslesäkerhet. Stockholm. 1977.

[11]Ratigan, J. L. "Groundwater Movements Around a Repository. Rock Mechanics Analyses". KBS Teknisk Rapport 54:04. Kärnbränslesäkerhet. Stockholm. 1977.

[12]Lindblom, U. E., Charlwood, R. G. and Gnirk, P. F. "Groundwater Movements Around a Repository. Final Report". KBS Teknisk Rapport 54:06. Kärnbränslesäkerhet. Stockholm. 1977.

[13]Burgess, A. S., Charlwood, R. G., Ratigan, J. L., Gnirk, P. F., Stille, H. and Lindblom, U. E. "Analyses of Groundwater Flow Around a High-Level Waste Repository in Crystalline Rock". OECD Nuclear Energy Agency. Workshop on Low-Flow, Low Permeability Measurements in Largely Impermeable Rocks. 1979.

[14]Snow, D. T. "Fracture Deformation and Changes in Permeability and Storage Upon Changes in Fluid Pressure". Q. Colorado School of Mines. Vol 63, (1). pp 201 - 244. 1968.

[15]Fisher, H. N. "An Interpretation of the Pressure and Flow Data for the Two Fractures of the Los Alamos Hot Dry Rock (HDR) Geothermal System". Energy Resources and Excavations Technology. Proc. 18th U.S. Symposium on Rock Mechanics. Keystone, Colorado. 1B4-1 to 1B4-8. 1977.

[16]Norton, D. and Knapp, R. "Transport in Hydrothermal Systems: The Nature of Porosity". Am. J. of Sci. Vc 227. pp 913 - 936. 1977.

[17]Jessop, A. M., Robertson, P. B. and Lewis, T. J. "A Brief Summary of Thermal Conductivity of Crystalline Rock". Canadian Department of Energy, Mines and Resources. Report 76-4. 1976.

[18]Webster, D. S. Proctor, J. F. and Marine, I. W. "Two Well Tracer Tests in Fractured Crystalline Rock". U.S. Geol. Survey Water Supply Paper 1544-1. 1970.

[19]Haggblom, H. "Calculations of Nuclide Migration in Rock and Porous Media, Penetrated by Water". KBS Teknisk Rapport 52. Kärnbränslesäkerhet. Stockholm. 1977.

[20]Lundstrom, L. and Stille, H. "Large-Scale Permeability Test of the Granite in Stripa Mine and Thermal Conductivity Test". KBS Teknisk Rapport. Kärnbränslesäkerhet. Stockholm.

DESCRIPTION AND APPLICATIONS OF THE FE3DGW AND CFEST THREE-DIMENSIONAL FINITE-ELEMENT MODELS

S. K. Gupta, C. R. Cole, C. T. Kincaid and F. E. Kaszeta
Pacific Northwest Laboratory
Richland, Washington 99352

The FE3DGW model is a finite-element three-dimensional isothermal saturated ground-water flow model for simulation of potentials, flow paths, and travel time in a complex multilayered system. The model has been used for regional ground-water basin studies and generic studies involving fracture flow as an equivalent porous media.

The CFEST (Coupled Flow, Energy, and Solute Transport) model is an extension of FE3DGW to address the problems in areas of seasonal energy storage in aquifers, disposal of chemical wastes in aquifers, storage of fresh water in saline aquifers, and salt-water intrusion into fresh ground-water flow systems. The model solves the partial differential equations describing single-phase fluid flow, energy transport by conduction and convection, and solute transport by dispersion, diffusion and convection.

SALIENT FEATURES OF THE MODELS

FE3DGW

Simulation of Multilayered System. FE3DGW has been designed to simulate large natural systems. It is capable of modeling complex multilayered systems by varying both the number and thickness of the hydrologic or geologic stratification layers. The modeled region can be conveniently subdivided to give greater detail in critical areas. Both point and distributed withdrawals and recharges are considered. FE3DGW can be used for either transient or steady-state solutions.

Storage Requirements and Costs. In FE3DGW, the core storage requirements and costs are reduced[5] to the extent that large, natural, multilayered systems are simulated efficiently on small computers. Data are efficiently processed through use of direct-access disk files and a partially compressed matrix for solution of the associated sparse and nonsymmetric system of equations. The intermediate results are stored for repeated retrieval at a fraction of the cost of computation.

Staged Execution Structure. For efficient simulation of field problems with complex geometry, this version of the model has been structured to execute in stages. The staged structure affords one the opportunity to thoroughly check the geometric structure of the domain, the physical parameters of the problems, and aspects of the solution sequence prior to making a complete run.

Plot Package. For the purposes of verification and visualization of input data and final results, a plot package is being integrated into the program. Displays of nodal locations, elements, and vertical log details will aid in the search for input-data errors. Contour plots of the interfaces between hydrogeologic strata will enable users to readily verify vertical logs and should enhance communications between interacting groups of hydrologists and geologists.

CFEST

Governing Equations. The partial differential equations (PDE) are based on:

- conservation of total liquid mass
- conservation of energy
- conservation of mass of a specific dissolved constituent within the liquid mass.

These three equations are solved in a cyclical-uncoupled solution scheme that employs the most current estimates of the variables (i.e., total head, temperature, and solute concentration) in the evaluation of nonlinear contributions and forcing functions.

Variable Density and Viscosity. Both density and viscosity are functions of the local pressure, temperature, and/or solute concentration.

Simulation Combinations. Various combinations of the PDE may be formulated and solved. A problem may be formulated for the solution of only fluid flow; fluid and energy transport; fluid and solute transport; or fluid, energy, and solute transport. Execution in stages allows efficient solution of complex problems.

GOVERNING EQUATIONS

FE3DGW

In this model, the governing equation is

$$\rho g(\omega C_w + C_p)\frac{\partial h}{\partial t} = \nabla \cdot K_{ij} \nabla h + Q \qquad (1)$$

The variable is the hydraulic head

$$h = \int_{p_o}^{p} \frac{dp}{\rho(p)} + Z \qquad (2)$$

CFEST

Fluid Flow:

$$(\rho K_{ij} h_{,j})_{,i} - Q = (\rho \ldots)_{,t} \qquad (3)$$

Energy Transport:

$$(E_{ij}T_{,j})_{,i} - (u_i H_E)_{,i} - H_L - Q(C_p'T')$$
$$= [\lambda_{ij} + (1-\theta)(\rho C_p)_r D_{ij}]T_{,ij} \qquad (4)$$

Solute Transport:

$$(D_{ij}C_{,j})_{,i} - (u_i C)_{,i} - QC' = (\theta C)_{,t} \qquad (5)$$

Fluid Density Model:

$$\rho(C,T,h_p) = \rho_o + [\partial\rho(1,T_o,h_{p_o}) - \rho_o]C$$
$$- \rho_o C_T(T - T_o) + \rho_o C_w(h_p - h_{p_o}) \qquad (6)$$

Porosity Model:

$$\theta = \theta_o[1 + C_r(h_p - h_{p_o})] \qquad (7)$$

The final form of the equations is acheived in two steps:

a. Density and porosity substitution. The models of density and porosity, Equations (6) and (7), are substituted into the flow, energy, and solute transport Equations (3, 4, and 5).

b. Collection of dependent variables. The cyclical solution scheme that has been adopted requires that the dependent variables (head, temperature, concentration) be treated as unknowns only when their respective equations (fluid flow, energy, solute) are being solved. Thus, temperature and concentration are assumed known when solving the fluid flow equation for head. Energy- and solute-transport equations are treated similarly. The cyclic sequence of solutions proceeds from fluid flow to energy and finally to solute transport. If successive iterates of this cycle fail to yield compatible results, the cycle is repeated.

In their final form, the equations are:

Fluid Flow:

$$(K_{ij}h_{,j})_{,i} - (\theta_o C_w + \theta_o C_r)h_{,t}$$
$$= q_o + \frac{dq_o}{dh_p}(h_{p_{out}} - h_p) - q_i - \frac{dq_i}{dh_p}(h_{p_{in}} - h_p)$$
$$- \theta_o C_T T_{,t} + [\partial\rho(1,T_o,h_{p_o}) - \rho_o]C_{,t} \qquad (8)$$

Energy Transport:

$$(E_{ij}T_{,j})_{,i} - (\rho u_i C_{pw}T)_{,i} + (\rho C_p)_r \theta_o C_r h_{,t}T$$
$$- [q_o + \frac{dq_o}{dh_p}(h_{p_{out}} - h_p)]C_{pw}T - AC_{pw}T$$
$$+ [-\theta_o U C_T + \theta\rho C_{pw} + (1-\theta)(\rho C_p)_r]T_{,t}$$
$$= H_L - [q_i + \frac{dq_i}{dh_p}(h_{p_{in}} - h_p)]C_p'T'$$
$$+ A(U_o - C_{pw}T_o) \qquad (9)$$

where $A = \theta_o C_w h_{,t} + \theta_o C_r h_{,t} + \theta[\partial\rho(1,T_o,h_{p_o}) - \rho_o]C_{,t}$

Solute Transport:

$$(\theta D_{ij}C_{,j})_{,i} - (u_i C)_{,i} - [q_o + \frac{dq_o}{dh_p}(h_{p_{out}} - h_p)]C$$
$$- (\theta_o C_w h_{,t} + \theta_o C_r h_{,t} - \theta_o C_T T_{,t})C$$
$$- (\theta[\partial\rho(1,T_o,h_{p_o}) - \rho_o]C + \theta)C_{,t}$$
$$= -[q_i + \frac{dq_i}{dh_p}(h_{p_{in}} - h_p)]C' \qquad (10)$$

Note: The most current estimates of density and porosity are employed in both the stiffness and load components of the equation. Further, the pressure-head values estimated previously are employed in the evaluation of fluid compressibility because of the term's relative importance.

NUMERICAL METHOD

The FE3DGW and CFEST codes reduce their partial differential equations to systems of algebraic equations through the use of the Galerkin finite-element method. FE3DGW uses mixed order isoparametric elements, while in CFEST only linear elements are used. For time derivative terms, a backward differencing scheme is adopted. The solution of the matrix equation uses a partially compressed matrix solver.[2] The non-zero coefficients are stored in one array and their corresponding column indices in another array. The row containing the minimum number of non-zero elements is used as a pivotal column to minimize round-off error. The system matrix is decomposed to an upper triangle. All the operations on the right-hand vector are stored for efficient solution by backward substitution until the stiffness coefficient matrix is altered due to change in time step or hydraulic properties.

COMPUTER CODE DOCUMENTATION AND AVAILABILITY

Both codes are written in FORTRAN IV and were developed on a PDP 11/45 at Pacific Northwest Laboratory. FE3DGW computer listings, a user's manual, and a few typical applications have been published.[3] The earlier versions of the flow models are reported in Gupta, Tanji, and Luthin 1975; Gupta and Tanji 1976; Gupta and Pinder 1977. Further refinement, verification with analytical solution, validation with field operations, and documentation of CFEST is underway.

VERIFICATION

FE3DGW was verified with the (1) Theis non-equilibrium solution (radial flow to a well pumping at a constant rate in an infinite and isotropic aquifer), (2) PATHS solution[11] (regional potential distribution in an aquifer system having an initial uniform gradient, large remote radial boundary and cavernous cylindrical reservoirs), and (3) Hantush (1959) drawdown distributions in the vicinity of a steady well draining an elastic strata.

CFEST, in addition to being verified by the above analytical solutions, has been verified with (1) a classical one-dimensional transient convection-diffusion problem with held boundary condition,[12] (2) a flux boundary problem[1] defining solute transport and energy transport, and (3) a radial transport analytical solution.[10]

APPLICATIONS

FE3DGW has been applied to the following problems:

Sutter Basin, California

Sutter Basin[6,8] lies in the central portion of the Sacramento Valley. It is a multi-layered system with volcanic rock outcrops at the Sutter Buttes and the Sutter Basin fault (Figure 1) in the valley. The hydraulic head (about 600 m caused by recharge in the Kione Sand at Sutter Buttes) has displaced marine connate water south and created a salt water mound at the Sutter Basin fault.

Long Island, New York

To evaluate alternative schemes for water supply and waste-water treatment for Long Island, New York, the ground-water system was analyzed three-dimensionally.[4] This ground-water basin has a very complex stratification having one to six geologic media separated by confining clay layers. The ground-water reservoir is wedge-shaped with southwardly increasing thickness. For mathematical representation of the stratification, major changes in each of the major hydrogeologic units were described by varying the size of the elements (Figure 2). Both the steady state and transient validations of the results were made using historical data.

Hypothetical Waste Repository in a Representative Salt Formation

To examine the consequences of the accidental release of radionuclides from a hypothetical nuclear waste repository located in a generic salt formation, FE3DGW was used to define the hydrologic flow detail (Figure 3). A hypothetical stratigraphy above the salt zone was assumed. The strata overlying and surrounding the salt contain water but are not considered prolific aquifers. The permeability range varied from 2×10^{-8} cm/sec of salt to 6.8×10^{-3} cm/sec of sand. The regional discharge site for the water within the various layers is assumed to be a river 5 km from the center of the repository.

Hypothetical Repository for Radioactive Waste in Hard Rock

FE3DGW was used to determine the flow paths and travel time from the repository in hard

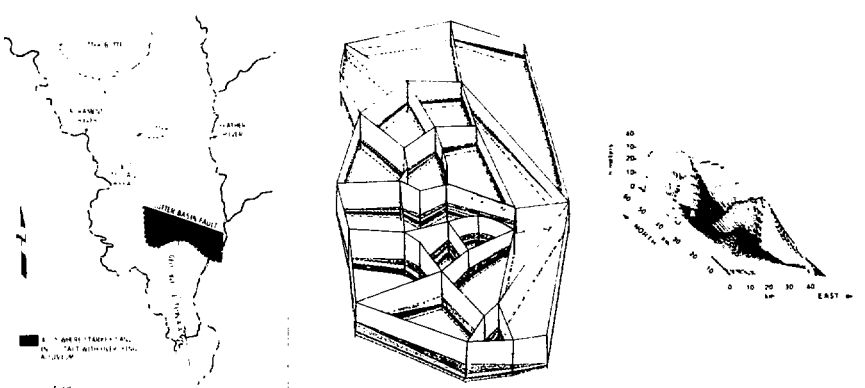

(a) Plan (b) 3-D Finite Element Grid (c) Simulated Steady State Hydraulic Head at Base of Post-Eocene Formation

FIGURE 1. Sutter Basin, California

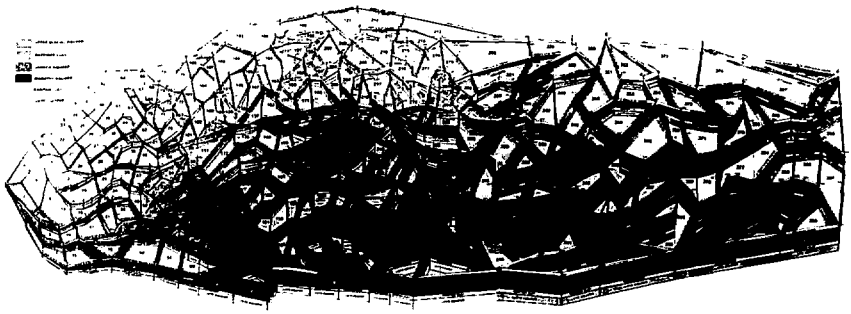

FIGURE 2. Three-Dimensional Finite-Element Grid of Ground-Water Reservoir Beneath Long Island, New York

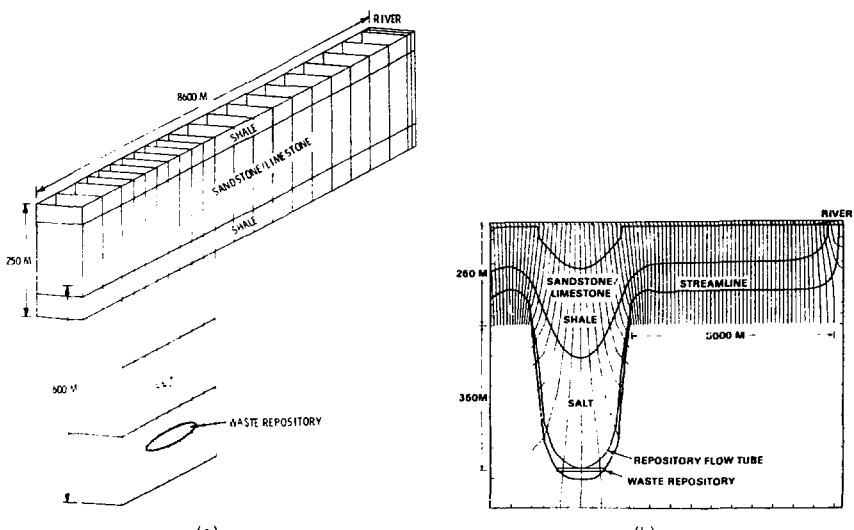

FIGURE 3. (a) Three-Dimensional Finite-Element Grid for Hypothetical Waste Repository in Representative Salt Formation;
(b) Contour Plot of the Model-Predicted Vertical Ground-Water Potentials with Superimposed Streamlines

granitic rock or gneiss with small discrete fracture planes or joints that are interconnected to some degree. Within the generic area lakes, rivers, and topography are considered (Figure 4). The element size, shape, and orientation are done according to surface-water bodies, topography, and structural properties of the region. The major fracture zones are represented by discrete elements with two additional thin elements to provide a transition zone from fractures to rock matrix.

Drawdown and Pumping Requirements from a Generic Mine

A real site in Precambrian hard crystalline rock is used for this study (Figure 5).

A three-dimensional finite-element grid is used to predict the pumping requirements for the mine and to determine the zone of influence of the drawdown.

WORK IN PROGRESS

Both FE3DGW and CFEST codes are currently under revision concerning:

- inclusion of options for double porosity and discrete fractures flow
- extension of the model to handle uncertainties in hydraulic properties and boundary conditions
- application of CFEST for coupled solution of flow, temperature, and solute in hypothetical repositories and to provide a means of coupling local, adjoining, and large regional basins.

SUMMARY

FE3DGW and CFEST are three-dimensional finite-element models suitable for simulation of detailed local, subregional, and coarse-grid large ground-water basins. The present version of the models considers faults and fractures as an equivalent porous media. Large fracture or fault zones are effectively simulated as discrete elements with higher permeability and/or porosity.

Further improvement is under way to include capabilities for double porosity, discrete fracture flow, and modeling uncertainties in hydraulic properties and boundary conditions.

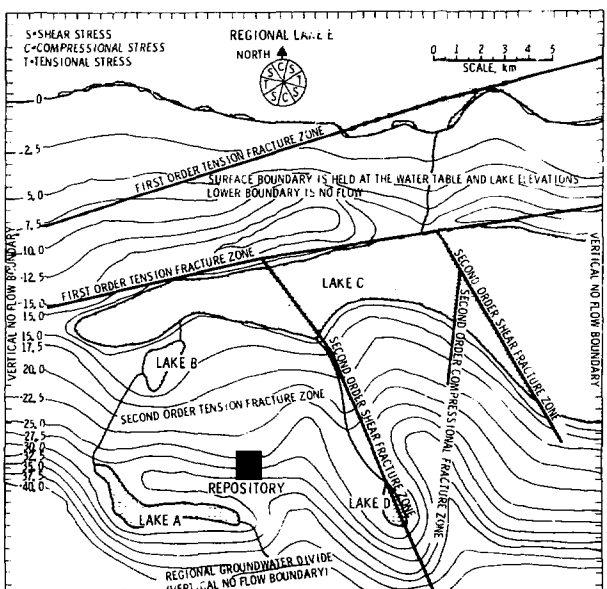

(a) Boundaries, Fractures and Water Table

FIGURE 4. Referen e Repository Site in Granite

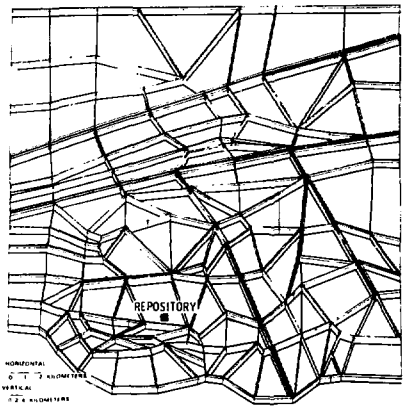

(b) Finite-Element Grid

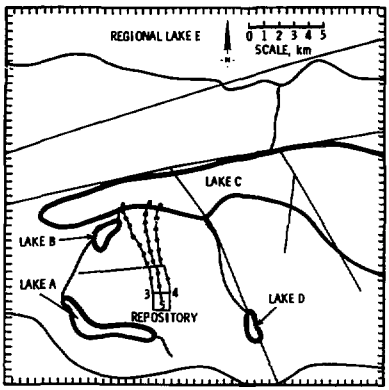

(c) Streamline X-Y Paths*

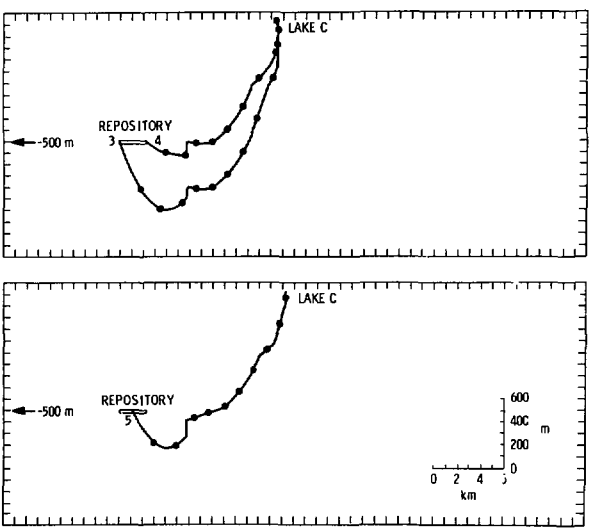

(d) Streamline X-Z Paths*

* Streamlines starting from upper left, upper right, and middle of the repository are numbered 3, 4, and 5, respectively. The dots along the streamline paths are placed 1,000 years apart in time.

FIGURE 4. *Reference Repository Site in Granite*

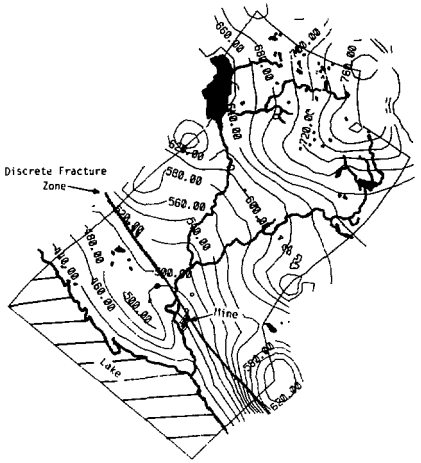

(a)

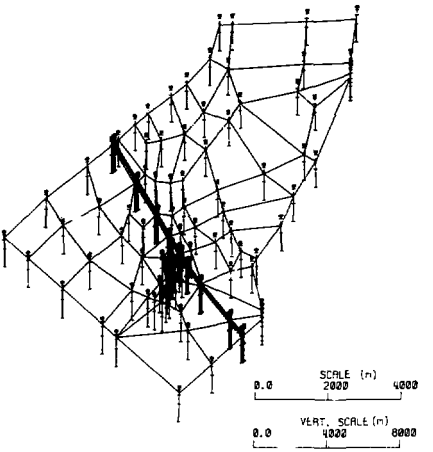

(b)

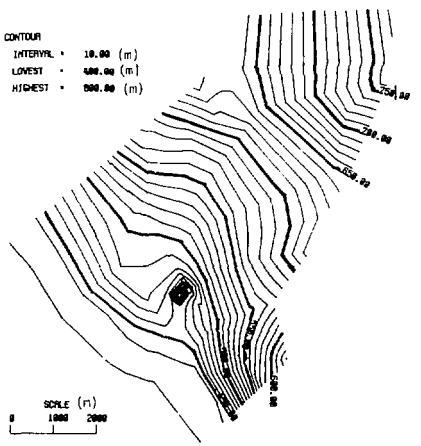

(c)

FIGURE 5. (a) Drainage, Water Table, Mine Locations and Boundary, Fractured Zone; (b) Finite-Element Grid; and (c) Contour Map of Potentials 150 m Below Ground Surface with Mining Pit

NOTATION

	Definitions	Units
C_p'	= Specific heat of injected fluid	$EM^{-1}°C^{-1}$
C_{pw}	= Specific heat of water	$EM^{-1}°C^{-1}$
$(\rho C_p)_r$	= Rock heat capacity per unit volume	$EL^{-3}°C^{-1}$
C_r	= Compressibility of porous media	L^{-1}
C_T	= Coefficient of thermal expansion of fluid aquifer fluid	$°C^{-1}$
C_w	= Compressibility of aquifer fluid	L^{-1}
C	= Concentration of solute, mass fraction	
C'	= Concentration of injected solute, mass fraction	
$D_{\alpha\beta}$	= Homogeneous, isotropic dispersion tensor for 3-D flow	L^2T^{-1}
$E_{\alpha\beta}$	= Apparent heat conductivity tensor, analogous to $D_{\alpha\beta}$; i.e., homogerous, isotropic	$E(LT°C)^{-1}$
g	= Acceleration due to gravity	LT^{-2}
h	= Hydraulic head = $Z + 1/g * \int_0^p \frac{dp}{\rho(p)}$	L
h_p	= Pressure head component of h	
h_{p_o}	= Reference pressure head for aquifer density	L
h_{p_θ}	Reference pressure head at which θ_o is defined	L
$h_{p_{out}}$, $h_{p_{in}}$	= Pressure head of withdrawal, injection	L
H_E	= Internal heat energy = $C_{pw}T$	EM^{-1}
H_L	= Rate of heat loss at boundary of domain	$EL^{-3}T^{-1}$

	Definitions	Units
$k_{\alpha\beta}$	= Intrinsic permeability of media	L^2
$K_{\alpha\beta}$	= Hydraulic conductivity (collinear) = $\rho g k_{\alpha\beta}/\mu$	LT^{-1}
p	= Pressure	$ML^{-1}L^{-3}$
q_o, q_i	= Mass rate of withdrawal (injection) of fluid	$MT^{-1}L^{-3}$
Q	= Strength of source or sink = $q_i + \frac{dq_i}{dh_p}(h_{p_{in}} - h_p) - q_o - \frac{dq_o}{dh_p}(h_{p_{out}} - h_p)$	$MT^{-1}L^{-3}$
t	= Time	T
T	= Temperature	°C
T'	= Injection fluid temperature	°C
T_o	= Reference temperature for density and internal energy	C
u_α	= Components of the Darcy fluid velocity	LT^{-1}
U	= Internal energy = $U_o + C_{pw}(T - T_o)$	EM^{-1}
Z	= Elevation above datum	L

Greek

α,β	= Cartesian component indices; i.e., 1, 2, and 3	
$\delta_{\alpha\beta}$	= Kronecker delta	
θ	= Porosity of aquifer @ h_p	
θ_o	= Porosity of aquifer @ h_{p_θ}	
μ	= Absolute viscosity	$M(LT)^{-1}$
ρ	= Density	ML^{-3}
ρ_o	= Reference density @ h_{p_o} T_o, C = 0	ML^{-3}

REFERENCES

1. Coats, K. H., and B. D. Smith. 1964. "Dead-End Pore Volume and Dispersion in Porous Media," S.P.E.J., pp. 73-84.

2. Cole, C. R., and S. K. Gupta. 1979. A Brief Description of the Three-Dimensional Finite-Element Ground-Water Flow Model Adapted for Waste Isolation Safety Assessments. PNL-2652, Pacific Northwest Laboratory, Richland, WA.

3. Gupta, S. K., C. R. Cole and F. W. Bond. 1979. Methodology for Release Consequence Analysis - Part III, Finite-Element Three-Dimensional Ground-Water (FE3DGW) Flow Model, Formulation Program Listings and User's Manual, PNL-2939, Pacific Northwest Laboratory, Richland, WA.

4. Gupta, S. K., and G. F. Pinder. 1977. Three-Dimensional Finite-Element Model for Multilayered Ground-Water Reservoir of Long Island, New York. Department of Civil Engineering, Princeton University, Princeton, NJ.

5. Gupta, S. K., and K. K. Tanji. 1976. "A New Approach in Reduction of Core Storage and Computational Time in Finite Element Solution and its Applications." In Proceedings of First International Conference on Finite Elements in Water Resources, Pentech Press, p. 2.173-2.193.

6. Gupta, S. K., and K. K. Tanji. 1976. "A Three-Dimensional Galerkin Finite-Element Solution of Flow Through Multi-aquifers in Sutter Basin, California," Water Resource Research. 12(2) p. 155-162.

7. Gupta, S. K., and K. K. Tanji. 1977. "Computer Program for Solution of Large, Sparse, Unsymmetric Systems of Linear Equations," Int. J. Num. Meth. in Eng., Vol. 11, p. 1251-1259.

8. Gupta, S. K., K. K. Tanji and J. N. Luthin. 1975. A Three-Dimensional Finite-Element Ground-Water Model. California Water Resource Center, Univ. of California, Davis, CA, Contribution No. 152, p. 119.

9. Hantush, M. S. 1959. "Nonsteady Flow to Flowing Wells in Leaky Aquifers," Journal of Geophysical Research, Vol 64, No. 8, p. 1043-1052.

10. Hoopes, J. A., and D. R. Harleman. 1967. "Dispersion in Radial Flow from a Recharge Well," J. Geophys. Res., p. 72.

11. Nelson, R. W., and J. A. Schur. 1978. A Preliminary Evaluation Capability for Some Two-Dimensional Ground-Water Contamination Problems, BCSR-38, Boeing Computer Services, Richland, WA.

12. Peaceman, D. W., and H. H. Rachford. 1962. "Numerical Calculations of Multidimensional Miscible Displacement," Soc, Petrol. Eng. J., p. 327-338.

GEOTHERMAL MODEL

K. H. Coats
INTERCOMP Resource Development and Engineering, Inc.
Houston, Texas

Abstract: This talk describes mathematical model equations for geothermal reservoirs and presents numerical results of an implicit, three-dimensional geothermal simulation model. Model stability allows inclusion of formation fractures and wellbores as grid blocks. Applications include illustrative natural convection problems in fractured-matrix geothermal reservoirs, single- and two-phase well behavior, fractured-matrix reservoir performance and well test interpretation, and extraction of energy from fractured hot dry rock.

References:

(1) K.H. Coats, "Geothermal Reservoir Modeling", SPE 6892, presented at the 52nd Annual Fall Technical Conference and Exhibition of the Society of Petroleum Engineers of AIME, Denver, Colorado, October 9-12, 1977.

(2) K.H. Coats, A.B. Ramesh, and A.G. Winestock, "Numerical Modeling of Thermal Reservoir Behavior", Oil Sands, p.399-410, 1977.

THE ROLE OF NUMERICAL MODELS IN APPLICATIONS TO THERMOHYDROLOGICAL FLOW IN FRACTURE ROCK MASSES

Charles R. Faust and James W. Mercer
GeoTrans, Inc.
Herndon, Virginia

INTRODUCTION

Thermohydrological flow in fractured rock masses involves complex processes. Fortunately, the state-of-the-art in numerical modeling has reached a point where it is possible to solve the equations describing many of these processes. Unfortunately, some of these processes are incompletely understood and available field-scale data for them are meager. Given these observations, is there a useful role that numerical models can serve in applications to thermohydrological flow in fractured rock? This question is the motivation for this brief communication. Before addressing this question, we first discuss the general topics of modeling objectives and model use, with emphasis on problem-dependent applications. We also review a recent application of a geothermal model to a fractured reservoir. The purposes of this example are to demonstrate the way in which complex models have been applied and the type of results that can be obtained from such applications. In this discussion we will refer primarily to deterministic models.

GENERAL MODEL USE

The overall objectives of any deterministic modeling application are to understand, characterize and predict the behavior of a real system or process. Several specific areas of model use contribute to meeting this overall objective. Among these are:

- understanding relevant physical processes
- conceptualization of actual field system
- data collection design
- data matching
- prediction

The first of these, understanding relevant physical processes, is a generic application; that is, it is not related to any specific field site. Much of the research in the numerical modeling of thermohydrological processes has involved this type of model use.

The remainder of the uses listed are associated with particular field applications; that is, they are site specific. All of these, except prediction, should be accomplished in an iterative manner. For example, early model use as a system conceptualization tool can provide guidance in the design of data collection activities. Further, matching observed data with calculated results can lead to a better concept of the system, and can pinpoint data deficiencies. Although not part of this iterative process, prediction depends on the other uses. Credible predictions of system behavior can be done only if an adequate match between observed data and model results is obtained. If data are insufficient to verify the model, then predictions will be less reliable.

Problem-Dependent Emphasis

The way in which models are most appropriately used is problem dependent. The important factors are the complexity of the system, the sufficiency of the data, and the conceptual understanding of the system.

Well understood systems having good data, and described by simple processes can be modeled reliably. Under these conditions, predictions should be credible and additional system conceptualization should be straightforward. An example of this type of application is ground-water flow in a well understood, porous, confined aquifer.

For poorly understood systems having little data and described by complex processes, models play a different but still important role. In this case, the use of the model as a predictive tool is not justified. Rather, models are best used in efforts to understand the physical processes, and in attempts to form a concept of particular field systems. The model results provide an idealized basis against which observed data can be compared, and perhaps explained. Further, the model can provide a consistent framework which can aid in explaining various observations, and in relating limited data. Thermohydrological flow in fractured rock masses is an example of this type of application.

MODELS OF COMPLEX SYSTEMS

When dealing with models of complex systems in geologic media, two problems must be recognized. The first is the uncertainty and incompleteness of field data. The second is the fact that it will never be possible to explain all the details of the observed behavior. The application of numerical models to thermohydrological flow in fractured media will always be hampered by these two problems.

The best way to reduce the severity of data uncertainty and model approximation is through history matching. For applications with uncertain data, we know that the match will be non-unique. In theory, either a statistical-optimization or a subjective approach can be used for history matching. In practice, however, the auto-

matic history matching methods are not well developed for complex processes. Consequently, the subjective approach is generally chosen. The subjective approach involves:

- determining what is the best comparison between observed data and calculated results;
- guaranteeing that the values of parameters giving the 'best match' are physically reasonable;
- assuring that 'major'aspects of the system behavior are explained.

Example

Details of this application and the numerical models used are given in our original report.[1] Only a brief summary is presented here, with the *emphasis being on the subjective aspects of the* history matching and system conceptualization. This example was chosen because the field problem is a geothermal reservoir in a highly fractured aquifer, which consists of pumice breccias and vitric tuffs.

This modeling study was made on the two-phase (water and steam) geothermal field at Wairakei, New Zealand. The purpose of the study was to consolidate existing information and data on the geothermal field and to develop a rational framework on how the system operates. The framework was a numerical model that incorporated:

- a conceptual description of the physics of fluid flow and heat transport,
- the thermodynamics of two-phase, single component water,
- a geometric description of the Wairakei field including boundary conditions and initial pressure and enthalpy conditions, and
- the hydrologic and heat transport parameters that characterize the Wairakei field.

The processes active at the Wairakei geothermal field are complex. Although information on the field appeared to be extensive, data were still incomplete in several ways. Consequently, it was recognized that the model application and history matching would be subjective.

In order to perform the analysis, it was necessary to set guidelines. It was required that determined parameters be physically reasonable and major aspects of the reservoir behavior be explained (or matched). For steady-state conditions, major reservoir aspects included observed initial fluid pressures and the distributed fluid and heat (convective and conductive) leakage at the surface. For transient conditions, these aspects included (1) a sharp decline in temperatures that occurred around 1962, (2) a differential drop in pressure between the top and bottom of the reservoir, (3) a pressure recovery that was observed during a partial shutdown of the field, and (4) changes in surface discharge characteristics during the first ten years of production.

Even with these guidelines, the history matching procedure was not straight forward. Several difficulties were encountered:

- there were too many parameters to adjust,
- the system response data were incomplete, and
- the response data that existed were of an indirect nature.

For example, fluid pressure in the reservoir was often determined from well-head pressures. Estimates of change in reservoir storage were based on gravity measurements. Both types of data had various assumptions and approximations implicitly included.

To overcome these difficulties, further guidelines were necessary. To reduce the large number of parameters that could be adjusted, most parameters were set to reasonable values. The few that were calibrated were those with the highest sensitivity. Response data were matched where available. Where absent, the computed results were required to be 'reasonable'. Finally, it was necessary to discriminate between direct and indirect data.

From the history matching procedure, several qualitative conclusions were drawn:

- From the steady-state match, it was clear that a steam cap existed prior to development - a conclusion not generally recognized at the beginning of the study;
- As development progressed, the steam cap spread areally and with depth;
- The temperature drop that occurred about 1963 could be explained by the steam cap falling below the top of the open interval of the well;
- Production in the reservoir was sustained primarily by mass leakage from below;
- Production is limited by the amount of mass available, not heat; and
- A highly fractured reservoir can be successfully approximated with a porous media model.

Several observations were not accounted for in this study:

- Although the pressure drop in the main production zone was simulated, the calculated pressure decline in the eastern production zone was not as high as observed;
- The connection of the Wairakei field to a field southeast of Wairakei was not considered, and
- The leakage coefficient for the base of the

reservoir appeared to be high. This final point suggests that the reservoir may be thicker than the 350 meters assumed in the model.

CONCLUSIONS

Model applications to thermohydrological flow in fractured media are not likely to be straightforward. The physical processes are complicated, the field systems often difficult to understand, and data for model verification are generally lacking. The primary use for models in this area will be in gaining a better understanding of the physical processes and in conceptualizing the behavior of actual systems.

Modeling studies of complex physical systems are generally unable to completely explain all details of observed behavior. In addition to uncertainties associated with interpretation of field measurements of subsurface conditions, numerical models, no matter how sophisticated, are approximations to nature. Because of these uncertainties, model calibration requires either subjective evaluation or statistical treatment. Statistical procedures for history matching of complex numerical models have not been sufficiently developed. This will necessitate the setting of subjective guidelines for model calibration.

A model based on subjective history matching procedures and incomplete data is obviously not a unique description of the system. Predictions will consequently have limited credibility. Qualitative predictions and sensitivity analysis still play an important role under such circumstances.

REFERENCE

1. Mercer, J.W., and C.R. Faust, 1979, Geothermal reservoir simulation 3: Application of liquid- and vapor-dominated hydrothermal modeling techniques to Wairakei, New Zealand, Water Resour. Res., vol. 15, no. 3, p. 653-671.

GEOTHERMAL RESERVOIR SIMULATION CAPABILITIES AT SYSTEMS, SCIENCE AND SOFTWARE

J. W. Pritchett
Systems, Science and Software
La Jolla, California

Summary

S^3's basic multiphase multidimensional compositional geothermal reservoir simulator is the MUSHRM code. The capabilities of this computer code are outlined in Figures 1-4; applications of the program over the years are summarized in Figure 5. In addition, the CHARL (useful for chemical waste disposal calculations) and LIGHTS (for single-phase long-term reservoir response simulations) codes are available (see Figures 6 and 7).

A typical application of MUSHRM to calculate the response of the Wairakei geothermal field in New Zealand is shown in Figures 8-17. The simulation involved a 2-D vertical section, located as shown in Figure 8, and the known discharge history was imposed (Figure 9 shows the sum over all wells of this history). The computational grid and stratigraphy employed is illustrated in Figure 10. Figure 11 shows favorable comparison between observed and computed pressure histories in the main part of the reservoir. Figure 12 shows the observed spatial variation in pressure drop, which compares well with the corresponding computed pressure distribution (Figure 13). The spatial extent of the two-phase (water/steam) region at Wairakei is known to have increased with time, and this behavior is reproduced by the computed results (Figures 14-16). Reasonably good qualitative agreement with the observed discharge enthalpy histories was also obtained (Figure 17): the disagreement is believed to be due to three-dimensional effects not taken into account in this simulation.

Figure 1

MUSHRM (MUlti-Species Hydrothermal Reserve Model)

- Unsteady flow of mass and heat in an heterogeneous porous medium (i.e., a geothermal reservoir)
- Finite-difference methods
- Flexible geometric capability
- Realistic stratigraphy
- Compositional Fluid Description
- Multiphase fluid mixtures
- Sub-model for production, injection wells
- Local instantaneous permeabilities depend on porosity
- Porosity changes with pressure, temperature, deposition
- May be coupled to finite-element subsidence simulator

Figure 2

MUSHRM Problem Geometries

- "Stretch" mesh (i.e., Δx depends on x)
- Any face of any zone may represent a boundary:
  - impermeable
  - specified flowrate
  - specified heat flux
  - specified temperature
  - specified pressure
- Various coordinate systems:
  - 1-D Slab (cross-section area and dip specified functions of x)
  - 1-D Radial (layer thickness and dip specified functions of r)
  - 1-D Spherical
  - 2-D Areal (layer thickness and dip specified function of x, y)
  - 2-D Vertical
  - 2-D Axisymmetric
  - 3-D Cartesian

Figure 3

MUSHRM Geological Description

The rock properties of each zone may be independently specified. These include:

- Density
- Heat capacity
- Thermal conductivity
- Initial porosity
- Initial directional permeabilities
- Relative permeability curves
- Porosity-permeability relation
- Bulk moduli (loading, unloading)
- Shear modulus
- Thermal expansion coefficient

Figure 4

MUSHRM Description of Pore Fluids

Constitutive packages currently available for:

- Liquid Water (1-component, 1-phase)
- Liquid Water/Steam (1-component, 2-phase)
- Liquid Water/Steam/Dissolved NaCl/Precipitated NaCl (2-component, 3-phase)
- Liquid Water/Dissolved Methane/Free Methane Gas (2-component, 2-phase)
- Liquid Water/Dissolved NaCl/ Dissolved Methane/Free Methane Gas (3-component, 2-phase)

Figure 5

MUSHRM Applications

Theoretical Studies

- Numerous comparisons with analytic/ approximate solutions
- Effects of fluid reinjection and well-patterns on reservoir performance
- Analyses of reservoir recharge by deep vertical faults
- Assessment of secondary terms ($P\delta V$ work, viscous dissipation) in the energy balance
- Determination of evaporative salt-deposition effects upon reservoir longevity
- Studies of pressure-drawdown well-tests for multiphase geothermal reservoirs
- Assessment of drive mechanisms (compressibility, compaction, gas) for geopressured reservoirs

Field Application

- Reproduction of Stanford bench-scale experiments
- Predictions for Salton Sea geothermal field
- Studies of East Mesa geothermal anomaly
- History-match and predictions for Wairakei
- Various applications for commercial customers

Figure 6

CHARM (CHemically-Active Reservoir Model)

- Two-Dimensional Geometry, stretch mesh
  (1) Axisymmetric, or
  (2) Areal with variable formation thickness
- Irregular grid capability with flexible boundary conditions
- Pore fluid is a compressible aqueous solution
- Rock properties (density, initial porosity, composition, conductivity, heat capacity directional permeabilities) may vary with position
- Local instantaneous permeability depends on precipitate deposition and pore erosion due to chemical reactions
- Fluid viscosity depends on temperature
- Two simultaneous chemical reactions provided for among solids and dissolved species. These may:
  (1) Dissolve rock matrix
  (2) Produce solid precipitates
  (3) Re-dissolve precipitates
  (4) Release or absorb heat
- Chemical reactions are non-equilibrium; rates are first-order in reactant concentrations with Arrhenius temperature dependence
- Rate coefficients and activation energies may be arbitrarily prescribed

Figure 7

LIGHTS (Liquid Incompressible Geothermal Heat Transfer Simulator)

- Three-dimensional (Cartesian) with "stretch" mesh
- Single-phase liquid unsteady flow
- Conductive and convective heat transfer
- Rock properties (porosity, density, heat capacity, conductivity, directional permeabilities) are functions of position
- Boussinesq approximation; fluid density independent of pressure (incompressible)
- Fluid properties (density, viscosity, thermal conductivity) depend on local instantaneous temperature

Applications so far

(1) Underground Heat Storage

(2) East Mesa Geothermal Field Studies

Figure 8

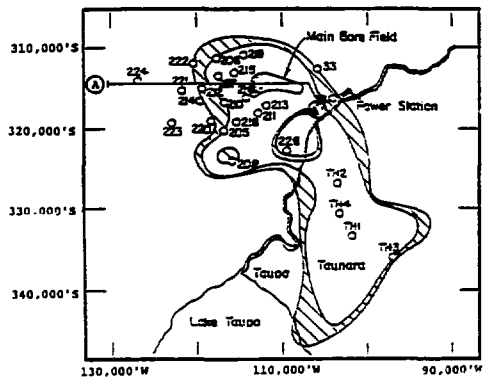

LOCATION OF VERTICAL SECTION

Figure 9

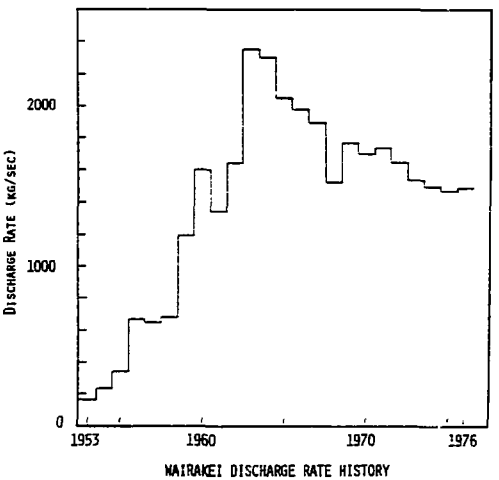

WAIRAKEI DISCHARGE RATE HISTORY

Figure 10

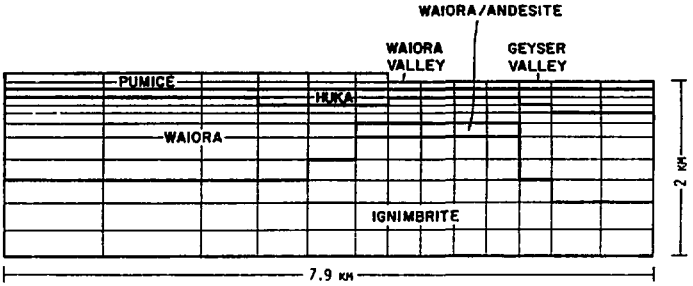

COMPUTATIONAL GRID AND STRATIGRAPHY

Figure 11

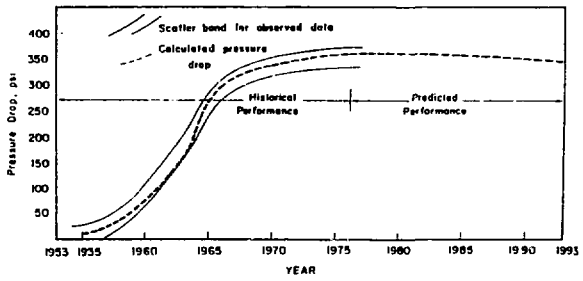

DEEP MAIN BOREFIELD PRESSURE DROP

Figure 12

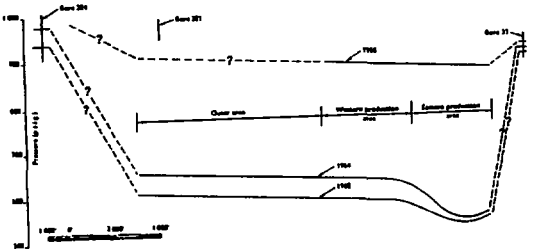

OBSERVED EAST-WEST PRESSURE DISTRIBUTIONS AT RL-900

Figure 13

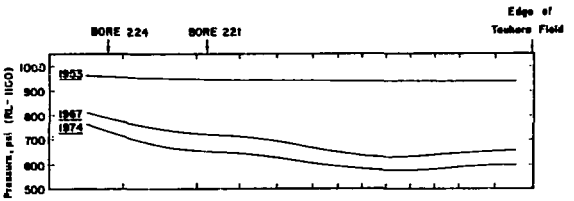

COMPUTED EAST-WEST PRESSURE DISTRIBUTIONS AT RL-1100

Figure 14

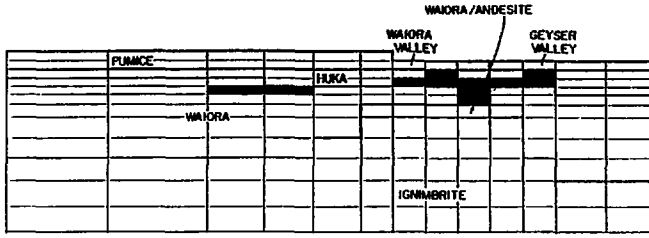

TWO-PHASE REGION -- JAN 1953

Figure 15

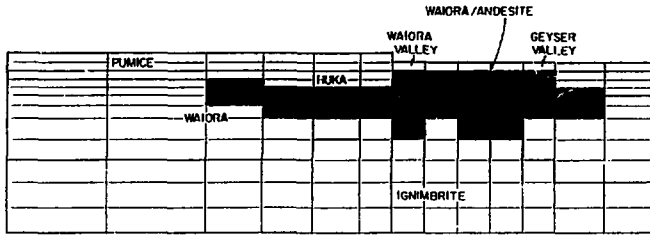

TWO-PHASE REGION -- JAN 1965

Figure 16

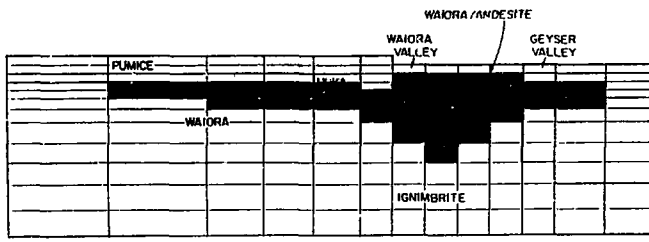

TWO-PHASE REGION -- JUNE 1977

Figure 17

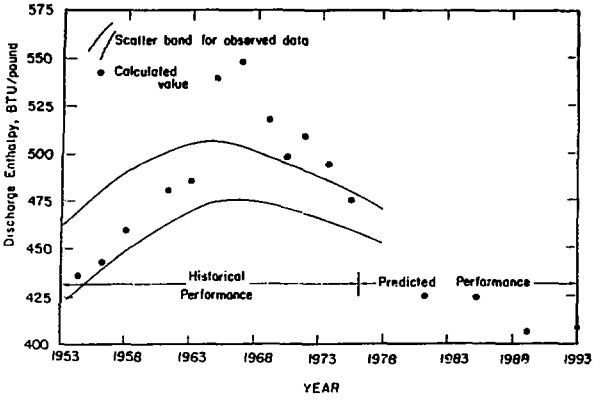

AVERAGE FIELD DISCHARGE ENTHALPY -- ALL WELLS

S^3 GEOTHERMAL RESERVOIR, WELL TEST, AND SUBSIDENCE MODELING

(Publications in Open Literature)

1. R.M. Knapp and T.D. Riney, (1975) "Numerical Simulation of Geopressured Geothermal Reservoirs," Proc. of First Geopressured Geothermal Energy Conference, University of Texas at Austin, June 2-4.

2. J.W. Pritchett, (1975) "Numerical Calculation of Multiphase Fluid and Heat Flow in Hydrothermal Reservoirs," Proc. Workshop on Geothermal Reservoir Engineering, Stanford, California, December 15-17.

3. L.F. Rice, (1976) "Pressure Drawdown and Build-up Analyses in Geothermal Reservoirs," Proceedings Eleventh Intersociety Energy Conversion Engineering Conference, State Line, Nevada, September 12 -17.

4. A.H. Nayfeh, D.H Brownell, Jr. and S.K. Garg, (1975) "Heat Exchange in a Fluid Percolationg Through Porous Media," Proceedings Society of Engineering Science Meeting, Austin, Texas, pp. 1125-1137, October.

5. D.H Brownell, Jr. S.K. Garg and J.W. Pritchett, (1975)"Computer Simulation of Geothermal Reservoirs. I. Governing Equations for Hydrothermal Systems," Society of Petroleum Engineers Preprint No SPE 5381. Also published under the title, "Governing Equations for Geothermal Reservoirs," Water Resources Research, Vol. 13, pp. 929-934, 1977. Reply to D.C. Helm, Vol. 15, pp. 727-729, 1979. Also correction, Vol. 15, p. 1671, 1979.

6. S.K. Garg. J.W. Pritchett, and D.H. Brownell, Jr., "Transport of Mass and Energy in Porous Media," Proceedings 2nd U.N. Geothermal Symposium, San Francisco, CA, pp. 1651-1656, May.

7. S.K. Garg, J.W. Pritchett, D.H. Brownell, Jr., and J. Sweet, (1975) "Multiphase Fluid Flow in Geologic Media and Land Surface Subsidence," Proceedings Society of Engineering Science Meeting, Austin, Texas (Invited talk), pp. 691-693, October.

8. T.R. Blake, and S.K. Garg, (1976) "On the Species Transport Equation for Flow in Porous Media," Water Resources Research, Vol. 12, pp. 748-750. Also reply to W.G. Gray and K.O'Neil, Vol. 13, p. 697, 1977.

9. S.K. Garg, (1975) "Land Surface Subsidence Associated with Geothermal Energy Production," Proceedings Workshop on Geothermal Reservoir Engineering, Stanford University, pp. 65-68, December 15-17.

10. S.K. Garg, D.H. Brownell, Jr. and J.W. Pritchett, (1977) "Dilatancy-Induced Fluid Migration and the Velocity Anomaly," Journal of Geophysical Research, Vol. 82, pp. 855-864.

11. S.K. Garg, J.W. Pritchett, L.F. Rice and D.H. Brownell, Jr., (1976) "Study of the Geothermal Production and Subsidence History of the Wairakei Field," Proceedings 17th U.S. Symposium on Rock Mechanics, Snowbird, Utah, pp. 3B3-1 to 3B3-5, August 25-27.

12. J.W. Pritchett, S.K. Garg, and D.H. Brownell, (1976) "Numerical Simulation of Production and Subsidence at Wairakei, N.Z.," Proceedings Second Workshop on Geothermal Reservoir Engineering, Stanford University, pp. 310-323, December 1-3.

13. S.K. Garg, J.W. Pritchett, (1977) "On Pressure Work, Viscous Dissipation and the Energy Balance Relation for Geothermal Reservoirs," Advances in Water Resources, Vol. 1, pp. 41-47.

14. J.W. Pritchett, S.K. Garg, and T.D. Riney, (1977) "Numerical Simulation of the Effects of Reinjection Upon the Performance of a Geopressured Geothermal Reservoir," Geothermal: State of the Art - Transactions Geothermal Resources Council Annual Meeting, San Diego, CA, pp. 245 -247, May 9-11. Also Proceedings of Third Geopressured Geothermal Energy Conference, pp. ES-73 to ES-83, University of Southwestern Louisiana, Lafayette, LA, 1977.

15. S.K. Garg and J.W. Pritchett, (1977) "Simulation of Drive Mechanisms in Geopressured Resevoirs," Proceedings 18th U.S. Symposium on Rock Mechanics, Keystone, Colorado, pp. 1B5-1 to 1B5-4, June 22-24.

16. R.M. Knapp, O.F. Isokrari, S.K. Garg, and J.W. Pritchett, (1977) "An Analysis of the Production from Geopressured Geothermal Aquifers," Society of Petroleum Engineers Preprint No. 6825.

17. T.D. Riney, (1977) "Geothermal Reservoir Modeling Needs from Exploration to Utilization," Proceedings EPRI Workshop on Geothermal Milestones, Kah-nee-ta, Oregon, August.

18. J.W. Pritchett and S.K. Garg, (1978/1979) "Flow in an Aquifer Charged with Hot Water from a Fault Zone," Pure and Applied Geophysics, Vol. 117, pp. 309-320. Also reprinted in Geothermics and Geothermal Energy (eds. L. Rybach and L. Stegena), Birkhauser Verlag, Basel, 1979.

19. S.K. Garg, and J.W. Pritchett, (1977) "Two-Phase Flow in Geopressured Geothermal Wells," Proceedings of Third Geopressured Geothermal Energy Conference, pp. ES-85 to ES-114, University of Southwestern Louisiana, Lafayette, LA. Also Energy Conversion, Vol. 18, pp. 45-51, 1978.

20. T.D. Riney, J.W. Pritchett and S.K. Garg, (1977) "Salton Sea Geothermal Reservoir Simulations," Proceedings Third Workshop on Geothermal Reservoir Engineering, Stanford University, pp. 178-184, December. Also Proceedings of the Geoterhmal Resources Council 1978 Annual Meeting, pp. 571-574, Hilo, Hawaii, July 1978.

21. S.K. Garg, (1978) "Pressure Transient Analysis for Two-Phase (Liquid Water/Steam) Geothermal Reservoirs," Proceedings Geothermal Resources Council 1978 Annual Meeting, pp. 203-206, July. Also Society of Petroleum Engineers Journal, Vol 20, pp. 206- 214, 1980.

22. S.K. Garg, T.D. Riney, and D.H. Brownell, Jr., (1978) "Preliminary Reservoir and Subsidence Simulations for the Austin-Bayou Geopressured Geothermal Prospect," Proceedings Fourth Workshop on Geothermal Reservoir Engineering, Stanford University, pp. 280-285, December.

23. S.K. Garg, and D.R. Kassoy, (1980) "Convective Heat and Mass Transfer in Hydrothermal Systems," in Geotermal Systems: Principles and Case Histories (eds. L. Rybach and P. Muffler), John Wiley, London, pp. 37-76.

24. S.K. Garg, L.F. Rice, and J.W. Pritchett, (1979) "Two-Dimensional Simulation of the Wairakei Geothermal Field," Expanding the Geothermal Frontier - Transactions Geothermal Resources Council Annual Meeting, Reno, Nevada, pp. 237-240,September 24-27.

25. S.K. Garg, (1979) "Reinjection of Fluids into a Producing Geopressured Reservoir," Proceedings of Fourth Geopressured Geothermal Conference, University of Texas at Austin, pp. 1000-1030, October.

26. J.W. Pritchett, (1979) "A Semi-Analytic Description of Two-Phase Flow Near Production Wells in Hydrothermal and Geopressured Reservoirs," Proceedings of the Fifth Workshop on Geothermal Engineering, pp. 173-182, Stanford University, December.

27. T.D. Riney, J.W. Pritchett, L.F. Rice, and S.K. Garg, (1979) "A Preliminary Model of the East Mesa Hydrothermal System," Proceedings of the Fifth Workshop on Geothermal Engineering, pp. 211-214, Stanford University, December.

28. J.W. Pritchett, (1980) "Determination of Effective Well-Block Radii for Numerical Reservoir Simulations," to appear in Water Resources Research.

29. T.D. Riney, J.W. Pritchett, and L.F. Rice (1980) "Three-Dimensional Model of East Mesa Hydrothermal System," Geothermal Energy for the 80's - Transactions Geothermal Resources Council Annual Meeting, pp. 467-470, Salt Lake City, Utah, September 9-11.

30. S.K. Garg, (1980) "Shale Recharge and Production Behavior of Geopressured Reservoirs," Geothermal Energy for the 80's - Transactions Geothermal Resources Council Annual Meeting, pp. 325-328, Salt Lake City, Utah, September 9-11.

SHAFT79

Karsten Pruess
Earth Sciences Division
Lawrence Berkeley Laboratory
University of California
Berkeley, California 94720

SHAFT79 (Simultaneous Heat And Fluid Transport) is an integrated finite difference program for computing two-phase non-isothermal flow in porous media. SHAFT79 solves the same equations as an earlier version, called SHAFT78, but uses much more efficient mathematical and numerical methods. The principal application for which SHAFT79 is designed is in geothermal reservoir simulation. The various aspects of the model are discussed in Pruess et al., 1979a-c,[1,2,3] and Pruess and Schroeder, 1979[4].

GOVERNING EQUATIONS

SHAFT79 solves coupled mass- and energy-balance equations of the following form.

$$\frac{\partial \phi \rho}{\partial t} = - \text{ div } \underline{F} + q$$

$$\frac{\partial U}{\partial t} = - \text{ div } \underline{G} + Q$$

Here ϕ is porosity (void fraction), ρ is fluid density, $\underline{F}$ is mass flux, q is a source term for mass generation, U is the volumetric internal energy of the rock/fluid mixture, $\underline{G}$ is energy flux, and Q is an energy source term.

Mass flux is given by Darcy's Law

$$\underline{F} = \sum_{\alpha} \underline{F}_{\alpha} = - \sum_{\alpha} \frac{k k_{r_\alpha}}{\nu_\alpha} \rho_\alpha (\nabla p - \rho_\alpha \underline{g})$$

α = vapor, liquid

where k, k_{r_α} are absolute and relative permeability, respectively, ν_α is viscosity, p is pressure and $\underline{g}$ is gravitational acceleration.

Energy flux contains conductive and convective terms

$$\underline{G} = - K \nabla T + \sum_{\alpha} h_\alpha \underline{F}_\alpha$$

where K is thermal conductivity of the rock/fluid mixture, T is temperature, and h_α is specific enthalpy of vapor (α = v) or liquid (α = ℓ).

The volumetric internal energy is

$$U = \phi u \rho + (1 - \phi) \rho_R C_R T$$

with u the specific internal energy of the (two-phase) fluid, ρ_R the rock density, and C_R the specific heat of the rock.

The main assumptions made in the above formulation are as follows: (1) The physical systems described by SHAFT79 are approximated as systems of porous rock saturated with one-component fluid in liquid and vapor form. (2) Except for porosity which can vary with pressure and temperature all other rock properties - density, specific heat, thermal conductivity, absolute permeability - are independent of temperature, pressure, or vapor saturation. (3) Liquid, vapor, and rock matrix are in local thermodynamic equilibrium, i.e., at the same temperature and pressure, at all times. (4) Capillary pressure is neglected.

The fluid properties (constitutive relations) are specified in tabular form. Thus, SHAFT79 can model the flow of any one-component fluid in porous rock.

NUMERICAL METHODS

Space discretization is achieved with the integrated finite difference method. This method allows a very flexible geometric description, because it does not distinguish between one-, two, or three-dimensional regular or irregular geometries. Time is discretized fully implictly as a first-order finite difference, resulting in the following finite difference equations.

$$D_n(\underline{X}^{k+1}) \quad \phi_n^{k+1} \rho_n^{k+1} - \phi_n^k \rho_n^k - \frac{\Delta t}{V_n} \left\{ \sum_m F_{nm}^{k+1} + V_n q_n^{k+1} \right\} = 0$$

$$E_n(\underline{X}^{k+1}) \quad \phi_n^{k+1} \rho_n^{k+1} u_n^{k+1} - \phi_n^k \rho_n^k u_n^k + \left[(1-\phi_n^{k+1}) \rho_R \right] C_R (T_n^{k+1} - T_n^k) - \frac{\Delta t}{V_n} \left\{ \sum_m G_{nm}^{k+1} + V_n Q_n^{k+1} \right\} = 0$$

Here n, m label the volume elements, and k labels the time step. $\underline{X}^{k+1} = (x_1^{k+1}, \ldots, x_N^{k+1}, u_1^{k-1}, \ldots u_N^{k+1})$ is the vector of the 2N unknowns for a system with N elements. Δt is the time step, $\Delta t = t^{k+1} - t^k$, V_n is the volume of element n, and

$$F_{nm} = A_{nm} \sum_{\alpha} k_{(nm)} \left(\frac{k_{r_\alpha}}{\nu_\alpha} \right)_{(nm)} (\rho_\alpha)_{(nm)} \times \left(\frac{P_m - P_n}{d_{nm}} - (\rho_\alpha)_{(nm)} g_{(nm)} \right)$$

is the mass flow from element m into element n, with interface area A_{nm} over a distance d_{nm}. An analogous definition holds for the energy flow G_{nm}. Whereas φ_n can vary with time, the apparent rock density $(1-\varphi_n)\rho_R$ is constant. Different weighting procedures can be selected for the various "interface quantities", labeled with subscript (nm) (harmonic weighting, spatial interpolation, upstream weighting).

The finite difference equations, above, are solved with the Newton/Raphson method. The set of linear equations arising at each iteration step is solved with an efficient direct solver, employing sparse storage techniques.[5]

COMPUTER CODE

SHAFT79 and a number of associated pre- and postprocessor programs are written in FORTRAN IV. The code is presently being used on the CDC 7600's at LBL and at Sandia/Albuquerque. Somewhat earlier versions have been installed on a UNIVAC 1108 and an IBM 370/168. Implementation on a Burroughs B-6800 is under way. A very comprehensive user's manual for the SHAFT78-version is presently being printed[1]. Much of it, including most of the preparation of input decks, still applies to SHAFT79. A new user's manual detailing data input to SHAFT79 is given in Pruess and Schroeder (1980)[6]. The input needed for SHAFT79 consists of several data blocks, which are provided by the user either as disk files or as data cards. Some of the data blocks are optional. The most general input structure is as follows:

BLOCK	DESCRIPTION
TITLE (first card)	One data card containing a header that will be printed on every page of output.
ROCKS	Material parameters for the various reservoir domains.
PARAM	Computational parameters (time stepping information, program options).
*ELEME	List of grid elements } MESH - information
*CONNE	List of interfaces (connections) } MESH - information
*GENER (optional)	List of mass or heat sinks/sources,
*INCON (optional)	List of initial conditions and (optional) restart-information
START (optional)	One data card allowing a more flexible initialization.
ENDCY (last card)	One card closing SHAFT79 input deck

The blocks which are labeled with a star(*) can be provided as disk files, in which case they would be omitted from the input deck. In addition to the data blocks indicated above, SHAFT79 requires an equation of state in tabular form to be provided through a disk file called TABLE.

Provisions for time-dependent source rates and position-dependent rock properties combined with the flexible geometry allow to describe a large variety of systems and processes. Any type of time-independent boundary condition can be realized. Time steps are semi-automatic, i.e., they have to be fed in by the user, but automatic adjustments will be made if no convergence is achieved. Two-dimensional contour plotting is available for display of results.

VALIDATION

SHAFT79 was validated against SHAFT78, which in turn was validated against a number of analytically solvable 1-phase flow problems, as well as against published numerical results for 2-phase flow problems.

APPLICATIONS

Table 1 summarizes simulation studies with SHAFT79.[4]

REFERENCES

1. Pruess, K., Schroeder R.C., Witherspoon, P.A., and Zerzan, J. M., SHAFT78, a two-phase multidimensional computer program for geothermal reservoir simulation, LBL-8264, 1979a.

2. Pruess, K., Zerzan, J.M., Schroeder, R.C., and Witherspoon, P.A., Description of the three-dimensional two-phase simulator SHAFT78 for use in geothermal reservoir studies, paper SPE-7699, presented at the Fifth Symposium on Reservoir Simulation, Denver, Colorado, 1979b.

3. Pruess, K., Bodvarsson, G., Schroeder, R.C., Witherspoon, P.A., Marconcini, R., Nari, G., and Ruffilli, C., Simulation of the depletion of two-phase geothermal reservoirs, paper SPE-8266, presented at the 54th Annual Fall Technical Conference and Exhibition of the SPE, Las Vegas, Nevada, 1979c.

4. Pruess, K. and Schroeder, R.C., Geothermal reservoir simulation with SHAFT79, LBL-10066, paper presented at the 5th Geothermal Reservoir Engineering Workshop, Stanford, California, 1979.

5. Duff, I.S., MA28 - a set of Fortran subroutines for sparse unsymmetric linear equations, Report AERE-R 8730, Harwell/Oxfordshire, Great Britain, 1977.

6. Pruess, K and Schroeder, R.C., SHAFT79 user's manual, LBL-10861, 1980.

GEOMETRY	TYPE OF PROBLEM	SIMULATED PROCESSES
1-D, rectangular	depletion of two-phase geothermal reservoirs	various production and injection schemes for reservoirs with uniform initial conditions or with sharp steam/water interfaces
1-D, cylindrical	two-phase flow near wells	production from two-phase zones; cold water injection into two-phase and superheated steam zones, respectively
2-D, rectangular	Krafla geothermal reservoir (Iceland)	different space and time patterns of production and injection
2-D, cylindrical	high level nuclear waste repository	long-term evolution of temperatures and pressures near a powerful heat source (in progress)
3-D, regular	two-phase interference test in Cerro Prieto (Mexico)	(in progress)
3-D, irregular	Serrazzano geothermal reservoir (Italy)	detailed field production from 1960 to 1966

Table 1: Simulation Studies with SHAFT79.

NUMERICAL MODEL CCC

G. S. Bodvarsson and M. J. Lippmann
Earth Sciences Division
Lawrence Berkeley Laboratory
University of California
Berkeley, California 94720

INTRODUCTION

The computer program CCC (conduction-convection-consolidation), developed at Lawrence Berkeley Laboratory, solves numerically the heat and mass flow equations for a fully saturated medium, and computes one-dimensional consolidation of the simulated systems. The model employs the Integrated Finite Difference Method (IFDM) in discretizing the saturated medium and formulating the governing equations. The sets of equations are solved either by an iterative solution technique (old version) or an efficient sparse solver (new version). The deformation of the medium is calculated using the one-dimensional consolidation theory of Terraghi. Details of the model are given by Lippmann et al., (1977), Mangold et al., (1979), and Bodvarsson et al., (1979).

In this paper, the numerical code will be described, validation examples given and areas of application discussed. Several example problems involving flow through fractured media will also be presented.

GOVERNING EQUATIONS

The governing mass and heat flow equations employed in the model are developed based on the principles of conservation of mass and energy. The mass flow equation can be written in integral form as

$$\frac{D}{Dt}\int_V \frac{S_s}{g} P dV = -\int_A \rho \vec{v}_d \cdot \vec{n} dA + \int_V G_f dV \qquad (1)$$

Equation (1) applies to any control element of volume V and surface area A, containing solids (V_s) and/or liquid water (V_f). The storage coefficient S_s describes the storage capacity of the element, and is related to the total compressibility C_T and the porosity ϕ through the expression

$$S_s = \phi \rho g C_T \qquad (2)$$

The energy equation can similarly be written in integral form as

$$\frac{D}{Dt}\int_V (\rho c)_M T dV = \int_A K_M \nabla T \cdot \vec{n} dA - \int_A \rho c_F \delta T \vec{v}_d \cdot \vec{n} dA + \int_V \dot{I} \, dV \qquad (3)$$

In equation (3), $(\rho c)_M$ represents the weighted heat capacity of the volume element; i.e.,

$$(\rho c)_M = \phi \rho_f c_f + (1 - \phi) \rho_s c_s \qquad (4)$$

In equation (3), the first term on the right hand side (RHS) represents heat-transfer by conduction as expressed by Fourier's law, K_M being the thermal conductivity of the rock-fluid mixture. The remaining terms on the RHS are the convective term and the source term, respectively. In the convective term, δT denotes the difference between the mean temperature of the volume element V and the interface temperature.

Equations (1) and (3) are coupled through the pressure and the temperature dependent parameters as well as through the convecting term. In the model, the fluxes are estimated using Darcy's law, which can be written as

$$\vec{v}_d = -\frac{k}{\mu}(\nabla P - \rho \vec{g}), \qquad (5)$$

where k is the absolute permeability, μ is the dynamic viscosity of the fluid, and $\vec{g}$ is the acceleration due to gravity.

Equations (1) and (3) are non-linear with pressure/temperature dependent parameters ρ, k, μ, K_M, and c. Furthermore, the parameters ϕ, S_s, and k are stress dependent.

In the development of the mathematical model used in the computer code, the following primary assumptions have been employed:

1) Darcy's law adequately describes fluid movement through fractured and porous media.

2) The rock and fluid are in thermal equilibrium at any given time.

3) Energy changes due to fluid compressibility, acceleration and viscous dissipation are neglected.

Assumptions 1 - 3 are usually employed in the numerical modeling of geothermal reservoirs.

Deformation

The model employs the one-dimensional theory of Terzaghi to calculate the deformation of the medium. The basic concept in the theory is the relationship between the effective stress σ' and the pore pressure P. For saturated media this expression can be written as

$$\sigma' = \sigma_N - P, \tag{6}$$

where σ_N denotes the normal stress (overburden). The effective stress can easily be calculated from equation (6) at any time, assuming that the normal stress σ_N is known.

The consolidation behavior of each material is described by the "e - log σ' curves," where e is the void ratio, related to the porosity ϕ by the expression

$$\phi = e/(1 + e) \tag{7}$$

In practice, consolidation tests are used to develop "e - log σ' curves" for each material. In the model this information is described by analytical expressions.

A typical consolidation curve consists of a so-called virgin curve and a series of parallel swelling-recompression curves (the model neglects hysteresis between swelling and recompression curves). When the material is loaded to levels never before attained, the deformation is given by the virgin curve, but for swelling, or load levels below the preconsolidation stress, the deformation is described by the swelling-recompression curves. In the model, the "e - log σ' curves" are generally approximated by straight lines, one of slope C_c (compression index, for virgin loading, and others of slope C_s (swelling index) for unloading/low level reloading.

The stress dependent parameters ϕ, S_s, and k, in equations (1) and (3), can easily be calculated given the consolidation curves for each material. The porosity is calculated using equation (7), and the specific storage S_s can be calculated using the following expression

$$S_s = \rho g [\phi\beta + a_v/(1 + e)]. \tag{8}$$

In equation (8), a_v is the coefficient of compressibility and can be expressed as

$$a_v = -\frac{de}{d\sigma'} = C_c/(2.303\ \sigma') \tag{9}$$

In calculating the permeability k, the empirical relation used is

$$k = k_o \exp\left[\frac{2.303(e - e_o)}{C_k}\right] \tag{10}$$

In equation (10), k_o and e_o are arbitrary reference values for the permeability and void ratio, respectively. For a given material, C_k is the slope of the best fitted line of void ratio (e) versus log k.

NUMERICAL FORMULATION

The model employs the Integrated Finite Difference Method (IFDM) to discretize the flow regime and to handle the spatial gradients. The flow regime is divided into arbitrarily-shaped polyhedrons, constructed by drawing perpendicular bisectors to lines connecting nodal points. This permits easy evaluation of the surface integrals in equations (1) and (3). Detailed descriptions of the IFDM are given by Edwards (1972).

The chief limitation of the method is that the finite difference gradient approximation is inadequate in handling tensorial properties such as the stress fields. Except for the procedure used in evaluating the gradients, the Integrated Finite Difference Method (IFDM) and the modified Galerkin Finite Element (with diagonal capacity matrix) are conceptually very similar (Narasimhan and Witherspoon, 1976). Both approaches derive their ability to handle complex geometries from the integral nature of the formulation.

In numerical notation the governing equations can be written as follows:

$$\text{mass balance} \quad \frac{(S_s V)_n}{g}\frac{\Delta P_n}{\Delta t} = \sum_m \left[\left(\frac{k\rho A}{\mu}\right)_{n,m} \frac{(P_m - P_n)}{D_{n,m} + D_{m,n}} - \left(\frac{k\rho^2 nA}{\mu}\right)_{n,m} R\right] + (G_s V_n) \tag{11}$$

$$\text{energy balance} \quad \left[(\rho c)_M V\right]_n \frac{\Delta T_n}{\Delta t} = \sum_m \left[\frac{(K_M A)_{n,m}}{D_{n,m} + D_{m,n}} (T_m - T_n) + \left(\frac{(\rho c_F Ak)}{\mu}\right)_{n,m} (T_{n,m} - \bar{T}_n)\left(\frac{P_m - P_n}{D_{n,m} + D_{m,n}} - \eta\rho g\right)\right] + (G_h V)_n \tag{12}$$

These equations are valid for an arbitrary node n connected to an arbitrary number of nodes m. The nodal point distances to the interface for node n and node m are represented by $D_{n,m}$ and $D_{m,n}$.

Upstream weighting

To evaluate the interface temperature $T_{n,m}$, the model employs an upstream weighting criterion:

$$T_{n,m} = aT_n + (1 - a)T_m \tag{13}$$

In equation (13), a, the upstream weighting factor, is restricted in value to the range of 0.5 - 1.0 for unconditional stability.

Implicit Formulation

In the model, the equations are solved implicitly to allow larger time steps to be taken. The implicit formulation is incorporated by means of the following expressions:

$$\begin{aligned} T_n^o &= T_n + \lambda\Delta T_n \\ T_m^o &= T_m + \lambda\Delta T_m \\ P_n^o &= P_n + \lambda\Delta P_n \\ P_m^o &= P_m + \lambda\Delta P_m \end{aligned} \tag{14}$$

The weighting factor λ is generally allowed to vary between 0.5 and 1.0 for unconditionally stable solutions, but it may also be specified as a constant. If λ is specified to be 0.0 during the simulation, a fully explicit solution scheme results (forward differencing) and the time step is restricted below to a critical stable value (see Narasimhan 1975). If $\lambda = 0.5$, the Crank Nicholson Scheme results; for $\lambda = 1.0$, a fully implicit (backward differencing) scheme is employed.

Spatial Gradients

The spatial gradients between nodes are estimated by a linear approximation, i.e.,

$$\tilde{\nabla}P = \frac{P_m - P_n}{D_{n,m} + D_{m,n}} \tag{15}$$

The permeability and thermal conductivity of the matrix and the density of the fluid at the interfaces are evaluated using the harmonic means to preserve continuity of flux at the interface, as for example:

$$k_{m,n} = k_m k_n \frac{D_{n,m} + D_{m,n}}{k_m D_{n,m} + k_n D_{m,n}} \tag{16}$$

Incorporating the above relations (equations 13-16) into the governing equations (equations 10 and 11), and simplifying, the equations can be written as

$$C_{n,n}\Delta P_n - C_{n,m}\Delta P_m = b_n \tag{17}$$

$$K_{i,i}\Delta T_n - K_{i,j}\Delta T_n + K_{i,n}\Delta P_n - K_{i,m}\Delta P_m = B_i \tag{18}$$

Solution Technique

Equations (17) and (18) can be combined for simultaneous solution into a single matrix equation

$$[A]\{X\} = \{b\} \tag{19}$$

In equation (19), the matrix [A] consists of the coefficients $C_{n,m}$ and $K_{i,j}$. These are in general a function of the temperature and pressure, and therefore the equations are non-linear. The vector {X} contains the unknowns (the ΔP and ΔT) and the vector {b} represents the known explicit quantities.

The sets of non-linear equations are solved using an efficient direct solver (Duff, 1977) and an iterative scheme for the non-linear coefficients. Basically, the solver uses LU decomposition and a Gaussian elimination procedure to solve a set of linear equations.

The matrix of coefficients (the [A] matrix) is preordered using permutation matrices P' and Q' such that the resultant matrix is in block lower triangular form. Gaussian elimination is then performed within each diagonal block in order to obtain factorization into the lower triangular (L_k) and the upper triangular (U_k). Finally, the factorization is used to solve the matrix equations. In this solution package (Duff, 1977), no restriction is placed upon the characteristics of the matrix of coefficients; i.e., it need not be symmetrical or of a specified degree of sparsity.

The non-linear coefficients are presently handled using an iteration scheme. Future development of the code includes incorporation the Newton-Raphson scheme for efficient and accurate determination of the non-linear coefficients.

CODE DESCRIPTION

Spatial Grid

In the model there is no restriction upon choice of basic block (node) shape or numbering of codes. The geometric configurations of the nodal elements can be arbitrary and the grid may be one, two, or three dimensional, with rectangular, cylindrical or spherical symmetry. Required input data are the dimensions of the nodes and the connections between nodes. For complex problems, the design of the mesh may create the most difficulty in using the program. Auxiliary computer

programs for mesh and input data generation are available for a number of grid systems, including the case with cylindrical or elliptical rings near a well, gradually changing to rectangular nodes in the far field. This mesh is relevant for the simulation of horizontal or inclined fractures intersecting either a well (cylindrical or elliptical cross sections) or other planar fractures within the rock mass (linear cross sections).

Material Properties

At present the code allows specification of up to twelve different materials. For each material the porosity, permeability, specific storage, thermal conductivity, heat capacity, and density of the solid must be specified. These parameters may be constant or may vary with temperature, and/or effective stress. The porosity and specific storage can vary with the effective stress, the permeability with both temperature and effective stress, and the thermal conductivity and heat capacity with temperature only. These relations are specified by tables, interpolated during each time step. Anistropic permeability can be handled by orienting the grid blocks parallel to the principle axes of anisotropy.

Fluid Properties

Input parameters are the fluid viscosity, heat capacity, density and compressibility of water. A constant value must be specified for the compressibility; other fluid properties may also be assumed constant. However, the code provides the option of specifying the viscosity and heat capacity as a function of temperature, and density as a function of temperature and pressure. An empirical formula is used for the density function, while the code interpolates input tables for the appropriate value of the viscosity and heat capacity during each time step.

Sources and Sinks

Mass and energy sources and sinks may be specified for any node. The rate may be constant or vary with time.

Initial Conditions

Initial values of pressure, temperature and preconsolidation stress must be specified for each grid block. If the restart option is utilized, the specified initial values must correspond to the final values obtained in the previous run.

Boundary Conditions

In the model, prescribed potential or flux boundaries may be used. The boundaries can be specified as constant or varying with time. Finite capacity wells (wellbore storage), as well as a heterogeneous flow regime (fractures) can easily be simulated.

Time Steps

There are several options for selecting the time steps to be taken during the simulation. The maximum and minimum time steps may be specified, or the time steps may be automatically determined based upon the maximum desired pressure and/or temperature changes during a time step. The problem is ended when one of several criteria is met. These include attainment of steady state, reaching the specified upper or lower limit for temperature and/or pressure, completing the required number of time steps, and reaching the specified maximum simulation time.

Output

Output is provided according to specified times or specified time steps. The pressure, temperature and first and second order derivatives are printed for each grid block. The fluid and energy fluxes are given for each connection. The mass and the energy balance are also included in the output.

VALIDATION

The code "CCC" has been validated against analytic solutions for fluid and heat flow, and against a field experiment for underground storage of hot water. The following is a list of selected problems:

Analytical Solutions (Fluid and Heat Flow)

1. Continuous Line Source: The Theis problem (1935) was solved for both early times (transient flow) and long term pseudo-steady radial flow.
2. Cold Water Injection in a Hot Reservoir: Avdonin's analytical results (1964) were matched for early and later times.
3. Doublet Problem: The temperature variations at the production well due to cold water injection were matched against the analytical results of Gringarten and Sauty (1975).
4. Conduction Problems: A number of conduction problems were solved and compared the analytical solution givens by Carslaw and Jaeger (1959).
5. Buoyancy Flow: The rate of thermal front tilting when injecting hot water into a cold reservoir was calculated and compared to results by Hellstrom (1979).

Fracture Flow Solutions

1. Vertical Fracture: The pressure response in a well intercepting a finite conductivity vertical fracture was calculated and compared to the semi-analytic solution of Cinco-Ley et al., (1978).

2. Horizontal Fracture: The pressure response in a well intercepting an infinite conductivity horizontal fracture was calculated and compared to the analytical solution of Gringarten (1971).

Field Experiments

The numerical code was validated against data from the Auburn University ATES Field experiments. Two cycles of injection, storage and production of hot water in a confined aquifer were modeled, yielding results that closely matched temperatures, pressures and energy recovery factors observed in the field (Tsang et al., 1979b).

APPLICATIONS

Our model has been applied to problems in the fields of geothermal reservoir engineering, aquifer thermal energy storage, well testing, radioactive waste isolation and in situ cool combustion.

Geothermal Reservoir Engineering

1. Simulation and reinjection studies have been made using data from the Cerro Prieto geothermal field (Lippmann et al., 1978; Tsang et al., 1979).
2. Generic studies have been made for injection and production in geothermal reservoirs (Lippmann et al., 1977a; 1979).
3. Theoretical studies have been made of subsidence in geothermal reservoirs due to fluid withdrawal (Lippman et al., 1976, 1977b).
4. Preliminary studies of flow through fractures in geothermal reservoirs are in progress (Bodvarsson et al., in preparation).

Aquifer Thermal Energy Storage

1. Many generic studies have been performed to demonstrate the feasibility of sensible heat storage in aquifers (Tsang et al., 1976, 1978a, 1978b).
2. The Auburn field experiments in aquifer storage were successfully modeled (Tsang et al., 1979b).

Well Testing

1. Studies of well behavior in a two-layered system with a temperature gradient have been made (Lippmann et al., 1978; Tsang et al., 1979a).
2. The effects of an alternate production-injection scheme on the temperature and the pressure response of a geothermal system have been studied (Lippmann et al., 1977; Tsang et al., 1978c).
3. A study was made of temperature effects in well testing in a single layer system (Mangold et al., 1979).

Radioactive Waste Isolation

1. A study was made to examine the conduction heat transfer near a repository (Chan et al., 1978).
2. A generic study was performed using a porous media approximation of a fracture system to examine effects of permeability anisotropy in a region around a repository. These simulations were for periods of up to 2000 years (Wang et al., in preparation).

In Situ Coal Combustion

Calculations were performed to investigate the time required for thermal effects to reach the surface from undergound combustion of a coal seam (Mangold et al., 1978).

EXAMPLES OF FRACTURE STUDIES USING CCC

In this section the capabilities of the numerical code CCC when applied to studies of fractured reservoirs will be demonstrated. The studies are subdivided into two categories: isothermal fracture studies, and non-isothermal fracture studies.

Isothermal Fracture Studies

1. Horizontal Fracture

Gringarten (1971) solved analytically the problem of isothermal fluid flow to a well intersecting a single horizontal fracture in a homogeneous porous reservoir. In his analytical approach to the problem, Gringarten made three important assumptions:

A. All of the flow to the well is through the fracture.

B. The flow per unit area into the fracture is uniform across the fracture surfaces (uniform flux assumption).

C. Gravity effects are negligible.

Figure 1 shows the type curves developed by Gringarten and a schematic figure of the model used.

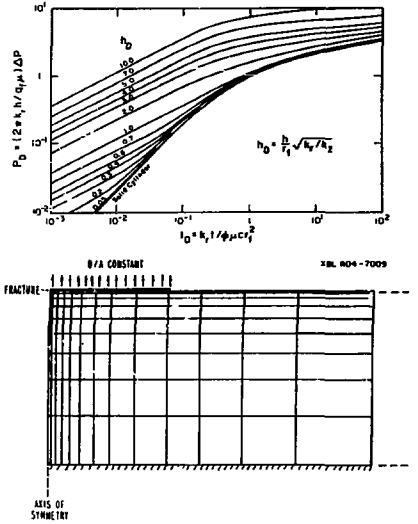

Fig. 2. Mesh used to validate CCC for flow through fractured media.

In order to validate CCC for flow through fractured media, we studied Gringarten's problem using the mesh shown in Figure 2. Based on Gringarten's first assumption it was not necessary to include a well element in the mesh. In order to satisfy the uniform flux assumption, sinks of variable strength were placed in the fracture elements. The strength of the sources were determined by the surface area of the elements. All of the elements used in the simulation were placed at the same elevation in order to exclude gravity from the calculations. Two cases with different h_D ($h_D = h/r_f(\sqrt{k_r/k_z})$) values were studied. Figure 3 shows the comparison between the numerical and the analytical solutions for $h_D = 1$. Similarly, a good agreement was found for the case of $h_D = 4$.

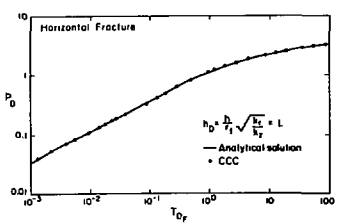

Fig. 3. Comparison between numerical and analytical solutions for $h_D = 1$.

2. Vertical Fracture

The problem of a well intercepting a single vertical fracture in a porous media reservoir was solved analytically by Cinco-Ley et al., 1978. The primary assumptions used in their analytical approach were as follows:

(1) the produced fluids enter the well only through the fracture

(2) gravity effects are negligible.

In the numerical simulation of this problem the mesh shown in Figure 4 was used. In order to satisfy the first assumption made by Cinco-Ley et al., the well element is connected only to the fracture elements, not to the elements representing the surrounding formation. Gravity is again excluded from the calculation by placing all of the nodes at the same elevation.

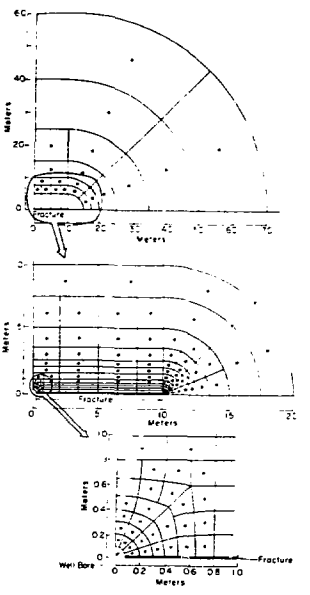

Fig. 4. Mesh used in the numerical simulation of the problem of a well intercepting a single vertical fracture.

Using the mesh shown in Figure 4, the case of $C_r = 100$ $\left(C_r = \frac{w\, k_f}{x_f k}\right)$ was numerically simulated.

Figure 5 shows the comparison between the numerical values obtained and the values given by Cinco-Ley et al. The excellent agreement did not warrant any additional comparison.

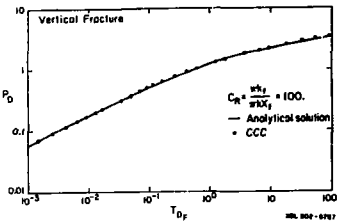

Non-Isothermal Fracture Studies

In this section, the problem of cold water injection into a fractured geothermal reservoir is considered. Reinjection of waste water can be effectively used to: dispose of waste water, maintain reservoir pressure and thus reduce the danger of subsidence, and maximize the energy recovery from a geothermal field. However, the use of injection in the development of geothermal fields has been limited, probably due to the common belief that the colder water will advance rapidly through the fracture and cause a premature breakthrough of the cold front at the production wells. This work can be considered as a first attempt to study the influence of fractures on cold water breakthrough at the production region when injection is used. The results can only be considered as estimates due to coarse grid used in the simulations. A more detailed description of this is given by Bodvarsson and Tsang (1980).

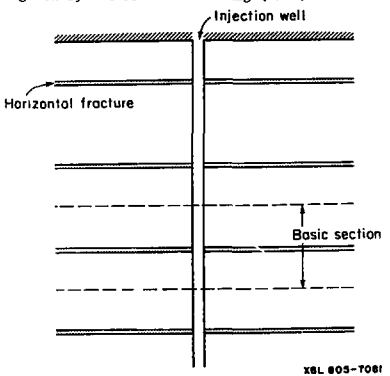

The problem considered involves a porous media geothermal reservoir containing equally spaced infinite horizontal fractures (Figure 6). Due to symmetry and the neglecting gravity effects, only half of the basic section shown in Figure 6 needed to be simulated. Thus the flow region considered consists of half a fracture and half of the rock matrix associated with each fracture. The mesh used in the study consisted of 144 elements, with fine elements close to the fracture and the well and larger elements farther away. Water at 100°C is injected through an element representing the injection well, and the fluid is allowed to flow directly from the well into both the fracture and the formation. The initial reservoir temperature is assumed to be 300°C. Table 1 gives some of the important parameters used in the study. Two cases were analyzed with different fracture spacing and different permeability ratios between the fracture and the rock matrix. In the first case a permeability ratio (K_D) of 10^3 was used as well as a fracture permeability of 1×10^{-10} m^2 (100 darcies) and a matrix permeability of 1×1^{-13} (100 md). For this case, a fracture spacing of 5 meters was assumed. Figure 7 shows the cumulative areal velocity of the thermal front in the fracture and the rock matrix versus time.

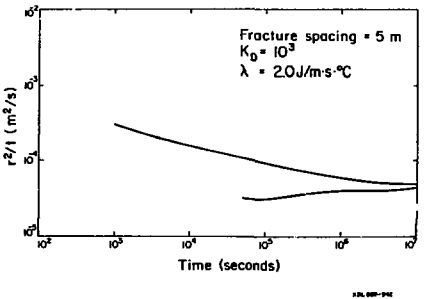

Here we define the thermal front as the 200°C isotherm. The cumulative areal velocity is calculated based upon the radial distance of the thermal front from the injection well and the time at which the radial distance is calculated. Figure 7 shows that at early times the cumulative areal velocity of the thermal front in the fracture is more than an order of magnitude larger that of the rock matrix. An accurate determination of the cumulative areal velocity of the rock matrix at early times was not possible because of the space discretization (mesh) used in the study. However, one must realize that for a radial system and an injection well injecting water at a constant rate into a porous media type reservoir, the cumulative areal velocity of the thermal front should be constant. As shown in Figure 7, the cumulative areal velocity of thermal front in the fracture decreases with time almost linearly at first but then gradually leveling off. On the

other hand, the cumulative areal velocity of the thermal front in the rock matrix slightly increases with time. The figure shows that the two curves are gradually converging, which indicates that although the thermal front initially advances faster in the fracture than in the rock matrix, eventually the thermal front in the rock matrix will catch up with the thermal front in the fracture, and after that they will advance at the same rate.

The decrease in the cumulative areal velocity of the thermal front in the fracture with time is due to the rapidly increasing surface area allowing heat transfer between the fracture and the rock matrix. During injection, the thermal front moves radially away from the injection well and the effective surface area for conductive and convective heat transfer increases as the square of the radial distance between the well and the front. The slight increase in the cumulative areal velocity of the thermal front in the rock matrix is probably due to cooling effects from the fracture.

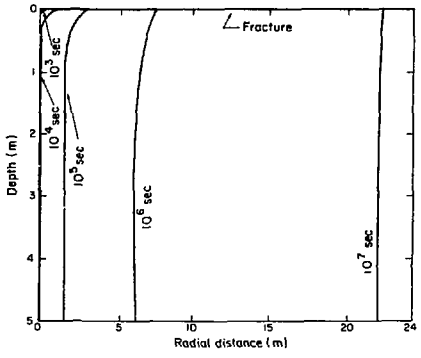

Figure 8 shows the location of the thermal front in the fracture and the rock matrix at different times. The figure shows clearly that at early times the thermal front in the fracture is well ahead of the thermal front in the rock matrix. However, after only 10^7 seconds (115 days), the thermal front in the rock matrix has almost completely caught up with the one in the fracture. It is of interest to note that only 23 meters away from the injection well, the two fronts almost coincide.

In the second run a permeability ratio (K_D) of 10^4 (the fracture permeability remained 10^{-10} m^2), and a fracture spacing of 10 meters was used; all other parameters remained the same. The results were similar throughout, although in this case the two fronts coincide farther away from the injection well.

The preliminary results obtained from this study indicate that for a reservoir with horizontal fractures, a premature invasion of colder water into the production region because of the higher permeability fractures may not cause an early breakthrough of cold water at the production wells. If the injection wells are properly located, the cold water sweep should be uniform and, consequently, the energy recovery from the field will be maximized. The appropriate spacing between the injection and the production wells will, however, depend upon many factors: the spacing and apertures of the fractures, the porosity and the thermal conductivity of the rock matrix, and the permeability ratio (K_D) between the fracture and the rock matrix.

REFERENCES

Avdonin, N. A., 1964; Some formulas for calculating the temperature field of a stratum subjected to thermal injection: Neft 'i Gaz, v. 3, p. 37-41.

Bodvarsson, G. S., Lippmann, M. J., and Narasimhan, T. N., 1979; Recent modifications of the numerical code "CCC": in Annual Report 1979 of the Earth Science Division, Lawrence Berkeley Laboratory, LBL-10795.

Bodvarsson, G. S., and Tsang, C. F., 1980; Injection into a fractured geothermal reservoir: to be published in the proceedings of the Geothermal Resources Council (GRC) Annual Meeting in Salt Lake City.

Carslaw, H. W. and Jaeger, J. C., 1959; Conduction of heat in solids, 2nd edition: Oxford University Press, Oxford, England.

Chan, T., Cook, N. G. W., and Tsang, C. F., 1978; Theoretical temperature fields for the Stripa Heater Project, 2 volumes: Technical Project Report no. 9, Swedish-American Cooperative Program on Radioactive Waste Storage in Mined Caverns in Crystalline Rock, Lawrence Berkeley Laboratory, LBL 7082, Berkeley California, September 1978.

Cinco-Ley, H., Samaniego, V. F., and Dominguez, A. N., 1978; Transient pressure behavior for a well with a finite-conductivity vertical fracture: Soc. Pet. Eng. J., August, 1978, p. 253-264.

Duff, I. S., 1977; MA28 - A set of Fortran subroutines for sparse unsymmetric linear equations: Report AERE - R 8730, Harwell/ Oxfordshire, Great Britain.

Gringarten, A. C., 1971; Unsteady-state pressure distribution created by a well with a single horizontal fracture, partial penetration or restricted entry: Ph. D. thesis, Stanford University.

Gringarten, A. C. and Sauty, J. P., 1975; A theoretical study of heat extraction from aquifers with uniform regional flow: Journal of Geophysical Research, v. 80, no. 35, p. 4956-4962.

Hellstrom, G., Tsang, C. F., and Claesson, J., 1979; Heat storage in aquifers. Buoyancy flow and thermal stratification problems: Department of Mathematical Physics, Lund Institute of Technology, Lund, Sweden.

Lippmann, M. J., Narasimhan, T. N., and Witherspoon, P. A., 1976; Numerical simulation of reservoir compaction in liquid dominated geothermal system: in Proceedings of the Anaheim Land Subsidence Symposium, IAHS-AISH Publication no. 121, December 1976, p. 179-189.

Lippmann, M. J., Tsang, C. F., and Witherspoon, P. A., 1977; Analysis of the response of geothermal reservoirs under injection and production procedures: SPE 6537, presented at the 47th Annual California Regional Meeting SPE-AIME, Bakersfield, California, April 1977.

Lippmann, M. J., Narasimhan, T. N., and Witherspoon, P. A., 1977; Modeling subsidence due to geothermal fluid production: Preprint 3107, ASCE Fall Convention, San Francisco, California, October 1977.

Lippmann, M. J., Bodvarsson, G. S., Witherspoon, P. A., and Rivera R., J., 1978; Preliminary simulation studies related to the Cerro Prieto Field: in Proceedings, First Symposium on the Cerro Prieto Geothermal Field, San Diego, California, Lawrence Berkeley Laboratory, LBL-7098, p. 375-383.

Lippmann, M. J. and Goyal, K. P., 1979; Numerical modeling studies of the Cerro Prieto Reservoir--A progress report: presented at the Second Symposium on the Cerro Prieto Geothermal Field, Mexicali, Mexico, October 1979.

Mangold, D., Wollenberg, H., and Tsang, C. F., 1978; Thermal effects in overlying sedimentary rock from in situ combustion of a coal seam: Lawrence Berkeley Laboratory, LBL-8172, Berkeley, California, September 1978.

Mangold, D. C., Tsang, C. F., Lippmann, J. J., and Witherspoon, P. A., 1979; A study of thermal effects in well test analyams: SPE-8232, presented at the 54th Annual Fall Technical Conference SPE-AIME, Las Vegas, Nevada, September 1979, Lawrence Berkeley Laboratory, LBL-9769.

Narasimhan, T. N., 1975; A unified numerical model for saturated-unsaturated groundwater flow: Ph.D. thesis, University of California, Berkeley, 244 p.

Theis, C. V., 1935; The relationship between the lowering of piezometric surface and the rate and duration of discharge using groundwater storage: Transactions American Geophysical Union, v. 2, p. 519-524.

Tsang, C. F., Lippmann, M. J., Goranson, C. B., and Witherspoon, P. A., 1976; Numerical modeling of cyclic storage of hot water in aquifers: presented at the Fall Annual Meeting of the American Geophysical Union, Symposium in Use of Aquifer Systems for Cyclic Storage of Water, San Francisco, California, December 1976, Lawrence Berkeley Laboratory, LBL-5929.

Tsang, C. F., Lippmann, M. J., and Witherspoon, P. A., 1978; Underground aquifer storage of hot water from solar energy collectors: in Proceedings of the International Solar Energy Congress, New Delhi, India, January 1978, Lawrence Berkeley Laboratory, LBL-7034.

Tsang, C. F., Buscheck, T., Mangold, D., and Lippmann, M. J., 1978; Mathematical modeling of thermal energy storage in aquifers: presented at the Thermal Energy storage in aquifers Workshop, Lawrence Berkeley Laboratory, Berkeley, California, May 1978, LBL-9970.

Tsang, C. F., Zerzan, M., et al, 1978; Numerical modeling of studies in well test analysis: in Proceedings of the Second Invitational Well Testing Symposium, Lawrence Berkeley Laboratory, Berkeley, California, October 1978, LBL-8883, p. 47-57.

Tsang, C. F., Buscheck, T. and Doughty, C., 1979; Aquifer thermal energy storage--a numerical simulation of Auburn University field experiments: Lawrence Berkeley Laboratory, LBL-10210.

DEVELOPMENT OF AN EXPLICIT FINITE-DIFFERENCE FLUID FLOW MODEL

R. Hofmann
Science Application Inc.
San Leandro, California 94577

SUMMARY

An explicit hydrological model has been developed and coupled to the STEALTH 2D code. It has been successfully tested in the uncoupled mode and is currently under further testing. This paper presents some preliminary results.

INTRODUCTION

For the past two days, all the speakers have been describing implicit and semi-implicit hydrological, numerical modeling techniques. Therefore, as a contrast, it might be interesting to show results of some recent work involving a fully explicit hydrological numerical model.

Last summer, the Office of Nuclear Waste Isolation (ONWI) funded Roger Hart, a graduate student from the University of Minnesota, to come to the San Leandro office of Science Applications, Inc. (SAI/SL), to construct and couple an explicit hydrologic model to an already existing coupled explicit, thermomechanical code. The specific job required that he develop an explicit porous medium, fluid-flow model based on Darcy's law and add it to the STEALTH 2D code[1].

TECHNICAL BACKGROUND

It is well known that explicit techniques have stability requirements that can impose severe economic restrictions on a calculational time step. However, recent developments in numerical scaling techniques are now making it possible to do (for reasonable computer cost) coupled quasi-static, thermomechanical, 10,000 to 100,000 year calculations using fully explicit techniques[2]. As a result, it now also appears economically feasible to do thermo-hydrologic-mechanical coupled calculations using explicit numerical equations.

Since, the thermal conduction and porous medium fluid-flow equations are both diffusion (parabolic) partial differential equations (if one uses Fourier's conduction law and Darcy's porous medium Law, respectively), it was possible for Roger to insert the fluid flow logic into STEALTH 2D by simply developing an algorithm from the existing heat conduction logic. Thus, the pore water flow model was coupled to the mechanical equilibrium equations in a way similar to the way that the heat conduction and mechanical equations are already coupled.

In nuclear waste isolation thermomechanical STEALTH calculations, the global (problem) time step is usually controlled by the stability requirements of the thermal phenomena while the mechanical response is computed using scaled momentum equations. By analogy in a hydrological-mechanical calculation in which stress is driven by pore water flow changes, the time-step would be controlled by the hydrology. In a thermo-hydrologic-mechanical calculation, either the thermal or the hydrology or some other constraint can be used to determine the problem time step while the slower mechanical response could be computed using time-step scaled equations[3].

An advantage of a fully explicit approach in coupled calculations, is the ease with which coupling mechanisms and complex constitutive behavior can be numerically included. In an explicit method one can concentrate on developing physically oriented constitutive models without spending an excessive amount of time on the numerics.

DESCRIPTION OF STEALTH

The STEALTH code system[4] solves fully time dependent equations, i.e., it can do mechanical transients as well as thermal transients. Quasi-static and static mechanical behavior are computed using time-step scaling and dynamic relaxation, respectively, applied to the fully time-dependent momentum equations. All the STEALTH codes can also perform large strain, large distortion, constitutively nonlinear calculations. STEALTH is basically a Lagrangian frame of reference continuum code, but it can also perform certain Eulerian frame of reference calculations using an advanced rezoning technique and certain structural response calculations using a finite element shell algorithm.

The STEALTH code system has one-, two-, and three-dimensional versions which offer several symmetries. The 2D version has sliplines which can be used to model discrete fractures. It's a public domain code system from EPRI and has four volumes of extensive documentation[5, 6, 7, 8]. To describe nonlinear constitutive effects, STEALTH can use standard material models or externally developed subroutines.

The STEALTH numerical equations are second order accurate in space and time for the mechanical solution and first order accurate in space for the thermal conduction equations. The Wilkin's finite-difference technique[9] is used to describe

partial derivatives (in particular, gradients of stress, velocity, etc.). This finite-difference approach is very similar to the approach used for eight-noded, isoparametric elements.

FLUID-FLOW MODEL TEST REQUIREMENTS

A set of relatively simple, analytic test problems were analyzed to check the validity of the fluid-flow model in the STEALTH 2D code. The following aspects of the fluid-flow calculations were checked:

- Are the potential gradient and direction of fluid-flow calculations correct for any model orientation?
- Is the calculation of total potential including the influence of gravity on the elevation head correct?
- What is the effect of fluid compressibility on the calculation?
- Is the model properly formulated for problems with a divergent (i.e., cylindrical) symmetry geometry?

These questions were answered by comparing the numerical results from STEALTH 2D to analytical solutions for selected transient fluid-flow problems. The analytic solutions[17] were obtained by taking advantage of the similarity between fluid flow and heat conduction.

DESCRIPTION OF TEST PROBLEMS AND RESULTS FROM STEALTH 2D

Three types of fluid-flow tests were performed.

Type 1. Potential boundary condition test.

Type 2. Fluid-flow boundary condition test.

Type 3. Pressurized well-bore simulation (cylindrical symmetry) test.

All three types used the same material properties. These properties are described below.

Fluid density	$\rho_f = 1000$ kg/m^3
Porosity	$n = 1$
Hydraulic conductivity	$K_\phi = 0.1$ m/sec
Fluid bulk modulus	$K_f = 10^6$ N/m^2, $(K_f \equiv 1/\beta)$.

The fluid bulk modulus was chosen so that the fluid is quite compressible (water's bulk modulus is $\sim 2 \times 10^9$ N/m^2). A highly compressible fluid was chosen to allow a larger time step in the fluid model calculation and to study the influence of the compressibility on the results.

The three test types were performed over transient time periods with types 1 and 3 being allowed to reach a steady state. Results for all the tests are presented as "snap-shot" plots of potential vs. distance across the body at selected times.

Although the two-dimensional code, STEALTH 2D, was used for these analyses, the test problems are all one-dimensional flow problems. The side boundaries were designated as impermeable in order to achieve the one-dimensional conditions. This kind of testing is severe in that the accuracy of the numerical model can be critically reviewed by observing the symmetric character of the computed results.

Test Type 1. Potential Boundary Condition Test.

For this test, a constant potential differential of 50 cm was applied to a mesh in various orientations in order to test both x- and y-components of the model. The orientations, illustrated in Figure 1, are:

- Orientation No. 1 - Vertical flow with gravity acting downward.
- Orientation No. 2 - Flow and gravity vector rotated 30^o counterclockwise.
- Orientation No. 3 - Flow and gravity vector rotated 25^o clockwise.
- Orientation No. 4 - Horizontal flow with no gravity effects.

In each case, the steady state condition consistent with the constant potential differential at the boundaries, is to be computed.

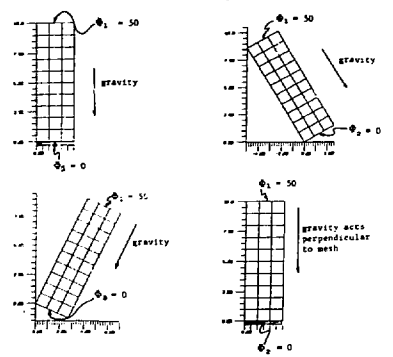

Figure 1. Fluid Flow Test Type 1 - Mesh Plots Showing Four Grid Orientations

Comparison of numerical and analytical results for the potential distribution is made in Figure 2 for the four cases. Agreement is quite good even though the grid is coarse. Better accuracy can be expected for a finer grid. Notice that for the first three grids, gravity provides an initial potential to the problem whereas for Orientaion No. 4, only the pore pressure influences the potential calculation.

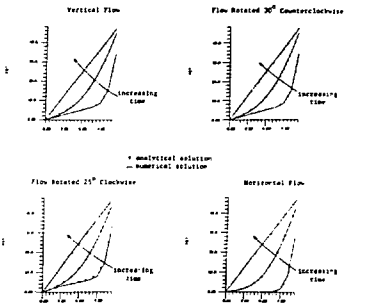

Figure 2. Fluid Flow Test Type 1 - Numerical and Analytical Results for Several Grid Orientations.

Test Type 2, Fluid-Flow Boundary Condition Test.

This test involves the effects of fluid building up in a mesh. An inward fluid flow of 0.5 m/sec was prescribed at one end of a grid while zero flow (impermeable boundary) was set at the other. The effect of gravity was not included. The mesh is shown in Figure 3 (a).

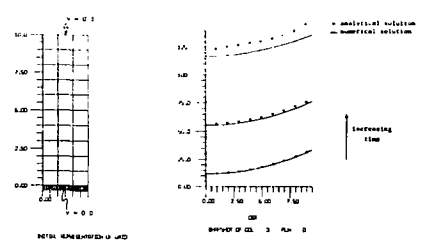

Figure 3. Fluid Flow Test Type 2 - Fluid Flow Boundary Condition.

Snapshots of the potential as a function of time are compared on the graph in Figure 3 (b) for three selected times. The influence of the fluid compressibility can be seen by observing that the numerical results for potential fall below the analytical results as time progresses. The reason for the difference in potentials at later times is because fluid density is not constant as is assumed for the analytical solution but is inversely related to the pore pressure. Thus, since the density increases with time, the pore pressure and potential are lower than they would be if the material was incompressible.

Since an analytical solution which included fluid compressibility was not used for this test, the accuracy of the numerical results was not verified. However, the difference between the numerical potential values and the analytical values showed an inversely proportional correspondence to the increase in fluid density with time, as would be expected. In later research, further analysis of the fluid compressibility will be made and additional validation performed.

Test Type 3, Pressurized Well-Bore Simulation.

This test case is typical of models used to simulate a constant pressure applied to the well-bore of a one-dimensional radial reservoir. For the case at hand, the pressure at the well-bore was set at 5000 N/m^2. Two approaches were examined for prescribing radial symmetry. They were:

1. describe the fluid mass storage equation in a two-dimensional axially symmetric form; and

2. define the grid using a two-dimensional translational symmetry geometry with a polar grid point description.

Approach 1 is illustrated by the grid in Figure 4 (a), where the radial direction is horizontal and the axial direction vertical. The grid representation for Approach 2 is shown in Figure 5 (a). As can be seen by the accompanying potential plots on each figure, results for both methods are very close to the analytical solution.

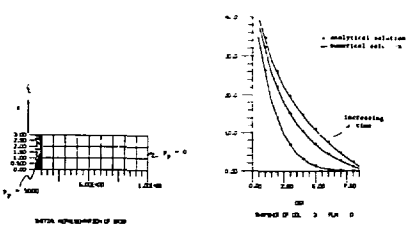

Figure 4. Fluid Flow Test Type 3 - Pressurized Wellbore Simulation 2-D Axial Symmetry Method.

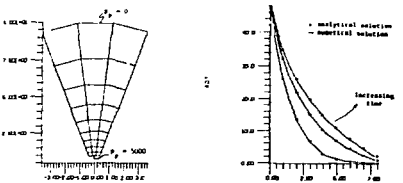

Figure 5. Fluid Flow Test Type 3 - Pressurized Wellbore Simulation 2-D Translational Symmetry Method.

STATUS

The current status of this development is as follows: Comparison of closed form and STEALTH computed, coupled stress fluid-flow consolidation cases are underway. So far the coupling seems to work. More testing is planned.

CONCLUSION

Explicit techniques can be used to cross check implicit and semi-implicit models. No judgment need be made about whether explicit or implicit is better or worse. Each have strengths and weaknesses. However, the results to date show that explicit techniques can be a reasonable additional tool in the bag of analytical tools for calculating coupled hydrological phenomena.

REFERENCES

1. K. Hart and R. Hofmann, "Hydrological Model in STEALTH 2D Code", OWI/Sub/79/E512-01300/8 SAI-FR-137-8), Office of Nuclear Waste Isolation, Battelle Memorial Institute, Columbus, Ohio, October 1979. Final report prepared by Science Applications, Inc., San Leandro, California.

2. K. K. Wahi, D. E. Maxwell and R. Hofmann, "The Thermomechanical Response of a One-Level Spent Fuel Nuclear Waste Repository", Y-OWI/SUB-78/16549/1 (SAI-FR-821-1), Office of Waste Isolation, Union Carbide Corporation, Oak Ridge, Tennessee, March 1978. Prepared by Science Applications, Inc., San Leandro, California.

3. D. E. Maxwell, R. Hofmann and K. K. Wahi, "An Optimization Study of the Explicit Finite-Difference Method for Quasi-Static Thermomechanical Simulations", Y/OWI/SUB-78/16549/3 (SAI-FR-821-3), Office of Waste Isolation, Union Carbide Corporation, Oak Ridge, Tennessee, March 1978. Prepared by Science Applications, Inc., San Leandro, California.

4. R. Hofmann, "STEALTH, A Lagrange Explicit Finite-Difference Code for Solids, Structural, and Thermohydraulic Analysis", EPRI NP-176-1, Electric Power Research Institute, Palo Alto, California, April 1978. Prepared by Science Applications, Inc., San Leandro, California.

5. R. Hofmann, "STEALTH, A Lagrange Explict Finite Difference Code for Solids, Structural, and Thermohydraulic Analysis", EPRI NP-260, Vol. 1, User's Manual, Electric Power Research Institute, Palo Alto, California, August 1976. Prepared by Science Applications, Inc., San Leandro, California.

6. R. Hofmann, "STEALTH, A Lagrange Explicit Finite-Difference Code for Solids, Structural, and Thermohydraulic Analysis", EPRI NP-260, Vol. 2, Sample and Verification Problems, Electric Power Research Institute, Palo Alto, California, August 1976. Prepared by Science Applications, Inc., San Leandro, California.

7. R. Hofmann, "STEALTH, A Lagrange Explicit Finite-Difference Code for Solids, Structural, and Thermohydraulic Analysis", EPRI NP-260, Vol. 3, Programmer's Manual, Electric Power Research Institute, Palo Alto, California, August 1976. Prepared by Science Applications, Inc., San Leandro, California.

8. B. I. Gerber, "STEALTH, A Lagrange Explicit *Finite-Difference Code for Solids*, Structural, and Thermohydraulic Analysis", EPRI-NP-260, Vol. 4, GRABIS Manual, Electric Power Research Institute, Palo Alto, California, August 1976. Prepared by Science Applications, Inc., San Leandro, California.

9. M. L. Wilkins, "Calculation of Elastic-Plastic Flow", UCRL-7322-Rev. 1, January 1969.

10. H. S. Carslaw and J. C. Jaeger, Conduction of heat in Solids, 2nd Edition, Oxford University Press, Oxford, 1959.

THE IMPORTANCE OF INCLUDING FRACTURES IN THERMOHYDROLOGICAL MODELING OF FLOW THROUGH POROUS MEDIA*

R. R. Eaton and D. E. Larson
Sandia National Laboratories**
Albuquerque, New Mexico 87185

ABSTRACT

This paper shows that computational models used to analyze the thermal and hydrologic characteristics of a nuclear waste repository site can give unrealistic results if the porous material matrix containing the repository is assumed fracture-free and completely rigid. Numerically modeling a repository in a homogenous porous media with an assumed permeability of 10^{-7} darcy results in calculated pore pressures which are four times larger than the local lithostatic load. These extreme pressures would degrade the integrity of host rock. It is concluded that the characteristics of the fractures within the material matrix must be considered in the computational model in order to obtain realistic results.

INTRODUCTION

A multi-dimensional two-phase computer code, SHAFT79,[1] has been used to analyze a proposed 1000 acre nuclear waste repository emplaced in argillite. The repository is assumed to contain spent fuel [$SF(UO_2)$] at a loading of 150 kW/acre and to be located at 600 m below the surface of the ground. It is also assumed that the argillite is saturated with water and that the drift was backfilled at the time of waste burial. The material properties used for these calculations are: argillite and drift permeability = 1×10^{-7} darcy, porosity = 9.1%, specific heat = 1046 J/kg-°C, thermal conductivity = 2.7 J/m-s-°C, and bulk density = 2530 kg/m^3. Argillite temperatures and pore pressures prior to waste emplacement were calculated by assuming the water table at the earth's surface, gravity = 9.8 m/s^2, and a geothermal heat flux of 1.5 μcal/cm^{2}s. Figure 1 gives the two-dimensional axisymmetric nodalization, with the repository located between $0 \le z \le 10$ and $0 \le R \le 1134$ m. The most critical input value affecting pore pressure is the assumed permeability of the argillite. The assigned value of 1×10^{-7} darcy falls in the middle of the reported range of shales in general (1×10^{-5} to 1×10^{-8} darcy).[2]

RESULTS AND CONCLUSIONS

Figure 2 shows temperature and pore pressure variation above the centerline of the repository at a radial location of 50 m for a time of 55 years after waste emplacement. The curve is significant because it demonstrates that for a distance of 200 m above the repository, the pore pressure exceeds the assumed local lithostatic load. Near the repository, the lithostatic load is surpassed by a factor of 4. It is, therefore, reasonable to assume that the rigidity of the rock would not be maintained at such extreme overpressures. If the rock was indeed completely homogeneous at t = 0, these calculated overpressures would likely create fractures. The fractures would result in an array of macro-sized homogeneous rock blocks. The presence of fractures around the blocks would provide channels with decreased resistance to fluid flow. Consequently, the increased volume of the fluid caused by thermal expansion would tend to flow out of the blocks and into the fractures at an increased rate and thus reduces maximum pressures experienced. If fractures existed at t = 0, the extremely high pore pressures and the corresponding local stress field would never develop. Additional cases for this geometry are presented in Reference 3.

A parametric study is currently underway from which it is hoped to quantify the importance of fractures surrounding the homogeneous macro-sized rock blocks that typically occur within the global repository region. Boundaries of the homogeneous blocks will be held at a specified pressure while the block is subjected to a given heat loading. Maximum pore pressures within the block will be a function of block size. This study should help define a range of conditions in which the strength

*This work was supported by the U.S. Department of Energy under contract DE-AC04-76DP00789.

**A U.S. Department of Energy facility.

of a homogeneous rock block might be exceeded and additional fractures generated.

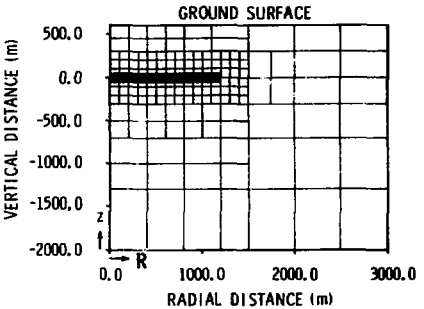

Figure 1. Axisymmetrix 2-D Grid System *Repository Located Between 0≤z≤10 and* 0_R_3034 m

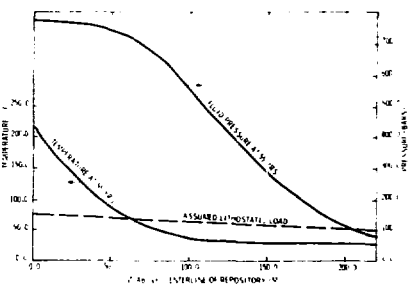

Figure 2. Geologic Medium Pressure and Temperature at R = 50.0 for 150 kW/acre Spent Fuel, Permeability = 1 x 10^{-7} darcy, Time After Burial = 55 yr

REFERENCES

1. K. Pruess, et al., SHAFT 78--A Two-Phase Multidimensional Computer Program for Geothermal Reservoir Simulation, LBL-8264, Lawrence Berkeley Laboratory, Earth Sciences Division, Berkeley, CA, 94720, 1980.

2. K. Magara, "Permeability Considerations in Generation of Abnormal Pressures," Soc. Petr. Engr., 11, pp. 236-242, 1971.

3. R. R. Eaton, W. D. Sundberg, D. E. Larson, and M. P. Sherman, Status of SHAFT78 With Respect to Modeling Radioactive Waste Burial in Eleana Argillite Including Calculations to Date, SAND79-1484, Sandia National Laboratories, Albuquerque, NM, 1979.

PANEL DISCUSSION

Chairman: J. O. Duguid, Office of Nuclear Waste Isolation

Panelists: K. H. Coats, Intercomp
J. E. Gale, University of Waterloo
R. E. Goodman, University of California, Berkeley
G. Hocking, Dames and Moore
C. R. Wilson, Lawrence Berkeley Laboratory

Editor: J. S. Y. Wang, Lawrence Berkeley Laboratory

DISCUSSION

The presentations in this workshop cover a wide spectrum of the state-of-the-art of modeling thermohydrological flows in fractured media. In addition to knowing "where we are" in our modeling capabilities, it is important to discuss "where we have to go" and "what we have to do to get there" in order to use the models for repository studies. In these proceedings, the stimulating discussions and comments from the panelists and participants are edited and organized to provide some insight into these questions of modeling.

Milestones in Repository Studies

The models are scheduled to be operational by 1986 for the study of thermomechanical influence on hydrological systems in fractured media. The models may not be verified in the field until large-scale, long-term studies are run. It is also likely that the verification of models for the repository scale will be extended over the fifty years of operation life of the repository.

According to the IRG Strategy 3, 1984 is the time for the decision on the choice among different media. Before this date we need to gather field data and develop modeling capabilities for different rock types.

Uncertainty in Input Parameters

Most of the input parameters for models cannot be determined exactly, and some can never be expressed in more definite form than a probability distribution. Therefore, models should be constructed to handle inputs of distributions for parameters. In many cases, the distributions are from the exponential family. The deterministic modeling may be tremendously biased if the parameters used are in the tails of the distributions.

If the distributions are continuous, the stochastic approaches can be used. For example, one can randomly sample the parameters with a Monte Carlo procedure and generate a distribution of results. To have a meaningful distribution, it may require many sampling and modeling steps.

For fractures, there is a great concern that the parameters may not only be distributed over wide ranges, but, more seriously, be distributed discontinuously. When the apertures of a few faults are very different from the distribution of apertures of other joints, these singular features must be taken into account separately. The basic knowledge of handling discontinuous distributions in stochastic modeling needs to be developed.

Discrete and Continuum Models

We need to know how far from the repository we need to go to use the continuum approach, and to what level of detail we need to measure the properties of the rock medium. To determine the scale, the discrete model should be compared with the continuum model using a consistent set of field data over a large rock mass. Work should be initiated to obtain a data set that could be used for this purpose.

For regional basin modeling, the porous medium approach may be used to model the direction and flux of flow. However, it is the velocity, not the flux, that we need as input in radionuclide transport modeling. It may be unsatisfactory to use Darcy flux and bulk porosity to estimate the velocity, especially in systems with fractures. The velocities in the fractures are very sensitive to the fracture apertures, and these may vary over orders of magnitude.

In regional studies, the water table can be modeled with different orderings of fractures or different sets of fractures intersecting the wells. The pressure distribution measured in the field will not in general uniquely determine the details of the fracture system. Experience from many basin studies of fractured systems shows that the porous medium models are very good for flow. But transport modeling with the porous medium approach has more problems.

Although the porous medium models may be satisfactory in modeling water levels, the discrete approach may be needed to model permeability tests with packed wellbore. The separation between packers is the characteristic length of the monitoring device in packer tests. When the packer spacing is comparable to the fracture spacing, the pressure responses are determined by the flow in the few fractures intersecting the interval. The relationship between monitoring and modeling should be specified. We must develop methods for measuring at the same scale as we model.

A low-permeability formation is essential for waste disposal. Human activities and waste emplacement could change the hydraulic gradient and induce flow along permeable paths. The fractures extending from the repository all the way to surface are potential leakage paths. For these fractures, the appropriate scale for porous medium modeling might not be easily determined and discrete modeling should be used.

The porous medium approximation is based on the concept that a meaningful average exists over a representative volume element which can be modeled as a grid block. It is assumed that the values of the parameters of the grid blocks can be measured in the laboratory or in the field. For fractured formations, it is unknown if the measured values represent a large enough volume. The variation of the permeability versus depth in same fractured media is one indication that the characteristics of flow through fractures can be quite different from the average flow through the pores in a porous medium.

For comparison between discrete fracture and porous medium models, the parameters of the equivalent continuum should be constructed consistently from the discrete data. Not enough work has been done using discrete data to build an equivalent continuum model. For example, there is a need to study the relevancy of the assumption of fracture continuity used in the derivation of the equivalent permeability tensor from the discrete fracture set data. More research is also needed to correlate the distributions of discrete data with the distributions of equivalent continuum parameters, taking into account the means, the standard deviations, etc.

Stripa Experiments

The LBL-SKBF experiments at Stripa, Sweden were discussed extensively. The field experiments measure the properties of a fractured rock mass on different scales. The underground large-scale macropermeability experiment, together with small-scale borehole tests at the same site, should generate a consistent set of data useful for the comparison of discrete and continuum models.

The macropermeability experiment measures the average hydrologic properties around a 33 m long x 5 m diameter drift, 335 m below surface in the granite formation adjacent to an abandoned iron mine. The fracture systems in Stripa have been extensively mapped. There are three near-vertical and one sub-horizontal sets with fracture spacings in the range of half of a meter. Fifteen 3" boreholes from 30 to 40 m long were drilled into the surrounding rock in different directions: five extending from the end of the drift, five radially outward at about 10 m from the end, and another five at about 20 m from the end. The borehole sample approximately 10^6 m^3 of rock mass in three-dimensional space with 10^2 m in each dimension. For each borehole, six packers are installed at approximately 5 m intevals. There are a total of 90 sampling zones which are individually connected by tubing to pressure gauges.

After packer installations, the inflow to the drift is measured by evaporating the seepage into the ventilation air while measuring the change in water vapor content between incoming and exhaust air streams. In order to measure this change in water vapor content, the drift has been sealed off and the wet and dry temperatures of the inlet and exhaust are taken. During the experiment, air in the drift will be kept at constant temperature. Preasures in the boreholes and water flow into the drift will be monitored until they are in a quasi-steady state. Several months may be required to reach quasi-equilibrium conditions. The average hydraulic conductivity of the surrounding rock is estimated to be about 10^{-10} m/sec, using the preliminary data of flow rate and pressures and the assumption of steady radial flow.

The directions of flow in the surrounding rock are difficult to measure. The flow field may be dominated by a few high permeability fractures. The pressure differences between different intervals in the boreholes were much less than were expected. The pressure gradients in the region surrounding the drift are also influenced by the extensive Stripa mine working adjacent to the granite rock. There are some noticeable gradients in the results as one proceeds from the top to the bottom. The complex pressure field may make the determination of anisotropy in the permeability tensor more difficult.

Since each interval in the boreholes is individually connected to the outside, different zones can be hydraulically connected together. This allows studies to be made of the effects of increasing axial zone lengths or the effects of integrating circumferentially the pressures at the same radial distance from the drift. Pressure pulses, tracer tests, and geochemical sampling can be performed from different zones.

To compare with the macropermeability measurements, the discrete fracture data will be generated by pressure tests from inclined boreholes drilled from the surface as well as from the bore holes surrounding the drift. The discrete data in boreholes form the basis for the derivation of the equilibrium continuum.

In view of the order of magnitude difference in the scales between the the results of wellbore testing and the ventilation experiment, it will be very good agreement if the permeability tensor from the discrete data is within an order of magnitude of the average macropermeability. One set of transient hydraulic responses between one borehole and other boreholes around the ventilation drift were discussed. Before the boreholes were packed, one of the radial holes produced about as much water as all the other fourteen holes combined. After this hole was sealed off, large pressure changes were measured throughout the fracture systems in a week. This is one indication that the

responses in the Stripa fracture system may be fast enough that the short-term, small-scale discrete measurements could be consistent with the long-term, large-scale average value. Therefore, the Stripa data could be used for the comparison of discrete and continuum models.

Transport Modeling

The safety of the repository is mainly determined by the transport of radionuclides. We need flow velocity as input to the transport model. As a result of the distributions of permeabilties and porosities, the velocities in a fractured medium have wide and discontinuous distributions. We need to be able to predict a distribution of velocities in order to understand the dispersion and transport of radionuclides.

The absorption by the rock matrix will significantly slow down the velocity of solute transport. In a discrete approach, the flows in the fractures are determined and the chemical diffusions in the rock matrix are modeled. It is of interest to compare the solution concentration of discrete model with that of the porous medium model.

Tracer tests are used to determine the flow velocity and solute transport. Although breakup curves can be calculated with analytical or numerical models, data analysis of tracer tests in the field are usually difficult. The loss of tracer mass in a fractured medium is one of the problems.

The problem of nuclide transport covers many orders of magnitude in the time and space scales. For the overall concern in the transport of nuclides, it is important to select the relevant scale. Over the time scale of thousands of years, the nuclides will spend short times in the fractures around the repository. For the modeling of an average dose over an aquifer in the future, the porous medium model may be used. On the other hand, it is not known if one could average over an aquifer. The contaminants could come out of one hole or one fracture instead of spreading over a large area. It is very difficult to define a dangerous or a safe dose.

We need to determine how much variation in waste dosage is associated with variations of fracture flow. This would provide information concerning what is important and what part of the problem we can neglect.

Age-Dating

In addition to permeability measurements, age-dating is an independent tool to study the movements of groundwater. For nearly impermeable rock with very slow flow, the differences in the ages of water at different locations may be detectable. One may expect to find older water at greater depth. If the flows measured from permeability tests and from age-dating are consistent, the answers will be more convincing.

The techniques of age-dating still need improvement. The age-dating method only estimates how long it takes for the water to get to a location. It does not indicate how long it will take to get to the biosphere discharge zones. One can find old rock water coming out of hillside springs. The conclusions from age-dating alone should be carefully evaluated.

A Proposed Field Test Procedure

A large-scale field test was proposed to run both the flow tests and the age-dating. A large shaft will be sunk to any appropriate depth in the formation of interest. From the shaft, long boreholes can be drilled into the surrounding rock mass at any depth and in any direction. Large shafts of several meters in diameter and long boreholes of several kilometers in length can be drilled with existing technologies. With the long boreholes, we can perform packer tests for fractures and sample the water at different locations to probe the three-dimensional flow field.

In each long borehole, a series of four sets of measurements can be performed. Firstly, the hole is packed off with long packers and short open zones. The steady state pressures are measured after shut-in to obtain the natural gradient along the hole. Then the waters are sampled and dated to estimate the natural water velocity from age differences. In the third set of measurements, high pressure water is injected into one of the zones and the permeabilities are measured from the induced pressure changes at other zones. After the steady state flow field is established, tracers are used to measure migration and to determine the porosity. The gradient, permeability and porosity are used to calculate an independent velocity value.

Although the licensing procedure for repositories has not been established, it is conceivable that shaft sinking, in-situ testing, age-dating, and tracer studies will take place prior to licensing the repository.

Thermal Effects

With the emplacement of waste heat sources, buoyancy flows will be induced and the stress field will be changed around the repository. Simple porous medium model and simple fracture models are being used to study generically the dependence of flow on permeability, waste type, repository location, the groundwater basin, etc. The capabilities of modeling flow-stress and flow-heat-stress couplings are being developed.

With elevated temperatures, many parameters of the formation will change. In repository studies, it is important that the natural system will not be perturbed irreversibly during the

thermal pulse. In principle, the thermal pulse can be controlled by lower waste loading density and longer surface cooling period. These are two of the important factors in repository design.

Modeling and Prediction

Numerical models are useful tools. We can simulate numericlly discrete fractures as small grid blocks. We can also handle transient behavior, discrete fracture porous block flow, and deformable fractures. The computer capacity and the lack of input data are the main limitations in our modeling capability.

There is concern that most of the existing models do not contain new concepts concerning the nature of flow in fractures. The governing equations are based on simple concepts which may or may not describe flow through fractures as they occur naturally or in the vicinity of the repository. The simple parallel-plate model does not take into account the roughness, the contact area, the in-filled material, the continuity and other features of fractures.

The models normally are calibrated with observed field data. There is a question of whether the fitted parameters are physically meaningful and representative of the formation. On the other hand, there is the view point that we should focus less on the complexity of the system and more on how we can simplify it in order to understand the results, the processes, and the system. The simple description of the formation which is used in matching a set of field data is not expected to represent accurately the details of the formation. Several field tests may be needed to understand the formation.

Models should be tested against data from laboratory experiments or field test sites before applying the model results. The reliability and credibility of our long-term prediction are largely untested. There is a need to quantify the confidence or uncertainty level of our modeling results in prediction.

SUMMARY

Key Points:

- The consensus that was sought was: where are we, where do we have to go, and what do we have to do to get there?
- Models should be constructed to accept a distribution of parameters. We can measure fracture orientation but everything else is difficult to measure. If distributions are continuous, stochastic methods could be used.
- We need to determine at what scale and to what level of detail we have to model flow (comparison of discrete with continuum models using a consistent data set). Work should be initiated to obtain a data set that could be used for this purpose.
- The pressure distribution measured in the field will not in general uniquely determine the details of the fracture systems.
- There is a relationship between monitoring and modeling. We must develop methods for measuring at the same scale as we model.
- Not enough work has been done on building an equivalent continuum model from discrete data.
- There is a possibility of using some of the Stripa data to compare discrete and continuum models.
- We need to be able to predict a distribution of velocities.
- We need to determine the sensitivity of variation in waste concentration to variations in fracture flow. This would provide information concerning which part of the problem we can neglect. We should focus less on the complexity of the system and more on how we can simplify it.
- Tracer tests and ground water dating should provide insight into the overall flow field of the system, and may indicate how the models of the system may be smplified.
- Ground water dating is an independent measure of permeability and may provide a means for verification of models.

Consensus reached:

- Models must be modified to accept distributions of parameters; we should be striving to use a stochastic approach.
- We need appropriate field data to determine where continuum models or where discrete models must be used.
- There appeared to be a strong feeling that continuum models with the capabiltiy of discrete fractures is an appropriate way to proceed in the future.

***

PROGRAM

***

NUMERICAL MODELING OF THERMO-HYDROLOGICAL FLOW IN FRACTURED ROCK MASSES

BUILDING 90 - 3RD FLOOR CONFERENCE ROOM
LAWRENCE BERKELEY LABORATORY
BERKELEY, CALIFORNIA 94720

FEBRUARY 19 - 20, 1980

TUESDAY, FEBRUARY 19

SESSION I

CHAIRMAN: C.F. TSANG

8:00 - 9:00		Registration
9:00 - 9:10	P.A. Witherspoon, LBL	Welcome
9:10 - 9:20	M. Lemcoe, ONWI	Welcome
9:20 - 9:40	J.S.Y. Wang, LBL	Introduction
9:40 - 10:10	P.J. Bourke, Harwell	Overview
Break		
10:30 - 11:00	T.N. Narasimhan, LBL	
11:15 - 11:45	J.O. Duguid, ONWI	
12:00 - 12:30	A. Shapiro, Princeton	

SESSION II

CHAIRMAN: P. Nelson

1:45 - 2:00	R. Thorpe, UCB
2:00 - 2:30	J. Noorishad, UCB
2:45 - 3:15	A. Runchal, Dames and Moore
Break	
3:45 - 4:15	S. Pahwa, Intera
4:30 - 5:00	A. Burgess, Acres / J. Ratigan, RE/SPEC
5:15 - 5:45	S. Gupta, BPNL
7:30 - 9:30	NO-HOST, INFORMAL DINNER

WEDNESDAY, FEBRUARY 20

SESSION III

CHAIRMAN: M. Wigley

9:00 - 9:30	K. Coats, Intercomp
9:40 - 10:10	C. Faust, Geotrans
Break	
10:35 - 11:05	J. Pritchett, S^3
11:15 - 11:45	K. Pruess / G. Bodvarsson, LBL
12:00 - 12:45	Short contributions on new developments
Lunch	

SESSION IV

CHAIRMAN: J.O. Duguid

1:30 - 3:30	Panel discussion Coats, Gale, Goodman, Hocking and Wilson.
3:30 - 4:00	Summary - J.S.Y. Wang and P.A. Witherspoon

LIST OF PARTICIPANTS

Gudmundur S. Bodvarsson
Earth Sciences Division
Lawrence Berkeley Laboratory
1 Cyclotron Road
Berkeley, CA 94720

Patrick J. Bourke
Chemical Technology Division
AERE Harwell
Oxfordshire OX11, ORA
ENGLAND

Anthony S. Burgess
Acres Consulting Services, Inc.
Liberty Bank Building
Main at Court
Buffalo, NY 14202

Paul L. Chambre
4171 Etcheverry Hall
U. C. Berkeley
Berkeley, CA 94720

Keith H. Coats
Intercomp
1201 Dairy Ashford
Houston, TX 77079

Lou H. Cohen
Earth Sciences Division
Lawrence Berkeley Laboratory
1 Cyclotron Road
Berkeley, CA 94720

Charles R. Cole
Battelle Pacific Northwest Laboratory
P. O. Box 999
Richland, WA 99352

Barry Dial
Science Application Inc.
2450 Washington Avenue, Suite 120
San Leandro, CA 94577

Tom W. Doe
Earth Sciences Division
Lawrence Berkeley Laboratory
1 Cyclotron Road
Berkeley, CA 94720

Kenneth W. Dormuth
Atomic Energy of Canada
Whiteshell Nuclear Research Est.
Pinawa
Manitobs ROE 1LO
CANADA

James O. Duguid
O.N.W.I.
Battelle Memorial Institute
505 King Avenue
Columbus, OH 43201

David B. Dunbar
3 Embarcadero Center, Suite 700
San Francisco, CA 94111

Roger R. Eaton
Div. 5511
Sandia Laboratories
Albuquerque, NM 87185

Charles R. Faust
Geotrans Inc.
P. O. Box 2550
Reston, VA 22090

John E. Gale
Earth Sciences Department
University of Waterloo
Waterloo
Ontario N2L 3G1
CANADA

Richard E. Goodman
434 B Davis
University of California, Berkeley
Berkeley, CA 94720

Gerald E. Grisak
Environment Canada
562 Booth Street
Ottawa
Ontario K1A 0E7
CANADA

Sumant K. Gupta
Department of Water and Land Resources
Battelle Pacific Northwest Laboratory
P. O. Box 999
Richland, WA 99352

Varuthamadhinn Guvanasen
Earth Sciences Division
Lawrence Berkeley Laboratory
1 Cyclotron Road
Berkeley, CA 94720

Grant Hocking
Advanced Technology Group
Dames and Moore
44 Mall Road
Burlington, MA 01803

Ron Hofmann
Science Application Inc.
2450 Washington Avenue, Suite 120
San Leandro, CA 94577

Paul A. Hsieh
Department of Hydrology and Water Resources
University of Arizona
Tucson, AZ 85721

Kenzi Karasaki
Etcheverry Hall
University of California
Berkeley, CA 94720

Mike M. Lemcoe
O.N.W.I.
Battelle Memorial Institute
505 King Avenue
Columbus, OH 43201

Marcelo J. Lippmann
Earth Sciences Division
Lawrence Berkeley Laboratory
1 Cyclotron Road
Berkeley, CA 94720

Jane C. Long
Earth Sciences Division
Lawrence Berkeley Laboratory
1 Cyclotron Road
Berkeley, CA 94720

Don C. Mangold
Earth Sciences Division
Lawrence Berkeley Laboratory
1 Cyclotron Road
Berkeley, CA 94720

Mark Mathews
LASL G-9
M.S. - 983, P. O. Box 1663
Los Alamos, NM 87545

Connie W. Miller
Earth Sciences Division
Lawrence Berkeley Laboratory
1 Cyclotron Road
Berkeley, CA 94720

Willard A. Murray
Lawrence Livermore Lab.
P. O. Box 808, L-390
Livermore, CA 94550

T.N. Narasimhan
Earth Sciences Division
Lawrence Berkeley Laboratory
1 Cyclotron Road
Berkeley, CA 94720

Phil H. Nelson
Earth Sciences Division
Lawrence Berkeley Laboratory
1 Cyclotron Road
Berkeley, CA 94720

Jahan Noorishad
Earth Science Division
Lawrence Berkeley Laboratory
1 Cyclotron Road
Berkeley, CA 94720

John D. Osnes
RE/SPEC
P. O. Box 725
Rapid City, South Dakota 57709

Michael J. O'Sullivan
Earth Sciences Division
Lawrence Berkeley Laboratory
1 Cyclotron Road
Berkeley, CA 94720

Suresh B. Pahwa
Intera Environmental Consultant, Inc.
11511 Katey Freeway, Suite 630
Houston, TX 77079

Walter Pelka
Inst. f. Wasserbau Wasserwirks
Reinisch-West Tech. Hochschule
Mies-van-der-Rohe Strasse 1
D-5100 Aachen
WEST GERMANY

John W. Pritchett
System, Science and Software
P. O. Box 1620
La Jolla, CA 92038

Karsten Pruess
Earth Sciences Division
Lawrence Berkeley Laboratory
1 Cyclotron Road
Berkeley, CA 94720

Anders Rasmuson
Royal Institute of Technology
Stockholm
SWEDEN

Joe L. Ratigan
3375 F Northwood Drive
Concord, CA 94520

Akshai K. Runchal
Dames and Moore
Suite 1000
1100 Glendon Avenue
Los Angeles, CA 90024

James E. Russell
Petroleum Engineering
Texas A & M University
1702 Todd Trail
College Station, TX 77840

Budhi Sagar
Dames & Moore
1100 Glendon Avenue, Suite 1000
Los Angeles, CA 90024

Christopher M. St. John
Department of Civil and Mineral Engineering
University of Minnesota
221 Church Street, S.E.
Minneapolis, MN 55455

Werner J. Schwarz
Earth Sciences Division
Lawrence Berkeley Laboratory
1 Cyclotron Road
Berkeley, CA 94720

Allen M. Shapiro
Department of Civil Engineering
Princeton University
Princeton, NJ 08540

Terry L. Simkin
Earth Sciences Division
Lawrence Berkeley Laboratory
1 Cyclotron Road
Berkeley, CA 94720

David T. Snow
Groundwater and Geological Engineering
6235 Turrett Drive
Colorado Springs, CO 80907

Michael L. Sorey
U.S.G.S.
345 Middlefield Road
Menlo Park, CA 94025

Becky Sterbentz
Earth Sciences Division
Lawrence Berkeley Laboratory
1 Cyclotron Road
Berkeley, CA 94720

Ren Jen Sun
U. S. Geological Survey
11113 Lombardy Road
Silver Spring, MD 20901

Richard Thorpe
Earth Sciences Division
Lawrence Berkeley Laboratory
1 Cyclotron Road
Berkeley, CA 94720

Jim Tracy
U.S.G.S.
12201 Sunrise Valley Road
Mail Stop 431
Reston, VA 22092

Chin Fu Tsang
Earth Sciences Division
Lawrence Berkeley Laboratory
1 Cyclotron Road
Berkeley, CA 94720

Yvonne Tsang
Earth Sciences Division
Lawrence Berkeley Laboratory
1 Cyclotron Road
Berkeley, CA 94720

Joseph S.Y. Wang
Earth Sciences Division
Lawrence Berkeley Laboratory
1 Cyclotron Road
Berkeley, CA 94720

Michael Wigley
O.N.W.I.
505 King Avenue
Columbus, OH 43201

Charles R. Wilson
Earth Sciences Division
Lawrence Berkeley Laboratory
1 Cyclotron Road
Berkeley, CA 94720

Alan Winslow
Lawrence Livermore Laboratory
P. O. Box 808 L200
Livermore, CA 94550

Paul A. Witherspoon
Earth Sciences Division
Lawrence Berkeley Laboratory
1 Cyclotron Road
Berkeley, CA 94720

GPO 789-120/2